

IN VIVO ANALYSIS OF OCULAR MORPHOLOGICAL CHANGES
DURING PHAKIC ACCOMMODATION

AMY LOUISE SHEPPARD

Doctor of Philosophy

ASTON UNIVERSITY

November 2010

This copy of the thesis has been supplied on the condition that anyone who consults it is understood to recognise that its copyright rests with its author and that no quotation from the thesis and no information from it may be published without proper acknowledgement.

ASTON UNIVERSITY

IN VIVO ANALYSIS OF OCULAR MORPHOLOGICAL CHANGES DURING PHAKIC ACCOMMODATION

AMY LOUISE SHEPPARD

Doctor of Philosophy

September 2010

Summary

The principal theme of this thesis is the *in vivo* examination of ocular morphological changes during phakic accommodation, with particular attention paid to the ciliary muscle and crystalline lens. The investigations detailed involved the application of high-resolution imaging techniques to facilitate the acquisition of new data to assist in the clarification of aspects of the accommodative system that were poorly understood.

A clinical evaluation of the newly available Grand Seiko Auto Ref/ Keratometer WAM-5500 optometer was undertaken to assess its value in the field of accommodation research. The device was found to be accurate and repeatable compared to subjective refraction, and has the added advantage of allowing dynamic data collection at a frequency of around 5 Hz. All of the subsequent investigations applied the WAM-5500 for determination of refractive error and objective accommodative responses.

Anterior segment optical coherence tomography (AS-OCT) based studies examined the morphology and contractile response of youthful and ageing ciliary muscle. Nasal *versus* temporal asymmetry was identified, with the temporal aspect being both thicker and demonstrating a greater contractile response. The ciliary muscle was longer in terms of both its anterior ($r = 0.49$, $P < 0.001$) and overall length ($r = 0.45$, $P = 0.02$) characteristics, in myopes. The myopic ciliary muscle does not appear to be merely stretched during axial elongation, as no significant relationship between thickness and refractive error was identified. The main contractile responses observed were a thickening of the anterior region and a shortening of the muscle, particularly anteriorly. Similar patterns of response were observed in subjects aged up to 70 years, supporting a lenscentric theory of presbyopia development.

Following the discovery of nasal/ temporal asymmetry in ciliary muscle morphology and response, an investigation was conducted to explore whether the regional variations in muscle contractility impacted on lens stability during accommodation. A bespoke programme was developed to analyse AS-OCT images and determine whether lens tilt and decentration varied between the relaxed and accommodated states. No significant accommodative difference in these parameters was identified, implying that any changes in lens stability with accommodation are very slight, as a possible consequence of vitreous support.

Novel three-dimensional magnetic resonance imaging (MRI) and analysis techniques were used to investigate changes in lens morphology and ocular conformation during accommodation. An accommodative reduction in lens equatorial diameter provides further evidence to support the Helmholtzian mechanism of accommodation, whilst the observed increase in lens volume challenges the widespread assertion that this structure is incompressible due to its high water content. Whole-eye MRI indicated that the volume of the vitreous chamber remains constant during accommodation. No significant changes in ocular conformation were detected using MRI.

The investigations detailed provide further insight into the mechanisms of accommodation and presbyopia, and represent a platform for future work in this field.

Key words: Accommodation, ciliary muscle, crystalline lens, ocular imaging, presbyopia.

ACKNOWLEDGEMENTS

I would like to thank my supervisors, Dr. Leon N. Davies, Dr. Mark Dunne and Professor James Wolffsohn for their guidance, support and continual encouragement over the last three years. Additionally, I wish to thank Professor Krish Singh and Dr. John Evans at Cardiff University School of Psychology for their time and assistance with my magnetic resonance imaging (MRI) projects, and Dr. Edward Mallen at Bradford University Optometry Department for his technical support.

Many thanks also to Bausch and Lomb, New York, for the funding to support my postgraduate studies.

I wish to extend warmest thanks to the staff and students at Aston University for their time and co-operation when participating in my numerous experiments. I am especially grateful to my postgraduate friends and colleagues in the Optometry Department, who have provided continual advice and support during my time back at Aston.

Finally, I am hugely grateful to Mom, Dad, Paul, Sarah and Carson for their love, understanding and encouragement.

CONTENTS

	Page
SUMMARY	2
ACKNOWLEDGEMENTS	3
CONTENTS	4
LIST OF TABLES	9
LIST OF FIGURES	10
CHAPTER 1 OCULAR ACCOMMODATION	
1.1 General introduction	13
1.2 Historical theories of accommodation	14
1.3 Present understanding of the mechanism of accommodation	15
1.4 Anatomy of the accommodative apparatus	17
1.4.1 Crystalline lens	18
1.4.2 Zonules	24
1.4.3 Ciliary body	26
1.4.4 Choroid	28
1.4.5 Auxiliary accommodative structures	29
1.5 Neural mechanism of accommodation	30
1.5.1 Ciliary muscle innervation	30
1.6 Components of accommodation	31
1.6.1 Reflex accommodation	31
1.6.2 Convergence accommodation	32
1.6.3 Proximal accommodation	32
1.6.4 Tonic accommodation	32
1.7 Accommodative microfluctuations	32
1.8 Presbyopia	34
1.8.1 Lenticular theories	35
1.8.2 Extralenticular theories	37
1.9 Summary	38
1.10 Aims of the thesis	39
CHAPTER 2 INSTRUMENTATION FOR <i>IN VIVO</i> ANALYSIS OF THE ACCOMMODATIVE STRUCTURES	
2.1 Introduction	41

2.2	Instrumentation for determination of refractive error and objective accommodation measurement	41
2.3	Validation of the of the Grand Seiko Auto Ref/ Keratometer WAM-5500	42
2.3.1	The Grand Seiko Auto Ref/ Keratometer WAM-5500	43
2.3.1a	Methods	44
2.3.1b	Results	47
2.3.1c	Discussion	56
2.4	Instrumentation for <i>in vivo</i> imaging of ocular accommodation	58
2.4.1	Scheimpflug imaging	58
2.4.2	Ophthalmophakometry	59
2.4.3	Ultrasound imaging	60
2.4.4	Anterior segment optical coherence tomography	61
2.4.5	Magnetic resonance imaging	65
2.5	Summary	69

CHAPTER 3 *IN VIVO* ANALYSIS OF CILIARY MUSCLE MORPHOLOGICAL CHANGES WITH ACCOMMODATION AND AXIAL AMETROPIA

3.1	Introduction	70
3.2	Methods	75
3.2.1	Sample size estimation	75
3.2.2	Subjects	76
3.2.3	Measurements	76
3.2.4	Ciliary muscle image acquisition and analysis	77
3.2.5	Statistical analysis	81
3.2.6	Repeatability	81
3.3	Results	82
3.3.1	Repeatability	82
3.3.2	Ciliary muscle biometry and changes with accommodation	83
3.4	Discussion	86
3.5	Conclusion	91

CHAPTER 4 THE EFFECT OF AGEING ON *IN VIVO* CILIARY MUSCLE MORPHOLOGY AND CONTRACTILITY

4.1	Introduction	93
4.2	Methods	96
4.2.1	Subjects	96

4.2.2	Measurements	97
4.2.3	Image analysis	98
4.2.4	Statistical analysis	99
4.3	Results	100
4.3.1	Ciliary muscle morphology	100
4.3.2	Ciliary muscle contractile response	103
4.4	Discussion	106
4.5	Conclusion	109

CHAPTER 5 PHAKIC LENS TILT AND DECENTRATION WITH ACCOMMODATION UTILISING ANTERIOR SEGMENT OPTICAL COHERENCE TOMOGRAPHY

5.1.	Introduction	111
5.2	Methods	115
5.2.1	Protocol development	115
5.2.2	Development of a computer programme for determination of lens tilt and decentration from AS-OCT images	116
5.2.3	Validity of programming	121
5.2.4	Main investigation	122
5.2.5	Measurements	123
5.2.6	Image acquisition	123
5.2.7	Image analysis	124
5.2.8	Statistical analysis	124
5.2.9	Repeatability	124
5.3	Results	125
5.3.1	Repeatability	125
5.3.2	Main investigation	126
5.4	Discussion	128
5.5	Conclusion	131

CHAPTER 6 THREE-DIMENSIONAL MAGNETIC RESONANCE IMAGING (MRI) OF THE PHAKIC CRYSTALLINE LENS DURING ACCOMMODATION

6.1	Introduction	132
6.2	Methods	138
6.2.1	MRI protocol development	139
6.2.2	Main protocol	141
6.2.3	MRI data analysis	142

6.2.4	Repeatability	143
6.2.5	Statistical analysis	145
6.3	Results	145
6.3.1	Repeatability	145
6.3.2	Main investigation	146
6.4	Discussion	154
6.5	Conclusion	157
CHAPTER 7 CHANGES IN THE POSTERIOR EYE WITH ACCOMMODATION		
7.1	Introduction	158
7.2	Methods	163
7.2.1	MRI data analysis	167
7.2.2	Statistical analysis	168
7.3	Results	169
7.3.1	<i>IOLMaster</i> derived retinal contour	170
7.3.2	MRI derived ocular conformation	171
7.4	Discussion	173
7.5	Conclusion	176
CHAPTER 8 CONCLUSIONS AND PLANS FOR FUTURE WORK		
8.1	General conclusions	177
8.2	Evaluation of experimental work: suggestions for improvement and plans for future research	179
8.3	Concluding statement	181
REFERENCES		182
APPENDICES		
A1	Aston University Human Sciences Ethical Committee acceptance of amendment to project 06/12	222
A2	Information and consent form for experimental participants at Aston University	224
A3	Aston University Human Sciences Ethical Committee acceptance of amendment to project 07/D	226
A4	CUBRIC volunteer information sheet, screening forms and consent form	228
A5	Data relating to Chapters 3 and 4	239

A6	Data relating to Chapter 5	251
A7	Data relating to Chapter 6	252
A8	Data relating to Chapter 7	254
SUPPORTING PUBLICATIONS		255

LIST OF TABLES

Table	Page(s)
1.1 Effect of age on <i>in vivo</i> measured lens dimensions	20-21
2.1 Comparison of the axis of the cylindrical component measured with the WAM-5500 and by subjective refraction	50
2.2 Intertest variability of the refractive results obtained from the final WAM-5500 autorefractor prescription	53
2.3 Accuracy of WAM-5500 pupil diameters assessed using calibrated artificial pupils	56
2.4 Summary of notable previous studies that have utilised AS-OCT to analyse ocular biometric changes with accommodation	64
3.1 Key findings from <i>in vitro</i> and <i>in vivo</i> studies of human ciliary muscle morphology	73
3.2 Mean values (\pm S.D.) for nasal and temporal ciliary muscle parameters with accommodative stimulus level	82
3.3 Repeatability of ciliary muscle biometric measures, assessed by imaging and analysing a single subject ten times at the minimal accommodative state	83
3.4 Intersession repeatability data of ciliary muscle biometric parameters measured at 0.19 D and 8.0 D accommodative demand levels	83
4.1 Change in ciliary muscle morphological characteristics with age	101
5.1 Summary of recent studies of phakic human lens tilt and decentration	112
5.2 Results of small pilot investigation to verify accuracy of the computer programme and associated methods	122
5.3 Repeatability of image analysis techniques	125
5.4 Intersession repeatability data	126
5.5 Mean values for lens tilt and decentration, relative to the cornea, in the relaxed and accommodated states	126
6.1 Summary of notable <i>in vivo</i> MRI studies of human phakic accommodation	134-135
6.2 Repeatability of <i>mri3dX</i> image analysis techniques	146
6.3 Intersession repeatability of complete MRI technique	146
6.4 Mean values of the six lens parameters measured in the current investigation, and the change in these parameters with accommodation	152-153
7.1 Intersession repeatability of temporal retinal contour measures with the <i>IOLMaster</i> , in the relaxed and accommodated states	170
7.2 Mean eye length measures, and change with accommodation, measured with the <i>IOLMaster</i>	171

LIST OF FIGURES

Figure	Page
1.1 Schematic diagram of the human accommodative apparatus	18
1.2 AS-OCT image of the crystalline lens of a 30 year old subject	22
1.3 Schematic view of the accommodative structures in the relaxed (unaccommodated) state	25
1.4 Traditional division of human ciliary muscle into three regions, based on the orientation of muscle fibres	27
1.5 Results of cross-sectional studies on the mean monocular amplitude of accommodation as a function of age	34
2.1 Operation of the Grand Seiko Auto Ref/ Keratometer WAM-5500	44
2.2 Difference in spherical component and MSE between the WAM-5500 and subjective, compared to the mean refractive error	48
2.3 Comparison of the frequency of differences between the objective and subjective refraction techniques for spherical component and MSE	49
2.4 Difference in cylindrical components measured with the WAM-5500 and by subjective refraction	51
2.5 Difference in J_0 and J_{45} vectors between the WAM-5500 and subjective refraction, compared to the mean	51
2.6 Difference in the horizontal and vertical corneal radii between the WAM-5500 and Javal-Schiotz keratometry compared to the mean	52
2.7 Tolerance of the WAM-5500 to longitudinal movements from the position of optimum focus whilst in high-speed mode	54
2.8 The dynamic refractive and pupillary response of a pre-presbyopic subject alternating attention between a distant and near fixation target	55
2.9 The Zeiss <i>Visante</i> AS-OCT showing a cross-sectional scan of the anterior segment, including the cornea and anterior portion of the crystalline lens	62
2.10 Axial T_2 -weighted MR image of both eyes and surrounding structures from a subject aged 26 years	66
3.1 Schematic diagram of laboratory set-up for imaging nasal ciliary muscle using AS-OCT	78
3.2 Measurement of ciliary muscle length and ciliary muscle anterior length	80
3.3 Measurement of ciliary muscle width parameters	80
3.4 Ciliary muscle total length and anterior length in relaxed state and in response to an 8 D stimulus	85
3.5 Sample images of temporal ciliary muscle morphology in a long, myopic	

	eye and an emmetropic eye	85
4.1a	Measurement of temporal ciliary muscle maximum thickness	98
4.1b	Measurement of distance from inner apex to scleral spur on the temporal side	99
4.2	Nasal and temporal ciliary muscle maximum width <i>versus</i> age	102
4.3	Nasal and temporal inner apex to scleral spur values <i>versus</i> age	103
4.4	Nasal and temporal CM25 <i>versus</i> age for minimum accommodation and in response to an 8.0 D stimulus	104
4.5	Nasal and temporal anterior ciliary muscle length in emmetropes <i>versus</i> age for minimum accommodation, and in response to an 8.0 D stimulus	105
4.6	Nasal and temporal anterior ciliary muscle length in myopes <i>versus</i> age for minimum accommodation, and in response to an 8.0 D stimulus	105
4.7	Nasal and temporal ciliary muscle total length in emmetropes <i>versus</i> age for minimum accommodation, and in response to an 8.0 D stimulus	105
4.8	Nasal and temporal ciliary muscle total length in myopes <i>versus</i> age for minimum accommodation, and in response to an 8.0 D stimulus	106
5.1	Anterior and posterior AS-OCT images for analysis of lens tilt and decentration	116
5.2	Execution of the initial stage of the computer programme	117
5.3	A movable line of calculated slope is used to locate the anterior and posterior corneal apices	118
5.4	The corneal axis is automatically drawn following location of the anterior and posterior corneal apices	119
5.5	Location of the intersections of the 9 vertical lines with the anterior and posterior lens surfaces	119
5.6	Lens tilt is the calculated difference in angles between the lenticular axis and the corneal axis	120
5.7	Dialogue box open during execution of the programme, displaying results for lens tilt and decentration relative to the cornea	121
5.8	Simplified schematic image constructed to confirm validity of the bespoke computer programme to measure lens tilt and decentration, relative to the cornea	122
5.9	Lens tilt in the unaccommodated state, and in response to an 8.0 D stimulus	127
5.10	Lens decentration in the unaccommodated state, and in response to an 8.0 D stimulus	128
6.1	Subject set-up for MRI	141
6.2	Image analysis using <i>mri3dX</i>	144

6.3	Visualisation of 3-D lens model using <i>Geomview</i> freeware software	144
6.4	Raw T ₂ -weighted axial images of a 20 year old subject scanned at the 0.17 and 8.0 D stimulus levels, and the corresponding 3-D lens models generated by <i>mri3dX</i>	147
6.5	Change in lens equatorial diameter and lens thickness with accommodation	148
6.6	Change in anterior and posterior lens surface radii of curvature during accommodation	149
6.7	Change in lens surface area with accommodation	150
6.8	Change in lens volume with accommodation	151
7.1	Adaptation of the Zeiss <i>IOLMaster</i> for determination of horizontal peripheral ocular dimensions	166
7.2	Sample 3-D models of the vitreous body and complete eye of a 20 year old emmetrope, viewed using <i>Geomview</i> software	169
7.3	Mean eye length as a function of field angle for emmetropic and myopic subjects at 0, 4 and 8 D stimulus vergences	172
7.4	Polynomial plots of nasal and temporal ocular contours from 25- 75 % of axial length at 0.17, 4.0 and 8.0 D stimulus levels	173

CHAPTER 1

OCULAR ACCOMMODATION

1.1. General introduction

Accommodation is defined as the dynamic change in refractive power of the eye to focus on objects at different distances (Millodot, 2008). The existence of an active focusing system was first demonstrated in the early seventeenth century by Scheiner, using his classic pinhole experiment (cited by Duke-Elder, 1970; Daxecker, 1992; Charman, 2008). Nearly four hundred years later, there is a general, but not universal, consensus on the mechanism of accommodation (Glasser *et al.*, 2006; Charman, 2008; Schachar and Koivula, 2008). Extensive research has so far failed to clarify numerous subtleties relating to the nature of accommodation and the inevitable loss of accommodative ability and near visual function with age, termed presbyopia (Strenk *et al.*, 1999; Dick, 2005; Glasser, 2008). Difficulties associated with imaging the accommodative structures *in vivo* have led many previous researchers to make assertions regarding the mechanism of human accommodation based on animal and/ or *in vitro* findings. However, recent advances in high-resolution ophthalmic imaging technology now enable the human accommodative apparatus to be more readily visualised *in vivo* (Baikoff *et al.*, 2004a; Koretz *et al.*, 2004; Konstantopoulos *et al.*, 2007; Wolffsohn and Davies, 2007a). Application of newer *in vivo* techniques can provide important information regarding the structure and function of the accommodative structures, whilst avoiding disruption of the complete system, as in *ex vivo* studies. The overall objectives of this thesis are to provide new data regarding the morphology of the key components of the human accommodative system, and investigate the biometric changes occurring in these structures during phakic accommodation. All of the empirical methodologies will involve application of *in vivo* techniques to examine natural, non-pharmacologically manipulated ocular accommodation.

Practically, such investigations could have widespread implications in ocular research. A more complete understanding of the morphology, action and age-related changes affecting the main accommodative structures would be valuable in the extensive and ongoing research directed at restoration of accommodation to the presbyopic eye (Charman, 2008; Glasser, 2008). All of the strategies currently available to provide dynamic focusing power to ageing eyes depend on a functional ciliary muscle, yet it is unclear exactly how the configuration and contractile responses of this structure change over time (Strenk *et al.*, 1999; Park *et al.*, 2008; Strenk *et al.*, 2010). Additionally, information on any refractive-error dependent variations in the morphological characteristics or responses of the

accommodative structures could be relevant to myopia research. An established link exists between myopia and near work/ accommodation (Adams and McBrien, 1992; Drexler *et al.*, 1998; Mutti *et al.*, 2002; Mutti, 2010), although it is unclear whether near work represents a genuine causative factor or is merely an association (Gilmartin, 2004).

Rather than providing an exhaustive review of previous literature related to the accommodation, this chapter considers key aspects most relevant to the thesis. The anatomy and function of the accommodative apparatus, and the age-related changes occurring in these structures, are detailed. An account of the theories of accommodation and presbyopia, including matters of continuing controversy, is also presented.

1.2. Historical theories of accommodation

Scheiner's simple pinhole experiment of 1619 (cited by Duke-Elder, 1970; Daxecker, 1992) confirmed the variable focusing capability of the youthful human eye. A needle viewed through two pinholes separated by a distance less than the pupil diameter appears single when the eye is focused on it, but doubles if observation is directed to an object at a different distance. Three needles are seen with three pinholes, *et cetera*. Descartes later correctly hypothesised in his 1637 *Traité de l'Homme* that the mechanism of accommodation involved changes in the shape and dioptric power of the crystalline lens, with an increase in curvature necessary to view near objects (cited by Atchison, 1995; Charman, 2008). Popular alternative theories at the time suggested that changes in corneal curvature or axial length result in the increased power of the eye when viewing near objects. However, in 1801 it was demonstrated that accommodative ability persists when the corneal power is neutralised, or the eye clamped to prevent axial length changes, thus the crystalline lens must be responsible for accommodation (Young, 1801). Evidence to support this conclusion was derived from the Purkinje imaging experiments of Langenbeck (1849) and Cramer (1853) that confirmed an increase in anterior lens surface curvature during accommodation (cited by Roman, 1995; Strenk *et al.*, 2005). At around the same time, in 1847, the presence of muscle tissue within the ciliary body was discovered independently by Bruecke and Bowman (cited by Duke-Elder, 1961) and subsequent theories included the ciliary muscle as a key element of the accommodative system. Cramer hypothesised that ciliary muscle contraction acted on the choroid to compress the vitreous and push it anteriorly against the posterior lens surface (cited by Fincham, 1937). Resistance to this pressure is provided by the iris, so the central part of the anterior lens surface, corresponding to the pupillary aperture, moves forwards and steepens, increasing the optical power of the eye. However, the demonstration of accommodative ability in an aniridic subject by von Graefe in 1861 soon discredited this theory (cited by Atchison, 1995).

Investigation of the Purkinje images provided the basis for von Helmholtz' (1855) now classical theory of accommodation. Using two luminous squares as an object and observing the Purkinje images when the eye is unaccommodated and then accommodated, he observed that the bright corneal Purkinje images remain almost stationary and unchanged, but those arising from the lens change position and become smaller with accommodation (cited by Duke-Elder, 1970). Crucially, Helmholtz included the zonules in his mechanism of accommodation. As the ciliary muscle contracts, the zonular fibres relax and the lens assumes a more convex shape, with a concurrent reduction in its equatorial diameter. However, this theory was not universally accepted and dissenters included Tscherning, who insisted in both of his theories that zonular fibres are under tension during accommodation (Tscherning, 1909). The observed downward movement of the lens due to gravity at high accommodative levels and the slackened appearance of an intact, but empty, capsule in an accommodating subject (Fincham, 1937) provided evidence to oppose Tscherning.

The mechanism described by Helmholtz, and elaborated by Gullstrand to include the choroid as the restoring force to ciliary muscle contraction (cited by Strenk *et al.*, 2005 and Charman, 2008), forms the basis of modern understanding of accommodation with overwhelming scientific evidence in support of the theory (Duke-Elder, 1970; Charman, 2008; Glasser, 2008). However, some nonconformist ideas continue to exist, notably the concept of a Tscherning-type system, whereby the zonules (specifically equatorial zonules) are under increased tension during accommodation, causing the lens equator to move outwards towards the sclera, with central steepening of the crystalline lens and peripheral flattening (Schachar, 2006; Schachar and Koivula, 2008). According to this controversial theory, the anterior and posterior zonules (inserting into the lens capsule) provide suspension for the lens only, whereas the equatorial zonules are responsible for instigating lens shape changes in response to ciliary muscle activity.

1.3. Present understanding of the mechanism of accommodation

Accommodation is achieved by the alteration in shape of the crystalline lens secondary to ciliary muscle contraction; a process governed principally by parasympathetic innervation of the ciliary smooth muscle. When the eye is unaccommodated and focus coincides with the eye's far point, the lens is held in a relatively flat and lower-powered state due to tension on the zonules. As the ciliary muscle contracts to accommodate, the majority of its mass shifts anteriorly and crucially, inwards, towards the optic axis, to reduce the diameter of the ciliary muscle collar (Gilmartin, 1995; Strenk *et al.*, 1999; Croft *et al.*, 2001). The decrease in ring diameter reduces the tension of the zonular fibres, allowing the elastic capsule enclosing the

lens to mould the young, flexible lens into a more convex and dioptrically-powerful form (Charman, 2008; Glasser, 2008).

During accommodation, the anterior lens surface undergoes the most significant increase in curvature and axial movement, resulting in the anterior chamber becoming shallower. Only slight steepening and posterior movement affects the posterior lens surface (Duke-Elder, 1970; Atchison, 1995; Drexler *et al.*, 1997; Croft *et al.*, 2001). The combined effect of these changes is an increase in lenticular axial thickness, and a small anterior shift of the centre of mass of the lens (Patnaik, 1967; Drexler *et al.*, 1997; Strenk *et al.*, 2004). The variability in response between the two lens surfaces may be attributable to more significant tensional changes affecting the anterior zonules and the greater thickness of the anterior capsule applying more elastic force to the crystalline lens substance (Ziebarth *et al.*, 2005). Additionally, vitreous body inertia may resist posterior movement of the posterior lens surface (Charman, 2008).

In conjunction with the axial thickening of the lens during accommodation, the general consensus is that lenticular equatorial diameter reduces (Brown, 1973a; Wilson, 1997; Strenk *et al.*, 1999; Jones *et al.*, 2007; Ostrin and Glasser, 2007a; Charman, 2008). Obtaining *in vivo* evidence from human subjects to support this assertion has historically been hampered by the presence of the iris, preventing direct viewing (by optical methods) of the lens periphery and its relationship with the ciliary muscle. Thus, previous investigators have relied on data obtained from atypical subjects, such as young albinos and aniridics (e.g. Fincham, 1937; Wilson, 1997). High-resolution magnetic resonance imaging (MRI) techniques enabling visualisation of the entire lens have been developed relatively recently, and indicate that lenticular diameter reduces by approximately 60- 90 μm per dioptre of accommodative response (Strenk *et al.*, 1999; Jones *et al.*, 2007; Kasthurirangan *et al.*, 2008; Hermans *et al.*, 2009).

The possible roles of the iris and vitreous body in the mechanism of human accommodation have also been disputed. It has been proposed that the iris sphincter aids accommodation by pulling the ciliary body further inwards and forwards to enable greater lenticular rounding (Crawford *et al.*, 1990), and pressure changes in the vitreous during accommodation may facilitate forward movement of the anterior lens surface to increase the accommodative response (Koretz and Handleman, 1982; Coleman, 1986). However, any contribution from these structures is likely to be relatively minor as accommodation has been observed in both aniridic subjects (Fincham, 1937) and those lacking a vitreous body (Fisher, 1982; Fisher, 1983).

The sequence of events that commences when ciliary muscle contraction ceases may be referred to as disaccommodation (Croft *et al.*, 2001; Glasser, 2008). During this process, the elastic choroid acts as a restoring force and the ciliary muscle is pulled posteriorly and outwards, along the inner scleral surface, into its unaccommodated configuration (Strenk *et al.*, 1999; Croft *et al.*, 2001). The rapidly increased tension in the equatorial zonules acts on the lens capsule to pull the lens into a flatter state. As the crystalline lens flattens, the anterior chamber deepens as the anterior lens surface moves posteriorly away from the cornea. A small anterior movement of the posterior lens surface also occurs, thus increasing vitreous chamber depth. The flattening of lenticular surface curvatures results in a decrease of the dioptric power of the eye (Croft *et al.*, 2001; Glasser, 2008; Davies *et al.*, 2010).

1.4. Anatomy of the accommodative apparatus

An appreciation of the structure and anatomy of the accommodative apparatus is required to fully comprehend the theories and controversies relating to human accommodation, and the investigations detailed in Chapters 3- 7. The following section considers in detail the anatomy of the crystalline lens, zonules, ciliary body, choroid and the auxiliary accommodative structures. Figure 1.1 illustrates the anatomical relationships between the major anterior segment components of the accommodative system.

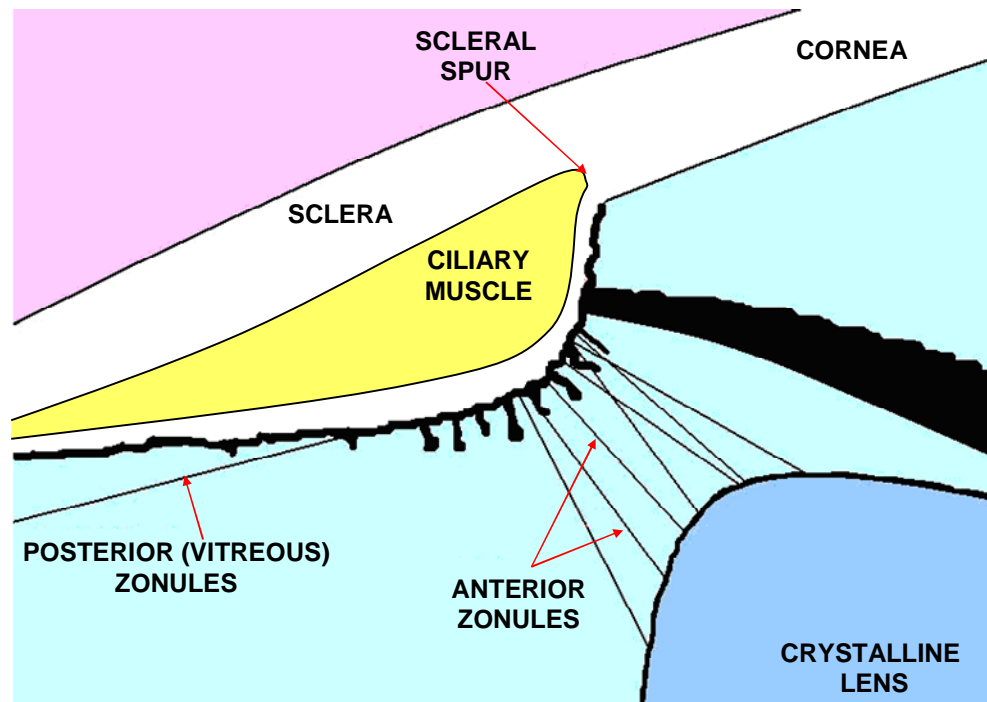


Figure 1.1. Schematic diagram of the human accommodative apparatus. As the ciliary muscle contracts during accommodation, the majority of its mass shifts anteriorly and inwards, reducing tension on the anterior zonules, allowing the elastic capsule to mould the crystalline lens into a more convex form.

1.4.1. Crystalline lens

The human crystalline lens is a complex, transparent structure, characterised by continuous growth throughout life (Koretz *et al.*, 1989; Pierscionek and Weale, 1995; Strenk *et al.*, 2004; Truscott, 2009). At 22 days' gestation, the lens begins as a thickening of surface ectoderm tissue known as the lens placode, which in turn, forms the hollow lens vesicle when it invaginates and moves below the surface ectoderm (Snell and Lemp, 1998). Primary lens fibres then develop, filling the vesicle, as the epithelial cells comprising its posterior wall undergo rapid elongation (Stafford, 2001). The fibres are packed with crystallins proteins, vital for the refractive properties of the lens, and upon losing their organelles do not divide or grow further. U-shaped secondary lens fibres, formed throughout life and which are not destroyed, develop from mitosis of anterior epithelial cells at the lens equator (Kaufman and Alm, 2003). Lens fibres are closely packed, and typically hexagonal in cross-section (Atchison, 1995; Snell and Lemp, 1998). As new fibres develop and cover their predecessors, the lens loses its sphericity and becomes more ellipsoidal in shape. The foetal secondary lens fibres meet at Y-sutures- simple junctions on either side of the lens. Postnatal fibres meet on the lens surfaces in increasingly complex patterns, creating 6 (simple star), 9 (star) and 12 (complex star) branch formations (Kuszak, 1995).

Lifelong growth of the lens results in an obvious change in lenticular dimensions with age. The effect of age on measured *in vivo* lens parameters is detailed in Table 1.1. The data highlight the notable increases in lens thickness and anterior surface curvature that occur with age. Such changes would be expected to cause an age-dependent increase in the optical power of the lens, and therefore a myopic shift in refractive error (Hemenger *et al.*, 1995). However, the lens actually becomes less powerful with increased age- a contradiction known as Brown's lens paradox (Brown, 1973a; Brown, 1973b; Dubbleman *et al.*, 2003). Changes to the refractive index distribution within the lens are believed to counteract the propensity for myopia caused by lens growth (Gilmartin, 1995; Koretz *et al.*, 2004). A gradient protein concentration and hence, gradient refractive index (GRIN) exists within the crystalline lens. *In vivo* high-resolution MRI studies (Jones *et al.*, 2007; Kasthurirangan *et al.*, 2008) have identified a central region of high refractive index (1.409 ± 0.008), accompanied by a sharp reduction in refractive index towards the lens periphery (peripheral index of 1.380 ± 0.004). The central and peripheral refractive index values do not vary significantly with age, in agreement with *in vitro* findings (Jones *et al.*, 2005), although older subjects exhibit a larger central plateau area of high index (mean change +0.83 mm along the axis and +0.56 mm along the equator between the age groups) with a steeper peripheral decline in refractive index compared to a younger cohort (Kasthurirangan *et al.*, 2008).

Parameter	Author and technique	Mean value	Change with age
Equatorial diameter (mm)	Atchison <i>et al.</i> (2008), 2-D MRI	Young cohort (19- 28 years): 9.19 ± 0.34. Older cohort (61-69 years): 9.51 ± 0.26	Small increase (+0.0075/ year)
	Kasthurirangan <i>et al.</i> (2008), 2-D MRI	Young cohort (19- 29 years): 9.12 ± 0.33. Older cohort (60-70 years): 9.39 ± 0.34	Small increase (+0.0067/ year)
	Jones <i>et al.</i> (2007), 2-D MRI	9.33 ± 0.33 (from 18-59 years)	No significant change
	Strenk <i>et al.</i> (1999), 2-D MRI	9.18 ± 0.29 (from 22-83 years)	No significant change
Central thickness (mm)	Atchison <i>et al.</i> (2008), ultrasonography	4.19 ± 0.47 (from 19- 69 years)	Increases (+0.024/ year)
	Kasthurirangan <i>et al.</i> (2008), 2-D MRI	Young cohort (19-29 years): 3.78 ± 0.22. Older cohort (60-70 years) 4.75 ± 0.38.	Increases (+0.023/ year)
	Richdale <i>et al.</i> (2008), AS-OCT	4.05 ± 0.20 (from 36- 50 years)	Increases (+0.021/ year)
	Dubbelman <i>et al.</i> (2001), Scheimpflug imaging	LT = 2.9 + 0.025 * age (cohort aged 16-65 years), e.g. 3.9 at age 40	Increases (+0.024/ year)
	Strenk <i>et al.</i> (1999), 2-D MRI	3.86 ± 0.46 (from 22-83 years)	Increases ($r^2 = 0.53$, $P < 0.0001$)
Anterior radius of curvature (mm)	Atchison <i>et al.</i> (2008), Scheimpflug imaging	10.32 ± 1.41 (from 19- 69 years)	Decreases (-0.044/ year)
	Dubbelman <i>et al.</i> (2001), Scheimpflug imaging	R = 12.9 – 0.057 * age (cohort aged 16-65 years), e.g. 10.62 at age 40.	Decreases (-0.057/ year)
	Koretz <i>et al.</i> (2001), Scheimpflug	R = 16.815 – 0.104 * age (cohort aged 18-	Decreases (-0.104/ year)

	imaging	70 years), e.g. 12.66 at age 40.	
Posterior radius of curvature (mm)	Atchison <i>et al.</i> (2008), Scheimpflug imaging	-6.77 ± 0.78 (from 19- 69 years)	No significant change
	Dubbelman <i>et al.</i> (2001), Scheimpflug imaging	R = -6.2 - 0.012 * age (cohort aged 16- 65 years), e.g.- 5.72 at age 40	Small decrease (-0.012/ year)
	Koretz <i>et al.</i> (2001), Scheimpflug imaging	R = -8.719 + 0.015 * age (cohort aged 18- 70 years), e.g. -8.12 at age 40.	Small decrease (-0.015/ year)

Table 1.1. Effect of age on *in vivo* measured lens dimensions. AS-OCT is anterior segment optical coherence tomography.

Viewing the crystalline lens in cross section (e.g. utilising a slitlamp or Scheimpflug camera) enables the various anatomical zones to be observed (Dubbleman *et al.*, 2003). Figure 1.2 shows a cross-sectional anterior segment optical coherence tomography (AS-OCT) scan centred on the crystalline lens, of a 30 year old subject.

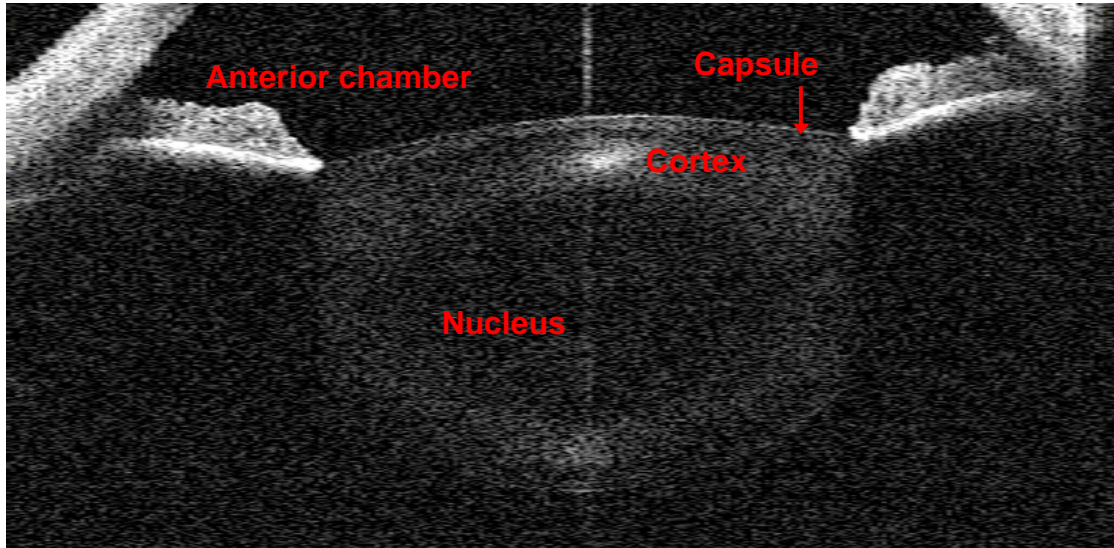


Figure 1.2. AS-OCT image of the crystalline lens of a 30 year old subject. The nucleus and cortex can be easily differentiated.

The nucleus is comprised of the oldest lens fibres, present at birth (Dubbleman *et al.*, 2003) and is the zone of highest refractive index within the lens due to the peak protein concentration of approximately 36% (Fisher and Pettet, 1973). The axial lens thickness increase that occurs with accommodation is due solely to the change in shape of the lens nucleus; the axial cortical thickness remains constant during accommodation (Hermans *et al.*, 2007). The cortex represents the fibre mass added postnatally and may be further subdivided according to the Oxford system into four zones of optical discontinuity (Patel and Bron, 2002). C1 and C4 are the outermost and innermost cortical areas, respectively. Zones C1 and C3 do not significantly thicken with age, despite lens fibres continuously being added to the surface of C1 α (Dubbleman *et al.*, 2003). New fibres pass through the C1 β zone and then remain in C2.

The cellular monolayer present over the anterior and equatorial lens cortex is the lens epithelium, derived from the original cells of the embryonic lens vesicle (Stafford, 2001). The epithelium has a number of functions; production of lens fibres takes place in its periphery, with the more central region important for the secretion of the capsular material and also the transport of ions and water between the aqueous and lens material (Snell and Lemp, 1998). Mitosis continuously occurs in the pre-equatorial region of the epithelium and new cells

move outwards to the lens equator (Atchison, 1995; Augusteyn, 2010). Here, they differentiate and are transformed into lens fibres. The new fibres elongate in the anterior direction underneath the lens epithelium, and in the posterior direction underneath the lens capsule (Snell and Lemp, 1998; Charman, 2008; Augusteyn, 2010), terminating in sutures on the anterior and posterior lens surfaces. During the process of elongation, cytoplasmic organelles and eventually nuclei, are lost, with only a few mitochondria remaining (Atchison, 1995; Lim *et al.*, 2009; Augusteyn, 2010).

The process by which new fibres are laid down, traversing the equatorial regions of the lens, suggests that lens diameter (in addition to thickness) should increase throughout life. *In vitro* data support this assertion, and indicate that lens diameter increases by over 1.0 mm between ages 20 and 95 years (Schachar, 2005; Rosen *et al.*, 2006; Augusteyn, 2010), although these data reflect the accommodated lens, free from zonular tension. Aside from the results of Atchison (2008; Table 1.1), *in vivo* MRI data contradict the *in vitro* observations. Strenk *et al.* (1999) and Jones *et al.* (2007) found no dependence of lens diameter on age, in subjects ranging from 18 to 83 years. Lens diameter, and its change with age, therefore remains a contentious issue.

Despite its cellular structure and high protein concentrations, the young human lens remarkably transmits nearly 100% of incident light. Optical homogeneity is key to effective light transmission (Patel and Bron, 2002; Truscott, 2009). Light scatter and absorption are minimised by the paucity of organelles within lens fibres, and the newer fibres containing nuclei are located in the equatorial region, screened by the iris. Lens transparency is also aided by the organisation of fibres into layers, with little extracellular space and precise arrangement of intracellular proteins meaning that there are no significant fluctuations in refractive index (Strenk *et al.*, 2005; Truscott, 2009).

The human lens is characterised by high water content throughout life, providing a solvent for crystallins proteins. Numerous *in vitro* investigations have examined the effect of age on lens water content, with no clear agreement between studies. Age-related increases in dry weight/ protein concentration imply that water must be lost from the central region of the lens until approximately 60 years of age (Nordmann *et al.*, 1974; Bours and Fodisch, 1986; Augusteyn, 2010), although direct measures of water content do not agree with this assertion. Van Heyningen (1972), Fisher and Pettet (1973) and Heys *et al.* (2005) have all measured constant nuclear water content with age, ranging from approximately 63 % (Fisher and Pettet, 1973) to 68 % (Heys *et al.*, 2005), whilst Siebinga *et al.* (1991) measured an age-dependent increase in the water content of the human lens nucleus. The high water

content has led to the theory that the lens is incompressible, thus its volume would not be expected to change during accommodation. Limited MRI data supports this prediction (Hermans *et al.*, 2009), although precise geometric modelling of the human lens suggests its volume should increase by approximately 2.6 % during accommodation (Gerometta *et al.*, 2007).

Encasing the whole crystalline lens is the capsule, an elastic basement membrane that fulfils the important function of moulding the deformable crystalline lens during accommodation (Snell and Lemp, 1998; Strenk *et al.*, 2005). The capsule appears structureless on slitlamp examination, but electron microscopy reveals a laminar structure, comprising layers of collagen filaments (Stafford, 2001). It is the lamellar arrangement of these filaments that results in the highly elastic nature of the capsule. The more dense, outer capsular layer contains zonular microfibrils in addition to collagen (Atchison, 1995). As the capsule grows throughout life to track the increased size of the crystalline lens, the anterior portion, produced by the anterior epithelium, continually thickens, reaching approximately 25 μm in adults (Remington, 2005). The thickness of the posterior capsule remains fairly constant with time, at approximately 5 μm (Krag and Andreassen, 2003). Into the equatorial region of the capsule, zonular fibres insert which connect the lens to the ciliary processes (Snell and Lemp, 1998), thus suspending the lens and enabling changes to the contractile state of the ciliary muscle to be translated to the lens mass.

1.4.2 Zonules

The delicate, zonular fibres comprise complex meshworks of fibrils (Kaufman and Alm, 2003). They are responsible for supporting the lens and facilitating accommodation and have been broadly differentiated into two categories: the main fibres (anterior and posterior/vitreous) and the tension or spanning fibres (Rohen, 1979), shown on Figure 1.3. The anterior zonules support the lens, extending from the ciliary processes of the anterior ciliary body, bridging the circumlenticular space and inserting into the equatorial region of the lens capsule, with many fibres crossing over each other (Glasser and Campbell, 1999; Charman, 2008). Rohen (1979) believed these anterior fibres attach to the lens capsule in three main sets, two of which insert 1.5 mm anterior and posterior to the lens equator and a third set of finer fibres linked to the equator itself. However, the appearance of three such distinct sets in scanning electron microscopy studies is now widely believed to be artefactual and due to *post mortem* tissue handling issues (Glasser and Campbell, 1999; Croft *et al.*, 2001). Longer, posterior zonular fibres (also known as vitreous zonules; Lutjen-Drecoll *et al.*, 2010) extend from the region of the ora serrata towards the valleys of the ciliary processes (Glasser, 2008; Wasilewski *et al.*, 2008; Lutjen-Drecoll *et al.*, 2010). Additionally, the anterior

and posterior systems are linked by shorter, intermediate, tension fibres that insert into the ciliary epithelium (Rohen, 1979). The exact function of these tensile fibres is not clear, but they are believed to behave as a fulcrum, providing precise leverage to enable rapid and accurate adjustments to the level of accommodation (Rohen, 1979; Gilmartin, 1995; Charman, 2008). Figure 1.3 shows the relationship of the zonules with the other accommodative structures.

Lifelong lens growth results in gradual changes to the geometry of zonular insertions into the lens capsule (Farnsworth and Burke, 1977; Farnsworth and Shyne, 1979; Sakabe *et al.*, 1998). Farnsworth and Shyne (1979) identified forward migration of the zonular attachments, away from the lens equator, as the lens diameter increases throughout life. More recently, Sakabe *et al.* (1998) have provided further evidence of this forward shift from examination of 223 cadaver eyes, observing that the zonular-free region of the anterior lens surface decreases in diameter with age. Mathematical and biophysical analysis of the relationship between lens and zonule indicates that with continued lens growth, the zonular insertions become more tangential to the lens surface, and therefore potentially less able to convey tension on the capsule (Koretz and Handelman, 1986; Koretz and Handelman, 1988). Whilst the geometry of zonular attachments varies throughout life, the extensible properties of the zonules remain constant between the ages of 15 -45 years (Fisher, 1986).

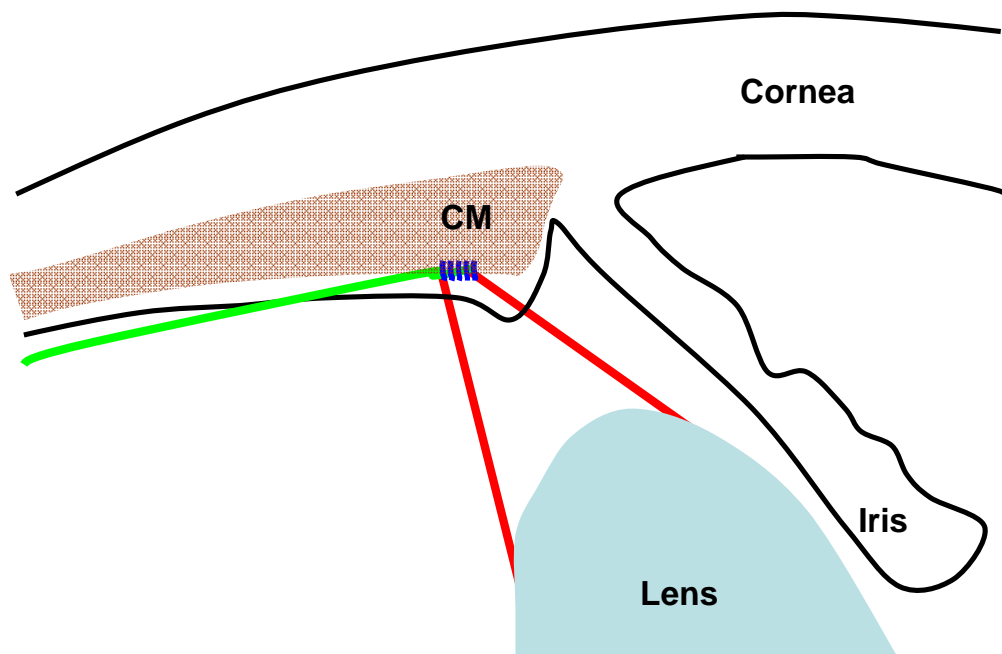


Figure 1.3. Schematic view of the accommodative structures in the relaxed (unaccommodated) state. The anterior zonules (red lines) are stretched by traction from the posterior/ vitreous zonules (green line). The tension in the anterior zonules keeps the lens in a flattened state for distance viewing. During accommodation, the forwards and inwards shift of ciliary muscle mass enables the shorter, tension fibre system (blue lines) to take up

the traction from the posterior zonules and release tension in the anterior zonules. The capsule is then able to mould the lens into its more spherical, accommodated form.

1.4.3. Ciliary body

The ciliary body is a complete ring of tissue that represents the anterior continuation of both the retina and choroid. It is roughly triangular in cross-section, the bulk of its mass comprising the ciliary muscle (Remington, 2005). The *in vitro* antero-posterior length of the ciliary body is greatest temporally, at approximately 5.76 mm in adults, compared to around 4.79 mm nasally (Aiello *et al.*, 1992). Functions of the ciliary body include secretion and support of zonular fibres, production of aqueous humour and nourishment of the lens, in addition to providing musculature for accommodation (Aiello *et al.*, 1992; Atchison, 1995; Tamm and Lütjen-Drecoll, 1996; Snell and Lemp, 1998).

The relatively flat, smooth, posterior portion of the ciliary body is the pars plana (orbicularis ciliaris), which is covered by longitudinally-oriented zonular fibres and contacts the vitreous (Tamm and Lütjen-Drecoll, 1996). In the most posterior region of the pars plana, posterior zonular fibres aggregate forming a broad plate connected to the ciliary body internal limiting membrane (ILM), which is continuous with the ILM of the retina (Atchison, 1995). The pars plicata (corona ciliaris) is the wider, anterior portion of the ciliary body, continuous with the posterior surface of the iris. The pars plicata is characterised by approximately 70 to 80 vascular ridges, the ciliary processes, which protrude freely into the posterior chamber (Tamm and Lütjen-Drecoll, 1996). Between ciliary processes, the zonular fibres pass in order to join the pars plicata surface. Aqueous humour is produced by the non-pigmented epithelium of the pars plicata and secreted into the posterior chamber of the eye from the ciliary processes (Kaufman and Alm, 2003). The crystalline lens equator is located approximately 1 to 1.5 mm centrally from the ciliary processes (Atchison, 1995; Tamm and Lütjen-Drecoll, 1996).

The ciliary body comprises six layers: the supraciliary lamina; ciliary muscle; stroma; basal lamina, epithelium and ILM, from the outer (scleral) to the inner (vitreous) aspect (Aiello *et al.*, 1992; Tamm and Lütjen-Drecoll, 1996). The supraciliary (or suprachoroidal) lamina is a fine layer of loose connective tissue, facilitating movement of the ciliary muscle against the sclera (Atchison, 1995; Tamm and Lütjen-Drecoll, 1996). Much of the bulk of the ciliary body is composed of the ciliary muscle, beneath the ciliary processes (Pardue and Sivak, 2000; Glasser *et al.*, 2001). Human ciliary muscle is classified as a rapidly-reacting multi-unit smooth muscle (Pardue and Sivak, 2000). Traditionally, the muscle has been sub-divided into three distinct regions, related to the orientation of smooth muscle bundles (Figure 1.4):

the longitudinal portion, running along the inner scleral surface and attached anteriorly to the scleral spur and trabecular meshwork; radial fibres forming a fan-like configuration from the irido-corneal angle towards the ciliary processes and circular fibres, running around the globe, parallel with the limbus (Tamm and Lütjen-Drecoll, 1996; Pardue and Sivak, 2000). However, detailed *in vitro* analysis of the muscle has revealed that these regions are not truly distinct, and during accommodation a reorganisation of the muscle fibres occurs, with the relative proportion of the longitudinal fibres decreasing whilst the proportion of the circular fibres increases (Lutjen, 1966). The reorganisation of fibres during accommodation, whereby a proportion of the longitudinal fibres are assumed to become radially or circularly oriented (Pardue and Sivak, 2000), explains the accommodative movement of the ciliary muscle, which is believed to shorten longitudinally, and thicken anteriorly, as the sphincter-like action of the circular fibres pulls the ciliary body closer to the lens (Duke-Elder, 1961; Strenk *et al.*, 1999).

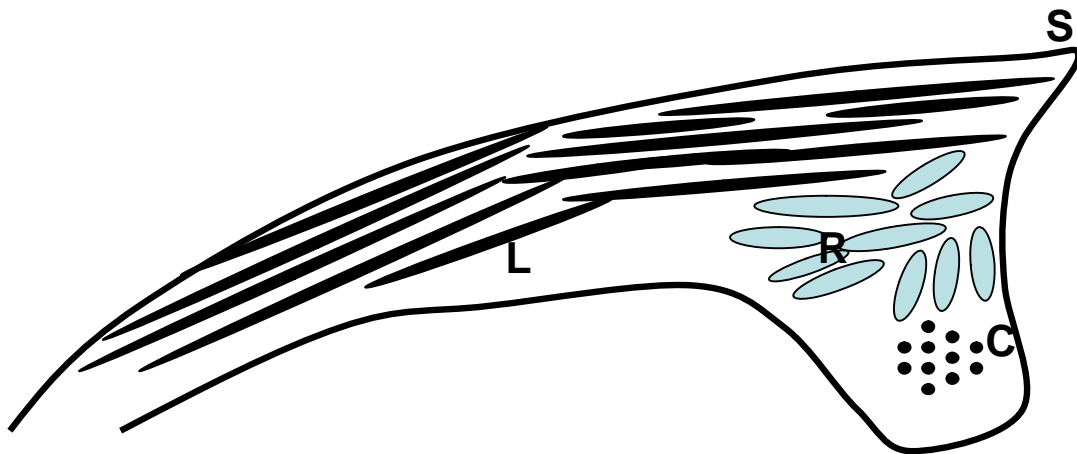


Figure 1.4. Traditional division of human ciliary muscle into three regions, based on the orientation of muscle fibres. The longitudinal fibres (L) run along the inner aspect of the sclera, terminating at the scleral spur (S). Circular fibres (C) run circularly around the globe, whilst the radial fibres (R) connect the other two groups and form a fan-like configuration.

The stroma of the ciliary body is highly vascular and also contains loose connective tissue and melanocytes (Mafee *et al.*, 2005). The stromal core of the ciliary processes features many leaky capillaries to provide the water and metabolites required for aqueous production. The three innermost layers of the ciliary body are relatively thin: the basal lamina is the continuation of Bruch's membrane of the choroid (Tamm and Lütjen-Drecoll, 1996); the epithelial layer consists of two single sheets of epithelium, the outer of which is heavily pigmented and continuous with the retinal pigment epithelium and anterior iris epithelium, whilst the inner non-pigmented layer is continuous with the neural retina and posterior iris epithelium. The ciliary body ILM is secreted by the non-pigmented epithelium and is continuous with the retinal ILM.

Age-related histological and morphological changes in human ciliary muscle have been described in detail by several previous authors using *in vitro* methods (e.g. Lutjen, 1966; Nishida and Mizutani, 1992; Tamm *et al.*, 1992a; Tamm and Lütjen-Drecoll, 1996; Pardue and Sivak, 2000). In neonate eyes, the ciliary muscle consists of evenly distributed individual fibres. Over time however, the fibres form bundles, separated by increasing amounts of connective tissue (Pardue and Sivak, 2000). Longitudinal fibres are always the most prevalent (Tamm *et al.*, 1992a), accounting for 41-69 % of muscle area, whilst the radial and circular fibres account for 25-47 % and 4-24 %, respectively (Pardue and Sivak, 2000). The relative proportions of the various fibre orientations changes with age (Nishida and Mizutani, 1992; Tamm *et al.*, 1992a; Pardue and Sivak, 2000), explaining the broad proportional ranges of area occupied by each fibre type. The percentage of circular fibres remains relatively stable throughout life, whilst the proportion of longitudinal fibres significantly decreases, and the quantity of radial fibres increases (Pardue and Sivak, 2000). Morphologically, the overall length and anterior length (distance from the point of maximum muscle thickness to the anterior tip) of the ciliary muscle decrease with age (Tamm *et al.*, 1992a; Pardue and Sivak, 2000), whilst there is a trend for maximum width to increase (Pardue and Sivak, 2000). In addition to the age-dependent shortening, there is a reduction in the distance from the scleral spur to the inner apex of the muscle, indicating that ageing human ciliary muscle adopts a more antero-inwards position, similar to that of the youthful, accommodating muscle (Tamm *et al.*, 1992a).

1.4.4. The choroid

The human choroid is primarily a vascular layer, fulfilling the key function of supplying oxygen and nutrients to the outer retina (Nickla and Wallman, 2010). It extends anteriorly, from the optic nerve, and is continuous with the pars plana of the ciliary body (Tamm and Lütjen-Drecoll, 1996). Throughout life, the choroid thins, from approximately 200 μm at birth, to 80 μm by 90 years of age (Ramrattan *et al.*, 1994). In addition to its extensive vascular component, the choroid also contains non-vascular smooth muscle cells (or myofibroblasts), first documented in the human eye by Mueller in 1859 (cited by Nickla and Wallman, 2010).

The role of the choroid in accommodation was detailed initially by Gullstrand in 1924, although there are relatively few recent reports describing the choroidal contribution to the mechanism of accommodation. The choroid and zonules together form an elastic system. In the relaxed (unaccommodated) state, the choroidal pulling force and the ciliary muscle force are in equilibrium with the pull of the lens capsule (Croft *et al.*, 2001). During accommodation, traction is taken up from the posterior zonules and choroid, facilitating

slackening of the anterior zonules and causing the choroid to slide anteriorly (Gilmartin, 1995). Mallen *et al.* (2006) postulated that a compensatory backwards displacement of the posterior region of the globe occurs to maintain a constant ocular volume, by transient increase in axial length. Mean axial length increases during accommodation of 58 μm in myopic subjects, and 37 μm in emmetropes have been reported (Mallen *et al.*, 2006), although Drexler *et al.* (1997) measured smaller changes, of 5.2 and 12.7 μm in myopic and emmetropic groups, respectively. During disaccommodation, the elastic choroid acts to restore the ciliary muscle to its relaxed, more posterior, configuration. Accommodation has therefore been described as a neuromuscular process in youthful eyes which modifies the natural tendency towards the unaccommodated state (Kaufman, 1992; Gilmartin, 1995)

1.4.5. Auxiliary accommodative structures

Some theories of accommodation propose a contributory effect from the vitreous and/ or iris. Coleman (1986) described the vitreous as the fourth most important accommodative structure after the lens, zonules and ciliary muscle. The vitreous accounts for approximately 80 % of ocular volume, lying between the posterior lens surface and retina. The outer vitreous membrane has elastic properties, resulting in a fairly spherical vitreous body configuration (Ljubimova and Eriksson, 2005), with an anterior pit (fossa patellaris) occupied by the crystalline lens. According to the theory of Coleman (1970, 1986), the ciliary body, zonular fibres and the hyaloid membrane, located between the posterior lens surface and the vitreous body, together form a diaphragm which determines the shape of the lens, related to vitreous pressure. Changes in the pressure gradient between the aqueous and vitreous body following ciliary muscle contraction, in conjunction with the hyaloid membrane diaphragm causes the lenticular surfaces to become more steeply curved and facilitates forward axial movement of the lens. However, Fisher's (1983) examination of the accommodative ability of a young subject following unilateral vitrectomy surgery provided evidence to oppose Coleman's hydraulic suspension theory. Neither accommodative amplitude, nor the magnitude of anterior lens pole movement was reduced in the vitrectomised eye, implying that the vitreous is not essential for effective accommodation. Furthermore, *in vitro* experiments have determined that normal accommodative changes in lens morphology can occur due to the forces imparted on the lens mass by the capsule alone, in the absence of the vitreous body (Glasser and Campbell, 1998; Koopmans *et al.*, 2003; Roorda and Glasser, 2004).

Weale (1992) cites the iris as an aid to human accommodation. The iris is a thin contractile diaphragm, containing a central aperture, the pupil. The iris root is continuous with the anterior region of the ciliary body. It is hypothesised that during accommodation, the iris

sphincter muscle, responsible for pupillary constriction, acts to pull the ciliary body further anteriorly and inwards (Weale, 1989), allowing for greater relaxation of zonular tension, and a higher amplitude of accommodation. Whilst accommodation has been observed in aniridic subjects (Fincham, 1937), a contributory role of the iris to the mechanism of human accommodation cannot be discounted (Charman, 2008).

1.5. Neural mechanism of accommodation

The accommodative response is primarily driven by a blurred retinal image, which is detected by the visual (striate) cortex (Campbell, 1954; Atchison, 1995; Charman, 2008). The afferent accommodative loop begins at the retina, from where the defocus signal is transmitted through the magnocellular layer of the lateral geniculate nucleus (LGN), and relayed to the visual cortex (Kaufman, 1992; Mays and Gamlin, 1995). The signal is also transmitted to parieto-temporal regions for further processing. The supranuclear signal is relayed to the Edinger-Westphal nucleus of the midbrain, and a motor command is formulated (Jumblatt, 1999). The efferent accommodative pathway comprises the oculomotor (third cranial) nerve, the ciliary ganglion and post-ganglionic short ciliary nerves, stimulating contraction of the ciliary muscle (Kaufman, 1992).

1.5.1. Ciliary muscle innervation

The autonomic nervous system (ANS) regulates structures that are not under voluntary control; for example, exocrine gland cells, cardiac muscle and smooth muscle, including the ciliary muscle (Cogan, 1937; Hopkins and Pearson, 2007). In common with most involuntary structures, ciliary smooth muscle receives dual innervation from both the parasympathetic (cholinergic) and sympathetic (adrenergic) divisions (Törnqvist, 1966; Toates, 1972; Gilmartin, 1986; Hopkins and Pearson, 2007), which usually have antagonistic effects. However, contraction of the ciliary muscle is induced predominantly by activity of the parasympathetic fibres of the third cranial nerve, originating from the Edinger-Westphal nucleus of the midbrain. The parasympathetic response, mediated by muscarinic receptors, is known to be rapid. Stimulation of the third cranial nerve in monkeys results in maximum accommodation after 1-2 seconds (Törnqvist, 1967). Human accommodation is stable after around 1 second, following a latent period of approximately 300 milliseconds (Campbell and Westheimer, 1960; Kasthurirangan and Glasser, 2006).

The possible role of the sympathetic branch of the ANS in accommodation has been disputed over many years. Functional sympathetic control is not proven merely by the presence of adrenoreceptors (Gilmartin, 1998). During the 1960s, Törnqvist conducted experiments utilising anaesthetised monkeys that provided some insight into this matter. In

the first, stimulation of the pre-ganglionic cervical sympathetic nerves caused a hyperopic shift in the monkeys that could not be negated by α -adrenoreceptor antagonists, but non-selective β -blocking drugs inhibited this negative accommodation (Törnqvist, 1966). Thus, sympathetic innervation of inhibitory β -receptors in ciliary muscle was proposed as the mechanism responsible for distance accommodation. Subsequently, accommodative changes following sympathetic nerve stimulation were discovered to develop too slowly to respond effectively to rapidly-changing stimuli in real-life situations. Maximal effect was reached 10-40 seconds after stimulation (Törnqvist, 1967). Törnqvist additionally observed that the magnitude of sympathetic inhibition was directly related to the corresponding level of parasympathetic activity. Support of this observation was provided by a later study (Hurwitz *et al.*, 1972) involving monkeys that induced positive accommodation by electrical stimulation of the midbrain, whilst stimulating and blocking ciliary muscle β -receptors by injecting propranolol (a β -receptor antagonist) and isoproterenol (a β -receptor agonist). A significant inhibitory effect of isoproterenol was only observed when accommodation levels were above 4 D. A comprehensive review of anatomical, physiological, pharmacological and clinical evidence regarding sympathetic input to accommodation concluded that the main features are that it is inhibitory in nature (mediated by inhibitory β -adrenergic receptors), small (less than 2 D), slow (20-40 seconds) and related to the background level of parasympathetic activity (Gilmartin, 1986). Additionally, more recent data has concluded that only approximately one third of the population have access to sympathetic inhibition during sustained near vision (Gilmartin *et al.*, 2002).

1.6. Components of accommodation

Gordon Heath (1956) distinguished four components of accommodation, namely reflex, convergence, proximal and tonic.

1.6.1. Reflex accommodation

In response to a blurred stimulus, the automatic adjustment of the dioptric power of the eye (over approximately a 2 D range) to maintain a clear retinal image of the object of regard is known as reflex accommodation (Charman, 2008). Heath (1956) proposed that reflex accommodation is the only component of accommodation to be influenced by retinal image quality.

1.6.2. Convergence accommodation

The near triad comprises accommodation, convergence and pupil miosis. The synkinesis of these systems is a result of their neural connection. Convergence accommodation describes the accommodation induced automatically by a change in convergence (Charman, 2008; Millodot, 2008), the magnitude of which is governed by an individual's convergence accommodation/ convergence (CA/ C) ratio.

1.6.3. Proximal accommodation

Proximal accommodation results from knowledge of an object's distance, or belief in its proximity (Heath, 1956; Rosenfield and Ciuffreda, 1991; Millodot, 2008). It may be elicited by the simple presentation of a near object, or when utilising a device such as a closed-view autorefractor (instrument myopia). Voluntary accommodation may be considered a form of proximal accommodation as a subject merely "thinking near" can stimulate an accommodative response (Provine and Enoch, 1975; Rosenfield and Ciuffreda, 1991).

1.6.4. Tonic accommodation

The slightly myopic state that occurs in the absence of an adequate visual stimulus e.g. darkness (Gilmartin *et al.*, 1984), ganzfeld (structureless/ empty field; Schor *et al.*, 1986), reduced visual acuity (Heath, 1956), low spatial frequency target (Kotulak and Schor, 1987) or pinhole viewing (Rosenfield *et al.*, 1991), is a result of the accommodative mechanism adopting an intermediate state of approximately 1 D (Heath, 1956; Millodot, 2008). The term tonic accommodation was initially used to describe this phenomenon because it was believed to result from the dual innervation of ciliary muscle, whereby an intermediate dioptric position would be assumed in the absence of an accommodative stimulus (Rosenfield *et al.*, 1993). However, the term is likely to be a misnomer as the probable explanation of the response is multifactorial, including non-optical aspects, such as auditory and vestibular input and mental imagery (Rosenfield *et al.*, 1993).

1.7. Accommodative microfluctuations

Rapid fluctuations about the mean level of accommodation when a subject fixates a stationary near object were first described in 1937 by Collins, using his pioneering infra-red optometer (cited by Charman and Heron, 1988). Accommodative microfluctuations are typically less than 0.25 D in magnitude (Collins *et al.*, 1995) and occur at a range of frequencies between 0 - 3 Hz (Heron and Schor, 1995). The temporal variations in the accommodative response are concentrated over two main frequency bands- a low frequency component (LFC) of <0.6 Hz and a high frequency component (HFC) of 1.0 – 2.3 Hz (Gray *et al.*, 1993b). Rather than representing instability in steady-state accommodation,

microfluctuations may have a functional role in maintaining the optimum mean accommodative response (Charman and Heron, 1988).

A range of investigations have studied the potential sources of the LFCs and HFCs and the factors that influence the incidence and magnitude of these components, drawing conclusions regarding the possible functional significance of accommodative microfluctuations. Several groups have observed an increase in low frequency fluctuations with smaller pupil sizes (Gray *et al.*, 1993a; Owens *et al.*, 1994; Stark and Atchison, 1997), although the HFC appears to be independent of pupil size, suggesting that LFCs may have a role in the accommodative feedback loop, providing maintenance of optimal retinal image contrast during steady viewing of a near target (Winn and Gilmartin, 1992). The LFC is also affected by target luminance (Gray *et al.*, 1993b), with very low luminance levels (0.002 – 0.004 cd m⁻²) leading to an obvious increase in power of this component. Again, the HFC is not altered by variation in this parameter, suggesting that HFCs are not under neurological control. Evidence to support this assertion has been provided from studies that have identified a significant correlation between arterial pulse rate and HFC frequency by simultaneously recording ocular accommodation and vascular pulse (Winn *et al.*, 1990; Collins *et al.*, 1995). The mechanism causing arterial pulse to impact the HFC is not yet known, but rhythmic variations in blood flow may affect the ciliary muscle ring diameter or the intraocular pressure pulse may displace the crystalline lens (Collins *et al.*, 1995). Thus, it is apparent that the source of HFCs is derived from arterial pulse effects (Winn *et al.*, 1990), although one study has identified an association between LFCs and the respiration cycle (Collins *et al.*, 1995).

Stimulus vergence is known to affect accommodative microfluctuations (Charman and Heron, 1988; Day *et al.*, 2006), with a number of authors having reported an increase in magnitude of the fluctuations as target vergence increases (Arnulf and Dupuy, 1960; Denieul, 1982; Kotulak and Schor, 1986). The study investigating the largest range of stimulus vergences (-9 to +3 D) identified an increase in the amplitude of microfluctuations up to -3 D, but then a subsequent decrease as target vergence rose further, with the fluctuations disappearing at stimulus vergences of approximately -6 D (Miege and Denieul, 1988). The reason proposed to explain this finding was based upon the lens zonules, with moderately relaxed zonules able to transmit the continuous tremor of the ciliary muscle, but the fully relaxed zonules at higher levels of accommodation are not able to do this.

To summarise, accommodative fluctuations may be categorised into LFCs and HFCs and the source of these components is different. The HFC appears to be derived from the effect

of arterial pulse and is independent of pupil size and target luminance. The LFC is a consequence of neurological control, although a link between LFCs and the respiration cycle may exist. LFCs may be important in maintenance of steady-state accommodation.

1.8. Presbyopia

The inevitable decline in accommodative amplitude begins well before adulthood is reached (Charman, 2008), although presbyopia does not usually manifest in North American and European individuals until approximately 42-48 years of age (Millodot, 2008). By age 55 years, the ability to accommodate is essentially non-existent. No standard definition of presbyopia exists, however a person may be considered presbyopic when near vision clarity is insufficient for their requirements (Gilmartin, 1995), usually corresponding to an accommodative amplitude below 3 D (Weale, 2000). Figure 1.5 summarises the results of notable published studies that have measured subjective monocular accommodative amplitude as a function of age. The results of the studies are remarkably similar and generally indicate a linear reduction in accommodative amplitude from childhood until the manifestation of presbyopia. Although a universal problem, the development of presbyopia and the relative contribution of age-related changes in the components of the accommodative system are not fully understood (Atchison, 1995; Pierscionek and Weale, 1995; Charman, 2008). A number of possible mechanisms have been described which may be broadly classified into lenticular and extralenticular theories.

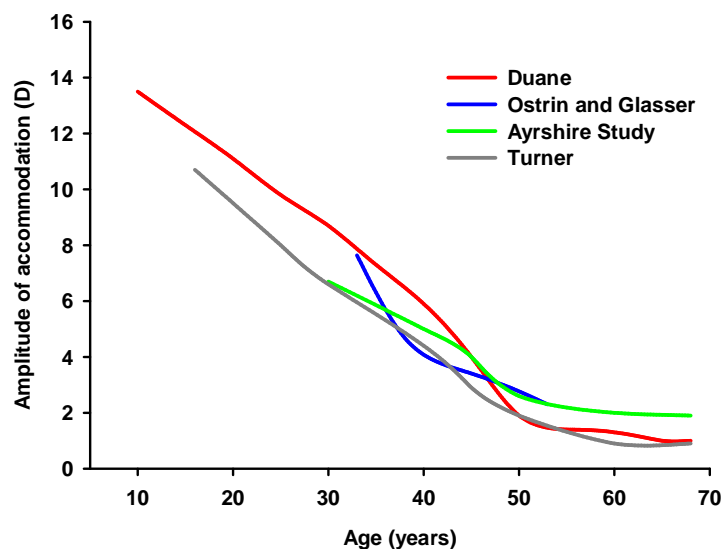


Figure 1.5. Results of cross-sectional studies on the mean monocular subjective amplitude of accommodation as a function of age. Data obtained from Duane (1922), Turner (1958), Ayrshire Study Circle (1964) and Ostrin and Glasser (2004).

1.8.1. Lenticular theories

Presbyopia is attributed to age-related changes in the crystalline lens and its capsule in the various lenticular theories. The continued growth of the lens during life and changes in the GRIN structure have been described previously (section 1.4.1) and Table 1.1 summarises the effect of growth on lens dimensions. Numerous *in vitro* experiments have investigated the mechanical properties of the lens and capsule (Fisher, 1969; Beers and Van der Heijde, 1994; Krag *et al.*, 1997; Glasser and Campbell, 1999; Weeber *et al.*, 2007), and it is clear that lens stiffening and a reduction in capsular elasticity are key factors in the development of presbyopia (Glasser, 2008), although many aspects of the accommodative system undergo age-related changes (Gilmartin, 1995; Charman, 2008). Nearly 40 years ago, Fisher discovered that Young's modulus of elasticity of the capsule decreases by around 50% between ages 20 and 40 years (Fisher, 1969). More recent experimentation has shown that the lens becomes more resistant to deformation by the capsule in older eyes (Glasser and Campbell, 1999). *In vitro* removal of the capsule has minimal effect on the lens shape after approximately age 50 years, but in younger eyes, capsular removal results in a significant reduction in lens power. As the water content of the human lens is believed to remain stable throughout life (Fisher and Pettet, 1973; Siebinga *et al.*, 1991; Heys *et al.*, 2005), altered lenticular mechanical characteristics have been attributed to adhesion and compaction of nuclear fibres (Fisher and Pettet, 1973; Pau and Kranz, 1991).

Lenticular theories of presbyopia may be further categorised into those that state presbyopia is essentially due to mechanical changes occurring in the lens and capsule with age (Hess-Gullstrand and Duane-Fincham theories) and the geometric theory, in which presbyopia is attributed to changes in lens size and shape. According to the Hess-Gullstrand theory, the ciliary muscle maintains its strength and the level of contraction required to produce a given dioptric change in accommodation remains constant throughout life. In the accommodating eye, as age advances, lens stiffness results in an increasing latent region of ciliary muscle contraction after the accommodative amplitude is reached, so further contraction would not influence the level of accommodation (Atchison, 1995; Strenk *et al.*, 1999). Evidence to support this hypothesis has been obtained from impedance cyclography studies that have measured the electrical resistance across the ciliary muscle (Swegmark, 1969) and concluded that ciliary muscle contraction remains normal until the age of 60 years. However, these data have been criticised as it is unclear exactly what the measurements represent, and it has been shown that a given level of accommodative demand does not consistently produce the same impedance (Saladin and Stark, 1975).

In contrast to the Hess-Gullstrand theory, weakening of the ciliary muscle has been implicated as the process leading to presbyopia (Duane, 1922; Duane, 1925). Instillation of highly diluted atropine drops was found to reduce the accommodative amplitude more rapidly in older subjects. Such findings would not be expected if ageing eyes had more ciliary muscle contraction in reserve at their amplitude of accommodation, compared to youthful eyes. Duane attributed his findings to an age-related weakening of the ciliary muscle. However, recent *in vivo* MRI investigations have demonstrated that the human ciliary muscle retains its contractile ability throughout life (Strenk *et al.*, 1999; Strenk *et al.*, 2006; Strenk *et al.*, 2010), as the ciliary muscle ring diameter reduces upon viewing a near stimulus, even in advanced presbyopes.

The lenticular explanation of presbyopia postulated by Fincham also involves ciliary muscle contraction (Fincham, 1937). Akin with the Hess-Gullstrand theory, Fincham proposed that the changes in the lens and capsule are important, but the contractile force necessary for each dioptre of accommodative response increases with age and the ciliary muscle is maximally contracted at the amplitude of accommodation, with no latency. Today, this proposal is commonly known as the Duane-Fincham theory and is supported by recent evidence that suggests older lenses require greater force to be exerted on the lens and capsule to induce a specific accommodative change (Glasser and Campbell, 1998; Glasser and Campbell, 1999).

Geometric theories attribute presbyopia to changes in the size and shape of the lens with age, rather than to changes in its mechanical characteristics. The increased size of the lens throughout life impacts on the geometry of zonular attachments (Farnsworth and Shyne, 1979; Gilmartin, 1995; Charman, 2008). A comprehensive study of 223 cadaver eyes demonstrated an age-related shift of the anterior zonular insertions, away from the lens equator (Sakabe *et al.*, 1998). The migration of lens zonules results in their insertions becoming more tangential to the lens surface, thus the ability of the zonules to impart tension on the capsule may be reduced in older eyes (Koretz and Handleman, 1986), although no experimental evidence exists to substantiate this hypothesis (Croft *et al.*, 2001).

The Modified Geometric Theory of presbyopia development (Strenk *et al.*, 2005) also states that lenticular growth results in the reduced ability of the lens to change shape and is consistent with *in vivo* MRI studies of accommodation that have documented an age-dependent reduction in ciliary ring diameter (Strenk *et al.*, 1999; Strenk *et al.*, 2006), maintenance of a constant lens diameter (Strenk *et al.*, 1999; Jones *et al.*, 2007), undiminished ciliary muscle contractile ability (Strenk *et al.*, 1999; Strenk *et al.*, 2010) and

antero-inward displacement of the ciliary muscle (Strenk *et al.*, 2010). According to this relatively new theory, the uveal tract acts as a complete unit in response to lens growth. The lens applies force onto the pupillary margin, which is translated to the iris root and ciliary muscle. A tangential force is also provided, as a result of scleral curvature. The combined effect of these forces is to cause an anterior and inwards shift of the ciliary muscle and iris root. The associated reduction in pupil diameter draws the pupil margin closer to the thicker, central region of the lens, accentuating the effect of lens thickness on ciliary muscle antero-inward displacement. As circumferential space diminishes due to the shift in ciliary muscle position, zonular tension is reduced in the unaccommodated state, causing both increased lens curvature and a decline in lens accommodative response.

Of the recent theories attempting to explain the mechanism resulting in presbyopia, it is that postulated by Schachar (1994; 2006) which is associated with the greatest controversy. Not only does this theory oppose more generally-accepted ideas, but Schachar performs presbyopia-correction surgery based upon his hypothesis. He asserts that as the lens grows, an increase in lens equatorial diameter, with an accompanying reduction in extralenticular space, causes a decline in zonular tension that limits accommodation. Scleral expansion surgery aiming to permanently restore resting equatorial zonular tension is available (Schachar, 2000), with subjective amplitudes of accommodation of up to 11.11 D reported post-operatively (Schachar, 1992). However, independent and objective analyses of patients following scleral expansion surgery have failed to identify an increase in accommodative amplitude in these subjects, compared to age-matched controls (Mathews, 1999; Ostrin *et al.*, 2004). Furthermore, these surgical techniques are based on the assumption that the ageing lens mass would still be capable of sufficient morphological change to increase the amplitude of accommodation.

1.8.2. Extralenticular theories

The numerous extralenticular theories attribute human presbyopia to ciliary muscle dysfunction or changes in the elastic properties of the zonules and/ or ciliary body. Ciliary muscle weakness was suggested by Duane (1925), although the work of Fisher (1977) on cadaver eyes indicated that the force of contraction of human ciliary muscle peaks at approximately 45 years of age, when the decline in accommodative amplitude is nearly complete (Ostrin and Glasser, 2004). Confirmation of the ability of ageing human ciliary muscle to contract has been provided by *in vitro* examination of muscle tissue exposed to pharmacological agents (Pardue and Sivak, 2000), and *in vivo* studies applying techniques such as ultrasound biomicroscopy (UBM; Park *et al.*, 2008) and MRI (Strenk *et al.*, 1999; Strenk *et al.*, 2006; Strenk *et al.*, 2010). Whilst there is strong evidence to support

maintenance of the contractual ability of ciliary muscle in presbyopic eyes, the muscular configurational changes could vary with age. Cataract surgery involving removal of the age-enlarged lens mass and implantation of an intraocular lens (IOL), allows the anteriorly-displaced ageing ciliary muscle to be restored to its youthful, more posterior position (Strenk *et al.*, 2010) and may also enhance its contractual response (Park *et al.*, 2008).

Decline in tissue elasticity is an established feature of ageing (Atchison, 1995), leading to the assertion that changes in ciliary body and choroidal elastic components could contribute to presbyopia. Bito and Miranda (1989) hypothesised that presbyopia is a loss of disaccommodative ability. According to their theory, in the young unaccommodated eye, the elastic antagonists of the ciliary body and choroid maintain tension on the lens and surrounding capsule via the zonules. With ciliary muscle contraction, the tension is released allowing the lens to assume a more spherical shape. In presbyopic eyes however, the elastic antagonists are unable to maintain tension, causing the lens to maintain a curved state, even in the absence of ciliary muscle contraction. Whilst this theory disregards possible age-related changes in lenticular and capsular elastic properties, it is consistent with the steepening of lens surface curvatures throughout life (Brown, 1974a; Dubbelman and Van der Heijde, 2001; Atchison *et al.*, 2008).

1.9. Summary

Human ocular accommodation functions reasonably effectively from around 4 months of age (Banks, 1980; Brookman, 1983), providing adequate near visual ability until the establishment of presbyopia, usually in the fifth decade of life. There is broad acceptance of the Helmholtzian mechanism of accommodation, with much empirical evidence to support this theory. However, a notable alternative model of accommodation has been proposed by Schachar, supported by mathematical substantiation (Schachar *et al.*, 1993b; Chien *et al.*, 2006) and limited experimental data (Schachar *et al.*, 1993a; Schachar and Cudmore, 1994; Schachar *et al.*, 1996; Schachar *et al.*, 2007; Schachar and Koivula, 2008). Difficulties associated with imaging the accommodative apparatus *in vivo* using high-resolution techniques have confounded efforts to invalidate Schachar's controversial theory, and the exact roles played by several ocular structures in accommodation remain unclear.

Further debate surrounds the processes responsible for presbyopia. Alterations in the viscoelastic properties of the enlarged lens mass, reducing its ability to be moulded by its capsule appear crucial, but the complete mechanism is likely to involve additional factors, including changes in extralenticular elastic tissue and the configuration of the ageing ciliary

muscle. Improved understanding of lenticular and extralenticular contributions to accommodation and presbyopia may be important in informing the development of strategies aiming to restore accommodative function to presbyopic eyes, particularly as currently-available methods generally target only the stiffened lens mass.

1.10. Aims of the thesis

The literature review presented in this chapter has highlighted numerous uncertainties relating to both the mechanism of accommodation, and the age-related changes affecting the accommodative structures which may be implicated in presbyopia development. Consequently, this thesis will address five pertinent topics related to accommodation and presbyopia, using only *in vivo* techniques that can visualise accommodative changes occurring in the natural, undisturbed system. The specific aims of the thesis are as follows:

1. To analyse the morphological characteristics and contractile responses of youthful human ciliary muscle *in vivo*, with regards to axial length/ ametropia.
2. To determine the age-related configurational and contractile changes affecting the ciliary muscle, which could be relevant to the development of presbyopia.
3. To devise a novel method to allow determination of lenticular tilt and decentration, relative to the cornea, using AS-OCT and apply this technique to investigate if lens stability changes during accommodation.
4. To develop and apply novel three-dimensional MRI techniques to analyse changes in lenticular morphology with accommodation. Of particular interest are the effects of accommodation on lens equatorial diameter, surface area and volume.
5. To utilise novel three-dimensional MRI methods to analyse changes in the posterior eye with accommodation amongst a cohort of youthful subjects.

The research will involve application of relatively new and complementary high-resolution imaging techniques that permit visualisation of the accommodative apparatus *in vivo*. The use of such methodologies will allow a high level of precision in examining the morphology of the accommodative structures, which has been difficult to achieve previously *in vivo*. A full account of the instrumentation used and validation of the techniques is provided in subsequent chapters. Previous experimental work has provided great insight into human

accommodation and presbyopia, but numerous questions remain unanswered. The thesis therefore seeks to provide clarification of a selection of related issues.

CHAPTER 2

INSTRUMENTATION FOR *IN VIVO* ANALYSIS OF THE ACCOMMODATIVE STRUCTURES

2.1. Introduction

The experimental chapters of the thesis involve the application of a range of advanced instrumentation to enable *in vivo* analysis of changes in both the anterior and posterior segments of the eye with accommodation. An account of the hardware used is provided in this chapter, with particular attention paid to anterior segment optical coherence tomography (AS-OCT) and high-resolution magnetic resonance imaging (MRI). Relevant findings from previously published studies utilising these techniques are included, in addition to full details of a new autorefractor validation study, performed prior to the acquisition of objective accommodative response and refractive error data.

2.2. Instrumentation for determination of refractive error and objective accommodation measurement

Each investigation detailed in the thesis describes changes in one or more of the ocular structures with accommodative effort. The accommodative response of an individual to particular stimulus vergence levels will vary due to a variety of factors including subject age (Duane, 1922; Atchison *et al.*, 1994), voluntary effort (Provine and Enoch, 1975) and the well-known phenomenon of accommodative lag, particularly for high amplitude targets (Wold *et al.*, 2003; Benjamin, 2006). Thus, it is important to measure the objective accommodative response to targets of various negative vergence, rather than assuming that stimulus demand is equivalent to response, as in many previously published studies (e.g. Dubbleman *et al.*, 2003; Baïkoff *et al.*, 2004b; Jones *et al.*, 2007; Schachar and Koivula, 2008), or using subjective measurements of accommodation, which are known to overestimate the true amplitude (Rosenfield and Cohen, 1996; Wold *et al.*, 2003; Ostrin and Glasser, 2004).

The term optometer describes any instrument designed to measure the refractive power of the eye (Millodot, 2008). Objective optometers, also known as autorefractors, calculate the vergence of light reflected from the retina to infer refractive error (Benjamin, 2006). In addition to on-axis refraction, autorefractors may be employed in accommodation research to determine peripheral refractive error (Dunne *et al.*, 1993; Davies and Mallen, 2009), accommodative responses to varying stimulus vergence levels (Manny *et al.*, 1993;

Richdale *et al.*, 2008) and microfluctuations (Winn and Gilmartin, 1992; Day *et al.*, 2006) that occur around the mean response level.

2.3. Validation of the Grand Seiko Auto Ref/ Keratometer WAM-5500

Previously-published studies have established that the majority of modern autorefractors are reliable and highly accurate compared to subjective refraction (McBrien and Millodot, 1985; Kinge *et al.*, 1996; Elliott *et al.*, 1997; Bullimore *et al.*, 1998; Mallen *et al.*, 2001; Davies *et al.*, 2003; Cleary *et al.*, 2009). Autorefractor readings are generally utilised as a starting point for subjective refraction in clinical practice, with previous studies indicating that prescribing from the objective findings alone results in limited patient satisfaction (Bullimore *et al.*, 1996; Strang *et al.*, 1998). As research interest in pseudophakic accommodation, particularly accommodating intraocular lenses (AIOLs) grows, it is of greater importance to measure accommodation objectively, rather than relying on subjective techniques that cannot differentiate between pseudoaccommodation and true accommodation. Pseudoaccommodation occurs due to a summation of non-accommodative influences including pupillary constriction leading to increased depth-of-field (Nakazawa and Ohtsuki, 1983); low-magnitude myopia (Elder *et al.*, 1996) or against-the-rule myopic astigmatism (Huber, 1981; Vezella and Calossi, 1993) and higher-order ocular aberrations (Pepose, 2008).

Most commercially available autorefractors utilise fixed internal targets in conjunction with fogging mechanisms to relax accommodation. However, this closed-view environment may induce instrument myopia (Smith, 1983; Rosenfield and Ciuffreda, 1991) and also restricts such devices to measurement of distance refractive error only. Therefore, the most appropriate autorefractors for research purposes should permit binocular viewing of external fixation targets in open-view formats. Additional features necessary for accommodation studies include a system to alter the vergence demand of near targets and the ability to measure refraction through small pupils due to the pupillary constriction that accompanies accommodative effort (Wolffsohn *et al.*, 2004; Win-Hall *et al.*, 2007). Only a very limited number of commercially available autorefractors meet these requirements, including the Shin-Nippon SRW-5000/ Grand Seiko WV-500 (Mallen *et al.*, 2001); the Shin-Nippon NVision-K 5001/ Grand-Seiko WR-5100K (Davies *et al.*, 2003) and the Tracey Visual Function Analyzer (Cleary *et al.*, 2009). Minimum pupil sizes stated by the manufacturers for these instruments are 2.9 mm, 2.3 mm and 2.5 mm, respectively.

2.3.1. The Grand Seiko Auto Ref/ Keratometer WAM-5500

The Grand Seiko Auto Ref/ Keratometer WAM-5500 (Grand Seiko Co. Ltd., Hiroshima, Japan) is a binocular open-field autorefractor and keratometer that also permits dynamic recording of refraction and pupil size by connection to an external PC via an RS-232 port. Refractive error is calculated in two stages, as with the SRW-5000/ WV-500, and details of the process have been described previously (Mallen *et al.*, 2001). An image of an infra-red measurement ring, which reflects strongly off the retina, is initially brought into rough focus by rapid movement of a lens on a motorised track. Subsequently, the toroidal refractive prescription is calculated by digital analysis of the image in multiple meridians. The instrument can measure refraction in the range of ± 22 D sphere and ± 10 D cylinder in increments of 0.01, 0.12 or 0.25 D for power, and 1° for cylinder axis. Central corneal radius is calculated by image analysis of an infra-red ring reflected off the cornea, the diameter of which is measured in 3 meridians separated by 60° . Corneal radii in the range 5.0 – 10.0 mm (0.01 mm steps) with refractive power of 33.75 – 67.50 D may be measured. Adjustment of vertex distance (to 0, 10, 12, 13.5 or 15 mm) is possible, and the manufacturer's specified minimum pupil diameter for refraction measurement is 2.3 mm. Pupil size data can be captured in both static and dynamic modes, by automatic detection of the iris boundary and subsequent superimposition of a best-fit circle. Measurement data are displayed on an internal 5.6 inch colour monitor, which permits visualisation of the pupil to enable alignment of the instrument with the subject's visual axis. Hard copies of data are available from the in-built thermal printer. In high-speed mode, mean spherical equivalent refractive error (MSE; equal to spherical component + cylindrical power/2) and pupil diameter can be recorded at a rate of 5 Hz by interfacing with a PC running the WAM communication system (WCS-1) software, allowing the objective measurement of a subject's dynamic accommodative response to a target.



Figure 2.1. Operation of the Grand Seiko Auto Ref/ Keratometer WAM-5500.

2.3.1a Methods

The purpose of this study was to determine the accuracy and repeatability of distance refraction and corneal curvature measurements obtained using the WAM-5500 in non-cycloplegic adult eyes by comparison with subjective refraction and Javal-Schiotz keratometry, performed by a qualified UK optometrist. Additionally, the ability of the instrument to provide dynamic recording of the accommodative response and pupil size with regards to use in accommodation research was assessed.

The study was approved by the Aston University ethics committee and the research followed the tenets of the declaration of Helsinki. Written, informed consent was obtained from all participants, following explanation of the nature and possible consequences of the study. Seventy-five subjects (54 female and 21 male), ranging in age from 18 to 69 years (mean: 25.12 ± 9.03 years) were recruited from the staff and student body of the Aston University Optometry Department.

WAM-5500 Static Mode

All subjects underwent an orthodox refraction routine on both eyes at 6 m, performed by an optometrist (ALS) masked to the participant's habitual prescription. Non-cycloplegic refraction was used, as this is the mainstay for adult prescribing by optometrists (Borish, 1975; Edwards and Llewellyn, 1988). Streak retinoscopy was followed by cross cylinder to

locate the cylindrical axis (in 2.5° increments) and its power (in 0.25 D increments). The spherical component was refined (in 0.25 D increments) with best sphere and binocular balancing. Endpoint criteria of maximum plus sphere and minimum minus cylinder power consistent with best visual acuity were used. Following subjective refraction, keratometry was performed on all eyes by a second optometrist (LND), with the Javal-Schiotz style keratometer (Topcon, Japan). Corneal radius of curvature (in 0.05 mm increments) and axis (in 2.5° increments) were measured in both the horizontal (from 0 – 42.5° and 135-180°) and vertical (45 – 132.5°) meridians following focusing of the instrument prior to each reading.

Autorefraction and autokeratometry were carried out at a second visit within 14 days of the subjective refraction, using the WAM-5500. Objective measurements were obtained utilising the same letter chart and testing room as the subjective refractions. The instrument was aligned with the visual axis of the eye being measured by instructing the subject to view a distance letter target, of the smallest size resolved binocularly without refractive correction. If the binocular unaided vision was less than 6/12, participants were asked to view the distant spotlight to minimise eye movements. Five refraction readings and single corneal curvature measures were obtained from each eye automatically when the instrument was adequately aligned with the eye being tested. Use of the automatic mode removes the need for the operator to judge subjectively when the measurement ring appears focused. Objective measurement of refractive error and corneal curvature on both eyes took less than 2 minutes per subject. Repeatability of these measures was determined by evaluating the differences between the 5 refraction readings taken per eye and additionally by repeating the autorefraction and autokeratometry on 44 eyes at a subsequent session, within a week of obtaining the initial results.

Statistical Techniques

Subjective and objective refraction results were entered into a spreadsheet in negative cylindrical form and the mean spherical equivalent (MSE) of each refraction was determined. Analysis of the astigmatic component of the results is problematic when standard clinical notation is used e.g. -1.75 DC x 135 (Bullimore *et al.*, 1998), thus two Jackson cross-cylinders were computed (Thibos *et al.*, 1997): at axis 0 (with power J_0 ; Equation 1) and at axis 45 (with power J_{45} ; Equation 2).

$$J_0 = -(\text{cylinder}/2)\cos(2*\text{axis}) \quad \text{Equation 1}$$

$$J_{45} = -(\text{cylinder}/2)\sin(2*\text{axis}) \quad \text{Equation 2}$$

Agreement between the WAM-5500 and subjective methods was evaluated for each of the components measured, by calculation of the mean of the differences (i.e. the bias) between the techniques, and the 95% confidence limits, as described by Bland and Altman (1986). Mixed-factor analysis of variance (ANOVA) was used to compare measures, with the two eyes of each subject considered as dependent variables.

WAM-5500 Dynamic Mode

The ability of the WAM-5500 to measure refraction accurately in its dynamic mode of operation was evaluated using the manufacturer's supplied model eye (of power -4.50 D), to avoid confounding effects such as subject head and eye movement that may occur with a cycloplegic human participant. The instrument was connected to a PC running the WCS-1 software via an RS-232 cable with the WAM-5500 set to Hi-Speed (continuous recording) mode, which allows refractive data collection at a temporal resolution of 5 Hz. No operator input is required during dynamic data collection, except depressing the WAM-5500 joystick button once to start recording, and once to stop at the end of the desired time frame. The software records dynamic results, including time (in seconds) of each reading; pupil size and MSE refraction, in the form of an *Excel* Comma Separated Values (CSV) file.

With the model eye positioned in its holder on the instrument chin rest, the measurement ring was brought as clearly into focus as possible by longitudinal movement of the autorefractor head. At this point, 10 continuous refraction recordings, each of 30 seconds duration were made to enable determination of the accuracy of the instrument in its dynamic mode. Additionally, the focusing tolerance of the WAM-5500 in continuous mode was evaluated by obtaining 50 dynamic refraction measures at 1 mm intervals of longitudinal shift as the instrument head was moved nearer and further from the model eye, resulting in increased blur of the measurement ring. Recordings were made across the full range of longitudinal movement that allowed measurements to be captured.

An investigation of the ability of the instrument to record refractive and pupil size responses dynamically to accommodative targets was made using a functionally emmetropic pre-presbyopic subject, corrected with hilafilcon B daily disposable soft contact lenses. The subject switched focus at 5 second intervals from a distant (Snellen letter) target to a 4 D high contrast (90%) Maltese cross accommodative stimulus.

2.3.1b Results

Subjectively-determined refractive errors ranged from -6.38 to +4.88 D MSE (mean MSE = -1.25 ± 2.18 D). The maximum level of astigmatism was 3.00 D. Corneal radii of curvature, measured by Javal-Schiotz keratometry, ranged from 7.2 to 9.1 mm (mean 7.81 ± 0.29 mm).

Validity

Validity of an autorefractor is generally expressed in terms of its agreement with subjective findings (Elliott *et al.*, 1997; Mallen *et al.*, 2001; Davies *et al.*, 2003). On average, the mean WAM-5500 prescriptions were similar to those found by subjective refraction (MSE: difference between WAM and subjective, -0.01 ± 0.38 D ($F_{(1, 148)} = 0.09$; $p = 0.77$); spherical component, difference 0.04 ± 0.41 D ($F_{(1, 148)} = 1.60$; $P = 0.21$). The cylindrical component was more negative than found by subjective refraction: difference -0.10 ± 0.34 D ($F_{(1, 148)} = 13.9$; $P = <0.001$), although J_{45} cylindrical vectors were very similar between the techniques (J_{45} difference 0.00 ± 0.15 D ($F_{(1, 148)} = 0.01$; $P = 0.92$)). The J_0 vector showed a slight statistically, but not clinically, significant positive bias of 0.04 ± 0.17 D ($F_{(1, 148)} = 7.87$; $P = 0.01$).

Figures 2.2a and 2.2b show the differences in the spherical component and MSE, respectively, between subjective and objective techniques, compared to the mean. Whilst there appears to be good agreement between WAM and subjective results for the majority of mean refractions between +1.00 D and -6.25 D, the outliers in the data sets are principally hyperopes above +2.00 D. Approximately 61 % of WAM-5500 spherical components were within ± 0.25 D of the subjective findings, and 74 % within ± 0.50 D (Figure 2.3a). For MSE, 57% of autorefractor readings were within ± 0.25 D of the subjective, and 73% within ± 0.50 D (Figure 2.3b).

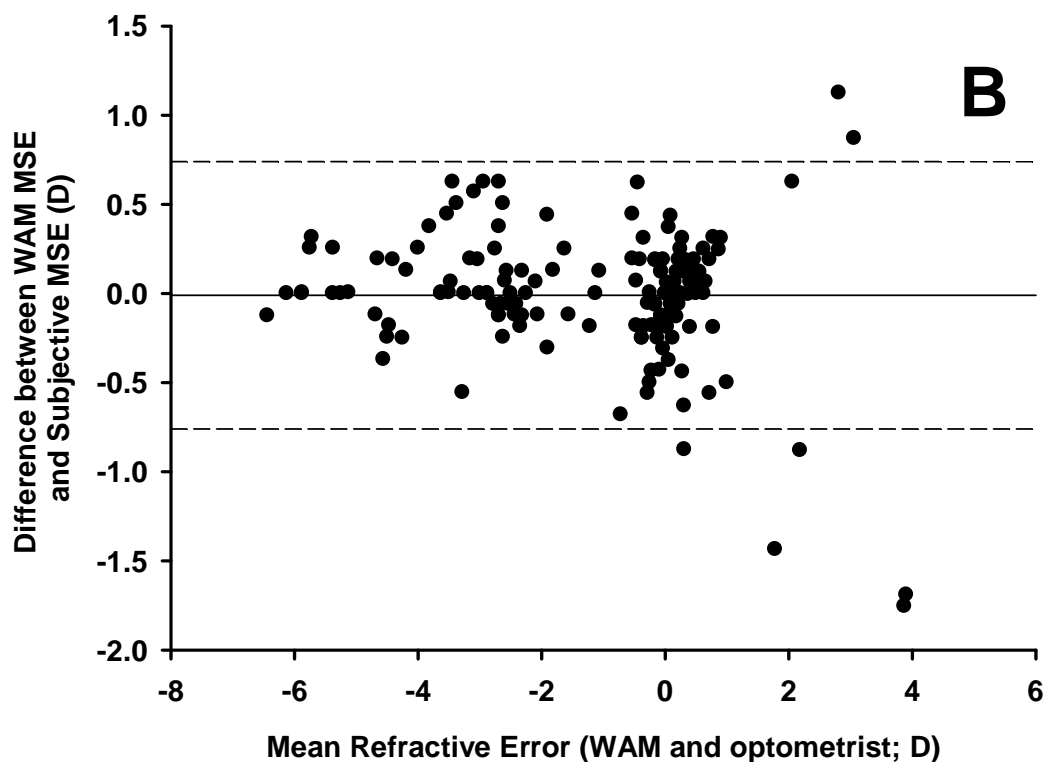
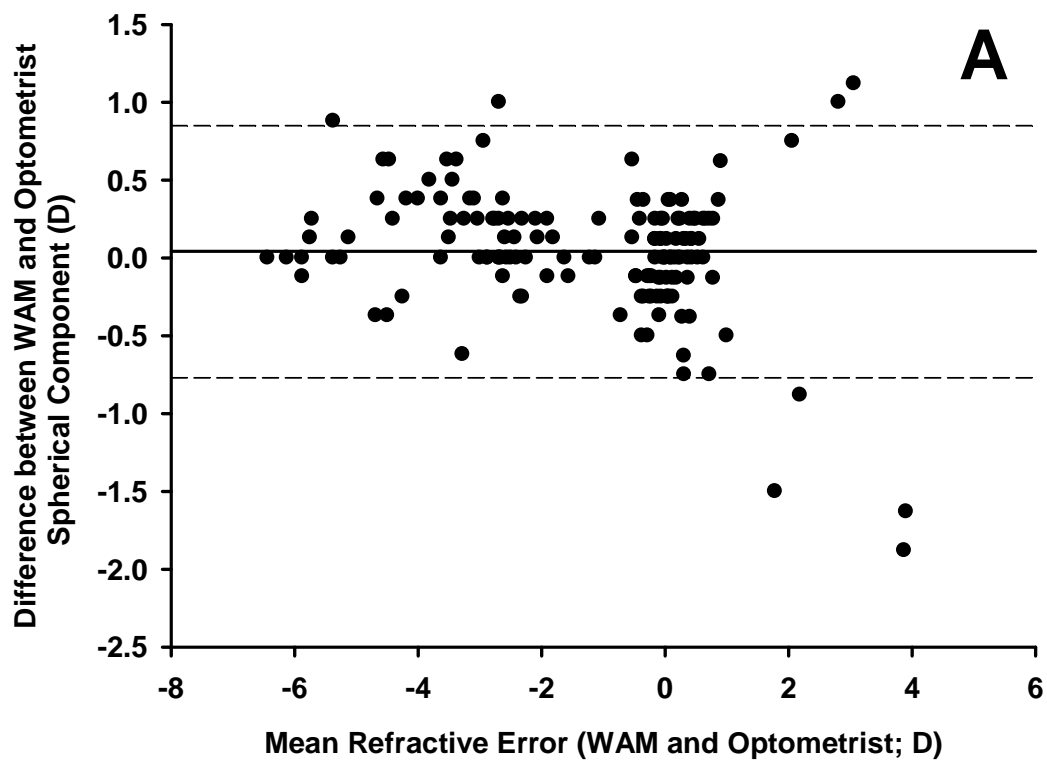


Figure 2.2. Difference in spherical component (A) and MSE (B) between the WAM-5500 and subjective, compared to the mean refractive error. Mean bias is indicated by the solid lines and the 95% confidence intervals by the dashed lines.

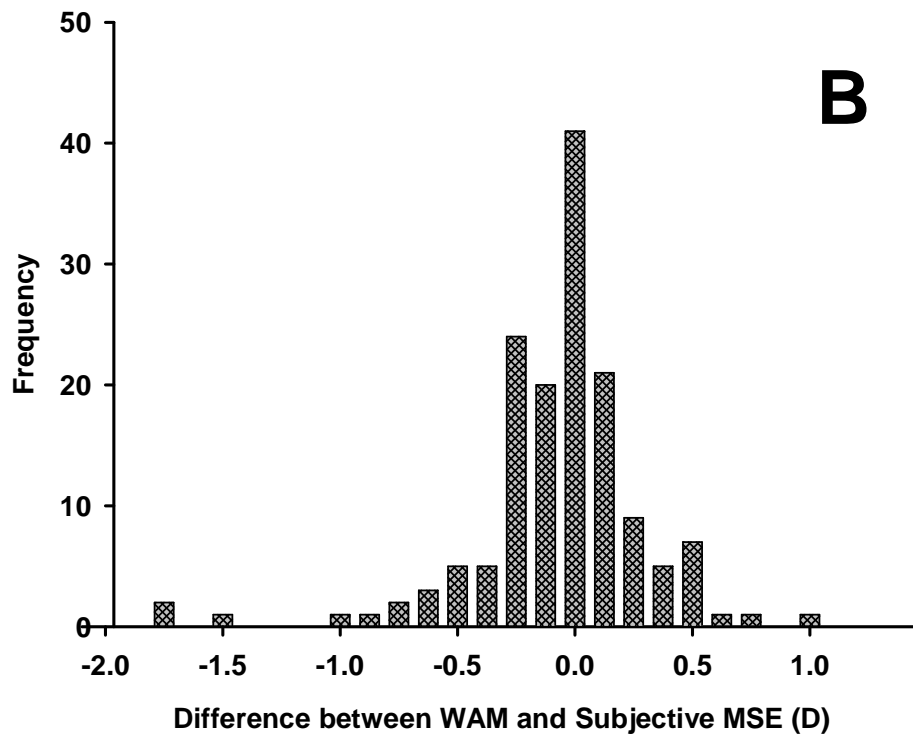
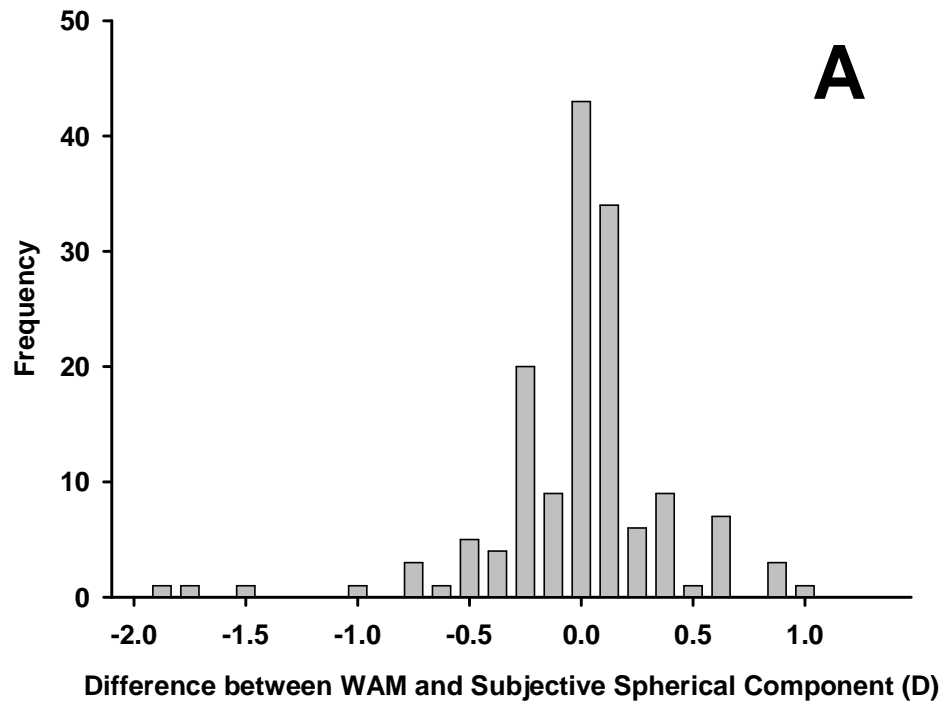


Figure 2.3. Comparison of the frequency of differences between the objective and subjective refraction techniques ($n = 150$ eyes) for spherical component (A) and MSE (B).

	All prescriptions with a cylindrical component n = 125	Prescriptions with a subjective cylindrical component ≥ 0.75 D n = 44
$\pm 5^\circ$	42 (34 %)	24 (55 %)
$\pm 10^\circ$	66 (53 %)	35 (80 %)
$\pm 15^\circ$	82 (66 %)	40 (91 %)
$\pm 20^\circ$	88 (70 %)	42 (95 %)

Table 2.1. Comparison of the axis of the cylindrical component measured with the WAM-5500 and by subjective refraction.

Table 2.1. details the agreement between subjective and autorefractor determination of cylinder axis. For all cylinder powers, 70 % of WAM-5500 axes were within $\pm 20^\circ$ of those found subjectively. However, for cylinder powers ≥ 0.75 D, the assessment of cylinder axis by the WAM 5500 was much improved, with 80 % within $\pm 10^\circ$, and 95% within $\pm 20^\circ$ of the subjective findings. Figures 2.4 and 2.5 show the differences in cylindrical component, and vectors J_0 and J_{45} compared to the mean values, respectively. Seventy-four percent of WAM cylinder components were within ± 0.25 D of the subjective findings, and 93 % within ± 0.50 D. Observation of the graphical data shows no clear bias in the difference in cylinder component determined by the WAM-5500 and subjectively with increasing magnitude of cylindrical component. In terms of cylinder vectors, there is an increase in positive bias of the J_0 component with increasing positive mean vector power, although no such bias is apparent for the J_{45} vector.

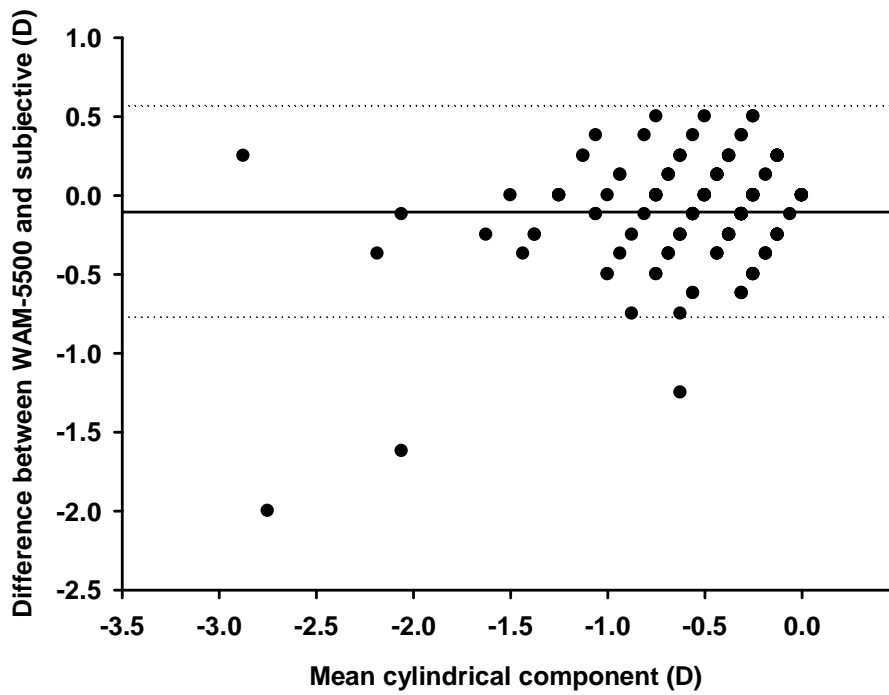


Figure 2.4. Difference in cylindrical components measured with the WAM-5500 and by subjective refraction ($n = 150$ eyes, although many of the data points overlaid each other). The solid line represents the mean bias, and the 95 % confidence intervals are indicated by the dotted lines.

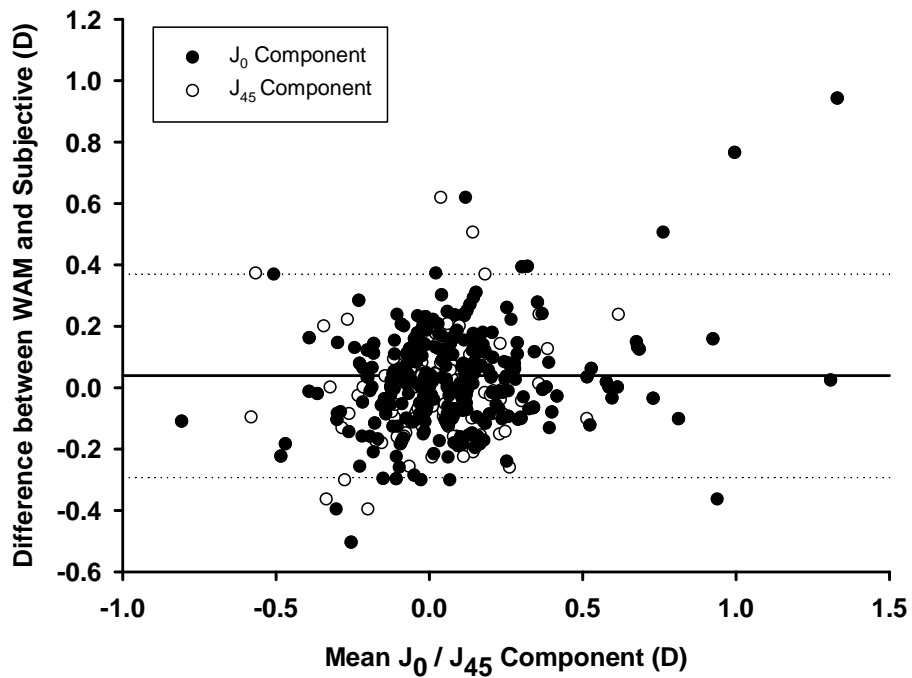


Figure 2.5. Difference in J_0 and J_{45} vectors between the WAM-5500 and subjective refraction, compared to the mean ($n = 150$ eyes). The solid line represents the mean bias for the J_0 vector, and the dotted lines show the 95 % confidence limits. The mean bias for the J_{45} vector was 0.00 ± 0.15 D.

Corneal curvature measured by the WAM-5500 was steeper than that determined subjectively by Javal-Schiotz keratometry (Figure 2.6). For the horizontal meridian, mean WAM-5500 bias was -0.05 ± 0.07 mm ($F_{(1, 148)} = 73.33$; $p = <0.001$), and for the vertical meridian, -0.06 ± 0.08 mm ($F_{(1, 148)} = 95.14$; $p = <0.001$). Generally good agreement was shown between the keratometric and WAM axes, with 49 % within $\pm 5^\circ$, 70% within $\pm 10^\circ$, 81 % within $\pm 15^\circ$, and 87 % within $\pm 20^\circ$. More consistent agreement between the WAM-5500 and Javal-Schiotz axes was found as corneal astigmatism increased. For corneal toricity ≥ 0.25 mm (on Javal-Schiotz), the mean difference between the Javal-Schiotz and WAM-5500 axes was $16.6 \pm 20.3^\circ$. However, for corneal toricity below this magnitude, the mean difference between Javal-Schiotz and WAM-5500 axes was $33.5 \pm 21.7^\circ$.

Calibrated spheres of radii 6.34, 7.93 and 8.72 mm were used to assess the accuracy and repeatability of keratometry readings obtained from the subjective and objective techniques. The mean bias of the optometrist using the Javal-Schiotz keratometer was slightly flat at $+0.003 \pm 0.012$ mm, whereas the mean bias of the WAM-5500 was of greater magnitude and steeper by -0.023 ± 0.025 mm.

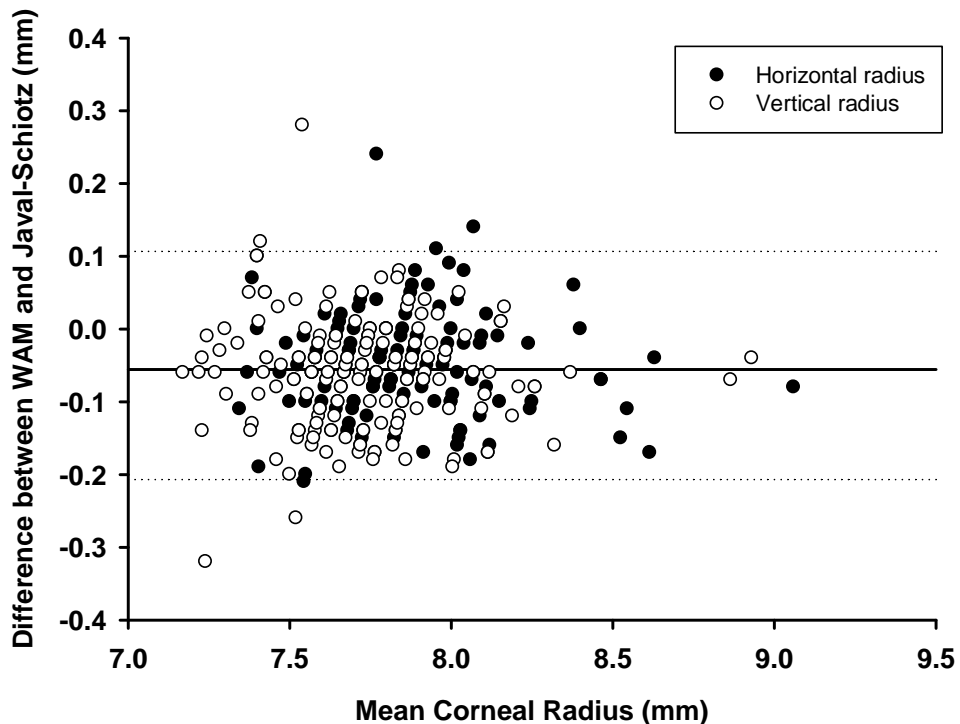


Figure 2.6. Difference in the horizontal and vertical corneal radii between the WAM-5500 and Javal-Schiotz keratometry compared to the mean ($n = 150$ eyes). The mean bias for the vertical meridian is indicated by the solid line (-0.06 mm), and the 95% confidence limits are shown by the dotted lines. The mean bias for the horizontal meridian was smaller, at -0.05 mm.

Repeatability

Both the intratest and intertest variability can be examined to evaluate the repeatability of automated refraction. The intratest variability was determined by calculation of the standard deviation of the 5 repeated readings acquired from each subject in one session. Mean intrasession repeatability was 0.09 D for the spherical component, 0.14 D for the cylindrical component, 0.09 for the MSE, 0.07 D and 0.06 D for the J_0 and J_{45} vectors, respectively.

	Sphere	Cylinder	MSE	J_0	J_{45}
Mean difference (D)	-0.04	-0.07	-0.07	-0.04	-0.01
SD of differences (D)	± 0.26	± 0.29	± 0.26	± 0.16	± 0.14
Within ± 0.12 D (%)	30	36	25	-	-
Within ± 0.25 D (%)	75	66	73	-	-
Within ± 0.50 D (%)	93	95	91	-	-
Within ± 1.00 D (%)	100	100	100	-	-

Table 2.2. Intertest variability of the refractive results obtained from the final WAM-5500 autorefractor prescription.

Intertest variability is arguably of greater importance (Mallen *et al.*, 2001; Davies *et al.*, 2003) as it requires realignment and remeasuring of subjects at a separate session. Table 2.2 details the intertest repeatability values for each of the refractive components measured. A slight myopic bias was demonstrated for all prescription elements on retesting (-0.04 D, -0.07 D, -0.07 D, -0.04 D and -0.01 D for sphere, cylinder power, MSE, J_0 and J_{45} , respectively). For sphere, cylinder power and MSE, over 90 % of retest values fell within ± 0.50 D of initial testing, and 100 % of retest values were within ± 1.00 D. Keratometric parameters were also found to have high intertest repeatability, with 63 % of all corneal radii within ± 0.05 mm of the initial value on retest, and 93 % within ± 0.10 mm. Mean intersession differences for the horizontal and vertical components were 0.00 ± 0.06 mm and 0.00 ± 0.07 mm, respectively.

Dynamic (high-speed) mode

Using the supplied model eye to record dynamically, the root-mean-square of the refractive fluctuations (i.e. the inherent noise level associated with dynamic recording) was 0.005 ± 0.0005 D, which is lower than measured by previous authors with both the Canon R-1 Autorefractometer (Owens, 1991) and the SRW-5000/ WV-500 (Wolffsohn *et al.*, 2001). Figure 2.7 shows the tolerance of the WAM-5500 to longitudinal movements away from the position of optimum focus whilst in dynamic mode, recording from the model eye. Beyond an 8 mm backwards movement, the device was unable to record dynamic data, although data capture was possible over the full physical range of forwards movement (+16 mm) of the instrument head. The focusing tolerance of the WAM-5500 was found to be good, as even a 1 mm movement in either axial direction was enough to cause noticeable blurring of the measurement ring on the internal monitor, the effect on the accuracy of the refractive data obtained was relatively minor. Even at the most anterior location possible, 16 mm from the position of optimum focus, the accuracy of the dynamic data collected was still within -0.25 D, despite the measurement ring being barely visible. Anterior or posterior movements from the point of optimum focus generally caused a negative shift in the accuracy of refraction data, although from 1- 5 mm of anterior movement, a positive shift is evident, which reduces to +0.004 D at 6 mm.

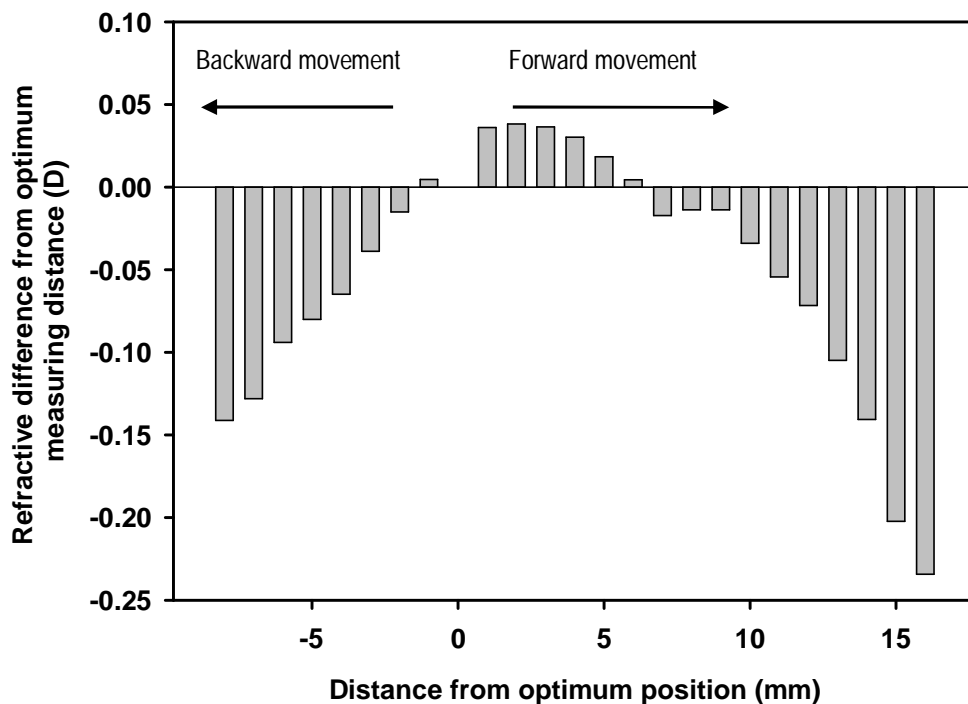


Figure 2.7. Tolerance of the WAM-5500 to longitudinal movements from the position of optimum focus whilst in high-speed (dynamic recording) mode. The WCS-1 software was unable to record any dynamic data beyond 8 mm of backwards movement, although data could be obtained until the instrument head was pushed fully forwards (to +16 mm).

Figure 2.8 illustrates graphically the refractive and pupil size data collected from a young subject switching fixation between a distance and near target. Pupil miosis associated with accommodation is evident. However, pupil size measures are not necessarily captured at every data collection point, which is visible on Figure 2.8 by the gaps in the pupillary size plot. The accuracy of WAM-5500 pupil diameter measures was assessed using calibrated artificial pupils, ranging in size from 4.49 to 7.46 mm. The results shown in Table 2.3 indicate a tendency for the instrument to slightly overestimate pupil size (except for the smallest diameter evaluated, with a mean bias of WAM-5500 pupil measures of $+0.11 \pm 0.19$ mm). The temporal resolution of the WAM-5500 in high-speed mode was found to be 4.2- 4.8 Hz when recording with the model eye and human subject, which is slightly lower than the 5 Hz stated by the manufacturer.

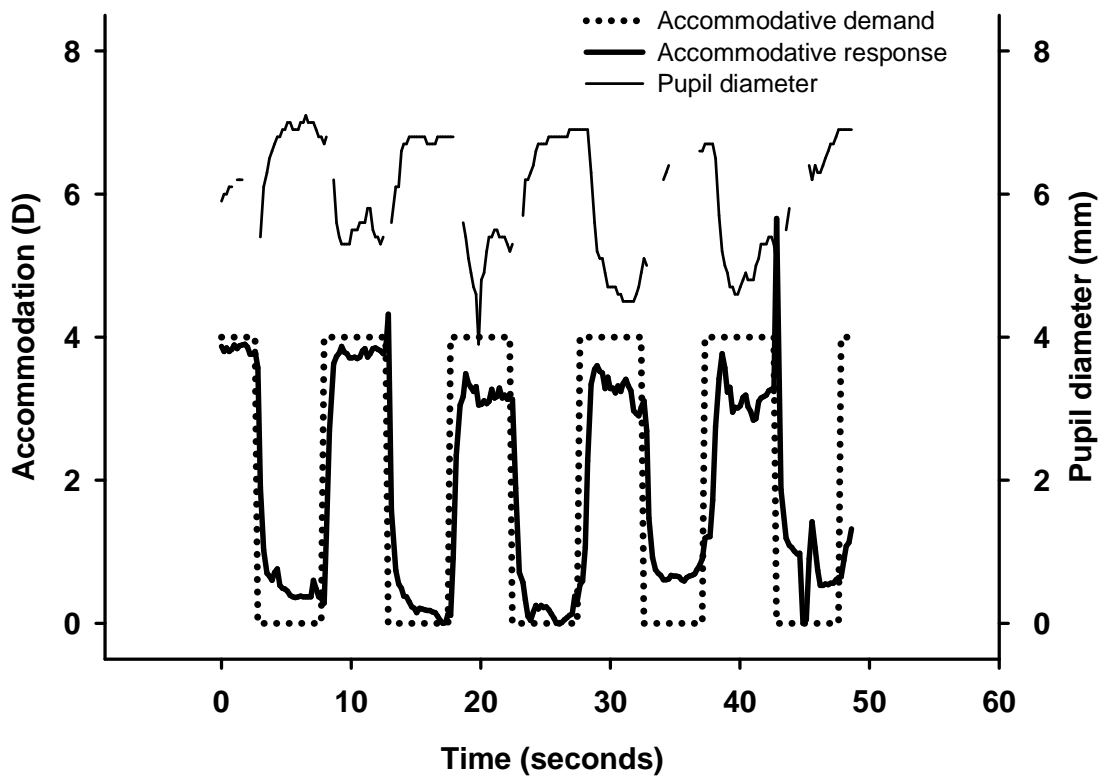


Figure 2.8. The dynamic refractive and pupillary response of a pre-presbyopic subject alternating attention between a distant (0.17 D) and near (4 D) fixation target. The gaps in the pupil size plot indicate times at which the WAM-5500 did not collect and record this data. The accommodation spike at 43 seconds is a blink artefact.

<i>Pupil diameter measured using digital callipers</i>	<i>Pupil diameter determined</i>	<i>Difference between WAM-5500 and digital calliper</i>
--	----------------------------------	---

<i>(mm)</i>	<i>by WAM-5500 (mm)</i>	<i>pupil diameter (mm)</i>
4.49 ± 0.01	4.30 ± 0.00	-0.13
5.14 ± 0.01	5.30 ± 0.00	+0.16
5.95 ± 0.00	6.27 ± 0.06	+0.32
7.46 ± 0.02	7.60 ± 0.02	+0.14

Table 2.3. Accuracy of WAM-5500 pupil diameters assessed using calibrated artificial pupils. Three measures were taken using the two techniques on each artificial pupil .The mean bias of WAM-5500 pupil measures was $+0.11 \pm 0.19$ mm.

2.3.1c Discussion

The WAM-5500 enables rapid, automatic and simultaneous acquisition of refractive, pupil size and keratometric data. Generally good agreement was found between the refractive techniques, with 57 % of WAM-5500 MSE values and 74 % of cylindrical components falling within ± 0.25 D of the subjective results. Similar levels of validity have been demonstrated with alternative autorefractors (McBrien and Millodot, 1985; Mallen *et al.*, 2001; Davies *et al.*, 2003; Cleary *et al.*, 2009). The significant underestimation of hyperopia by the WAM-5500 in a small number of subjects, compared to subjective refraction (Figures 2.2a and 2.2b), is likely due to their accommodation not being fully relaxed, despite the binocular, open-view design of the WAM-5500. McBrien and Millodot (1985) suggest a green spotlight as an effective target to relax accommodation when using an open-view autorefractor.

Accurate determination of cylinder axis by the WAM-5500 was notably improved for levels of astigmatism ≥ 0.75 D (Table 2.1.), where precise axis location is vital, as significant errors are likely to have > 0.1 logMAR effect on distance acuity. Corneal curvature data showed close agreement in terms of axis between the WAM-5500 and traditional keratometry, with half of all objective axes within $\pm 5^\circ$ of those found with the Javal-Schiotz keratometer. There was a negative bias of approximately -0.05 mm (in both horizontal and vertical meridians) in corneal radii of curvature measured by the WAM-5500 compared to Javal-Schiotz keratometry, which is unlikely to affect soft contact lens choices, but could be important when selecting appropriate rigid gas permeable lenses, where back optic zone radii are generally specified in 0.05 mm steps.

Intertest repeatability of the WAM-5500 was high, with 75% of spherical components, 66% of cylindrical components, and 73 % of MSEs falling within ± 0.25 D of the initial measurement on retesting. These values compare favourably with other commercially available autorefractors (Mallen *et al.*, 2001; Davies *et al.*, 2003; Cleary *et al.*, 2009).

As well as being a valid, repeatable and rapid autorefractor for use in general optometric practice, the additional features of the WAM-5500 make it a potentially valuable tool for accommodation research. Preparing the instrument for dynamic recording of refraction and pupil size is simple and quick, with no requirements for significant user modification of the machine or bespoke software, as may be necessary with alternative autorefractors (Pugh and Winn, 1988; Wolffsohn *et al.*, 2004). Straightforward recording of dynamic refractive and pupil size data may be beneficial in post-operative evaluation of the performance of implanted accommodating intraocular lenses, as true accommodative dioptric power changes could be distinguished from pseudo-accommodation which may result from an increased depth of focus e.g. due to pupil miosis (Wold *et al.*, 2003; Glasser, 2008). Despite this potential use of the WAM-5500 in accommodation research, the temporal resolution of 4.2- 4.8 Hz is too low to enable evaluation of accommodative microfluctuations. The characteristics, source and role of these microfluctuations have received much research interest over recent years (e.g. Charman and Heron, 1988; Winn and Gilmartin, 1992; Heron and Schor, 1995; Stark and Atchison, 1997; Gray *et al.*, 2000; Day *et al.*, 2006). Sampling well above the Nyquist frequency, which is twice the highest frequency of interest present in the signal, is necessary to avoid errors in studying accommodative microfluctuations (Pugh *et al.*, 1987). Previous studies have used sampling rates of 35 Hz and above (Gray *et al.*, 1993a Heron and Schor, 1995; Stark and Atchison, 1997; Day *et al.*, 2006), which is far higher than currently possible with the WAM-5500. Furthermore, the possible research uses of the instrument could be extended by the manufacturer in future designs by modification of the instrument head to allow measurement of a wider range of peripheral refractive errors. Peripheral refraction is believed to be relevant in eye development and myopia progression (Hoogerheide *et al.*, 1971; Atchison *et al.*, 2006; Mutti *et al.*, 2007; Davies and Mallen, 2009) and consequently, interest in the measurement of these off-axis refractions has recently grown (Fedtke *et al.*, 2009). The present binocular open-view design allows measurement of peripheral refraction to a horizontal eccentricity of around 30° only, due to the casing that frames the viewing window. Modification of the design of the viewing window could allow the maximum peripheral testing angle to be extended to levels greater than 30°, which is possible using alternative techniques such as peripheral retinoscopy (Anderson and Thibos, 1999) and manual optometers (Millodot, 1981).

Thus, the WAM-5500 Auto Ref/ Keratometer represents a reliable and valid objective refraction tool for both general optometric practice and research allowing collection of data including on-axis and peripheral refraction, pupil diameter and low temporal frequency dynamic recordings.

2.4. Instrumentation for *in vivo* imaging of ocular accommodation

Imaging may be defined as the visual representation of an object, typically in the form of an objective recording (Wolffsohn and Peterson, 2006). Following the advent of retinal photography in the late nineteenth century (Jackman and Webster, 1886), a range of advanced techniques have been developed to image ocular structures. The ability to visualise and objectively record both internal and external regions of the eye is important for detecting, monitoring and recording ocular disease, abnormality and trauma (Konstantopoulos *et al.*, 2007; Wolffsohn and Davies, 2007b; Nolan, 2008). Additionally, the use of these techniques as research tools enables a better understanding of the anatomy and physiology of ocular structures, particularly when *in vivo* imaging is possible. The ability to visualise the active human accommodative apparatus *in vivo* is advantageous, as *in vitro* investigations may be affected by *post mortem* tissue changes (Weale, 1999; Kasthurirangan *et al.*, 2008) in addition to storage and handling processes (Strenk *et al.*, 2004; Werner *et al.*, 2008).

The key techniques currently employed for *in vivo* imaging of the accommodative structures that also permit quantification of biometric changes are Scheimpflug imaging (Brown, 1972; Brown, 1974a; Koretz *et al.*, 2001; Dubbleman *et al.*, 2005); ophthalmophakometry (Phillips *et al.*, 1988; Kirschkamp *et al.*, 2004); ultrasound biomicroscopy (UBM; Beers and Van der Heijde, 1994; Van der Heijde *et al.*, 1996); AS-OCT (Baikoff *et al.*, 2004b; Baikoff *et al.*, 2005; Davies *et al.*, 2008; Richdale *et al.*, 2008) and high-resolution MRI (Strenk *et al.*, 1999; Strenk *et al.*, 2006; Jones *et al.*, 2007).

2.4.1. Scheimpflug Imaging

Scheimpflug devices use a camera perpendicular to a slit-beam creating an optic section of the cornea and crystalline lens to image the anterior segment (Koretz *et al.*, 2004). The technique has been used to assess corneal thickness (Morgan *et al.*, 2002) and topography (Abad *et al.*, 2007), anterior chamber depth (Buehl *et al.*, 2006) and lens surface curvatures (Koretz *et al.*, 2001), in addition to evaluating intraocular lenses (de Castro *et al.*, 2007). An unprocessed Scheimpflug image is subject to two types of distortion; the first is due to the geometry of the Scheimpflug system and the tilt of the camera and can be remedied easily (Dubbleman *et al.*, 2005). The other mode of distortion arises because optical structures are imaged through the preceding optical surfaces (Wolffsohn and Davies, 2007b) and is not constant, varying with factors including corneal curvature, anterior chamber depth and lens curvature. Previous studies of anterior segment biometry have not always corrected for this second type of distortion.

Scheimpflug photography was employed by Brown during the 1970s to conduct his pioneering research into accommodation and lens ageing. Increases in lens thickness and surface curvatures with accommodation and ageing were established (Brown, 1972; Brown, 1974a). More recent studies, utilising Scheimpflug images corrected for both types of distortion have demonstrated that the anterior lens surface assumes a more hyperbolic shape during accommodation and the lens equivalent refractive index increases by 0.0013 ± 0.0009 per dioptre of accommodation (Dubbleman *et al.*, 2005). Scheimpflug evaluation of the lens internal structure determined that increased lens thickness with accommodation is due solely to changes in the lens nucleus, the cortical thickness remaining constant. Additionally, the increased thickness of the cortex with age is attributable to changes in the C2 zone only. Zones C1 and C3 do not alter appreciably with age (Dubbleman *et al.*, 2003).

Recent Scheimpflug imaging systems, such as the *Pentacam* (Oculus, Germany) are able to create three-dimensional representations of the anterior chamber by rotating around the visual axis and acquiring multiple images (Rabsilber *et al.*, 2006). Although excellent quality images may be obtained non-invasively (Baikoff, 2006), Scheimpflug imaging does not permit visualisation of the lens equator, zonular fibres and ciliary body as these structures are screened by the iris (Koretz *et al.*, 2004).

2.4.2. Ophthalmophakometry

Since their initial description in 1832, the Purkinje images reflected from the anterior and posterior corneal surfaces (PI and PII, respectively) and the anterior and posterior lens surfaces (PIII and PIV, respectively), have been utilised to measure properties of the cornea and crystalline lens (Rosales and Marcos, 2006; de Castro *et al.*, 2007). Linear equations have been proposed (Phillips *et al.*, 1988) that relate the positions of PI, PIII and PIV relative to a central reference point (e.g. pupil centre), as a function of eye rotation and also crystalline lens tilt and decentration. More recent studies have provided validation of this methodology (Barry *et al.*, 2001) and employed the linear equations. Ocular surface alignment appears to be independent of accommodative state (Kirschkamp *et al.*, 2004) and it is possible using only ophthalmophakometry to non-invasively assess corneal and crystalline lens alignment (Dunne *et al.*, 2005). The tilt and decentration of both the natural crystalline lens (Dunne *et al.*, 2005) and implanted IOLs (de Castro *et al.*, 2007) have been assessed using ophthalmophakometry.

2.4.3. Ultrasound Imaging

Ophthalmic ultrasound imaging is a contact technique based on the reflection of high frequency acoustic pulses, generated by piezoelectric components (Wolffsohn and Davies, 2007b), from ocular tissue interfaces and the resultant detection of reflected sound waves (Konstantopoulos *et al.*, 2007) to generate an A-scan. B-scan sectional imaging is facilitated by scanning the probe across the eye. High frequency ultrasound biomicroscopy (UBM) of the anterior segment has been in use since the early 1990s (Pavlin *et al.*, 1992) and utilises an approximately 50 MHz transducer (compared to 10-20 MHz for whole-eye ultrasonography) to image ocular structures, permitting visualisation behind opaque corneas. Higher frequency UBM permits a tissue penetration of just 4-5 mm, but with improved resolution: axial resolution is around 25 μm and transverse resolution approximately 50 μm (Nolan, 2008). UBM typically requires the subject to be supine as the eye is immersed in a saline bath using an eye cup positioned directly onto the globe, which can be uncomfortable for the patient and may also potentially distort angle structures (Konstantopoulos *et al.*, 2007). High frequency UBM has been employed in recent studies to assess the movement of implanted IOLs (Muftuoglu *et al.*, 2005; Stachs *et al.*, 2006).

A-scan ultrasound imaging enables accommodative changes in lens thickness (LT), anterior chamber depth (ACD) and anterior segment length (LT + ACD) to be measured. Static ocular biometric changes with accommodation induced either pharmacologically or by Edinger-Westphal nucleus electrical stimulation, have been assessed with A-scan ultrasonography in rhesus monkeys (Koretz *et al.*, 1987a). Continuous A-scan ultrasound biometry has enabled measurement of dynamic accommodative biometric changes in humans (Van der Heijde *et al.*, 1996) and rhesus monkeys (Vilipuru and Glasser, 2005). However, human studies involving natural accommodative responses, induced by viewing near targets, are hindered by the problem of the ultrasonography probe covering the eye being measured meaning it is not possible to simultaneously record accommodative refractive and biometric changes in the same eye (Van der Heijde *et al.*, 1996; Vilipuru and Glasser, 2005).

2.4.4. Anterior Segment Optical Coherence Tomography

OCT enables non-invasive *in vivo* cross-sectional imaging of ocular structures (Baikoff, 2006; Wolffsohn and Davies, 2007a; Werner *et al.*, 2008). The technique is available for retinal or anterior segment imaging (Drexler and Fujimoto, 2007). Since the first device became commercially available in 1995, OCT has been used extensively for evaluation of retinal disease (Drexler, 2007), including diabetic retinopathy (Polito *et al.*, 2006), macular

hole (Bakri *et al.*, 2007) and macular degeneration (Pieroni *et al.*, 2006) as the technique allows sectioning through the retinal layers (Wolffsohn, 2008). Anterior segment OCT is a more recent development, first conceived in 1994 (Izatt *et al.*, 1994), becoming a reality in 2001, when a high speed AS-OCT providing good quality images became available. Clinically, AS-OCT has a range of applications, including determination of corneal thickness (Li *et al.*, 2006) and anterior chamber depth (Baikoff *et al.*, 2004a; Baikoff, 2006), accurate sizing of phakic IOLs (Goldsmith *et al.*, 2005), evaluation of implanted IOLs (Wirbelauer *et al.*, 2005; Baikoff, 2006), corneal grafts (Ardiomand *et al.*, 2007) and trabeculectomy blebs (Singh *et al.*, 2007) and the detection of angle-closure glaucoma (Radhakrishnan *et al.*, 2005; Nolan *et al.*, 2007).

OCT technology utilises a light source split into a reference beam, which undergoes reflection by a mirror, and a measurement beam that is reflected by the ocular structures (Wolffsohn, 2008). If light from the reference beam and the measurement beam travel identical optical distances before being recombined, coherent (positive) interference occurs, which is measured by an interferometer (Wolffsohn and Davies, 2007b). Varying the optical length of the reference path at each scanning spot determines the axial depth of tissues, building an A-scan. The scanning spot moves laterally across the eye, and multiple A-scans are aligned to construct a two-dimensional cross-sectional image that may be measured or used for diagnostic purposes. The AS-OCT light source is a long wavelength (1310 nm) superluminescent diode. The longer wavelength (compared to 830 nm for retinal imaging) affords better penetration of light-scattering tissues such as the sclera, thus the iridocorneal angle and ciliary body can be visualised (Konstantopoulos *et al.*, 2007). However, the pigmented iris blocks the 1310 nm wavelength, preventing imaging of the lens equator and zonules (Wolffsohn and Peterson, 2006).

Currently, two AS-OCT instruments are commercially available (Nolan, 2008): the *Visante* stand-alone OCT (Carl Zeiss Meditec Inc., Dublin, CA, USA) and the slit-lamp OCT (Heidelberg Engineering, GmbH, Heidelberg, Germany) which combines a slit-lamp and AS-OCT. Only the former of these devices is employed in the investigations detailed in the thesis, so the slit-lamp OCT will not be considered further, although many of the following details and issues are relevant to both machines. The *Visante* OCT offers standard imaging and high resolution corneal imaging modes. Standard mode utilises 256 A-scans per line sampling, with an image width of 16 mm, and depth of 6 mm (Zeiss, 2006) to provide a broad view of the anterior segment. High resolution 10 mm x 3 mm corneal scanning employs 512 A-scans per line sampling. Scanning is rapid, with up to 2048 A-scans per

second, and according to the manufacturer, optical axial and transverse resolutions are down to 18 μm and 60 μm , respectively.

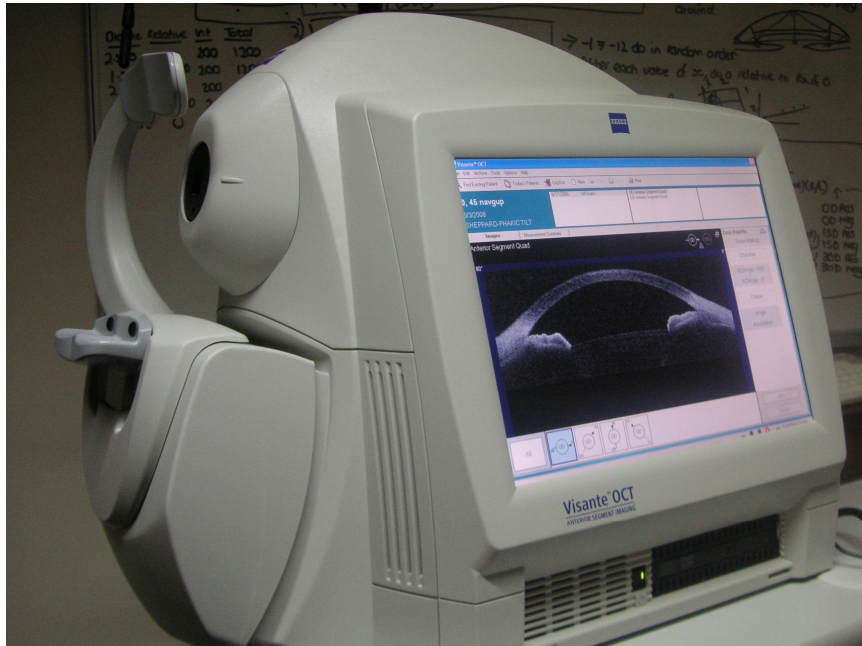


Figure 2.9. The Zeiss *Visante* AS-OCT showing a cross-sectional scan of the anterior segment, including the cornea and anterior portion of the crystalline lens.

Any technique involving the passage of light or sound waves through media with curved surfaces and varying refractive indices is subject to optical distortion (Wolffsohn, 2008), and AS-OCT is no exception. The in-built *Visante* software (versions 1.0 or 2.0) reduces this distortion by using edge detection algorithms to identify and fit the corneal surfaces and subsequently assigns appropriate refractive indices to each portion of the image- an index of 1.000 (air) is applied to the region anterior to the cornea, 1.338 (cornea) for the area within the corneal boundaries, and 1.343 (aqueous humour) for structures posterior to the cornea. Despite the improved accuracy provided by the software for measuring the ocular components, compared to using uncorrected images, some error remains. A relatively recent study (Dunne *et al.*, 2007) utilising physical model eyes with known dimensions determined, for example, that corneal thickness is overestimated by approximately 60 μm with the AS-OCT software; this represents a significant inaccuracy given that central corneal thickness is generally in the region of 550 μm (Lackner *et al.*, 2005; Buehl *et al.*, 2006). AS-OCT instrument distortion correction factors have been derived to reduce the errors in measurement of axial distances, and a scheme developed to enable determination of surface curvatures with clinically-acceptable accuracy (Dunne *et al.*, 2007).

AS-OCT is a useful modality for assessing anterior eye changes with accommodation. The image capture procedure is non-contact and simple to perform, with the patient seated and fixating an internal pinwheel target. Target vergence is adjustable in 0.25 D increments to compensate for the subject's spherical equivalent refractive error, or to provide an accommodative stimulus for the eye being imaged (Baikoff *et al.*, 2004a; Baikoff *et al.*, 2004b; Richdale *et al.*, 2008). Despite the lens equator and zonules not being visible, a variety of factors which may vary with accommodation can be measured from the cross-sectional images obtained, including anterior chamber depth in phakic and pseudophakic eyes (Baikoff *et al.*, 2004b; Davies *et al.*, 2008), lens axial thickness (Baikoff *et al.*, 2004a; Davies *et al.*, 2008; Richdale *et al.*, 2008) and surface curvatures (Dunne *et al.*, 2007), pupil diameter (Baikoff *et al.*, 2004a) and ciliary body thickness (Bailey *et al.*, 2008). The supplied *Visante* software includes a calliper tool, allowing anterior segment dimensions (but not curvatures) to be rapidly determined, without the need for exporting images from the machine.

To date, relatively few studies have utilised AS-OCT to examine ocular biometric changes with accommodation despite its relative ease of use and potential for measuring a wide range of variables. Table 2.4 summarises notable AS-OCT investigations into accommodation. In addition to quantifying the expected increase in lens thickness with age (Richdale *et al.*, 2008) and accommodation (Baikoff *et al.*, 2004a; Davies *et al.*, 2008; Richdale *et al.*, 2008), Davies *et al.*, (2008) demonstrated using AS-OCT data that accommodative biometric changes appear to be non-linear and biphasic. Forward shifting of the anterior lens surface was identified as the primary accommodative change until approximately 1.5 D response, with minimal movement of the posterior surface. Beyond 1.5 D response, the posterior lens surface moved backwards, but to a lesser degree than the forwards movement of the anterior surface. Schachar and Koivula (2008) analysed the light intensity of the anterior lens surface in a small cohort of subjects implanted with phakic IOLs. Increased reflectance of light from the anterior lens surface was observed with accommodation. The authors postulated that this change was due to increased zonular tension with ciliary muscle contraction, leading to greater stress on the anterior lens surface, and contradicting the Helmholtzian theory of accommodation.

Author & study title	Cohort characteristics	Results	Implications
Baikoff et al. 2004 Static and dynamic analysis of the anterior segment with optical coherence tomography.	n = 56 (range 7 – 82 years)	Per dioptre of accommodative stimulus, the crystalline lens anterior pole moves forwards by 30 µm, pupil diameter decreases by 0.15 mm and anterior lens radius of curvature steepens by 0.3 mm.	AS-OCT is a useful, relatively simple method of examining biometric changes with accommodation. Good image quality is possible even with opacified corneas.
Davies et al. 2008 <i>In vivo</i> biometric evaluation of phakic and pseudophakic eyes during accommodation with optical coherence tomography.	n = 32 phakic (aged 18 – 36 years) and 15 pseudophakic (aged 44- 85 years) implanted with the Kellen Tetraflex accommodating IOL	Lens thickness increases by 72.6 µm/ D accommodation in the phakic cohort. Biometric changes demonstrated a non-linear biphasic response. Anterior chamber depth (ACD) decreases by 52.8 µm/ D and increases by 353.8 µm/ D in the phakic and pseudophakic groups, respectively.	Crystalline lens biometric changes, particularly regarding the posterior lens surface (PLS) are non-linear and biphasic. Up to 1.5 D response, forwards movement of the anterior lens surface (ALS) is the main component of the response- after this point, backward shift of the PLS also contributes
Richdale et al. 2008 Lens thickness with age and accommodation by optical coherence tomography.	n = 22 (range 36 – 50 years)	Lens thickness increases by 51 ± 19 µm/ D of accommodation and increases with age by 21 µm/ year.	Lens thickness changes reported compare well with previous ultrasound and Scheimpflug measures.
Schachar and Koivula, 2008 The stress on the anterior lens surface during human <i>in vivo</i> accommodation.	n = 9 (range 25 – 38 years), all implanted with a phakic refractive IOL	Stress on the lens capsule was inferred from the intensity of light reflected from this structure on AS-OCT images. During accommodation, the intensity of the anterior lens surface increased significantly, suggesting an increase in zonular tension	Contradicts the Helmholtzian mechanism of accommodation, implying that zonular tension increases with accommodation.

Table 2.4. Summary of notable previous studies that have utilised AS-OCT to analyse ocular biometric changes with accommodation.

2.4.5. Magnetic Resonance Imaging

Unlike other imaging techniques, high-resolution MRI enables *in vivo* visualisation of the whole crystalline lens and its relationship with other anterior segment structures (Strenk *et al.*, 1999; Strenk *et al.*, 2006). Soft tissue contrast is excellent, and images free from optical distortion can be acquired in any plane (Strenk *et al.*, 2004; Jones *et al.*, 2007). Clinically, MRI has been used in the diagnosis and management of a number of ocular disorders, including space-occupying lesions (Ben Simon *et al.*, 2005), soft tissue injury (Kolk *et al.*, 2005), extraocular muscle abnormalities (Sa *et al.*, 2005) and congenital abnormalities (Chaudhry *et al.*, 2007). Despite a number of advantages, the clinical and research applications of MRI have been limited (Singh *et al.*, 2006), partly due to its expense (Strenk *et al.*, 2006; Wolffsohn and Davies, 2007b).

MRI uses the principle of nuclear magnetic resonance to image the internal structures of the body (Wolffsohn and Davies, 2007b). The nuclear spins of protons within tissues usually have no fixed orientation, but when surrounded by a strong magnetic field, for example, when a patient enters an MRI scanner, the nuclear spins tend to align along the field (Hornak, 2008). Application of a radiofrequency (RF) pulse with a specific frequency results in the spins being flipped out of the longitudinal plane, and into the transverse plane; a 90° RF pulse application (Liney, 2005a). When the pulse terminates, the RF coil is able to detect a spatially localised signal as the spins dephase (T_2 decay and T_1 recovery) and return to their initial state of equilibrium (T_1 relaxation). The intensity of the signal is dependent on several factors, including the RF pulse and varying magnetic field gradient, in addition to tissue characteristics and proton density. Application of linear changes to the magnetic field enables an image to be constructed.

The appearance of various tissues and how an image is weighted is governed by pulse sequences controlling the RF pulse. MRI images may be T_1 -weighted, T_2 -weighted or proton density-weighted (Liney, 2005a; Hornak, 2008). Normal soft tissue structures are shown optimally on T_1 -weighted images; fat appears bright, whilst water and fluids appear as intermediate signal intensity. T_1 -weighted images can be acquired with relatively fast scanning times (Obata *et al.*, 2006). T_2 -weighted images (e.g. Figure 2.10) show optimally fluids and pathology (including inflammation or tumours), with fluids appearing bright and fat dark. Proton density-weighted images minimise T_1 and T_2 weighting, with signal contrast dependent only on the density of spins within a tissue.



Fig. 2.10. Axial T₂- weighted MR image of both eyes and surrounding structures from a subject aged 26 years. The fluid filled chambers of the eye appear hyperintense, whilst the crystalline lenses are dark.

MRI is a safe imaging modality, involving no ionising radiation. The magnetic fields required for MRI are very powerful, typically 0.3 to 3 Teslas (compared to the Earth's average magnetic field strength of 50 picoTeslas; Wolffsohn and Davies, 2007) and implanted metal in devices including pacemakers and cochlear implants, represent the main contraindication to the technique. Ferromagnetic material can become displaced causing injury to internal organs and may also lead to imaging artefacts (Hornak, 2008).

Since the late 1990s, high-resolution two-dimensional (2D) MRI has been employed in a range of *in vitro* and *in vivo* investigations related to accommodation and accommodative structures. *In vitro* MRI studies of isolated crystalline lenses have provided some important information regarding optical and physical lenticular changes with age. Refractive index maps of excised human crystalline lenses generated from high-resolution MR images, have indicated an age-dependent flattening of the central profile and steepening of the equatorial peripheral region, with a possible reduction in the index of the nucleus (Moffat *et al.*, 2002; Jones and Pope, 2004; Jones *et al.*, 2005), providing a plausible explanation for Brown's lens paradox (Brown, 1974a; Brown, 1974b). A primary advantage of *in vitro* lenticular studies is the fact that lenses may be carefully aligned within the scanner and long scan times are not a problem as there is no potential for motion artefacts due to blinking or fixational eye movements (Kasthurirangan *et al.*, 2008). However certain methodological

problems are associated with *in vitro* studies, including tissue handling and storage, and *post mortem* deformation of the lens (Weale, 1999; Koretz *et al.*, 2004; Ziebarth *et al.*, 2008). Additionally, zonular tension is absent in the excised lens and it is not possible to obtain information on physiological changes with accommodation, or the relationship of the lens with other anterior eye structures (Jones *et al.*, 2005; Jones *et al.*, 2007).

In vivo MRI studies into accommodation have exploited the fact that it is possible to present stimuli of varying accommodative demands within the confines of the scanner, using targets positioned in close proximity to the eyes (Strenk *et al.*, 1999; Jones *et al.*, 2007; Kasthurirangan *et al.*, 2008) or minus-powered trial lenses to view a distant target through a mirror (Hermans *et al.*, 2009). The resultant changes to the accommodative structures in one or both of a subject's eyes may be imaged. All previous MRI studies of accommodation have utilised a distant target of minimal accommodative demand, in addition to a single near stimulus with a vergence close to, or exceeding, the accommodative amplitude of the subjects. Such an approach may have represented the only option to visualise the physiological changes that occur with accommodation if there were imaging limitations arising from poor signal to noise ratios (SNRs) or in-plane resolution. However, use of just two demand levels provides no information relating to the dose-effect of accommodative structural changes with varying stimulus vergence.

The key findings of these *in vivo* studies include more evidence to support the Helmholtzian mechanism of accommodation, as increased lens axial thickness with accommodation appears to be accompanied by a concurrent reduction in equatorial diameter (Strenk *et al.*, 1999; Jones *et al.*, 2007; Hermans *et al.*, 2009). With both accommodation and advancing age, increases in the cross-sectional area of the crystalline lens are confined to its anterior portion. Posterior lens cross-sectional area appears to be independent of both age and accommodation (Strenk *et al.*, 2004). Significantly, 2-D MRI studies have demonstrated that although the ciliary ring diameter decreases with age, the ciliary muscle maintains its contractile ability long after the development of presbyopia (Strenk *et al.*, 1999; Strenk *et al.*, 2006). The lenticular theory of presbyopia is supported by this finding, which may also have implications for attempts to restore accommodative function to presbyopic eyes.

With the exception of the Hermans *et al.*, (2009) study, all of the *in vivo* accommodative MRI studies have imaged a single, 3 mm thick axial slice of the eye in its relaxed and accommodated states. Some debate exists over the validity of this 2-D approach, as it is possible that the MRI acquisition planes could vary as a result of subject head motion and the natural convergent and excyclotorsional eye movements that accompany

accommodation, leading to erroneous conclusions to be drawn regarding the magnitude of the physiological changes observed (Pope *et al.*, 2008; Schachar *et al.*, 2008). Furthermore, Demer *et al.* (2003) imaged the human extraocular muscles of 8 subjects during accommodation and convergence using this method and found no statistically significant difference in equatorial lens diameter between the relaxed and accommodated states.

To negate problems associated with finite slice thickness in 2-D imaging, three-dimensional (3-D) MRI techniques have been proposed to image the accommodative structures (Strenk *et al.*, 1999; Singh *et al.*, 2006; Hermans *et al.*, 2009; Langner *et al.*, 2010). Singh *et al.*, (2006) first described the shape of the whole eye in 3-D following acquisition of MRI data with high resolution in all three directions. Previous authors had only surmised 3-D shape from several 2-D slices (e.g. Cheng *et al.*, 1992; Chau *et al.*, 2004; Atchison *et al.*, 2005). A 3-D approach to analysing the accommodative structures with high-resolution MRI would remove the error associated with finite slice thickness and provide more robust data regarding change in lens equatorial diameter with age and accommodation, in addition to addressing the question of lens volume and surface area. To date, one previously published study has used 3-D MRI to analyse these factors with varying stimulus demand. On a cohort of five young subjects, Hermans *et al.*, (2009) inferred lens volume from 3-D MRI data divided into eight parts. A Canny filter was applied to determine the lenticular boundaries in these regions, allowing a subsequent calculation of volume. No change in lens volume was measured between relaxed and maximal accommodative effort, whilst lens equatorial diameter decreased with accommodation. Two further recent studies (Richdale *et al.*, 2009; Langner *et al.* 2010) have used ultra-high field 7-Tesla MRI to image the ocular structures in 3-D. Richdale *et al.* (2009) utilised a voxel size of 0.038 mm³ to examine the *in vivo* human eye. However, field variability from the air-tissue interface along the eyelid margin at 7 T resulted in considerable image artefacts, thus it was necessary to tape the eyelids closed. Whilst the high-resolution images obtained could provide information regarding structural changes with age, the closed eye environment currently limits the application of this approach in accommodation research. Langner *et al.* (2010) assessed the anterior segment of several species, including humans, *ex vivo*, and the rabbit eye *in vivo* at 7.1 T, providing data on lens volume and surface area. The techniques described in this investigation could not be applied to human eyes *in vivo* due to the small inner tube diameter (200.5 mm) of the ultra- high field scanner. Furthermore, the 30 minute scan acquisition time would be unsuitable for assessing multiple vergence demand levels.

2.5. Summary

Both AS-OCT and high-resolution MRI are potentially valuable tools in accommodation research. AS-OCT is widely available and comfortable for subjects, but is affected by optical distortion and does not allow visualisation of the lens equator. Despite its expense, MRI overcomes these disadvantages, allowing imaging of the entire lens and its surrounding structures. MRI scanning protocols do require careful planning to permit high resolution and SNRs, whilst maintaining reasonable scan acquisition times. Regardless of the imaging technique(s) used, it is important to measure the objective accommodative responses to enable accurate quantification of the change in biometric variables per dioptre of accommodation.

Supporting publication: Sheppard, A. L. and Davies, L. N. (2010a). Clinical evaluation of the Grand Seiko Auto Ref/ Keratometer WAM-5500. *Ophthalmic and Physiological Optics*. **30**, 143-151.

CHAPTER 3

IN VIVO ANALYSIS OF CILIARY MUSCLE MORPHOLOGICAL CHANGES WITH ACCOMMODATION AND AXIAL AMETROPIA

3.1. Introduction

The exact mechanism of accommodation and the changes in the accommodative apparatus that lead to presbyopia are yet to be elucidated. Despite over 150 years of continuing research since von Helmholtz (1855) proposed his classical theory of accommodation, precise details of factors including how ciliary muscle contraction influences zonular tension, and the roles of the posterior zonules, iris and vitreous body remain unclear (Coleman, 1986; Atchison, 1995; Croft *et al.*, 2001; Charman, 2008). The process of accommodation is undisputedly governed by ciliary muscle contraction (von Helmholtz, 1855; Glasser *et al.*, 2006; Ostrin and Glasser, 2007a), with the resultant forward and inward shift of its mass towards the lens equator causing a reduction in zonular tension (Glasser and Kaufman, 1999; Charman, 2008), allowing the elastic capsule to mould the young lens into a thicker, more convex and dioptrically powerful form (von Helmholtz, 1855; Ehrmann *et al.*, 2008).

To gain a more complete understanding of the mechanism of accommodation, the structure and function of human and animal (particularly primate) ciliary muscle has been examined in detail by previous authors using both *in vitro* and *in vivo* techniques. The position of the ciliary body, screened by the iris, has traditionally hindered *in vivo* observation of its morphology and accommodative movements (Pardue and Sivak, 2000; Strenk *et al.*, 2006; Park *et al.*, 2008). *In vivo* primate studies, utilising iridectomised animals allow direct visualisation of the ciliary muscle and its relationship with the lens equator (Neider *et al.*, 1990). The rhesus monkey (*Macaca mulatta*) is considered to be the optimum animal model for the study of human accommodation due to close similarities in accommodative structures (Koretz *et al.*, 1987b; Ostrin and Glasser, 2007b) and mechanism (Koretz *et al.*, 1987a; Glasser and Kaufman, 1999; Glasser *et al.*, 2006), and the development of presbyopia on comparable relative timescales (Bito *et al.*, 1982; Kaufman *et al.*, 1982; Wasilewski *et al.*, 2008). Furthermore, implantation of an electrode into the Edinger-Westphal nucleus, which provides parasympathetic innervation of the ciliary muscle via the ciliary ganglion, permits accurate control of both the amplitude and duration of the accommodative response by application of a controlled stimulus current (Crawford *et al.*, 1989; Neider *et al.*, 1990; Vilipuru and Glasser, 2005). Studies utilising Edinger-Westphal stimulation of accommodation in the rhesus monkey have demonstrated linear associations between accommodative response and various ocular biometric correlates including anterior

chamber depth and lens thickness (Vilipuru and Glasser, 2005), and movements of the ciliary processes and lens edge (Ostrin and Glasser, 2007a). Further studies have concluded that whilst the ciliary body maintains much of its ability to move centripetally with accommodative effort (Croft *et al.*, 2008), the forward shift of the ciliary body is lost with age in the rhesus monkey (Croft *et al.*, 2006a; Croft *et al.*, 2009). Glasser *et al.* (2001) performed ultrasound biomicroscopy of the ciliary region in cyclopleged monkeys *in vivo*, revealing several significant nasal *versus* temporal biometric asymmetries. The ciliary body was found to be longer, with a larger area and greater zonule length temporally, compared to the nasal aspect. To date, nasal/ temporal asymmetry of the ciliary body has not been detected *in vivo* in humans.

In vitro monkey studies have analysed *post-mortem* ciliary muscle sections to attempt to identify age-dependent changes, which could contribute to the development of presbyopia. Isolated ciliary muscle strips from both young and presbyopic monkeys continue to contract in response to pharmacological agents (Tamm *et al.*, 1992b; Poyer *et al.*, 1993) and there is no decrease in the quantity or affinity of muscarinic receptors with age (Bito *et al.*, 1982). However, presbyopic monkey samples in which the posterior attachment of the ciliary muscle is intact do not contract in response to muscarinic agonists (Tamm *et al.*, 1992b). Additionally, the elastic tendons forming the posterior attachments become thicker with age and show increased levels of microfibrils (Tamm *et al.*, 1991). These findings indicate that decreased compliance of the posterior insertion of rhesus monkey ciliary muscle, which is essential to allow its forwards and inwards accommodative movement and the restoration of its position during disaccommodation (Tamm and Lütjen-Drecoll, 1996), could be an important factor in the development of presbyopia.

In humans, analysis of *post-mortem* ciliary body tissue from eyes exposed to high doses of pharmacological agents before dissection has demonstrated that the muscle maintains its ability to contract throughout life (Pardue and Sivak, 2000). Eyes from donors of 1 day to 107 years of age exhibited shortening of the ciliary muscle length and narrowing of the width at the thickest point in response to pilocarpine administration. Further *in vitro* studies have identified nasal *versus* temporal asymmetry in human ciliary body morphology, with the temporal aspect being significantly longer at all ages (Streeten, 1985; Aiello *et al.*, 1992). To date, this nasal/ temporal disparity has not been observed *in vivo*. Total *in vitro* ciliary body length in adult subjects is approximately 4.79 mm nasally, and 5.76 mm temporally (Aiello *et al.*, 1992). Table 3.1 summarises the key findings of significant *in vitro* and *in vivo* investigations of human ciliary muscle morphology.

More recently, several investigations have employed ultrasound biomicroscopy to analyse *in vivo* the morphology and configurational changes of the human ciliary muscle with accommodation. In youthful eyes, with accommodative effort, Ma and Chen (2004) observed that the thickness of the anterior, but not the posterior, portion of the ciliary body increased. In presbyopic subjects, the contractility of the ciliary muscle (as inferred by its centripetal movement) in response to pilocarpine administration significantly increases following cataract extraction (Park *et al.*, 2008). Lenticular sclerosis may, therefore, hinder ciliary body contractility by exerting tension via the zonules. The effects of cataract surgery, whereby the thickened, presbyopic lens mass is removed and a significantly thinner intraocular lens (IOL) is implanted into the capsular bag, which undergoes postoperative fibrosis and contraction, may alter anterior segment geometry in such a way to allow the centripetal movement to be restored.

Authors & study title	Study type	Cohort characteristics	Key findings	Implications
Aiello et al. 1992 Postnatal development of the ciliary body and pars plana	<i>In vitro</i> histologic investigation	n = 76 children's eyes (donor ages 0 – 6 years) n = 5 adult eyes for comparison	Mean CB lengths: Age <6 months = 3.06 mm (nasal), 3.31 mm (temporal) Adults = 4.79 mm (nasal), 5.76 mm (temporal)	Temporal ciliary body is longer than nasal at all ages. Ciliary body is substantial in length at birth, but continues to grow into adulthood.
Pardue and Sivak, 2000 Age-related changes in human ciliary muscle	<i>In vitro</i> Eyes treated with atropine or pilocarpine to simulate relaxed and accommodated ciliary muscle (CM) states. Eyes subsequently dissected and CM examined by light microscopy	n = 16 pairs of eyes (donor ages 0 – 107 years)	Main pilocarpine induced change was shortening of CM at all ages. Mean CM length with atropine = 3.87 mm and with pilocarpine = 3.51 mm	Isolated CM maintains its contractile ability throughout life and shortens with accommodation.
Marchini et al. 2003 Effects of 0.005 % latanoprost on ocular anterior structures and ciliary body thickness	<i>In vivo</i> , with ultrasound biomicroscopy (UBM). Ciliary body (CB) morphology analysed before and after treatment with topical latanoprost	n = 30 ocular hypertensives/ primary open angle glaucoma patients (mean age 59.3 years)	CB2 = 434 µm before treatment, and 536 µm after treatment	Topical latanoprost causes CB thickening, supporting the theory of increased aqueous outflow through extracellular CM spaces to reduce intraocular pressure.
Oliveira et al. 2005 Ciliary body thickness increases with increasing axial myopia	<i>In vivo</i> , with UBM	n = 75 (mean age 51.8 years)	Mean CB2 values vary with refractive error status: Myopes = 490 µm Emmetropes = 362 µm Hyperopes = 317 µm	Strong association between CB2 and refractive error. CB2 increases with axial length and myopia.
Bailey et al. 2008 Ciliary body thickness and refractive error in children	<i>In vivo</i> , with anterior segment optical coherence tomography (AS-OCT)	n = 53 children (mean age 11.8 years)	Mean CB in myopes = 630 µm and emmetropes = 574 µm. CB2 strongly correlated with axial length and myopia	Hypertrophy of ciliary muscle could be implicated in myopigenesis, as it could cause accommodative dysfunction which is central to the retinal defocus model of myopia development.

Table 3.1. Key findings from *in vitro* and *in vivo* studies of human ciliary muscle morphology. CB2 is ciliary body thickness, measured 2 mm posterior to the scleral spur.

In addition to changes with accommodation, the morphologic characteristics of the ciliary muscle have been studied with regard to refractive error *in vivo* utilising ultrasound biomicroscopy (Oliveira *et al.*, 2005; Muftuoglu *et al.*, 2009) and AS-OCT (Bailey *et al.*, 2008). Oliveira *et al.* (2005) first reported increased ciliary body thickness in adults with high axial myopia, contravening the intuitive expectation that this structure would be attenuated in longer, more myopic eyes, and the findings of van Alphen (1986), who demonstrated significant thinning of human ciliary muscle with *in vitro* expansion of the globe. The association between axial myopia and greater ciliary body thickness has been confirmed in subjects with unilateral high myopia (Muftuoglu *et al.*, 2009), and children aged 8 to 15 years (Bailey *et al.*, 2008; Schultz *et al.*, 2009), although the reason for this thickening is unclear. Bailey *et al.*, (2008) suggest that ciliary muscle hypertrophy and thickening may lead to poorer contractile responses and the accommodative dysfunction which is central to the hyperopic defocus model of myopigenesis, where the resultant retinal defocus is accompanied by axial elongation and myopia (Hung and Ciuffreda, 2000; Gwiazda *et al.*, 2005; Langaas *et al.*, 2008). However, it is not known whether accommodative dysfunction constitutes a cause or effect of myopia (Gwiazda *et al.*, 1993; Mutti *et al.*, 2006).

The morphology and accommodative configuration of the human ciliary muscle is therefore of significant interest, in relation to the mechanism of accommodation and, as a consequence of recent findings, its link with refractive error. Whilst *in vitro* studies have furthered understanding of human and primate accommodation, the precise impact of *post mortem* tissue changes cannot be known (Strenk *et al.*, 2004; Werner *et al.*, 2008) and samples from dissected eyes may not represent normally-responding ciliary muscle. Additionally, the effects of ischaemia may alter the response of the muscle to topically-applied pharmacological agents such as pilocarpine (Pardue and Sivak, 2000). Thus, *in vivo* approaches to analysing the ciliary body may be more valid, particularly because the entire accommodative apparatus remains intact. Hitherto, UBM has been most frequently used to acquire high resolution *in vivo* images of the relaxed and accommodating ciliary body in humans (e.g. Stachs *et al.*, 2002; Marchini *et al.*, 2003; Ma and Chen, 2004; Park *et al.*, 2008) and primates (e.g. Glasser *et al.*, 2001; Croft *et al.*, 2006a; Wasilewski *et al.*, 2008). However, the contact nature of the technique and requirement for the subject to be supine could potentially alter anterior segment geometry (Fledelius, 1997; Konstantopoulos *et al.*, 2007).

AS-OCT represents a relatively new methodology for imaging the anterior segment, including the ciliary body (Bailey *et al.*, 2008; Schultz *et al.*, 2009). The non-contact nature

of the technique is advantageous, and subjects can sit in a natural, upright position. In high-resolution corneal imaging mode, axial resolution of 8 μm is possible (Nubile *et al.*, 2008). Ocular biometric changes with accommodation, including anterior chamber depth, lens thickness and anterior segment length have been studied by previous authors (Davies *et al.*, 2008; Richdale *et al.*, 2008) using the *Visante* (Carl Zeiss Meditec Inc., Dublin, California, USA) device. However, Richdale *et al.* plotted accommodative biometric changes against stimulus, rather than response, which may lead to underestimation of physiological responses per dioptre of accommodation. Whilst the relaxed ciliary body has been imaged with AS-OCT to investigate the link between thickness and refractive error (Bailey *et al.*, 2008; Schultz *et al.*, 2009), no previously-published study has analysed accommodative changes in this structure with AS-OCT.

The aim of this *in vivo* study is to further the author's previous work (Sheppard and Davies, 2009a; 2009b) and use AS-OCT to provide new data regarding human ciliary muscle morphology and accommodative characteristics. Furthermore, nasal *versus* temporal asymmetry in ciliary muscle morphology and response will be investigated, along with a possible link to axial ametropia.

3.2. Methods

3.2.1 Sample size estimation

Prior to recruitment of subjects for the main study, a pilot investigation was conducted in order to highlight potential problems with the protocol and to acquire initial data to assist in the determination of required sample size for the project. Pilot data were necessary for sample size estimation in this instance to determine standard deviations of the accommodative biometric measures (Eng, 2003), which have not previously been studied in this manner *in vivo*. Fifteen young subjects (mean age 23.2 ± 3.1 years) participated in the pilot study, and were imaged in both the relaxed state and at 4.0 D stimulus vergence. The differences in means between the two demand levels, and standard deviations of ciliary muscle thickness and length parameters were used in sample size calculations, carried out with *SigmaPlot* statistical and graphing software (Version 11, Systat Software Inc., Chicago, Illinois, USA). The maximum number of subjects required for any of the individual parameters was 23, which was therefore used as a minimum level for subject recruitment, to ensure adequate statistical power of results, and also to allow for attrition.

3.2.2 Subjects

50 pre-presbyopic volunteers (29 female, 21 male), aged 19 to 34 years of age (mean age 25.8 ± 4.5 years) with no previous history of ocular abnormality or intraocular surgery were recruited using email announcements at Aston University. Participants in the pilot study were remeasured during the main investigation, which took place several months later. Subjects with all types of refractive error were included, provided their prescription (including astigmatic component, if applicable) was amenable to correction with daily disposable soft contact lenses (*Focus Dailies* and *Focus Dailies Toric*: nelfilcon A, 69 % water content; Ciba Vision, Duluth, Georgia, USA). The parameter ranges for these contact lenses meant subjects with spherical refractive errors greater than -10.00 DS or +6.00 DS were excluded from the investigation, as were those with oblique cylinders > 0.50 DC, or orthogonal cylinders > 1.50 DC. The study was approved by the Ethics Committee of Aston University (see Appendix 1) and was performed in accordance with the tenets of the Declaration of Helsinki. Written, informed consent was obtained from all participants (see Appendix 2 for copy of consent form) following explanation of the nature and possible consequences of the study.

3.2.3 Measurements

Refractive error was determined in both eyes from the mean of five open-view distance autorefractor readings obtained with the Grand Seiko Auto Ref/ Keratometer *WAM-5500* (Grand Seiko Co. Ltd., Hiroshima, Japan). The *WAM-5500* is a binocular open-field autorefractor and keratometer which has been validated and found to be repeatable and accurate compared to subjective refraction (Sheppard and Davies, 2010a). Subjects with spherical or astigmatic refractive error > 0.50 D in either eye were corrected with *Focus Dailies* or *Focus Dailies Toric* disposable soft contact lenses. Functional emmetropia was necessary to ensure near-identical accommodative demand for each subject. All further measurements were taken from the right eye only.

Objective accommodative responses were determined using the *WAM-5500* autorefractor whilst subjects fixated Maltese cross targets in free space at -4 D and -8 D stimulus vergences, presented in random order. The targets subtended a constant angular subtense of 4.6° . Average target luminance and Michelson contrast values were 34.0 cd/m^2 and 82 %, and 30.5 cd/m^2 and 80 %, for the 4 D and 8 D stimuli, respectively. Static accommodation responses have been found to be comparable across this range of target luminances (Johnson, 1976). The left eye was occluded with a patch during measurement of the response and subjects were instructed to “carefully focus” (Stark and Atchison, 1994) on the centre of the Maltese cross to induce both voluntary and reflex

accommodation (Radhakrishnan and Charman, 2007a). It was ensured at this stage that participants had sufficient subjective accommodative amplitude to maintain clarity of the 8.0 D stimulus, required for ciliary muscle imaging. Five readings were obtained at each stimulus level, and the mean of these values was used in conjunction with the distance autorefractor results to determine the objective accommodative response.

Axial lengths were obtained from the mean of five partial coherence laser interferometry (PCI) readings, using the commercially-available *IOLMaster* (Carl Zeiss Meditec, Inc., Dublin, CA). The *IOLMaster* is a high-resolution non-contact device developed principally for determination of ocular biometry prior to cataract extraction with intraocular lens implantation (Santodomingo-Rubido *et al.*, 2002) and has a resolution of 0.01 mm for axial length measures (Drexler *et al.*, 1998; Mallen *et al.*, 2006). For subjects corrected with soft contact lenses, axial length measurement was conducted at the end of data collection, following lens removal.

3.2.4 Ciliary Muscle Image Acquisition and Analysis

Images were obtained of nasal and temporal ciliary muscle of the right eye at stimulus vergence levels of -0.19 D, -4 D and -8 D. The high vergence level of -8 D was selected to induce near-maximal non-pharmacologically induced accommodative changes in ciliary muscle. The AS-OCT was set to high-resolution corneal mode for all imaging, providing axial resolution of approximately 8 μm (Baikoff, 2006). The device employs low-coherence interferometry, with a 1310 nm superluminescent light-emitting diode. The scanning spot moves rapidly across the eye, acquiring 512 A-scans in 0.25 seconds in high resolution mode, to generate a 2-dimensional image covering an area measuring 10 mm in width and 3 mm in depth. The scanning plane was set horizontally, at 0°, throughout the investigation.

Maltese cross targets were used for fixation, positioned at an angle of 40°, such that the eccentric gaze of the subject, whilst their head was in the primary position on the chin and forehead rest, allowed images centred on the ciliary muscle, rather than the cornea, to be captured. 40° represented the minimum level of horizontal eye movement needed to view the distant targets, beyond the AS-OCT device, and meant that the optical axis of the instrument was through the sclera, rather than the cornea, reducing optical distortion. The distant target was viewed through a mirror, resulting in a stimulus vergence of -0.19 D. Near targets, subtending 4.6°, were suspended in free space from an adjustable apparatus mounted on the AS-OCT headrest (Figure 3.1). Average luminance and Michelson contrast values were 38 cd/m^2 and 81 %, and 32 cd/m^2 and 78 % for the 4 D

and 8 D stimuli, respectively. For each of the two sides of the eye imaged, all targets were positioned along the same axis, with subjects asked to ensure that the near stimuli appeared directly over the distant Maltese cross to reduce the possibility of varying acquisition planes. Targets of the varying stimulus vergence levels were presented in random order, and multiple images were acquired of nasal and temporal ciliary muscle in each accommodative state, ensuring good visibility of the muscle in at least three images wherever possible. During the image capture process, which lasted approximately 5-10 seconds per scan, subjects were again asked to “carefully focus” on the centre of the cross. A code was used to store the multiple image sets for each subject on the AS-OCT hard-drive, such that the examiner performing *post hoc* analysis of ciliary muscle biometry was masked to the stimulus demand level and the refractive error of the individual.

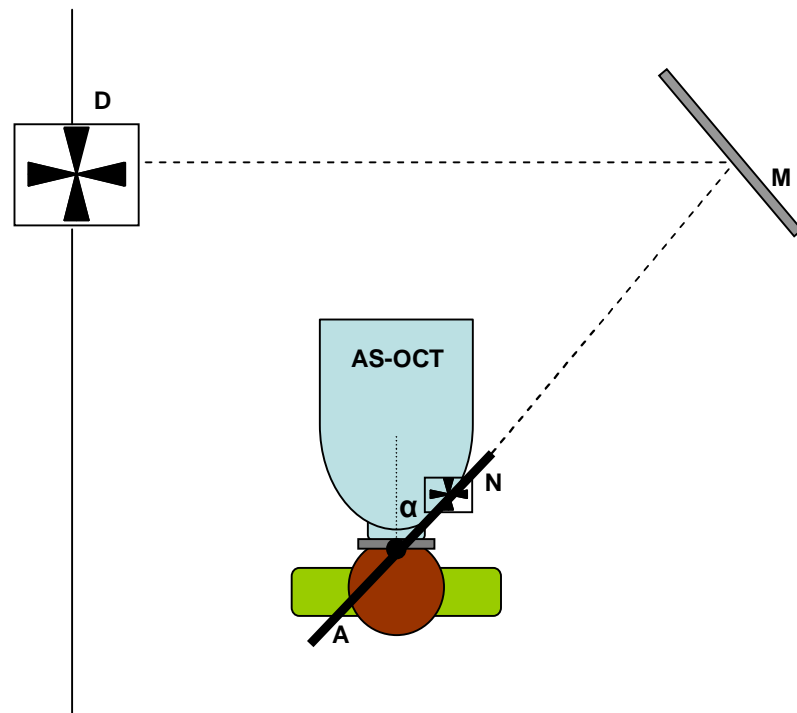


Figure 3.1. Schematic diagram of laboratory set-up for imaging nasal ciliary muscle using the AS-OCT. The subject views a near Maltese cross (N) at either -4.0 or -8.0 D stimulus vergence, attached to an adjustable apparatus (A) mounted on the AS-OCT headrest. Angle $\alpha = 40^\circ$. To image the relaxed ciliary muscle, the near target is removed from the apparatus, allowing the subject to view via a mirror (M), a distant Maltese cross (D) positioned on the laboratory wall, resulting in a stimulus vergence of -0.19 D. For clarity, the mirror and distant target used for imaging temporal ciliary muscle have been omitted from the diagram, although these were present throughout the investigation.

Image analysis was performed by one examiner (ALS) using the inbuilt *Visante* software (version 2.0), which utilises edge detection algorithms to locate corneal surfaces and assign appropriate refractive indices to each portion of the image and adjust its dimensions (Baikoff *et al.*, 2004a). An index of 1.000 (air) is applied to the region anterior to the cornea, 1.338 (cornea) for the area within the corneal boundaries, and 1.343 (aqueous humour) for structures posterior to the cornea (Richdale *et al.*, 2008). A refractive index of 1.000 was applied to the whole image prior to taking measurements, using the “Edit Surfaces” option. Following adjustment of the applied refractive index, the *Visante* callipers were used to measure a range of ciliary muscle biometric characteristics. The software allows up to seven callipers to be positioned simultaneously on each image, with the option of hiding from view those not required, for example, if obscuring the region required for another measure. Overall visible ciliary muscle length was defined as the antero-posterior distance from the scleral spur, representing the anterior insertion, to the posterior tip of the ciliary muscle (Fig. 3.2). Due to intra-individual variability in the relative visibility of these landmarks on different images, each subject’s images for one stimulus vergence level were examined before measurements were taken, with adjustment of brightness and contrast settings where necessary, to facilitate localisation of these points. Additionally, *Visante* software version 2.0 allows the operator to magnify the image, and more accurately place the callipers. Anterior length was measured from the point of maximum width of the ciliary muscle to the scleral spur. To obtain this measurement, a calliper was first placed along the widest portion of the ciliary muscle, and a second calliper, perpendicular to the first, was used to determine the distance from the widest region to the scleral spur (Fig. 3.2). In addition to lengths, a range of width measurements were obtained, judged from the ciliary muscle-sclera boundary, to the pigmented ciliary epithelium. Width measurements (including determination of maximum width) were always obtained using a calliper positioned perpendicular to the ciliary muscle-sclera boundary. Three key width measures were acquired, selected because of the known anterior shift of the ciliary muscle with contraction (Duke-Elder, 1961; Tamm and Lütjen-Drecoll, 1996; Ma and Chen, 2004). Using knowledge of the pre-determined overall length, the width of the muscle was determined at the point 25 % of the total length posterior to the scleral spur (CM25; Fig.3.3). Similar measures were obtained at locations 50 % and 75 % of the overall ciliary muscle length posterior to the scleral spur (CM50 and CM75, respectively; Fig. 3.3). Additionally, the ciliary muscle thickness at a set location 2 mm posterior to the scleral spur was determined (CM2). Bailey *et al.* (2008) included this width measurement in image analysis, and found it was negatively correlated with refractive error in children.

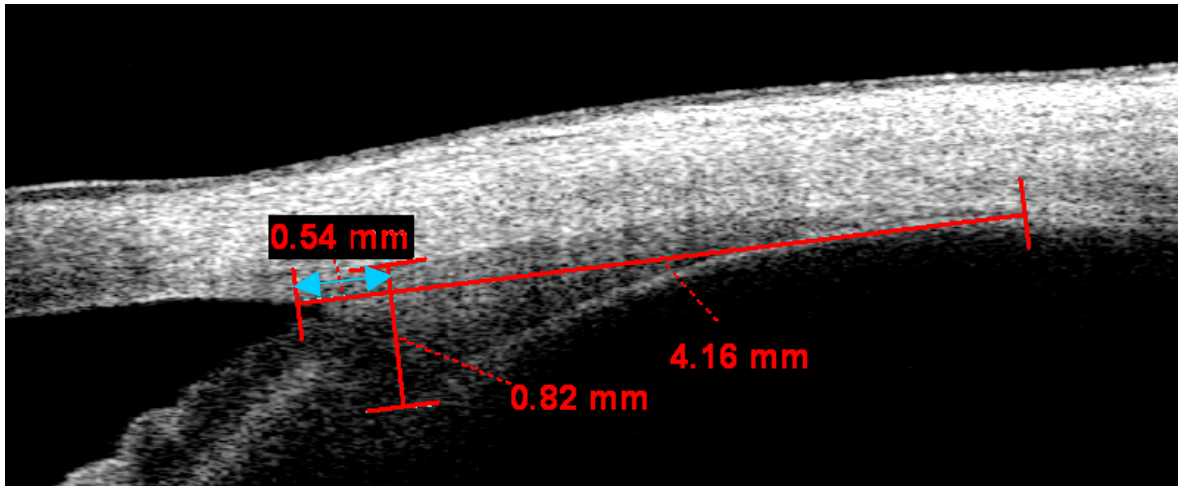


Figure 3.2. Measurement of ciliary muscle length, from the scleral spur to posterior visible limit (here, 4.16 mm) and ciliary muscle anterior length, from the point of maximum width (indicated by the calliper 0.82 mm in length) to the scleral spur (here, 0.54 mm; double-ended arrow)

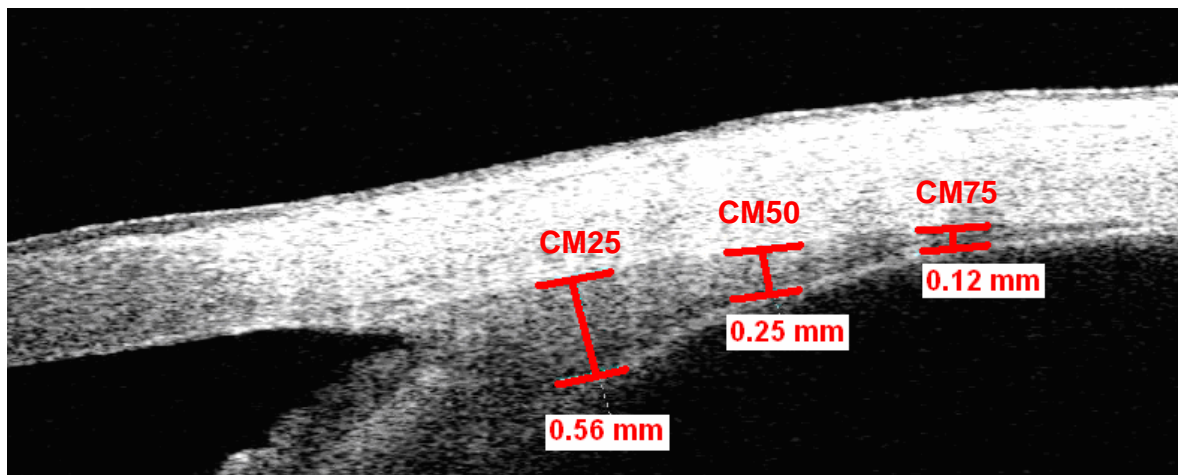


Figure 3.3. Measurement of ciliary muscle width parameters (in same eye as Fig. 3.2). CM25, CM50 and CM75 are ciliary muscle widths at 25, 50 and 75 % of total ciliary muscle length, respectively. Here, CM25 is 0.56 mm, CM50 is 0.25 mm and CM75 is 0.12 mm.

The refractive index of 1.000 applied during image analysis would not be appropriate for analysis of thickness measures, and would cause an overestimation of these parameters, as the index of the ciliary muscle is significantly higher than this value. Reports in the literature suggest the refractive index of the ciliary muscle to be in the region of 1.382 (Tearney *et al.*, 1995; Dirckx *et al.*, 2005), so all thickness measures were divided by this value to provide more realistic data. Following analysis of the three images of nasal and temporal ciliary muscle for each accommodative state, in which the muscle appeared best defined, mean values for each of the length and width parameters (adjusted for refractive index) were entered into a spreadsheet (*Excel*; Microsoft, Redmond, WA) and used for statistical analyses. Knowledge of the objective responses to the -4 D and -8 D stimuli allowed determination of the changes in ciliary muscle parameters per dioptre of accommodation for

each subject. Using mean values of ciliary muscle response per dioptre of objective accommodation, from all 50 participants, allows description of the cohort as a whole.

3.2.5 Statistical Analysis

The relationship between axial length and both ciliary muscle overall length and anterior length was determined using linear regression analysis, performed with *SigmaPlot* graphing software (Version 11, Systat Software Inc., Chicago, Illinois, USA). To assess the differences in ciliary muscle parameters with accommodation, and to determine whether any changes observed were dependent on either axial length or nasal/ temporal aspect, two-way mixed factor Analyses of Variance (ANOVAs) were performed using *SPSS* statistical software (Version 15, SPSS Inc., an IBM Company, Chicago, Illinois, USA). Eyes were classified into tertiles based on axial length for ANOVA purposes. Demand, the within subjects factor, was assigned three levels, of 0.19, 4 and 8 D, whilst the side (nasal or temporal) and axial length (short, medium or long) were designated between-subjects factors. A significance level of $\alpha = 0.05$ was used throughout analysis.

3.2.6 Repeatability

The repeatability of ciliary muscle measures and examiner interpretation was assessed initially by imaging and analysing the ciliary muscle of a single subject ten times at -0.19 D stimulus vergence. The subject removed and repositioned their head on the AS-OCT forehead and chin rest before each image was acquired. Furthermore, to assess intersession repeatability, the temporal ciliary muscle of a subset of ten subjects was imaged at -0.19 D (minimal) and 8.0 D (maximal) stimulus vergence at a second session, within two weeks of the initial visit. The temporal ciliary muscle aspect was chosen for intersession repeatability measures as it has been shown that the scleral spur is most easily discernible on the nasal side (Sakata *et al.*, 2008), thus it would be expected that temporal ciliary muscle measures would be associated with greater variability. The bias for each ciliary muscle parameter was calculated from the mean difference in measures between visits and paired t-tests used to determine whether the levels of bias were significantly different from zero. The limits of agreement (LoA), i.e. the interval over which 95 % of the differences between the two visits lie (Altman and Bland, 1983; Bland and Altman, 1986) were established using the standard deviation (SD) of differences with the following formula:

$$\text{LoA} = \text{bias} \pm (1.96 * \text{SD of differences}) \quad \text{Equation 3}$$

3.3. Results

A wide range of refractive error was found amongst the cohort, from -9.50 to +0.88 D mean sphere equivalent (MSE; mean -2.00 ± 2.62 D) and consequently, axial lengths were broadly spread, from 22.17 to 28.12 mm (mean 24.49 ± 1.13 mm). Mean objective accommodative responses to the 4.0 and 8.0 D stimuli were 2.82 ± 0.58 D and 5.44 ± 0.97 D, respectively. The general characteristics of ciliary muscle biometric parameters at stimulus levels of 0.19, 4.0 and 8.0 D are summarised in Table 3.2.

CM parameter	NASAL			TEMPORAL		
	0.19 D	4.0 D	8.0 D	0.19 D	4.0 D	8.0 D
Overall length (μm)	4630 \pm 470	4470 \pm 460	4440 \pm 480	4810 \pm 690	4620 \pm 590	4520 \pm 610
Anterior length (μm)	860 \pm 120	780 \pm 110	750 \pm 130	900 \pm 140	740 \pm 150	680 \pm 150
CM25 (μm)	535 \pm 51	550 \pm 51	564 \pm 58	550 \pm 51	571 \pm 58	586 \pm 72
CM50 (μm)	297 \pm 43	297 \pm 36	297 \pm 43	347 \pm 43	333 \pm 43	333 \pm 51
CM75 (μm)	152 \pm 22	152 \pm 15	152 \pm 22	174 \pm 22	166 \pm 22	166 \pm 22
CM2 (μm)	347 \pm 58	340 \pm 58	340 \pm 58	405 \pm 58	384 \pm 65	384 \pm 65

Table 3.2. Mean values (\pm S.D.) for nasal and temporal ciliary muscle parameters with accommodative stimulus level. n = 50 eyes.

3.3.1 Repeatability

The repeatability results of ciliary muscle measures assessed by imaging and analysing a single subject ten times at -0.19 D stimulus vergence are shown in Table 3.3, whilst intersession repeatability is summarised in Table 3.4. None of the amounts of bias reported in table 3.4 are statistically significantly different from zero, (using paired t-tests) at either the minimal or maximal accommodative stimulus level.

CM Parameter	Mean value and S.D. (μm)
Overall length	4570 \pm 32.2
Anterior length	870 \pm 26.4
CM25	485 \pm 9.6
CM50	326 \pm 11.4
CM75	166 \pm 5.1
CM2	369 \pm 27.5

Table 3.3. Repeatability of ciliary muscle biometric measures, assessed by imaging and analysing a single subject ten times at the minimal accommodative state.

Parameter	0.19 D stimulus level			8 D stimulus level		
	Bias	SD of differences	95 % LoA	Bias	SD of differences	95 % LoA
Overall length (μm)	-15.0	105.9	-222.8, +192.8	-39.7	95.8	-227.5, +148.1
Anterior length (μm)	-4.0	46.0	-94.2, +86.2	18.3	16.3	-13.7, +50.3
CM25 (μm)	-5.8	11.4	-28.1, +16.4	5.6	10.3	-14.7, +25.8
CM50 (μm)	2.9	12.4	-21.3, +27.2	2.5	10.3	-17.6, +22.6
CM75 (μm)	0.3	3.7	-6.9, +7.5	0.6	10.3	-19.5, +20.7
CM2 (μm)	-3.5	12.1	-27.4, +20.2	6.8	15.5	-23.5, +37.1

Table 3.4. Intersession repeatability data of ciliary muscle biometric parameters measured at 0.19 D and 8.0 D accommodative demand levels. None of the measures of bias are significantly different from zero (paired t-tests).

3.3.2 Ciliary Muscle Biometry and Changes with Accommodation

Mean relaxed ciliary muscle overall length was 4630 \pm 470 μm and 4810 \pm 690 μm on the nasal and temporal aspects, respectively, although the difference between sides was not significant ($F = 1.67$, $P = 0.2$). Anterior length comprised on average, 18.5 % of overall ciliary muscle length in the relaxed state, and was also independent of nasal/ temporal aspect ($F = 2.18$, $P = 0.12$). A positive correlation was identified between axial length and both overall ciliary muscle length and anterior length (Figure 3.4; $r = 0.34$, $P = 0.02$ and $r =$

0.49, $P < 0.001$, respectively). Figure 3.5 shows a sample image of ciliary muscle morphology on the temporal side in a long eye (axial length 28.12 mm) and an emmetropic eye in the shortest tertile (axial length 23.70 mm). The overall ciliary muscle length and anterior length are both noticeably greater in the longer eye.

A statistically significant reduction in both overall ciliary muscle length, and anterior length was found with accommodative effort (Figure 3.4; $F = 42.9$, $P < 0.001$ and $F = 177.2$, $P < 0.001$, respectively). The shortening with accommodation was not dependent on axial length for either overall or anterior length ciliary muscle measures ($F = 0.43$, $P = 0.79$ and $F = 0.60$, $P = 0.67$), although the anterior length showed a significantly greater accommodative reduction on the temporal, compared to the nasal, side ($F = 20.6$, $P < 0.001$). The greatest magnitude of changes in ciliary muscle overall length and anterior length occurred between the 0.19 to 4.0 D, rather than 4.0 to 8.0 D, stimulus levels. For the temporal aspect, overall length decreased on average by $80 \pm 100 \mu\text{m}$ and $50 \pm 120 \mu\text{m}$ per dioptre of accommodative response between the 0.19 to 4.0, and 4.0 to 8.0 D demand levels, respectively. Anterior length reduced by $60 \pm 40 \mu\text{m}$ and $30 \pm 30 \mu\text{m}$ per dioptre of response between the lower and higher demand levels, respectively. It is therefore apparent that most of the shortening in overall ciliary muscle length is as a result of a reduction in the anterior portion, which constitutes only approximately 19 % of overall length in the relaxed state. The mean reductions in anterior length were significantly smaller on the nasal side: $-30 \pm 14 \mu\text{m}$ from 0.19 to 4.0 D and $-20 \pm 20 \mu\text{m}$ from 4.0 to 8.0 D.

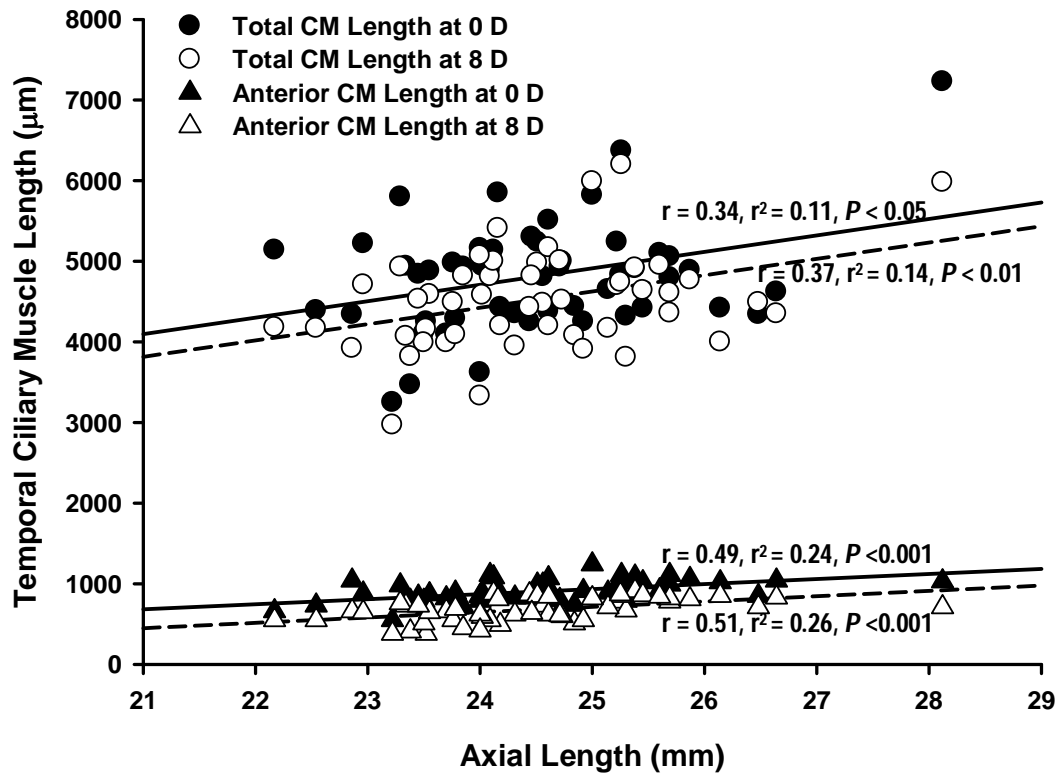


Figure 3.4. Ciliary muscle total length and anterior length in relaxed state and in response to 8 D stimulus. Both ciliary muscle length measures, particularly anterior length, show a positive correlation with axial length. With accommodation, a contractile shortening of ciliary muscle occurs, the majority of which is accounted for by a reduction in the anterior length, which comprises only approximately 19 % of overall length in the relaxed state.

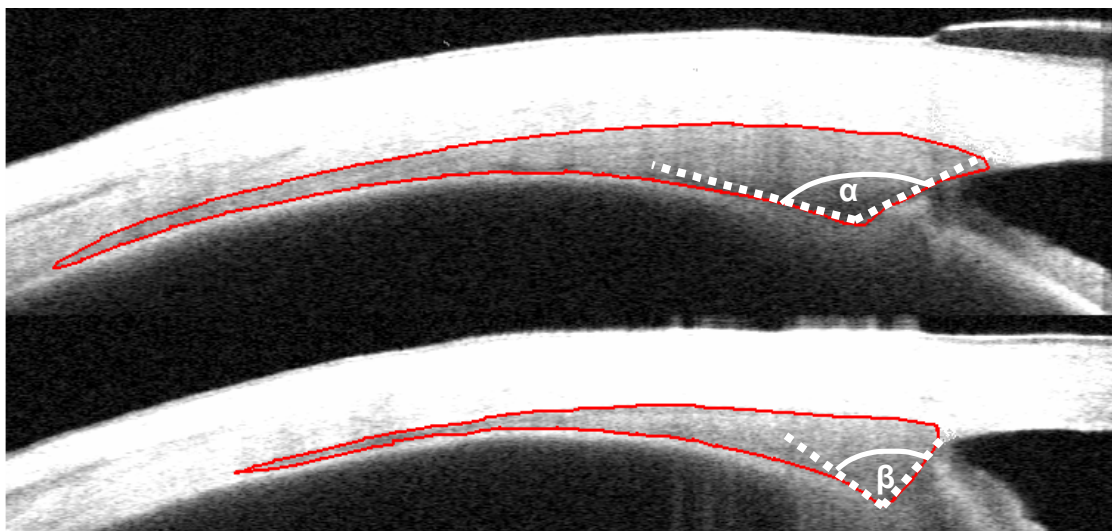


Figure 3.5. Sample images of temporal ciliary muscle morphology in a long, myopic eye (axial length 28.12 mm; upper image) and an emmetropic eye (axial length 23.7 mm; lower image). Ciliary muscle overall length (6580 µm and 4800 µm in the long and short eyes, respectively) and anterior length (from the thickest point to the

scleral spur; 1030 μm and 810 μm in the long and short eyes, respectively) are both noticeably greater in the longer eye. Additionally, the ciliary muscle inner apical angle is larger in the myopic eye ($\alpha = 138^\circ$, $\beta = 92^\circ$).

Considering ciliary muscle thickness, the most anterior portion measured, namely CM25, represented the thickest region at all accommodative stimulus levels, with the more posterior CM50 and CM75 becoming progressively thinner (Table 3.2). The proportional measures of ciliary muscle thickness (CM25, CM50 and CM75) were not dependent on axial length (CM25: $F = 0.16$, $P = 0.86$; CM50: $F = 0.83$, $P = 0.44$; CM75: $F = 2.17$, $P = 0.12$), although CM50 and CM75 were significantly thicker on the temporal, compared to the nasal, aspect ($F = 21.2$, $P < 0.001$ and $F = 15.3$, $P < 0.001$ for CM50 and CM75, respectively). There was a trend for CM25 to be thicker also on the temporal side, although this was not statistically significant ($F = 3.16$, $P = 0.08$). With accommodative effort, there was a statistically significant thickening of CM25 ($F = 46.2$, $P < 0.001$) but neither CM50 nor CM75 changed significantly with accommodation ($F = 1.90$, $P = 0.15$; $F = 1.84$, $P = 0.16$, respectively). A mean increase in CM25 of $7.1 \pm 6.4 \mu\text{m}$ per dioptre of accommodative response was identified.

CM2 thickness measures, taken at a constant 2 mm posterior to the scleral spur are unrelated to the overall length of the ciliary muscle. A trend for CM2 to increase with axial length was identified, although this was not statistically significant at the 0.05 level ($F = 2.84$, $P = 0.06$). CM2 was found to be significantly thicker on the temporal side, compared to the nasal aspect ($F = 17.8$, $P < 0.001$). Mean values in the relaxed state were $347 \pm 58 \mu\text{m}$ and $405 \pm 58 \mu\text{m}$, on the nasal and temporal sides, respectively. Accommodative effort caused a statistically significant thinning of CM2 ($F = 13.1$, $P < 0.001$), particularly on the temporal side ($F = 3.4$, $P = 0.04$), with the vast majority of the change occurring between the 0.19 to 4.0 D stimuli, rather than 4.0 to 8.0 D. Mean changes in CM2 thickness per dioptre of accommodative response were $-2.2 \pm 11 \mu\text{m}$ from 0.19 to 4.0 D and $0 \pm 19 \mu\text{m}$ from 4.0 to 8.0 D on the nasal side. Temporally, these changes were greater, at $-7.0 \pm 13 \mu\text{m}/\text{D}$ of accommodative response from 0.19 to 4.0 D stimuli and $-1.1 \pm 12 \mu\text{m}$ between the 4.0 and 8.0 D levels.

3.4. Discussion

There is a paucity of literature documenting *in vivo* changes in human ciliary muscle biometry with accommodation. Recent advances in ophthalmic imaging technology allow the ciliary muscle to be more easily visualised, and imaged with sufficient resolution to detect accommodative changes. To date, this study is the largest reporting the relaxed and

accommodated morphological characteristics of ciliary muscle biometry in an adult population, using AS-OCT.

In the unaccommodated state, the ciliary muscle was found to be significantly longer, both in terms of overall length and anterior length, in eyes with a greater axial length. No statistically significant nasal *versus* temporal difference in ciliary muscle length measures was identified. The proportional measures of ciliary muscle thickness (CM25, CM50 and CM75) were not dependent upon axial length, although CM2, measured at a fixed distance of 2 mm posterior to the scleral spur, showed a trend towards being thicker in longer eyes ($F = 2.84$, $P = 0.06$). Regarding nasal *versus* temporal thickness characteristics, CM50, CM75 and CM2 were all significantly greater temporally. For the most anterior location measured, CM25, the nasal/temporal asymmetry was less pronounced ($F = 3.16$, $P = 0.08$). Nasal *versus* temporal differences in human ciliary muscle thickness have not been reported in an *in vivo* study previously, and the relevance of this asymmetry is unclear. It is feasible that a stronger contractile response would occur on the side where the ciliary muscle is thickest; the greater accommodative shortening of the anterior portion of the ciliary muscle on the temporal side ($F = 20.6$, $P < 0.001$) observed in this study supports this premise. Nasal/ temporal variation in ciliary muscle morphology and contractile response could have implications in strategies being developed to surgically restore accommodation to presbyopic eyes, such as accommodating intraocular lenses and capsular bag refilling. Ocular asymmetry in the anatomy of the ciliary region has been documented in living rhesus monkeys (Glasser *et al.*, 2001), and it has been suggested that nasal/ temporal anatomical variations may be a functional necessity in primates, enabling alignment of the lenticular axes on the object of regard and maintaining binocular single vision during the convergent eye movements that accompany accommodation.

Previously published studies have identified a strong negative correlation between refractive error/ axial length and ciliary body thickness, particularly at the point 2 mm posterior to the scleral spur (CB2). Bailey *et al.* (2008) used AS-OCT with an applied refractive index of 1.000 to measure ciliary body thickness in children. After adjustment of their results to the 1.382 index used in the present investigation, they found the mean nasal CB2 to be 415 μm in emmetropes and 455 μm in myopes, whilst Schultz *et al.* (2009) reported a mean nasal CB2 of 437 μm in children with refractive errors from -6.00 to +3.44 D, but of the same age range. Using equivalent methodology as these investigations, the present study has identified a considerably thinner mean nasal CM2 (equivalent to CB2) in adults aged 19 – 34 years, of 340 μm in emmetropes, and 356 μm in myopes. AS-OCT findings therefore, imply that the ciliary muscle is at its thickest during childhood and becomes thinner in adulthood,

when eye growth has ceased, and refractive error stabilised. UBM analysis of a cohort of adults of average age 51.8 years identified mean CB2 to be 490 μm in myopes, and 362 μm in emmetropes, but did not assess youthful subjects (Oliveira *et al.*, 2005). Further investigation using identical methodology across a broad range of age groups is needed to clarify the effect of age on ciliary muscle thickness and the possible implications this may have on refractive error development. Furthermore, thickness measurements taken at a fixed distance from the scleral spur do not take into account the fact that ciliary muscle overall length varies significantly with refractive error, so a point 2 mm from the scleral spur may represent an anatomically different region of the ciliary body in varying refractive error groups. Proportional thickness measures employed in the present investigation (such as CM25, CM50 and CM75) may be more valid in analysing subjects of different refractive error and ensuring that similar regions of the ciliary muscle are compared.

Whilst the present investigation has identified a weaker association between ciliary muscle thickness measures and refractive error than previously published studies, a positive correlation between ciliary muscle length and axial length was found (Fig. 3.4). The correlation with axial length was greater for anterior length measures ($r = 0.49$, $r^2 = 0.24$, $P < 0.001$) than for overall ciliary muscle length ($r = 0.34$, $r^2 = 0.11$, $P = 0.017$). A possible explanation for this observation is that the scleral spur was more readily identifiable in many images than the posterior limit of the ciliary muscle, meaning that the anterior length measures were associated with slightly reduced variability compared with the overall values of muscle length, as indicated by the standard deviations of the repeatability measurements (Table 3.3 and Table 3.4).

Hitherto, no *in vivo* study has documented human ciliary muscle lengths. However, the mean overall relaxed ciliary muscle length measures determined in this investigation of 4.63 mm nasally, and 4.81 mm temporally, are in accordance with previous *in vitro* reports. Pardue and Sivak (2000) found a mean ciliary muscle length of 3.87 mm in atropine-treated eyes, whilst Aiello *et al.* (1992) determined mean lengths of 4.79 mm on the nasal side, and 5.76 mm temporally, although their sample consisted of just 5 adult eyes. The finding that the ciliary muscle is longer in myopic eyes is unsurprising: one would expect the morphology of the ciliary body to alter with elongation of the globe. van Alphen (1986) observed marked thinning of the ciliary body with *in vitro* globe expansion, although the findings of the present study indicate that the ciliary muscle is not simply stretched as the eye elongates. The ciliary muscle was not found to be attenuated in myopic subjects as would be predicted from stretching alone, in fact, no significant relationship between ciliary muscle thickness and refractive error was identified. It seems likely, therefore, that axial elongation is

accompanied by some radial growth/ thickening of the ciliary muscle during myopigenesis. The greater anterior ciliary muscle length in longer eyes indicates that the structure grows in the antero-posterior direction as the globe elongates, with the scleral spur as the fixed anchor point. Figure 3.5 supports this assertion: the inner apical angle of the ciliary muscle is clearly larger in the myopic eye compared to the emmetropic subject. However, *in vivo* measurements of this angle are required to confirm the finding.

The key accommodative changes in ciliary muscle morphology identified in the present investigation are a contractile shortening of both overall length and anterior length, and a thickening of CM25; the most anterior of the thickness measures. These observations support the generally-accepted model of ciliary muscle action during accommodation, whereby the majority of the muscle mass shifts anteriorly and inwards to reduce zonular tension (von Helmholtz, 1855; Atchison, 1995; Croft *et al.*, 2001; Charman, 2008). Whilst the accommodative forward shift of ciliary muscle has been observed *in vivo* in rhesus monkeys using UBM (Croft *et al.*, 2006a; Wasilewski *et al.*, 2008), the movement has not been visualised previously in human subjects, as the iris normally prevents exploration of the ciliary region with most available imaging techniques. Furthermore, a recently-published human *in vivo* MRI study found no change in the antero-posterior position of the ciliary muscle with accommodative effort in either young or presbyopic subjects (Strenk *et al.*, 2010), suggesting that only a centripetal rather than a forward and centripetal shift of muscle mass occurs during accommodation. A case report of accommodation in a 19 year old albino using AS-OCT also failed to observe a concurrent forward shift of the ciliary body with its centripetal accommodative movement (Baikoff *et al.*, 2004b). However the images were not centred on the ciliary region, nor captured in high-resolution mode, and accommodative changes in a single albino subject cannot be considered representative of the population as a whole. The present study found that anterior ciliary muscle length decreased significantly with accommodation, while CM25 thickened. Between 0.19 and 4 D stimulus levels, anterior length reduced on average by $30 \pm 30 \mu\text{m}$ per dioptre of response nasally, and $60 \pm 40 \mu\text{m}/\text{D}$ of accommodation, temporally. This shortening of anterior length represents a movement of the thickest region of the ciliary muscle towards the cornea, i.e. evidence of forward shift of the main muscle mass, whilst the thickening of CM25 by approximately $11 \pm 16 \mu\text{m}/\text{D}$ of response on both sides is indicative of the centripetal ciliary muscle movement.

Therefore, *in vivo* support of anterior, as well as centripetal, ciliary muscle movement with accommodation in a relatively large cohort of human subjects is provided for the first time. However, in addition to the implications of the study, there are limitations which should also be considered. Firstly, the objective measures of accommodation were acquired prior to AS-

OCT scanning and may not represent the precise level of accommodation exerted by each subject during image capture. Simultaneous measurement of refraction and ciliary muscle imaging would be preferable, particularly because of the eccentric (40°) angle required for image acquisition. However, the dimensions of the *Visante* device, which screens much of the subject's face, may hinder such attempts. An appliance mounted on the AS-OCT headrest, employing a beam splitter linked to an autorefractor is being considered and could be custom-manufactured in the future to facilitate simultaneous measurement of accommodation during scanning.

In order to visualise the complete ciliary muscle, it was necessary for subjects to view an eccentrically-positioned target, at an angle of 40°. Therefore, the images of temporal ciliary muscle were captured during convergence, but the nasal muscle was imaged during abduction, which does not represent the natural convergent state of the eye during accommodation. It is not possible to image the entire right nasal ciliary muscle during convergence, with AS-OCT. However, peripheral refraction measures have been found not to vary depending on whether a subject moves their eye or their head (Radhakrishnan and Charman, 2008) implying that the state of convergence does not directly alter refraction. Neither the accommodative response therefore, or the ciliary muscle parameters should have been significantly confounded by state of convergence.

In the present investigation and other previously published studies (e.g. Bailey *et al.* 2008; Schultz *et al.* 2009), optical distortion arising from imaging the ciliary muscle through the overlying sclera has not been accounted for. Consequently, the absolute values of the ciliary muscle parameters described may not accurately reflect the true measures. However, the effect of optical distortion would not vary between the relaxed and accommodated states, meaning that the observations of accommodative changes (e.g. shortening of length and anterior length, and thickening of the anterior portion) are valid. It is also feasible that significant inter-individual differences in scleral thickness could alter the level of optical distortion, and therefore the measurement of ciliary muscle parameters. Similar future investigations could therefore measure scleral thickness, and potentially exclude participants with unusually thick or thin scleras.

As with any two-dimensional imaging technique, there is the potential for image acquisition planes to vary between measurements. To reduce the associated impact, multiple images were acquired and analysed at each stimulus level, and the average values used for statistical analyses. Whilst data collection for this study was underway, an update to the *Visante* software was released (Version 2.0). All analysis was performed with the new

software, which gives the option of zooming whilst viewing images, allowing for easier identification of ciliary muscle boundaries. However, the software update also includes a novel enhanced high resolution imaging mode which takes several scans and automatically generates an averaged image of improved quality than was previously possible. As the majority of data had been collected by the time the new software was released, the enhanced mode was not used for imaging, rather the original high resolution imaging mode was employed to maintain consistency. For future ciliary muscle imaging the authors intend to utilise the enhanced acquisition mode and it is anticipated that the improved detail will reduce the variability of measurements. Even with enhanced image acquisition, determination of the ciliary muscle boundaries, e.g. the posterior visible limit, could still occasionally prove problematic, as in this study. The *post hoc* measurement of ciliary muscle parameters using the manufacturer's software is relatively simple and could be performed by any researcher with access to the *Visante* device, although the subjective nature of the technique is not ideal. The authors are currently exploring the possibility of using custom-developed software with edge detection algorithms to derive objective measures of ciliary muscle parameters. An objective method of analysing the images could enable multiple images to be analysed and averaged more rapidly and reliably than at present.

3.5 Conclusion

In summary, this study has reported for the first time *in vivo* biometric characteristics of relaxed and contracting human ciliary muscle amongst a relatively large adult cohort, using AS-OCT. The ciliary muscle is longer in eyes with axial myopia, and there are nasal/temporal asymmetries in both morphology and accommodative changes in all refractive error groups. The main accommodative changes observed were a shortening of muscle length, particularly in the anterior portion and a thickening of CM25. These findings support the broadly-accepted theory of anterior as well as inward shift of human ciliary muscle mass during accommodation. AS-OCT is a valid and accessible tool for analysing human ciliary muscle, and could be further employed to analyse morphological and contractile characteristics of the muscle with age, which could be relevant to the development of presbyopia.

Supporting publications:

Sheppard A.L. and Davies L. N. (2010b). *In vivo* analysis of ciliary muscle morphological changes with accommodation and axial ametropia. *Investigative Ophthalmology and Visual Science*. In press. doi: 10.1167/iovs.10-5787

Sheppard A.L. and Davies L. N. (2009a). Changes in human ciliary muscle biometry with accommodation: an anterior segment optical coherence tomography study. *Ophthalmic and Physiological Optics*. **29**, 668 (Abstract).

Sheppard A.L. and Davies L. N. (2009b). *In vivo* changes in human ciliary muscle biometry with accommodation. *Investigative Ophthalmology and Visual Science*. **50**, E-Abstract 2796.

CHAPTER 4

THE EFFECT OF AGEING ON *IN VIVO* CILIARY MUSCLE MORPHOLOGY AND CONTRACTILITY

4.1. Introduction

Despite widespread ongoing research directed at restoring accommodation to the ageing eye, the processes responsible for the development of presbyopia are not fully understood (Gilmartin, 1995; Strenk *et al.*, 2005; Charman, 2008; Glasser, 2008). Although lenticular changes are generally accepted to be of major importance (Glasser, 2008; Ziebarth *et al.*, 2008; Truscott, 2009), the precise effects of age on the other components of the accommodative system, and the possible interactions between these changes, remain unclear (Atchison, 1995; Pierscionek and Weale, 1995; Charman, 2008). The crystalline lens is known to increase in mass and axial thickness throughout life, as a consequence of the continual formation of cortical lens fibres (Davson, 1990; Dubbleman *et al.*, 2003). *In vitro* experimentation has demonstrated that the isolated human lens becomes more resistant to deformation with age (Glasser and Campbell, 1999), and thus unable to change shape to provide variable dioptric power. Although much evidence exists to support the lenscentric view of presbyopia development, age-related changes in associated structures including the ciliary muscle (Pardue and Sivak, 2000), choroid (Tamm *et al.*, 1991; Tamm *et al.*, 1992b) and vitreous body (Harocopos *et al.*, 2004) are also likely to have a contributory effect. Of particular relevance is the effect of ageing on ciliary muscle configuration and function, as all of the potential strategies aimed at restoring accommodation to the presbyopic eye, including capsular refilling and increasingly-popular accommodating intraocular lens implants (AIOLs; Glasser, 2008; Sheppard *et al.*, 2010), rely on the continued action of this muscle throughout life.

Age-related changes in ciliary muscle have been documented previously, from a range of primate studies and *in vitro* investigations. *In vivo* data describing the effects of age on human ciliary muscle morphology and function are scarce (Strenk *et al.*, 2005), as the iris prevents direct visualisation of the ciliary region (Park *et al.*, 2008). *Post mortem* microscopic examination of human ciliary body tissue sections has revealed that the ciliary muscle decreases in both length and area with age (Tamm *et al.*, 1992a; Pardue and Sivak, 2000). Pardue and Sivak (2000) found that anterior ciliary muscle length (measured perpendicular from the line of maximum muscle thickness, to the scleral spur) showed a greater reduction with age than overall length measures: in a relatively small sample of 16 pairs of eyes, mean anterior length was approximately 680 μm in donors aged under 34

years, and 550 μm in older eyes aged up to 107 years. Furthermore, the age-related trends for maximum muscle thickness to increase (Pardue and Sivak, 2000), whilst the distance from the scleral spur to the inner apex of the ciliary muscle decreases (Tamm *et al.*, 1992a), indicate that the human ciliary muscle adopts a more anterior-inward position with advancing age. *In vivo* MRI data support this assertion: reductions in both ciliary muscle ring diameter (Strenk *et al.*, 1999; Strenk *et al.*, 2006) and axial distance from cornea to muscle apex (Strenk *et al.*, 2010) have been observed in presbyopic subjects.

In the primate eye, age-related nasal/ temporal biometric asymmetry develops in the ciliary region. *In vivo* ultrasound biomicroscopic examination of rhesus monkey eyes has identified a more significant reduction in temporal, compared to nasal, circumlental space (CLS) with age (Glasser *et al.*, 2001; Croft *et al.*, 2006b). Additionally, age and temporal CLS (but not nasal CLS) are together a better indicator of accommodative amplitude than age alone (Croft *et al.*, 2006b), suggesting that some process linked to presbyopia development may predominantly impact the temporal aspect of the eye. No such age-related asymmetry has been detected in the human eye using either *in vitro* or *in vivo* methods, although previous authors have failed to clarify the region of ciliary muscle investigated (e.g. Tamm *et al.*, 1992a; Pardue and Sivak, 2000; Strenk *et al.*, 2006). Chapter 3 reports significantly greater ciliary muscle thickness and contractile response (as inferred by reduced anterior length), on the temporal side, compared to the nasal aspect. The observed differences in both morphology and contraction highlight the need to consider nasal and temporal ciliary muscle regions separately.

Ciliary muscle contractile changes with age have previously been more widely studied in the primate eye, partly because surgical iridectomy permits visualisation of the ciliary body (Croft *et al.*, 2006b). *In vivo* investigations have indicated that ageing rhesus monkey ciliary muscle maintains its centripetal contractile response (Croft *et al.*, 2008), but the associated forwards movement is significantly reduced (Croft *et al.*, 2006a; Croft *et al.*, 2009). Furthermore, *in vitro*, the pharmacologically-induced contractile responses of isolated strips of monkey ciliary muscle do not vary markedly with age (Tamm *et al.*, 1992b; Poyer *et al.*, 1993), but in ocular sections where the posterior limit of the muscle is undisturbed, the response to muscarinic agonists is lost in older eyes (Tamm *et al.*, 1992b). An age-related accumulation of inelastic collagenous material has been postulated to cause reduced compliance of the posterior insertion of the ciliary muscle, restricting anterior mobility and contributing to presbyopia (Tamm *et al.*, 1991).

Conversely, in the human eye, the effects of age on ciliary muscle contractility are contentious, with some contradictory findings in previously published studies. Human ciliary muscle has been shown *in vitro* to maintain its contractile response to pilocarpine administration, demonstrating a reduction in length and maximum width, even in eyes with advanced presbyopia (Pardue and Sivak, 2000). However, *in vitro* studies alone are insufficient to confirm the contractile changes in ciliary muscle with age (Strenk *et al.*, 1999). *Post mortem* tissue changes and ischaemic effects could alter the response of the muscle to topically-applied pharmacological agents (Pardue and Sivak, 2000). Furthermore, samples from sectioned eyes may not accurately reflect the *in vivo* responses of human ciliary muscle.

Hitherto, high resolution MRI (Strenk *et al.*, 1999; Strenk *et al.*, 2006; Strenk *et al.*, 2010) and ultrasound biomicroscopy (UBM; Park *et al.*, 2008) have been utilised to analyse *in vivo* the contractility of ageing ciliary muscle. Park *et al.* (2008) observed minimal inwards ciliary body movement following pilocarpine administration in a cohort of 15 presbyopic subjects (mean age 65.3 years) prior to cataract surgery. Post-operatively, pharmacologically-induced centripetal movement significantly increased, suggesting that lenticular sclerotic changes may hinder ciliary muscle contractility in older eyes, due to altered anterior segment geometry. In contrast to these findings, published MRI data indicate that the inwards contractile movement of the ciliary muscle is undiminished by age (Strenk *et al.*, 1999; Strenk *et al.*, 2006), and not affected by intraocular lens (IOL) implantation (Strenk *et al.*, 2006). Human ciliary muscle ring diameter decreases by approximately 0.025 mm per year, but the mean reduction of 0.64 ± 0.05 mm in this parameter in response to an 8 D stimulus was found to be independent of subject age. In pseudophakic eyes, the contractile change in ciliary muscle ring diameter was statistically identical to contralateral phakic eyes (Strenk *et al.*, 2006). A further, recently-published, MRI study analysing ciliary muscle action *in vivo* identified an age-independent increase in ciliary muscle thickness with accommodation, in volunteers aged from 22- 91 years (Strenk *et al.*, 2010). However, no anterior contractile movement of the muscle apex was observed in any of the 32 phakic subjects, challenging the generally-accepted model of accommodation, in which a concurrent forwards and inwards shift of ciliary muscle mass acts to reduce tension on the zonules (von Helmholtz, 1855; Croft *et al.*, 2001; Charman, 2008).

The majority of available evidence, therefore, from both *in vitro* and *in vivo* studies, indicates that human ciliary muscle maintains its contractile ability long after the onset of presbyopia, although whether the nature of the response varies with age is less obvious. Pilocarpine is known to cause powerful ciliary muscle contraction and act as a superstimulus to

accommodation (Koepl *et al.*, 2005; Kriechbaum *et al.*, 2005; Uthoff *et al.*, 2009), so the use of such pharmacological agents should ideally be avoided to analyse natural ciliary muscle function *in vivo*. The findings detailed in Chapter 3 provide support for an anterior, as well as centripetal, shift of ciliary muscle mass during stimulus-driven accommodation, but whether this pattern of response persists in older eyes is unknown.

Regarding ciliary muscle morphology, age-related reductions in length (particularly of the anterior portion) and area have been documented *in vitro*, but not yet confirmed *in vivo*. *In vitro* and MRI data indicate that the human ciliary muscle increases in maximum width throughout life, and slowly adopts a more anterior-inward position. Possible nasal *versus* temporal variations in age-dependent morphological changes have not previously been investigated in the human eye, although asymmetry has been shown to develop in the monkey ciliary region. There is a lack of published *in vivo* data collected using the same high-resolution methodology across a broad range of age groups documenting the effects of age on human ciliary muscle morphology and contractility. Anterior segment optical coherence tomography (AS-OCT) has been shown in Chapter 3 to be a valid tool for analysis of ciliary muscle biometry, with an axial resolution of up to 8 μm (Nubile *et al.*, 2008), which is superior to the values of 0.156 mm (Strenk *et al.*, 1999; Strenk *et al.*, 2006) and more recently, 0.078 mm (Strenk *et al.*, 2010), reported in previous MRI based studies.

The aim of this study, therefore, is to provide new high-resolution *in vivo* data on the age-related changes in human ciliary muscle morphology, utilising AS-OCT. The possible development of nasal *versus* temporal asymmetry in these changes will be explored, with a consideration of the implication on presbyopia development. Furthermore, the accommodative responses of ageing ciliary muscle will be compared to those of young eyes to attempt to clarify the effects of age on contractility. An improved understanding of ciliary muscle morphology and function with advancing age would assist in the development of strategies aimed at restoring accommodation to the presbyopic eye.

4.2. Methods

4.2.1 Subjects

A cohort aged 35 years and over was required for the study, to investigate ciliary muscle characteristics from incipient presbyopia onwards. The data acquired from this sample were compared with the young cohort described in Chapter 3 (Sheppard and Davies, 2010b), aged 19- 34 years (mean 25.8 ± 4.5 years). Twenty nine older volunteers aged 35- 70 years, with no history of ocular abnormality or intraocular surgery were recruited for the study, using email announcements at Aston University. The mean age of older participants

was 46.3 ± 10.2 years. Subjects with all types of refractive error were included, provided their distance prescription (including astigmatic component, if applicable) was amenable to correction with daily disposable soft contact lenses (*Focus Dailies* and *Focus Dailies Toric*: nelfilcon A, 69 % water content; Ciba Vision, Duluth, Georgia, USA). The parameter ranges for these contact lenses meant subjects with spherical refractive errors greater than -10.00 DS or +6.00 DS were excluded from the investigation, as were those with oblique cylinders > 0.50 DC, or orthogonal cylinders > 1.50 DC. The study was approved by the Ethics Committee of Aston University (see Appendix 1) and was performed in accordance with the tenets of the Declaration of Helsinki. Written, informed consent was obtained from all participants (see Appendix 2 for copy of consent form) following explanation of the nature and possible consequences of the study.

The younger and older cohorts together comprised 79 subjects (40 female, 39 male) aged 19-70 years (mean 33.3 ± 12.2 years). The complete sample therefore represented youthful ciliary muscle, through to incipient and established presbyopia.

4.2.2 Measurements

Data were collected from the older cohort using the methods detailed in Chapter 3 (Sheppard and Davies, 2010b). In brief, the process involved initial determination of objective refractive error in both eyes using the Grand Seiko Auto Ref/ Keratometer WAM-5500 (Grand Seiko Co. Ltd., Hiroshima, Japan; Sheppard and Davies, 2010a). Subjects with spherical or astigmatic error >0.50 D in either eye were corrected with *Focus Dailies* or *Focus Dailies Toric* disposable soft contact lenses to provide functional emmetropia at infinity, ensuring the accommodative demand was comparable for all participants. All further measurements were taken from the right eye only.

Objective responses to 4.0 and 8.0 D accommodative stimuli (Maltese crosses) were determined with the WAM-5500, whilst the left eye was occluded with a patch. Many of the older participants were unable to attain/ maintain clarity of either the 4.0 or 8.0 D targets, but were instructed to concentrate on the Maltese cross and make an effort to focus on it (Stark and Atchison, 1994). Blurred targets have been shown to stimulate ciliary muscle contraction, even in advanced presbyopes (Strenk *et al.*, 1999; Strenk *et al.*, 2006; Strenk *et al.*, 2010). Axial length was next determined from the mean of 5 readings obtained with the Zeiss *IOLMaster* (Santodomingo-Rubido *et al.*, 2002). For those subjects corrected with soft contact lenses, axial length was measured once the lenses had been removed, following ciliary muscle image acquisition.

AS-OCT images were obtained of nasal and temporal ciliary muscle in the relaxed state and whilst viewing 4.0 and 8.0 D accommodative stimuli, as previously described in section 3.2. All participants were instructed to “carefully focus” on the accommodative stimuli during image acquisition, even if they were unable to maintain a clear image of the target. Imaging was performed with the AS-OCT in high-resolution corneal mode throughout.

4.2.3 Image analysis

In the same manner described in section 3.2, image analysis was performed by one examiner (ALS) using the inbuilt *Visante* software (version 2.0). The examiner was masked to the accommodative state of subjects by use of a code to save image sets following scan acquisition. A refractive index of 1.000 was manually applied to all images prior to analysis. In addition to the ciliary muscle length and thickness measures detailed in Chapter 3, two further parameters, which may be relevant to the development of presbyopia, were determined from the OCT images. Ciliary muscle maximum thickness (Figure 4.1a) was measured using a calliper extending from the inner apex of the muscle to the muscle/ sclera boundary. As with all thickness measures detailed in the investigation, the calliper was positioned perpendicular to the muscle/ sclera interface. The distance from the scleral spur to the inner apex of the muscle (Figure 4.1b) was also determined to investigate the age-related shift in ciliary muscle location.

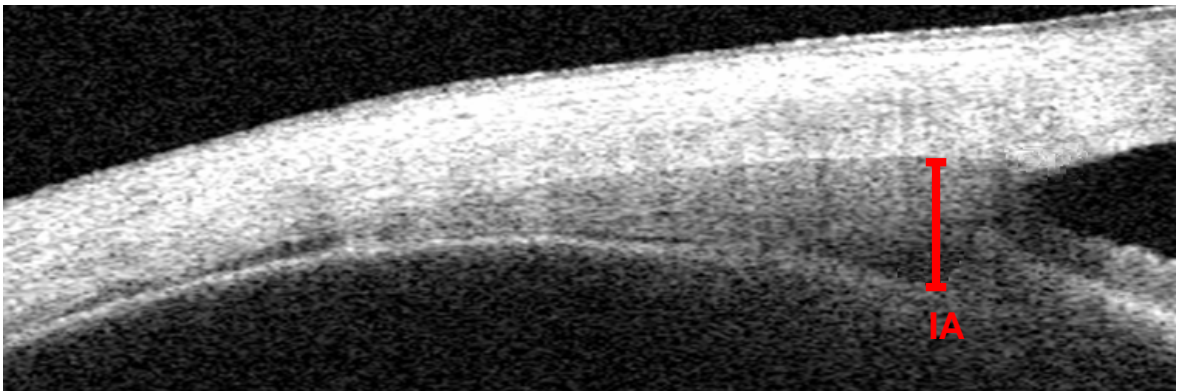


Figure 4.1a. Measurement of temporal ciliary muscle maximum thickness. A calliper positioned at the inner apex (IA) is extended to the ciliary muscle/ sclera interface. Here, maximum thickness = 0.66 mm (emmetropic subject, aged 26 years).

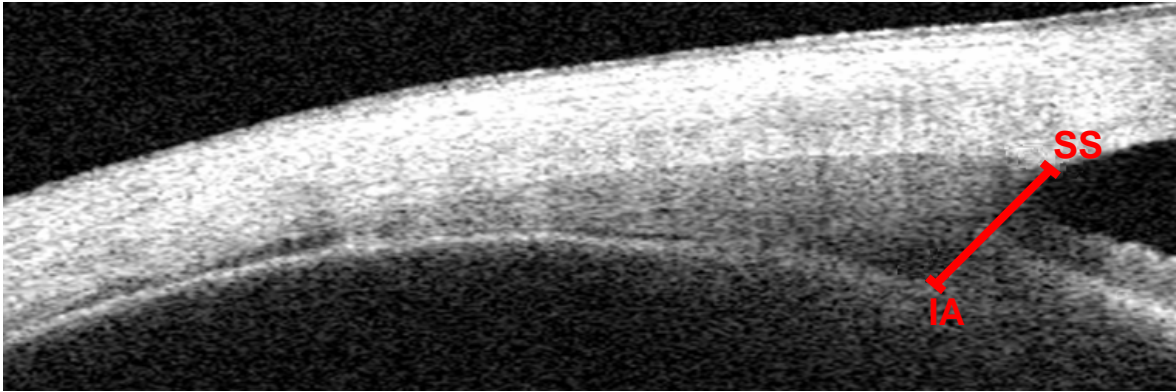


Figure 4.1b. Measurement of distance from inner apex (IA) to scleral spur (SS) on the temporal side. Here, distance from inner apex to scleral spur = 1.08 mm (same eye as Fig. 4.1a).

Following analysis of the three nasal and temporal images in which the ciliary muscle was most clearly defined, using an applied refractive index of 1.000, all width measures were divided by 1.382, which is a more valid index for the ciliary muscle (Tearney *et al.*, 1995; Dirckx *et al.*, 2005). Mean values for all length and width measures (adjusted for refractive index) were entered into a spreadsheet (*Excel*; Microsoft, Redmond, Washington, USA) and used for statistical analyses.

4.2.4 Statistical analysis

Linear regression analysis using *SigmaPlot* graphing software (Version 11, Systat Software Inc., Chicago, Illinois, USA) was performed to determine the effect of age (independent variable) on nasal and temporal ciliary muscle morphological characteristics. The mean and standard deviation for each parameter was calculated if significant correlation with age was not found at the $\alpha = 0.05$ level. To investigate the effect of age on ciliary muscle contractile responses, the difference between CM25, overall length and anterior length (the main parameters which showed an accommodative change in Chapter 3) at 0.17 and 8.0 D was calculated for each subject. Linear regression analysis was then used to determine any dependence of the magnitude of response with age.

Emmetropic and myopic eyes were considered separately, whilst the few hyperopic participants were analysed in conjunction with the emmetropes, as these eyes have not undergone myopic axial elongation, which has been proposed as a cause of altered ciliary muscle characteristics (Sheppard and Davies, 2010b)

4.3. Results

The total cohort of 79 subjects comprised 45 emmetropes/ hyperopes (mean spherical equivalent; MSE: -0.75 to +2.33 D) with a mean age of 34.7 ± 12.8 years, and 34 myopes (MSE > -0.75 D), with a mean age of 31.5 ± 11.5 years. A wide range of refractive error was found amongst the whole cohort, ranging from -9.50 D to +2.33 D MSE, which was reflected by the broad spread of axial lengths, from 21.75 to 28.12 mm (mean 24.31 ± 1.20 mm). Mean refractive error and axial length values for the emmetropic participants (including the 6 hyperopes, with MSE > +1.00 D) were $+0.31 \pm 0.70$ D and 23.68 ± 0.83 mm, respectively, and -3.87 ± 2.21 D and 25.00 ± 1.17 mm, respectively, for the myopes. Table 4.1 summarises the effect of age on nasal and temporal ciliary muscle biometric characteristics.

4.3.1 Ciliary muscle morphology

Regarding ciliary muscle length measures, neither total length nor anterior length demonstrated a significant dependence on age in myopic eyes, for either the nasal (total length: $r = 0.325$, $P = 0.065$; anterior length: $r = 0.113$, $P = 0.523$) or temporal (total length: $r = 0.253$, $P = 0.150$; anterior length: $r = 0.183$, $P = 0.300$) aspects. In emmetropic eyes, ciliary muscle anterior length decreased significantly with age both nasally ($r = 0.461$, $P = 0.001$) and temporally ($r = 0.619$, $P < 0.001$), whilst no age-related change in overall length was identified for either the nasal ($r = 0.232$, $P = 0.126$) or temporal ($r = 0.009$, $P = 0.952$) side.

Changes in thickness measures with age also displayed some refractive-group dependent asymmetry. CM2, measured at a fixed 2 mm position posterior to the scleral spur, did not demonstrate a significant age-related change in myopic eyes, either nasally ($r = 0.119$, $P = 0.504$), or temporally ($r = 0.196$, $P = 0.266$). However, in emmetropic eyes, CM2 reduced with age on the temporal side, by $2.08 \mu\text{m}/\text{year}$ ($r = 0.387$, $P = 0.009$), but remained constant nasally ($r = 0.193$, $P = 0.009$), with a mean value of $327 \pm 59 \mu\text{m}$.

Table 4.1. Change in ciliary muscle morphological characteristics with age. n = 45 emmetropes/ hyperopes (MSE -0.75 - +2.33 D), mean age 34.7 ± 12.8 years, and 34 myopes (MSE < -0.75 D), mean age 31.5 ± 11.5 years

<i>Ciliary muscle parameter</i>	<i>Side</i>	<i>Change with age</i>	
		<i>Emmetropes</i>	<i>Myopes</i>
Total length	Nasal	No significant change. Mean = 4.53 ± 0.57 mm	No significant change. Mean = 4.84 ± 0.65 mm
	Temporal	No significant change. Mean = 4.69 ± 0.66 mm	No significant change. Mean = 5.07 ± 0.77 mm
Anterior length	Nasal	Decreases: Nasal AL (mm) = 0.989-(0.00546 * age). R = 0.461, P = 0.001	No significant change. Mean = 0.91 ± 0.15 mm
	Temporal	Decreases: Temporal AL (mm) = 1.080-(0.00895 * age). R = 0.619, P < 0.001	No significant change. Mean = 0.92 ± 0.15 mm
CM25	Nasal	No significant change. Mean = 528 ± 44 µm	No significant change. Mean = 541 ± 62 µm
	Temporal	No significant change. Mean = 541 ± 50 µm	No significant change. Mean = 546 ± 66 µm
CM50	Nasal	No significant change. Mean = 284 ± 42 µm	No significant change. Mean = 304 ± 43 µm
	Temporal	Decreases: Temporal CM50 (µm) = 383 – (1.940 * age). R = 0.448, P = 0.002	Decreases: Temporal CM50 (µm) = 581 – (3.810 * age). R = 0.538, P = 0.001
CM75	Nasal	No significant change. Mean = 143 ± 22 µm	No significant change. Mean = 157 ± 22 µm
	Temporal	Decreases: Temporal CM75 (µm) = 184 – (0.760 * age). R = 0.380, P = 0.010	Decreases: Temporal CM50 (µm) = 276 – (1.26 * age). R = 0.410, P = 0.016
CM2	Nasal	No significant change. Mean = 327 ± 59 µm	No significant change. Mean = 372 ± 72 µm
	Temporal	Decreases: Temporal CM2 (µm) = 434 – (2.079 * age). R = 0.387, P = 0.009	No significant change. Mean = 419 ± 74 µm

Regarding the proportional measures of ciliary muscle thickness, the most anterior of these parameters, CM25, did not show any dependence on age either nasally (emmetropes: $r = 0.149$, $P = 0.365$; myopes: $r = 0.019$, $P = 0.917$) or temporally (emmetropes: $r = 0.009$, $P = 0.956$; myopes: $r = 0.211$, $P = 0.231$), for either refractive group. The more posterior CM50 and CM75 parameters showed an age dependent reduction in thickness on the temporal side for both refractive error groups (CM50: emmetropes $r = 0.365$, $P = 0.022$; myopes $r = 0.538$, $P = 0.001$. CM75: emmetropes $r = 0.338$, $P = 0.036$; myopes $r = 0.410$, $P = 0.016$), although nasally, no significant age-related change was identified for either of these measures (CM50: emmetropes $r = 0.076$, $P = 0.647$; myopes $r = 0.129$, $P = 0.469$. CM75: emmetropes $r = 0.037$, $P = 0.821$; myopes $r = 0.288$, $P = 0.100$).

Ciliary muscle maximum width and distance from inner apex to scleral spur measures were obtained from only 37 of the 79 participants, due to technical problems encountered with the *Visante* device (hard-drive failure and unrecoverable image files). Despite the reduced data sets, the power of all statistical tests performed to ascertain the effect of age on these parameters was 0.80 or above. Ciliary muscle maximum width increased significantly with age, by $2.8 \mu\text{m}/\text{year}$ nasally ($r = 0.54$, $P < 0.001$) and $3.0 \mu\text{m}/\text{year}$ temporally ($r = 0.44$, $P = 0.007$). No significant difference between nasal and temporal maximum width measures was identified ($P = 0.673$). Figure 4.2 illustrates graphically the effect of age on maximum ciliary muscle width.

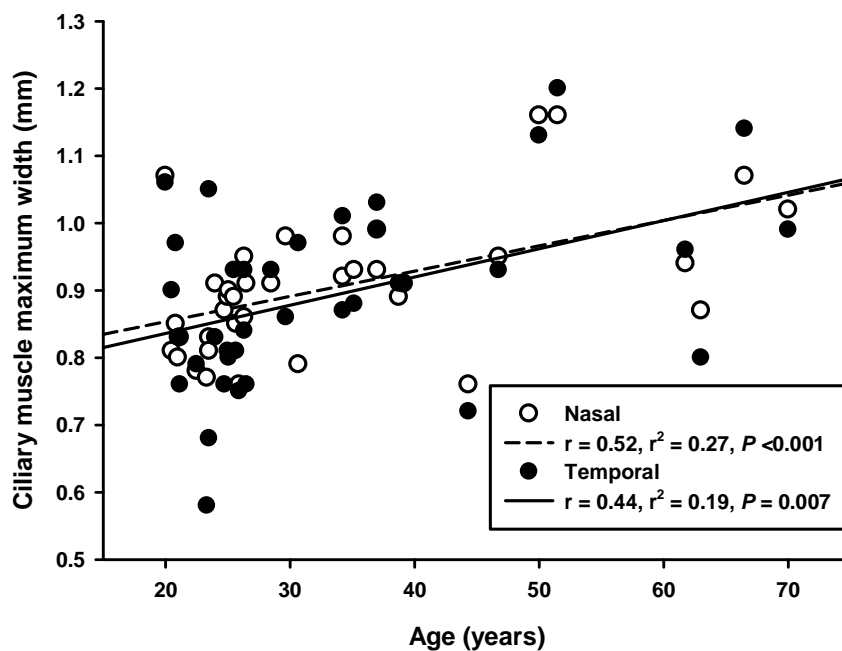


Figure 4.2. Nasal and temporal ciliary muscle maximum width *versus* age. $n = 37$ participants.

The distance from the inner apex of the ciliary muscle to the scleral spur decreased significantly with age on both the nasal and temporal aspects ($r = 0.47$; $P = 0.004$ and $r = 0.43$; $P = 0.009$, respectively). The reduction was similar on both sides: the decrease was $4.7 \mu\text{m}/\text{year}$ nasally, and $4.1 \mu\text{m}/\text{year}$ temporally. No significant difference was identified between the nasal and temporal inner apex to scleral spur measures ($P = 0.550$). Figure 4.3 illustrates the relationship between age and ciliary muscle inner apex to scleral spur values.

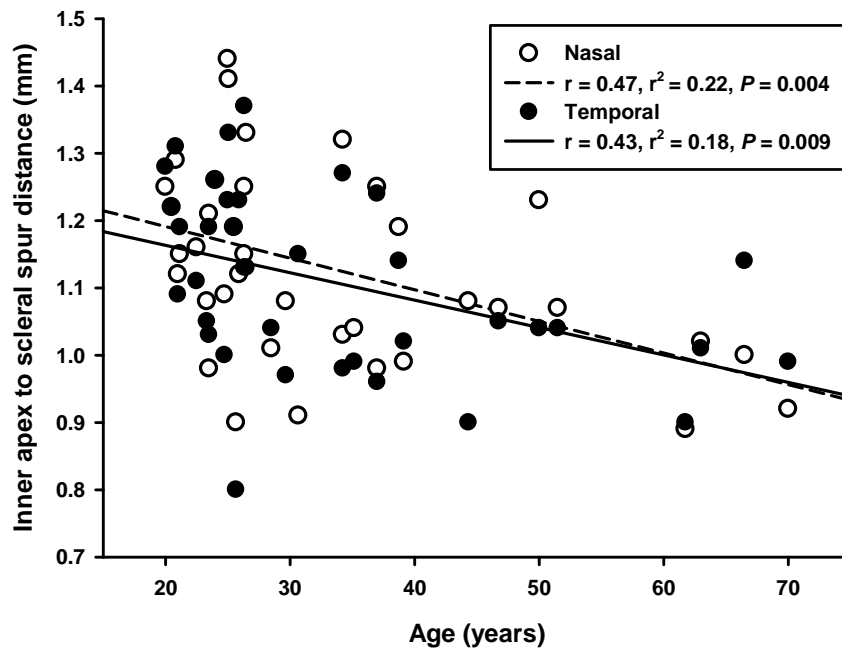


Figure 4.3. Nasal and temporal inner apex to scleral spur values *versus* age. $n = 37$ subjects.

4.3.2 Ciliary muscle contractile response

CM25 (shown in Chapter 3 to increase significantly with accommodation in youthful eyes) thickens in response to an accommodative stimulus throughout life. Figure 4.4 illustrates graphically the change in nasal and temporal CM25 with accommodative effort *versus* age. Linear regression analysis revealed the magnitude of accommodative thickening of CM25 was not dependent on age for either the nasal or temporal aspects ($r = 0.001$, $r^2 = 0.000$, $P = 0.994$ and $r = 0.202$, $r^2 = 0.041$, $P = 0.090$, for nasal and temporal CM25, respectively).

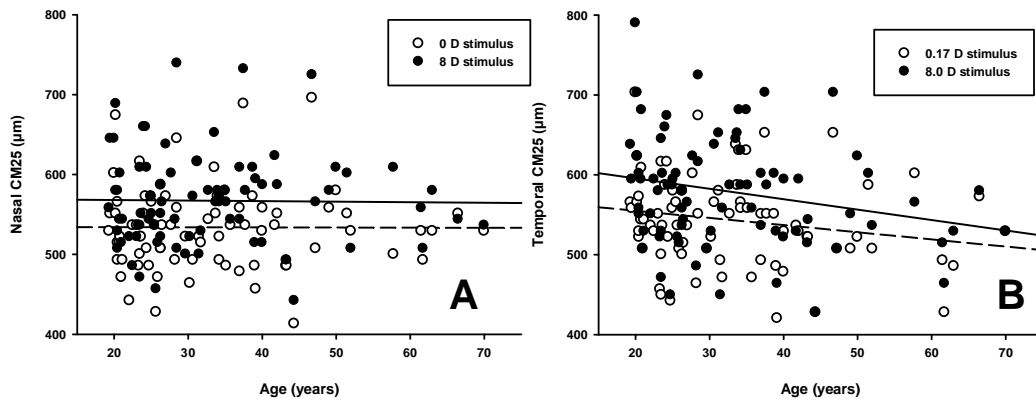


Figure 4.4. Nasal (A) and temporal (B) CM25 versus age for minimum accommodation (open circles and dashed regression line) and in response to an 8.0 D stimulus (filled circles and solid regression line). $n = 79$ subjects.

In conjunction with the thickening of CM25, Chapter 3 highlighted a shortening of ciliary muscle anterior length and overall length measures during accommodation. Both overall length and anterior length continue to reduce with accommodative effort throughout life. Figures 4.5 and 4.6 illustrate the change in nasal and temporal ciliary muscle anterior length in response to an 8.0 D accommodative stimulus against subject age in emmetropes and myopes, respectively. In both refractive groups, the magnitude of change in anterior length during near vision is statistically unchanged with age on both the nasal ($r = 0.254$, $P = 0.161$ and $r = 0.056$, $P = 0.755$, for emmetropes and myopes respectively) and temporal ($r = 0.061$, $P = 0.741$ and $r = 0.116$, $P = 0.514$, for emmetropes and myopes respectively) sides. Furthermore, the reduction in overall length during accommodative effort also remains statistically constant with age both nasally ($r = 0.049$, $P = 0.750$ and $r = 0.073$, $P = 0.680$, for emmetropes and myopes respectively) and temporally ($r = 0.075$, $P = 0.624$ and $r = 0.047$, $P = 0.791$, for emmetropes and myopes respectively). Figures 4.7 and 4.8 show the effect of age on nasal and temporal ciliary muscle overall length changes in response to an 8.0 D accommodative stimulus.

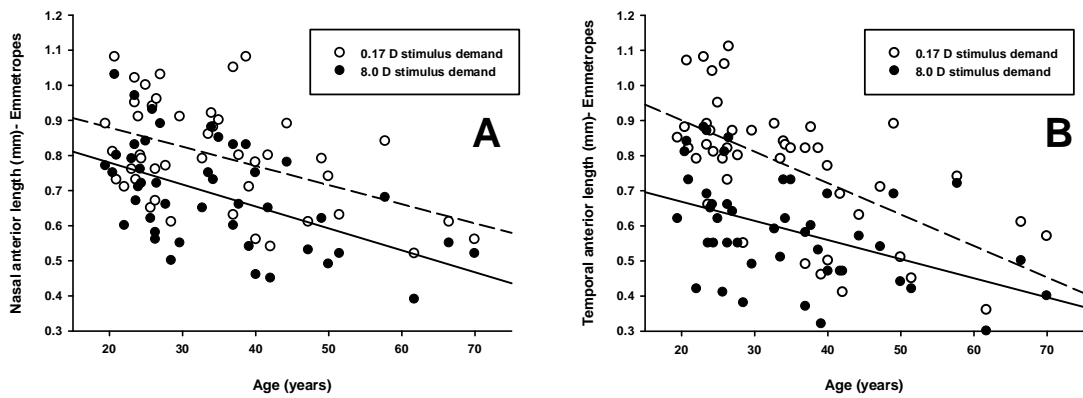


Figure 4.5. Nasal (A) and temporal (B) anterior ciliary muscle length in emmetropes *versus* age for minimum accommodation (open circles and dashed regression line) and in response to an 8.0 D stimulus (filled circles and solid regression line). n = 45 subjects.

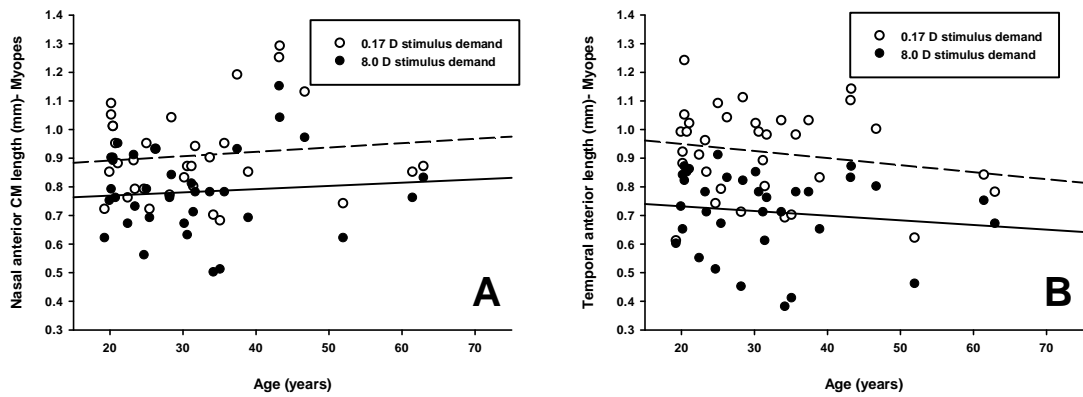


Figure 4.6. Nasal (A) and temporal (B) ciliary muscle anterior length in myopes *versus* age for minimum accommodation (open circles and dashed regression line) and in response to an 8.0 D stimulus (filled circles and solid regression line). n = 34 subjects.

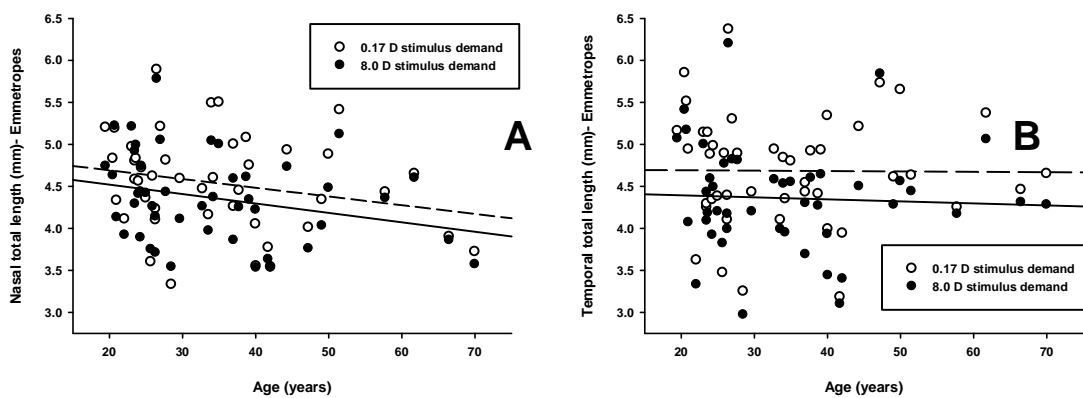


Figure 4.7. Nasal (A) and temporal (B) ciliary muscle total length in emmetropes *versus* age for minimum accommodation (open circles and dashed regression line) and in response to an 8.0 D stimulus (filled circles and solid regression line). n = 45 subjects.

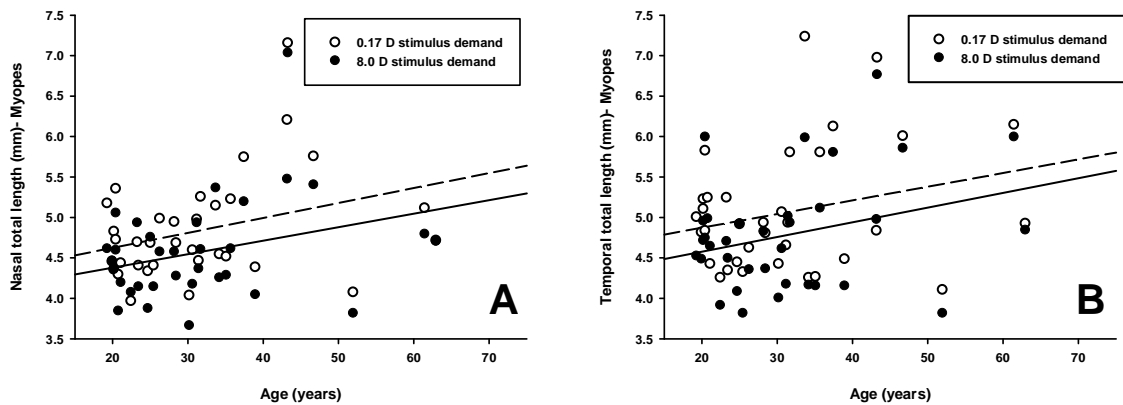


Figure 4.8. Nasal (A) and temporal (B) ciliary muscle total length in myopes *versus* age for minimum accommodation (open circles and dashed regression line) and in response to an 8.0 D stimulus (filled circles and solid regression line). $n = 34$ subjects.

4.4. Discussion

There are limited published data documenting the effect of age on human ciliary muscle morphology and contractility. Previous *in vitro* and *in vivo* studies of ciliary muscle biometry have used narrow age-bands of subjects and/ or small cohort sizes. The present investigation represents the largest *in vivo* study to date to investigate relaxed and contracted ciliary muscle characteristics across a broad range of subject ages.

In the relaxed state, the anterior portion of the ciliary muscle becomes thicker throughout life, as reflected by the age-related increase in maximum width values, of approximately $3 \mu\text{m}/\text{year}$. More posteriorly, CM25 is unchanged in both refractive groups with age, whilst CM50 and CM75 become progressively thinner temporally. Regarding ciliary muscle lengths, the overall length is unchanged with age for both refractive groups, whilst anterior length measures decrease on both sides in emmetropic, but not myopic, eyes. Furthermore, the distance from the muscle inner apex to the scleral spur demonstrates a significant reduction with age, of approximately $4 \mu\text{m}/\text{year}$. Overall, the observed changes reflect a general antero-inwards shift of ciliary muscle mass throughout life. The anterior thickening of the ciliary muscle is in agreement with a recent *in vivo* MRI study (Strenk *et al.*, 2010) and earlier *in vitro* data (Pardue and Sivak, 2000). Increased thickness of the anterior portion of the muscle may be a consequence of the age-related build-up of connective tissue observed in human *post mortem* samples (Pardue and Sivak, 2000), particularly in the radial and circular regions (Nishida and Mizutani, 1992; Tamm *et al.*, 1992a), and/ or a change in the relative proportions of different fibre orientations. The quantity of circular (Nishida and

Mizutani, 1992) and radial (Pardue and Sivak, 2000) fibres, compared to the longitudinal portion, may increase with age, resulting in a bulging of the anterior portion of the ciliary muscle. Thinning of the posterior region of the human ciliary muscle has not previously been documented, although the present study has identified a significant reduction in temporal CM50 and CM75 in both refractive groups. Chapter 3 highlighted increased thickness of CM50 and CM75 parameters on the temporal side, compared to the nasal aspect, in youthful eyes. The age-dependent decrease in posterior thickness may be a consequence of a reduction in longitudinally-orientated muscle fibres, compared to radial and circular fibres, on the temporal side. Tamm *et al.* (1992a) measured an *in vitro* decrease in the cross-sectional area of the longitudinal portion of the muscle in older eyes, but did not state from which region of the globe (i.e. nasal/ temporal/ superior/ inferior) the samples were obtained.

Hitherto, age-dependent changes in ciliary muscle length and distance from the inner apex to scleral spur have been observed in several *in vitro* investigations, but not previously reported *in vivo*. The reduction in distance from inner apex to scleral spur is in accordance with the *in vitro* data of Tamm *et al.* (1992a) from donor eyes aged 33- 87 years. No other previously published study has investigated the change in this parameter in the human eye with age. Ciliary muscle length changes with age have been more widely investigated, with some disagreement between studies. Tamm *et al.* (1992a) documented a continuous and significant decline in overall length with age, whereas Pardue and Sivak (2000) found no statistically significant change in this parameter, although the length of the anterior portion showed a substantial reduction. The present study has identified no significant age-dependent change in ciliary muscle total length with age, in either emmetropes or myopes, although the anterior length reduced significantly in the emmetropic group. Chapter 3 identified a positive correlation between axial length and both anterior and overall length measures, suggesting that the ciliary muscle elongates during myopigenesis. The maintenance of a constant anterior muscle length with age in myopic subjects suggests that the forces responsible for elongation of the globe are still present in later life, and inhibit the anterior shift of ciliary muscle mass that occurs in emmetropes.

The mechanism responsible for the age-related anterior shift in ciliary muscle mass is unclear. According to the Modified Geometric Theory of presbyopia development, postulated by Strenk *et al.* (2005), growth of the lens results in antero-inwards movement of the uveal tract, through forces transmitted via the pupillary margin to the iris root. As the lens becomes progressively thicker throughout life, ever-increasing force is applied to the pupillary margin (which is in contact with the anterior lens surface) and translated to the iris root and ciliary

muscle. In addition to an anterior movement of the ciliary muscle, an inwards displacement simultaneously occurs, due to the constraining effect of the curved sclera. The antero-inwards movement of the uvea leads to reduced pupil diameter, causing the pupillary margin to become increasingly nearer to the thicker part of the lens, and augmenting the forces applied by the lens. An alternative possible explanation for age-related anterior and inwards displacement of the ciliary muscle is based on the migration of zonules over the surface of the lens throughout life. Pardue and Sivak (2000) hypothesised that the forward migration of zonular insertions into the lens capsule (Farnsworth and Shyne, 1979; Sakabe *et al.*, 1998) due to lens thickening with advancing age, causes an anterior and inwards pull on the ciliary body. Regardless of the cause of the altered position of the ciliary body with advancing age, the results of the present study imply that the anterior shift of muscle mass in emmetropic eyes is insignificant to the development of presbyopia, as myopes (in which a reduction in anterior length is not seen) also lose all accommodative ability by approximately 50-55 years of age.

Regarding ciliary muscle function in the ageing eye, the results of the present study suggest that there is no significant decrease in the contractile ability of the muscle, even in eyes with established presbyopia. The main accommodative changes in ciliary muscle morphology observed in Chapter 3 were a reduction in overall length and anterior length measures, with a concurrent thickening of CM25. Figures 4.4 to 4.8 inclusive indicate that these parameters show the same changes in response to a near stimulus throughout life: linear regression analysis of the change in each measure between the minimal and 8.0 D stimulus levels *versus* age showed no statistical dependence of the magnitude of change on subject age. The data support a lensocentric model of presbyopia development, whereby continued growth and alterations in lenticular viscoelastic properties reduce the ability of the capsule to mould the lens into an accommodated form. Furthermore, the anterior migration of zonular insertions over the enlarged lens, such that they become more tangential to the lenticular surface with advancing age, may act to reduce the ability of the zonules to impart tension on the capsule. The observed ciliary muscle configurational changes appear to be passive elements in the development of presbyopia, particularly due to the refractive group asymmetry of anterior length changes.

In considering the findings of the current investigation, attention must be paid to the limitations of the study. The technical problems encountered with the AS-OCT meant it was not possible to obtain ciliary muscle maximum width and inner apex to scleral spur measures from all participants. Due to the reduced data set, it was not feasible to compare the age-related changes in these parameters in emmetropes *versus* hyperopes. Whilst inner

apex to scleral spur measures decreased with age (in $n = 37$ participants, mixed refractive errors), suggesting an anterior displacement of the ciliary muscle with age, the anterior length was found to significantly decrease only in emmetropic eyes. It is possible that refractive group differences exist in the age-related changes in inner apex to scleral spur and maximum thickness measures, which were not detected in the current study. Additional further investigation could serve to clarify this matter.

The current study was limited to investigation of ciliary muscle biometry in phakic volunteers. However, the impact of cataract extraction and intraocular lens (IOL) implantation on ciliary muscle configuration and contractility is relevant to the attempted correction of presbyopia with accommodating IOLs that rely on continued function of the ciliary muscle throughout life to induce either axial movement of an optic, or a change in surface curvature, to generate an increase in dioptric power. Previous studies that have analysed ciliary muscle morphology and contraction in phakic and pseudophakic eyes have produced some contradictory results. Park *et al.* (2008) used ultrasound biomicroscopy to evaluate centripetal ciliary muscle movement following pilocarpine administration to stimulate accommodation. Minimal centripetal movement was observed in patients prior to cataract surgery, but significant movement was restored following IOL implantation. However, the MRI data of Strenk *et al.* (2006) suggested that ciliary muscle contractility (as inferred by reduction in ciliary muscle ring diameter in response to a near stimulus) remained constant throughout life, and was unaffected by cataract surgery with IOL implantation. Further MRI data from the same group (Strenk *et al.*, 2010) adds further uncertainty to the matter, as ciliary muscle thickening with accommodative effort was only observed in phakic volunteers aged 22- 91 years; pseudophakes showed no ciliary muscle thickening in response to a near visual stimulus, suggesting at least a partial reduction in ciliary muscle response following cataract surgery. To provide clarification of these issues, the methodology employed in the present study could be applied to a cohort of phakic *versus* pseudophakic volunteers, or alternatively, to a group of patients awaiting cataract surgery to compare pre- and post-operative ciliary muscle morphology and contractility.

4.5 Conclusion

The human ciliary muscle undergoes age-dependent changes in morphology that suggest an antero-inwards displacement of muscle mass, particularly in emmetropic eyes. The morphological changes observed appear not to affect the ability of the muscle to contract, even in established presbyopes, thus supporting a lenticular model of presbyopia development. Further work is required to investigate the effect of cataract extraction with IOL implantation on ciliary muscle biometric characteristics. Such data would be valuable in

the development of strategies aimed at restoring accommodative function to presbyopic eyes.

Supporting Publication:

Sheppard A. L. and Davies L. N. (2010). The effect of ageing on *in vivo* human ciliary muscle morphology and contractility. *Investigative Ophthalmology and Visual Science* (In press).

CHAPTER 5

PHAKIC LENS TILT AND DECENTRATION WITH ACCOMMODATION UTILISING ANTERIOR SEGMENT OPTICAL COHERENCE TOMOGRAPHY

5.1. Introduction

Recent clinical literature includes many studies of post-operative intraocular lens (IOL) tilt and decentration, using a range of methodologies (e.g. Guyton *et al.*, 1990; Hayashi *et al.*, 1997; Mutlu *et al.*, 1998; Kim and Shyn, 2001; Mutlu *et al.*, 2005; de Castro *et al.*, 2007; Verbruggen *et al.*, 2007). As both cataract surgical procedures and implant designs have progressed, measures of IOL tilt and decentration, which may degrade retinal image quality (Atchison, 1991; Mester *et al.*, 2009), have developed greater clinical significance. However, less attention has been directed towards measurement of lens tilt and alignment in the healthy, phakic eye. Despite a paucity of data describing natural crystalline lens tilt and decentration, such information could be valuable in IOL research, as perfect alignment of the implant with the cornea may not be necessary, or feasible, in all eyes (Dunne *et al.*, 2005).

Hitherto, the most frequently used technique to determine tilt and decentration of the phakic crystalline lens is phakometry, although one recent investigation reports findings from a small cohort utilising magnetic resonance imaging (MRI; Chang *et al.*, 2007). Table 5.1 provides a summary of recently published studies that have analysed natural lens tilt and alignment *in vivo*. Reported mean lens tilt values from these studies are variable, ranging from a minimal $0.2 \pm 0.8^\circ$ temporally (Kirschkamp *et al.*, 2004) to $4.62 \pm 3.18^\circ$ temporally (Schaeffel, 2008). The broad range of values documented could be a result of several factors, either individually or interacting to produce a greater effect. True population differences could be present, although it is impossible to exclude potential technical discrepancies without some subjects being analysed with more than one of the described methodologies. Furthermore, with the exception of the Dunne *et al.* (2005) study, lens tilt has been determined from relatively small cohorts, leading to the problem of one or two outliers causing a significant increase in the calculated mean values. The results of Schaeffel (2008), based on 11 subjects, include an individual with a measured phakic lens tilt of 10.24° , a value far exceeding that observed by other authors. While reported absolute values vary, Table 5.1 highlights a tendency for lens tilt to be in the temporal direction in the phakic human eye. Temporal lens tilt has been suggested to be an evolutionary remnant from non-binocular mammalian ancestors (Schaeffel, 2008).

Author	Method	Cohort size	Mean lens tilt (°)	Mean lens decentration (mm)
Kirschkamp et al. (2004)	Phakometry, keratometry & ultrasonography	9	H = +0.2 ± 0.8	H = -0.1 ± 0.2
Dunne et al. (2005)	Phakometry	45	H = +0.2 ± 1.8	H = +0.1 ± 0.1
Rosales & Marcos (2006)	Phakometry	17	H = -0.87 ± 2.16 V = +2.3 ± 2.33	H = -0.28 ± 0.12 V = -0.06 ± 0.08 Relative to pupil centre
Chang et al. (2007)	MRI	6	3.0 ± 2.4 (ALS) 2.7 ± 1.6 (PLS)	H = +0.05 ± 0.14 V = -0.29 ± 0.45
Schaeffel (2008)	Phakometry	11	H = +4.62 ± 3.18 V = -1.7 ± 0.49 Relative to fixation axis	H = +0.10 ± 0.08 V = -0.31 ± 0.09 Relative to pupil centre

Table 5.1. Summary of recent studies of phakic human lens tilt and decentration. H and V are the horizontal and vertical directions, respectively. Regarding lens tilt, positive values of horizontal tilt indicate tilt to the temporal side, whilst positive values of vertical tilt signify that the superior edge of the lens is nearer to the cornea than the inferior edge (forwards tilt). For decentration, positive horizontal values indicate temporal decentration, whilst positive vertical values signify upwards displacement. Regarding the data of Chang *et al.*, (2007) the direction of mean tilt was not specified, but ALS and PLS are the anterior and posterior lens surfaces, respectively

Regarding phakic lens decentration, published studies indicate generally good alignment between the cornea and crystalline lens, although direct comparisons are not possible, due to the variations in definition of decentration between authors. Kirschkamp *et al.* (2004), Dunne *et al.* (2005) and Rosales and Marcos (2006) defined decentration as the distance between the lens tilt axis and corneal axis; Chang *et al.* (2007) measured the distance from the lens centre to corneal axis, whilst Schaeffel (2008) determined the distance from lens centre to pupil centre. Use of pupillary centre as the reference point from which to judge lens decentration may lead to a temporal bias in results, as the pupil is generally displaced nasally, by approximately 0.25 mm (Rabbetts, 1998). Reported horizontal lens decentrations range from just 0.1 ± 0.1 mm temporally (Dunne *et al.*, 2005) to 0.28 ± 0.12 mm nasally (Rosales and Marcos, 2006). Although no consensus exists over whether horizontal decentration is usually nasal or temporal, in the vertical meridian, the lens appears to be inferiorly displaced. Table 5.1 highlights that all studies reporting vertical alignment have identified a downwards displacement, ranging from a minimal 0.06 ± 0.08 mm (Rosales and

Marcos, 2006) to approximately 0.3 mm (Chang *et al.*, 2007; Schaeffel, 2008), potentially due to the effects of gravity (Schaeffel, 2008).

Rather than measuring phakic lens tilt and decentration at just one fixed vergence level, or not controlling accommodative demand, several previous authors have documented lens position in the monkey and human eye during accommodation, through direct or indirect methods. Potential changes in lens tilt and alignment are significant as instability of the lens during accommodation implies reduced zonular tension with ciliary muscle contraction, providing additional evidence to support Helmholtz' theory of accommodation (von Helmholtz, 1855). Furthermore, variation in lens position may account for the changes in wavefront aberrations that occur during accommodation (He *et al.*, 2000; Sokolowska and Thorn, 2003).

In the rhesus monkey, Glasser and Kaufman (1999) observed movement of a lenticular opacity under the influence of gravity, regardless of head position, through slitlamp video recording of a single accommodating specimen. More recently, Rosales *et al.* (2008) performed phakometry on 4 eyes of 2 monkeys in the relaxed and accommodated states. Contrary to the observations of Glasser and Kaufman (1999), no significant change in lens centration was detected during accommodation, although tilt around the horizontal axis changed at a rate of 0.15 ± 0.25 °/D. Similar confounding results have been documented in the accommodating human eye. Phakometry- based studies (Sokolowska and Thorn, 2003; Kirschkamp *et al.*, 2004) have shown no change in lens centration during accommodation to a 4 D stimulus, although Sokolowska and Thorn (2003) measured a change in horizontal tilt during near vision. No variation in lens tilt with accommodation was detected by Kirschkamp *et al.* (2004). However, He *et al.* (2010) measured saccadic lens instability during ciliary muscle contraction utilising a dual Purkinje image eye tracker to compare the positions of Purkinje image 1 (P1; anterior corneal surface) and P4 (posterior lens surface). The saccadic "lens wobble artifact" (Deubel and Bridgeman, 1995) was found to increase with stimulus demand in the presbyopic cohort examined, indicating that lens stability does reduce during accommodation, as a consequence of slackened zonular tension.

Additionally, increases in astigmatic refractive error have been postulated as indirect evidence of lens tilting with accommodation in humans (Fletcher, 1951; Radhakrishnan and Charman, 2007b). The reported levels of astigmatic change during accommodation do, however, differ significantly from one another. In relatively recent studies, Tsukamoto *et al.* (2000) found the greatest change, with 0.8 D of with-the-rule astigmatism induced by a 2 D stimulus. Cheng *et al.* (2004) and Radhakrishnan and Charman (2007b) identified more

modest increases, of 0.021 DC per dioptre of response and 0.036 DC/ D, respectively, whilst Mutti *et al.* (2001) observed no significant change in astigmatism during accommodation.

In summary, *in vivo* studies of phakic human lens tilt and alignment, and changes in these parameters with accommodation, are scarce. The results of the few studies to date show no consensus on levels of natural tilt and decentration, although the unaccommodated lens appears to be inferiorly displaced (Rosales and Marcos, 2006; Chang *et al.*, 2007; Schaeffel, 2008). In the accommodated eye, according to the mechanism described by Helmholtz (1855), an increase in lenticular tilt and decentration would be expected, as a result of lens instability whilst zonular tension is reduced. However, only one study that has directly measured lens stability with accommodation has identified an accommodative increase in instability (He *et al.*, 2010). Interestingly, this is the study that employed the greatest range of stimulus vergences: up to -8.0 D, compared to the 4.0 D demand level utilised by Sokolowska and Thorn (2003) and Kirschkamp *et al.* (2004). The outcome measure reported by He *et al.* (2010) was lens wobble, which unfortunately does not differentiate between tilt and decentration. Increased with-the-rule astigmatism during near viewing (Tsukamoto *et al.*, 2000; Cheng *et al.*, 2004) provides further, indirect, evidence for accommodative lens tilting (Radhakrishnan and Charman, 2007b), but the refractive changes observed could potentially result from other factors such as narrowing of the palpebral aperture (Han *et al.*, 2007) or natural eye movements (Steffen *et al.*, 2000; Buehren *et al.*, 2003).

Hitherto, the methods used to analyse directly phakic human lens tilt and alignment *in vivo* have been limited to phakometry-based techniques and MRI. MRI is an expensive and relatively inaccessible imaging methodology, and potential subjects could be precluded from participation due to risk factors such as migraines, heart disease and implanted metal devices/ fragments. Whilst phakometry requires less sophisticated equipment, the set-ups described in previous studies are bespoke, and as such, may be time-consuming to develop. Anterior segment optical coherence tomography (AS-OCT) is a commercially available high-resolution imaging technique that has been suggested for use in analysis of IOL positioning (Montes-Mico *et al.*, 2009), although no published study to date has measured lens tilt and decentration with this method.

The aim of this study is to develop an AS-OCT based technique that permits measurement of phakic crystalline lens tilt and alignment, relative to the cornea. The methodology will be applied to analyse phakic lens tilt and decentration in youthful eyes, in the relaxed and

accommodated states. It is anticipated that the data will assist in clarifying the natural alignment and tilt of the crystalline lens *in vivo*. Use of a high vergence stimulus (-8.0 D) should make accommodative changes in these parameters more obvious. It is feasible that sectorial differences in ciliary muscle contractility could have a significant impact on lens stability during accommodation (Radhakrishnan and Charman, 2007b). Results will therefore be considered in light of the findings detailed in Chapter 3, of a thicker (and possibly more powerful) ciliary muscle on the temporal aspect of the eye, thus building on the author's previous work.

5.2. Methods

5.2.1 Protocol development

To determine phakic lens tilt and decentration, relative to the cornea, using AS-OCT, it is necessary to acquire images including both corneal and both lenticular surfaces. In Anterior Segment Single mode, the axial field of view of the *Visante* device permits visualisation of both corneal surfaces along with the anterior lens surface only. It is therefore necessary to capture a second image, penetrating further into the eye, showing both lenticular surfaces (but not the cornea). The anterior and posterior scans described (Figs. 5.1a and 5.1b, respectively) are needed in conjunction with one another for the calculation of phakic lens tilt and decentration. Image sets can be rapidly obtained along any desired meridian using AS-OCT. The manufacturer's supplied software (version 1.0) allows post hoc distance measurements using callipers, and angle determination, but no tools exist that would enable assessment of lenticular tilt and alignment. It was therefore necessary to develop a bespoke semi-automated computer programme to calculate lens tilt and alignment, relative to the cornea, from exported AS-OCT images.

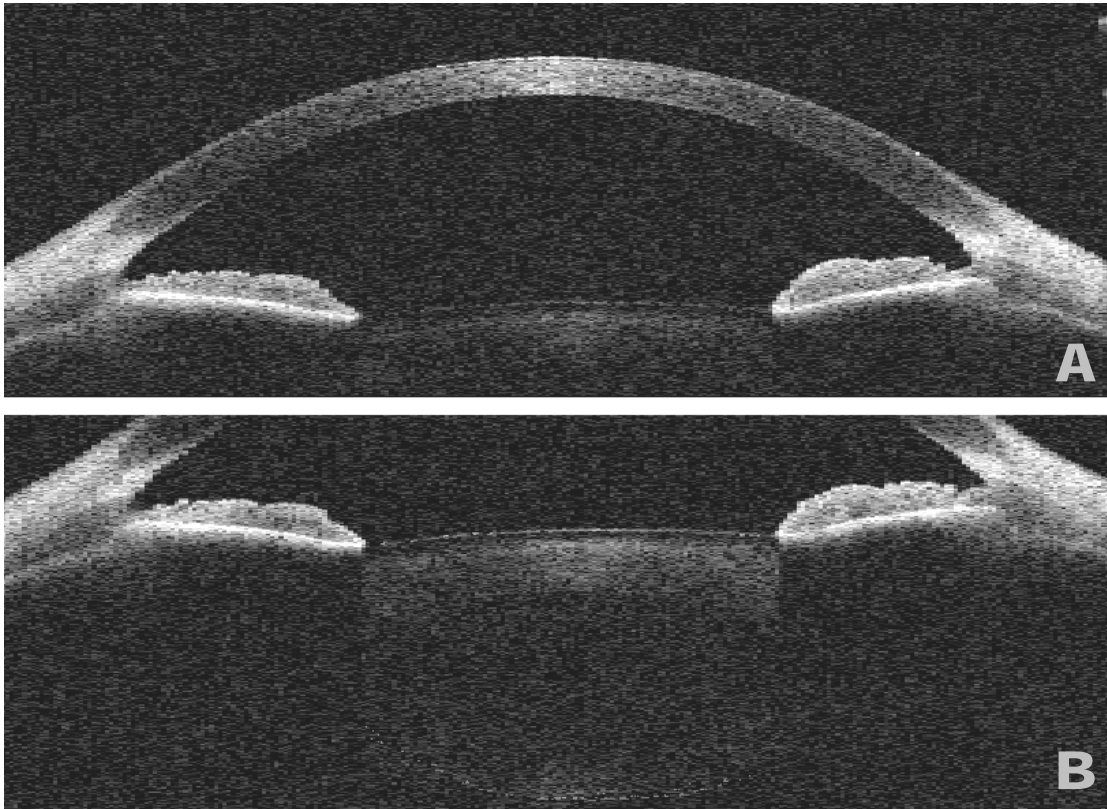


Figure 5.1. Anterior (A) and posterior (B) AS-OCT images for analysis of lens tilt and decentration. The anterior image includes both corneal surfaces and the anterior lens surface, whilst image B contains both lens surfaces. The common features on the two images are the irido-corneal angles.

5.2.2. Development of a computer programme for determination of lens tilt and decentration from AS-OCT images

A *Liberty Basic 4.0* (Shoptalk Systems, Framingham, Massachusetts, USA) computer programme was written by the author to facilitate the analysis of AS-OCT extracted bitmap images and determine lens tilt and decentration relative to the cornea. Manual input is required throughout running of the programme, as the user is asked to define various landmarks on the images using left and right mouse clicks. All AS-OCT data for analysis are exported as 816 * 638 pixel bitmaps, thus the x and y co-ordinates of selected points can be used for the calculations performed automatically during execution of the programme. The three key stages of the programme can be summarised as follows:

1. Determination of corneal axis from analysis of the anterior image.
2. Location of lenticular axis, using the posterior image.
3. Calculation of lens tilt and decentration relative to the cornea.

5.2.2a Determination of corneal axis

Stage one initially prompts the user to locate the irido-corneal angles (Figure 5.2; small white squares) on the anterior image, which are used by the programme as anatomical landmarks to divide the cornea into 12 equally-sized segments with 13 visible lines. The intersections of the anterior and posterior corneal surfaces with the vertical lines are specified by the user (Fig. 5.2; red spots indicate the defined points) and the programme determines the x and y co-ordinates of the midpoints between the anterior and posterior corneal intersections: these values are used to determine the regression coefficient (Equation 4) of the line formed by the corneal midpoint coordinates.

$$b = \frac{\sum (x - \bar{x})(y - \bar{y})}{\sum (x - \bar{x})^2}$$

Equation 4

The constant a is estimated by:

$$a = \bar{y} - b\bar{x}$$

Equation 5

The fitted regression line is therefore:

$$y = a + bx$$

Equation 6

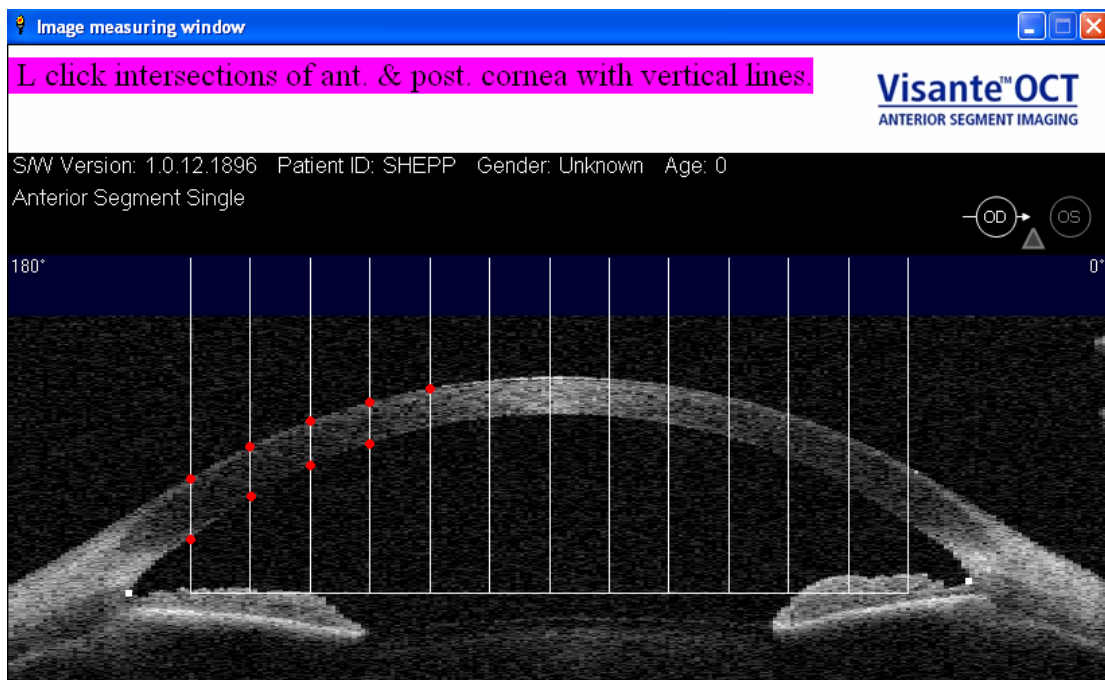


Figure 5.2. Execution of the initial stage of the computer programme. Following location of the irido-corneal angles (white squares), the user specifies the points at which the 13 vertical lines dividing the cornea into 12 equal segments intersect the anterior and posterior corneal surfaces (red dots).

Having calculated the slope of the line formed by the corneal midpoint values, the programme draws a movable line with the same slope on the anterior scan (Figure 5.3; red line). The operator moves the line using \uparrow and \downarrow keyboard input, and specifies the location of the anterior and posterior corneal apices (i.e. the most anterior, and least posterior points at which the line touches the corneal surfaces). The midpoint of these locations (in both the x and y directions) is calculated, and a line of an angle 90° to that of the corneal slope is drawn (Fig. 5.4; bold red line) from this point; it is this line that represents the corneal axis.

As the corneal surfaces are not visible in the more posterior scan, to be used for the later stages of analysis, it is necessary for the user to again locate the irido-corneal angles, between which a line is drawn. Identifying the point at which the corneal axis crosses this line provides a reference point that allows the axis to be redrawn, provided the angles are visible, on the posterior image.

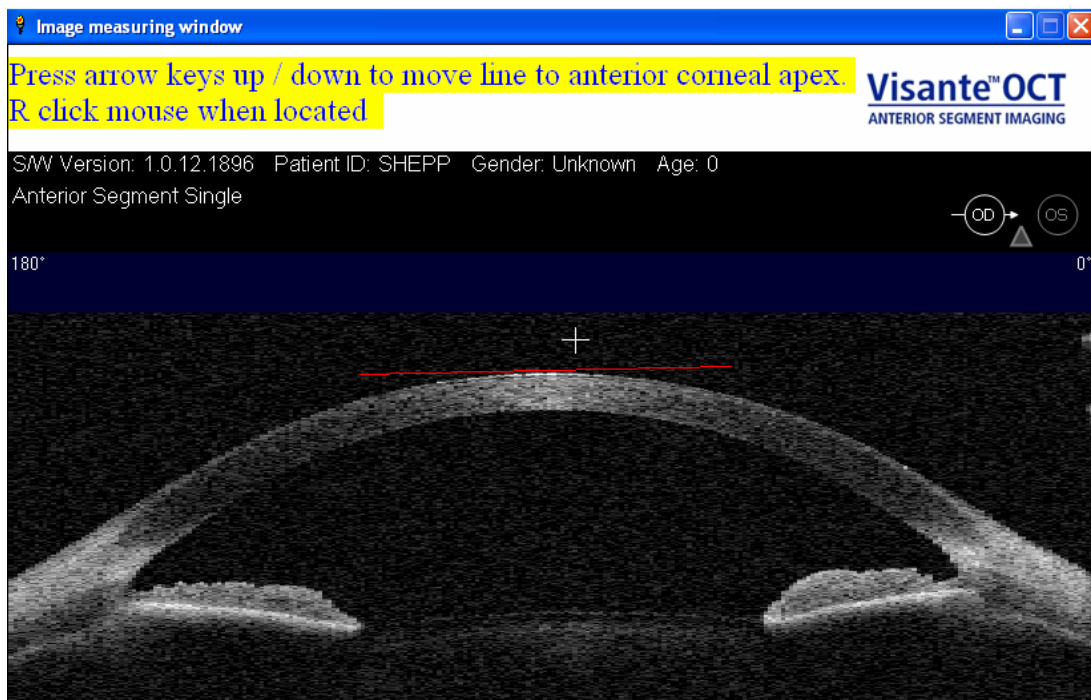


Figure 5.3. A movable line of calculated slope is used to locate the anterior and posterior corneal apices.

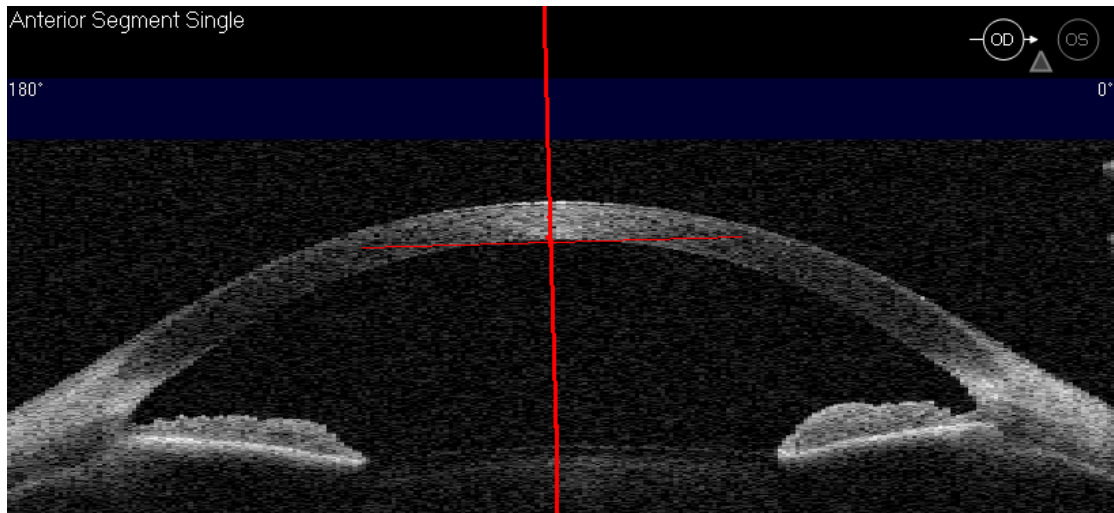


Figure 5.4. The corneal axis (bold red line) is automatically drawn following location of the anterior and posterior corneal apices.

5.2.2b Location of lenticular axis

Following selection and opening of the more posterior bitmap image, the operator is prompted to indicate the visible limits of the crystalline lens (i.e. the widest horizontal portion of the lens where it is possible to visualise both the anterior and posterior surfaces, normally corresponding to the pupillary aperture), to allow 9 vertical lines to be automatically drawn that pass through both the anterior and posterior lenticular surfaces (Fig. 5.5). In the same manner as described previously, the intersections of these lines with the anterior and posterior lens surfaces are identified by the user (Fig. 5.5; red dots), enabling the programme to determine the midpoints of these locations (Fig. 5.5; purple spots). Equations 4, 5 and 6 are used to calculate the slope of the line formed by these midpoint values and the lenticular axis (Fig. 5.6; purple line) is determined in the same way as the cornea, following operator location of the anterior and posterior lens apices.

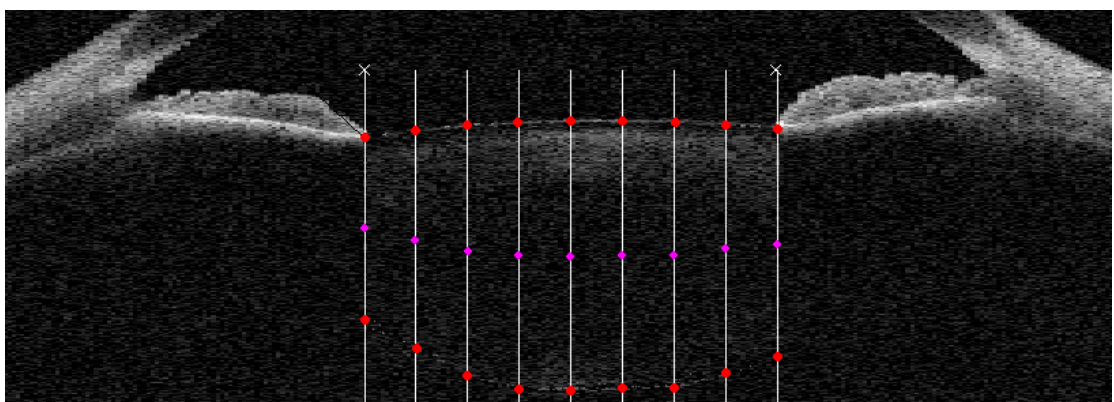


Figure 5.5. Location of the intersections of the 9 vertical lines with the anterior and posterior lens surfaces (red dots). The programme calculates the slope of the line formed by the midpoint values (purple dots).

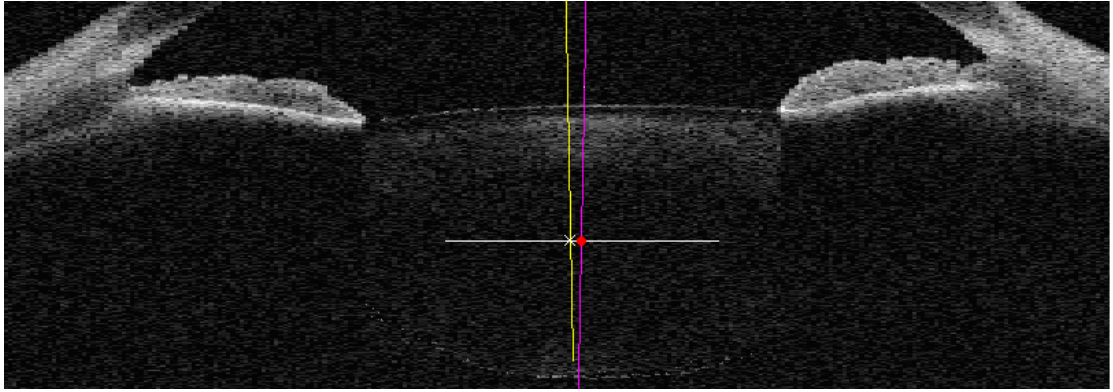


Figure 5.6. Lens tilt is the calculated difference in angles between the lenticular axis (purple) and the corneal axis (yellow). Lens decentration relative to the cornea is the horizontal separation of the corneal axis and the lens centre (i.e. horizontal distance from red dot to white cross).

5.2.2c Calculation of lens tilt and decentration relative to the cornea

Following identification of the lenticular axis, it is necessary to redraw the corneal axis on the posterior image for determination of lens tilt and alignment. The operator is again required to indicate the locations of the irido-corneal angles, and using the previously determined coordinates for the point at which the corneal axis intersects a line between these points, the programme draws the corneal axis (Fig. 5.6; yellow line). Lens tilt is defined as the angular difference between the corneal and lenticular axes, and the result is displayed in the dialogue box (Fig. 5.7), which is open throughout execution of the programme.

Finally, to determine lens decentration, the user is required to indicate the intersection of the corneal axis with a horizontal line originating from the lens centre (Fig. 5.6). The horizontal distance between these points corresponds to the lens decentration. A previously determined pixel to millimetre conversion factor of 1 pixel = 0.022 mm (Dunne *et al.*, 2007) is used to calculate lens decentration, the result of which is displayed in the dialogue box (Fig. 5.7).

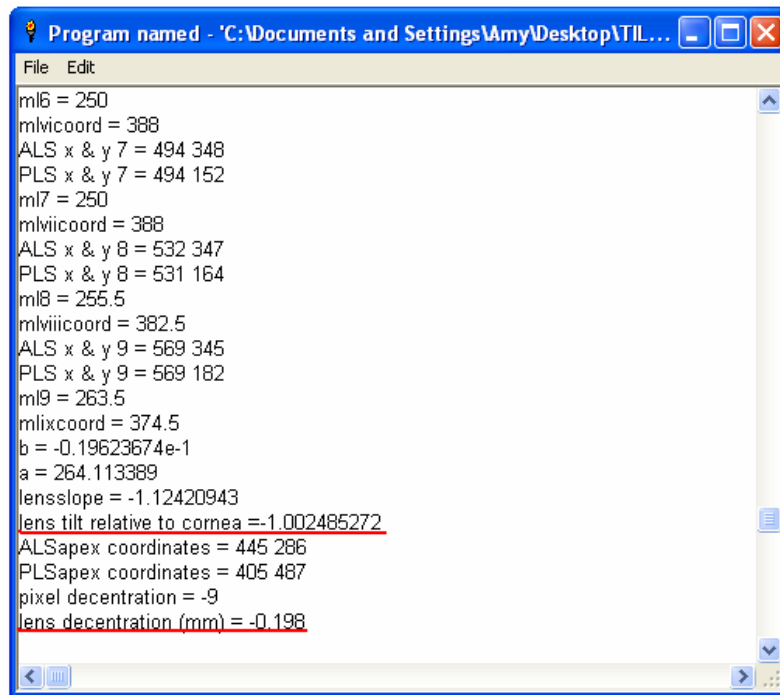


Figure 5.7. Dialogue box open during execution of the programme, displaying results for lens tilt and decentration relative to the cornea.

Measures of tilt and decentration may produce positive or negative values. According to the programme, for horizontal scans, negative values for tilt indicate nasal tilt (i.e. the nasal aspect of the lens is displaced backwards relative to the cornea), whilst negative decentration indicates that the lens is decentred nasally (relative to the cornea). For vertical scans, negative tilt indicates that the superior edge of the lens is tilted backwards, whilst negative decentration represents superior displacement of the lens relative to the cornea.

5.2.3 Validity of programming

Before application of the programme to images of human eyes, it was necessary to confirm accuracy of the computer programming (particularly regarding the automated calculations performed) and validity of the methods involved, by conducting a small pilot investigation. Simplified schematic images, based upon AS-OCT scans, of eyes incorporating 0, 5 and 10° of lenticular tilt, and 0 mm of lens decentration, relative to the cornea (e.g. Fig. 5.8) were constructed using *Powerpoint* presentation software (Microsoft, Redmond, Washington, USA) and converted to 816 * 638 bitmap files. The sample images were analysed 10 times to provide an indication of the inherent error involved in execution of the programme, which requires significant user input. Table 5.2 summarises the results of the pilot study, which confirmed accuracy of the computer programming, and also demonstrated that the error associated with user input is relatively small, compared to previously-published mean values of lens tilt and decentration (Table 5.1).

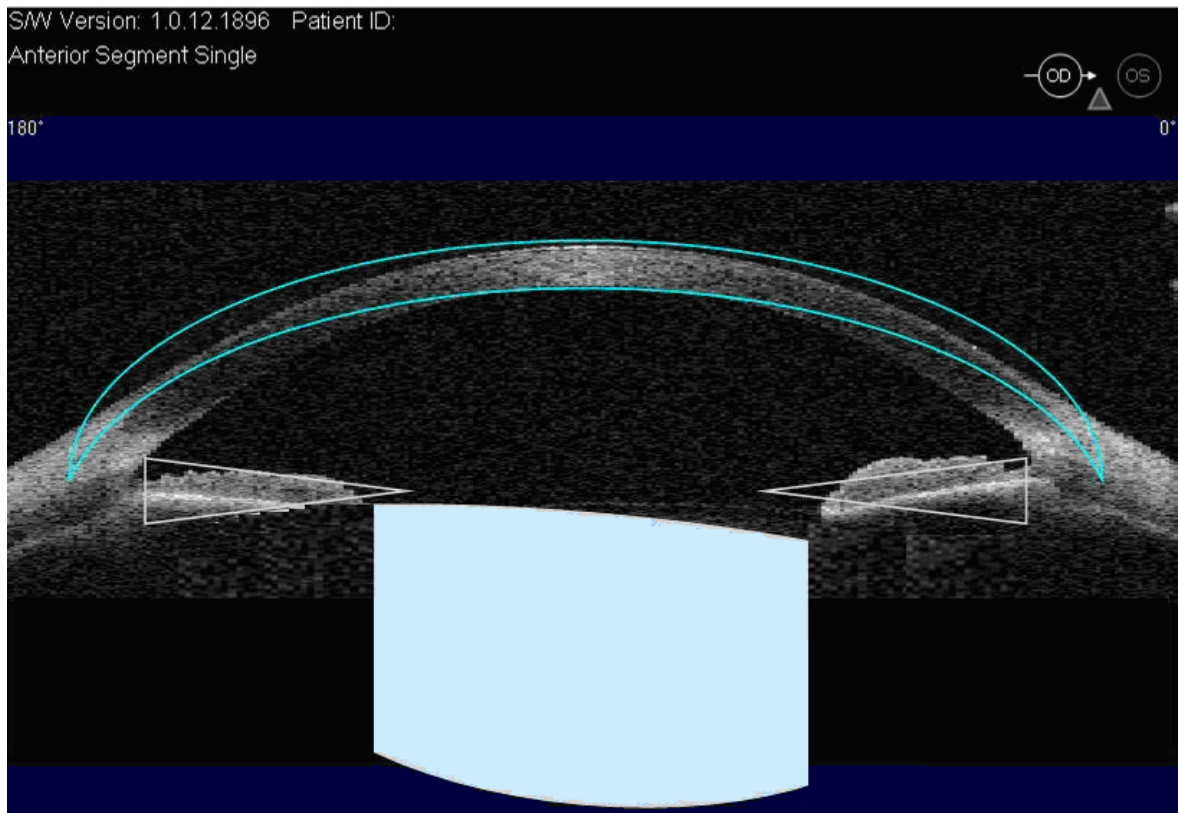


Figure 5.8. Simplified schematic image constructed to confirm validity of the bespoke computer programme to measure lens tilt and decentration, relative to the cornea. Here, lens tilt = -5° and lens decentration = 0 mm.

<i>Actual lens tilt and decentration, relative to cornea</i>	<i>0°, 0 mm</i>	<i>-5°, 0 mm</i>	<i>-10°, 0 mm</i>
Calculated mean lens tilt (\pm SD)	$0.093 \pm 0.078^\circ$	$-5.102 \pm 0.090^\circ$	$-9.892 \pm 0.074^\circ$
Calculated mean lens decentration (\pm SD)	-0.033 ± 0.052 mm	0.032 ± 0.069 mm	0.039 ± 0.091 mm

Table 5.2. Results of small pilot investigation to verify accuracy of the computer programme and associated methods. Images were constructed of eyes incorporating 0, 5 and 10° of lens tilt, with 0 mm decentration, relative to the cornea. Each image was analysed 10 times to indicate the error associated with user input.

5.2.4. Main investigation

20 pre-presbyopic volunteers (12 females, 8 males), aged 19 to 34 years of age (mean age 26.5 ± 4.5 years) with no previous history of ocular abnormality or intraocular surgery were recruited using email announcements at Aston University. A young cohort was selected to ensure participants had high amplitudes of accommodation. Subjects with all types of

refractive error were included, provided the mean spherical equivalent refractive error (MSE) of their right eye was within the range that could be corrected by the *Visante* optometer to allow both the internal pinwheel target to be seen clearly in the unaccommodated state, and the stimulus vergence to be adjusted to -8.0 D. Volunteers with an MSE outside of the broad range of -27.00 to +20.00 D were therefore excluded from the study, as were participants with cylindrical powers exceeding 0.75 DC, as the *Visante* optometer cannot make adjustment for astigmatic refractive errors. The study was approved by the Ethics Committee of Aston University (see Appendix 1), and was performed in accordance with the Declaration of Helsinki. Written, informed consent was obtained from all subjects (see Appendix 2 for copy of consent form) following explanation of the nature and possible consequences of the study.

5.2.5 Measurements

All measurements were taken from the right eye only. Refractive error was determined from the mean of five open-view distance autorefractor readings, obtained with the Grand Seiko Auto Ref/ Keratometer *WAM-5500* (Grand Seiko Co. Ltd., Hiroshima, Japan; Sheppard and Davies, 2010a). Objective accommodative response to an 8.0 D stimulus was measured with the *WAM-5500*, whilst subjects fixated a Maltese cross target in free space at a distance of 12.5 cm from the right eye. The Maltese cross had an angular subtense of 4.6° and the average target luminance and Michelson contrast of the stimulus was 30.5 cd/ m² and 80 %, respectively. The left eye was occluded with a patch during measurement of the accommodative response, and it was ensured at this stage that subjects had sufficient monocular amplitude of accommodation to maintain clarity of the 8.0 D stimulus, as would be required for AS-OCT imaging.

5.2.6 Image acquisition

Images of the right eye only were obtained, whilst the left eye was occluded by a patch. All imaging was performed in Anterior Segment Single mode, which provides sufficient horizontal field of view to visualise the entire cornea and the irido-corneal angles on the left and right of the image. 256 A-scans, penetrating to a tissue depth of 6mm, are performed in this mode to generate each 2-D image (Zeiss, 2006). Subjects were instructed to keep their heads as still as possible throughout scan acquisition. Scans were initially obtained in the unaccommodated state, whilst participants fixated the internal pinwheel target, which is automatically adjusted by the *Visante* depending on the specified distance refractive error. Images were acquired in the relaxed state first to avoid the problem of incomplete relaxation of accommodation confounding the results. Anterior images featuring the whole cornea, iris and anterior lens surface (Fig. 5.1a), and posterior images, comprising the limbal region, iris

and both crystalline lens surfaces (Fig. 5.1b) were captured with the scan line direction set at 0° (horizontal) and 90° (vertical). It is possible to set the scan line at any orientation from 0- 359°, however 0 and 90° angles were selected to enable quantification of lens tilt and decentration relative to the cornea, in the horizontal and vertical meridians, allowing comparison with previously-published data (e.g. Kirschkamp *et al.*, 2004; Dunne *et al.*, 2005; Rosales and Marcos, 2006; de Castro *et al.*, 2007; Schaeffel, 2008). The same image set was subsequently acquired from each subject in the accommodated state, with the stimulus power set to Distance MSE – 8.00 D (e.g. -9.00 D for a -1.00 DS myope).

5.2.7 Image analysis

Scans were exported from the AS-OCT as bitmap files following adjustment of the refractive index applied by the Visante software (version 1.0.12.1896), which uses edge detection algorithms to identify the corneal surfaces and assign an appropriate refractive index to each region of the image (Dunne *et al.*, 2007; Bailey *et al.*, 2008). As the posterior image did not contain either corneal surface, an index of 1.000 was manually applied to all regions of both images. Image analysis was performed on a PC running the bespoke programme. For each subject, the programme was executed to calculate lens tilt and decentration relative to the cornea in the horizontal and vertical meridians, at both the 0 and 8.0 D stimulus demand levels. Data were entered into a spreadsheet (*SigmaPlot* Version 11; Systat Software Inc., Chicago, Illinois, USA) for statistical analyses.

5.2.8 Statistical analysis

Statistical analysis was performed using *SigmaPlot* graphing software. Paired t-tests were used to identify significant differences in lens tilt and/ or decentration between the relaxed and accommodated states, with the significance level set at $\alpha = 0.05$ throughout analysis.

5.2.9 Repeatability

The repeatability of both the analysis technique (applied to human data) and the complete experimental protocol was examined. Firstly, to determine the repeatability of human image analysis with the bespoke programme, the images of a single subject in the unaccommodated state, acquired with the scan line direction set at 0°, were analysed 10 times. The mean values of both tilt and decentration were calculated, in addition to the standard deviation (SD) and standard error (SE) of the measures.

To assess intersession repeatability of the entire protocol, a subset of ten participants returned within a fortnight of their initial visit, and were rescanned at both the 0 and 8.0 D stimulus levels. The bias for horizontal lens tilt and decentration relative to the cornea at

each demand level was calculated from the mean difference in measures between visits and paired t-tests used to determine whether the levels of bias were significantly different from zero. The limits of agreement (LoA), i.e. the interval over which 95 % of the differences between the two visits lie (Altman and Bland, 1983; Bland and Altman, 1986) were established using the standard deviation (SD) of differences with the following formula:

$$\text{LoA} = \text{bias} \pm (1.96 * \text{SD of differences})$$

Equation 3

5.3. Results

5.3.1 Repeatability

The results obtained from analysing a single image set ten times are displayed in Table 5.3, whilst the intersession repeatability data regarding the complete methodology are shown in Table 5.4. A small degree of error associated with the analysis technique is highlighted by table 5.3, probably reflecting the requirement of the operator to manually locate various landmarks on the AS-OCT images. The intersession repeatability of the entire technique is fair, with none of the degrees of bias reported in table 5.4 being significantly different to zero (paired t-tests).

<i>Repeat</i>	<i>Lens tilt (°)</i>	<i>Lens decentration (mm)</i>
1	0.320	-0.132
2	0.220	-0.143
3	0.578	-0.154
4	0.526	-0.154
5	0.330	-0.176
6	0.277	-0.154
7	0.541	-0.110
8	0.489	-0.132
9	0.323	-0.176
10	0.403	-0.088
Mean	0.401	-0.142
SD	0.125	0.028
SE	0.040	0.009

Table 5.3. Repeatability of image analysis techniques. A single subject was analysed 10 times at the 0 D stimulus level, with the scan line direction set at 0°.

<i>Parameter</i>	<i>0 D stimulus level</i>			<i>8 D stimulus level</i>		
	<i>Bias</i>	<i>SD of differences</i>	<i>95 % LoA</i>	<i>Bias</i>	<i>SD of differences</i>	<i>95 % LoA</i>

Horizontal lens tilt (°)	-0.067	0.247	-0.551, +0.417	-0.051	0.292	-0.623, +0.521
Horizontal lens decentration (mm)	-0.032	0.178	-0.381, +0.317	+0.060	0.108	-0.152, +0.272

Table 5.4. Intersession repeatability data. Ten subjects attended two sessions, 7- 14 days apart. Horizontal lens tilt and decentration were analysed, by setting the scan line direction to 0°.

5.3.2 Main investigation

A broad range of refractive error was identified amongst the cohort of 20 youthful subjects, from -9.50 to +0.88 D mean sphere equivalent (MSE; mean -2.21 ± 2.78 D). Mean objective accommodative response to the 8.0 D stimulus was 5.48 ± 0.95 D, reflecting the lag of accommodation known to occur at high vergence demands. Table 5.5 summarises the results of lens tilt and decentration, relative to the cornea, in the relaxed and accommodated states for the complete cohort.

Demand level	<i>Lens tilt (°)</i>		<i>Lens decentration (mm)</i>	
	0 D	8.0 D	0 D	8.0 D
Horizontal	-0.185 ± 0.845	-0.262 ± 0.758	-0.111 ± 0.271	-0.110 ± 0.189
Vertical	0.411 ± 0.628	0.455 ± 0.639	0.102 ± 0.196	0.121 ± 0.226

Table 5.5. Mean values for lens tilt and decentration, relative to the cornea in relaxed and accommodated states. n = 20 youthful subjects. For horizontal scans, negative values of tilt indicate nasal tilt (i.e. nasal edge of lens displaced backwards), whilst negative values for decentration represent nasal displacement of the lens, relative to the cornea. For vertical scans, positive values of lens tilt indicate that the superior edge of the lens is moved forwards, whilst positive values of decentration indicate inferior displacement of the lens, relative to the cornea.

The mean values stated in Table 5.5 indicate that the crystalline lens is tilted slightly nasally and forwards in both the relaxed and accommodated states. Figure 5.9 graphically illustrates the lens tilt in both conditions for all subjects, and highlights significant variation between individuals in lens tilt, ranging from -1.25 to $+1.91^\circ$ horizontally, and -0.96 to $+1.58^\circ$ vertically in the unaccommodated state. There was no significant difference in lens tilt

between the relaxed and accommodated conditions for either the horizontal or vertical meridians ($t = 0.656$, $P = 0.518$ and $t = -0.576$, $P = 0.571$, respectively).

Regarding lenticular decentration, the lens was found on average, to be displaced slightly inferiorly and nasally. Again, there was significant variation between subjects with decentration in the unaccommodated state ranging from -0.80 to $+0.30$ mm horizontally, and -0.22 to $+0.34$ mm vertically. Figure 5.10 illustrates lens decentration for all participants in the relaxed and accommodated conditions. No significant difference was identified in lens decentration, relative to the cornea, between the unaccommodated and accommodated states, in either the horizontal or vertical meridian ($t = -0.011$, $P = 0.992$ and $t = -0.500$, $P = 0.623$, respectively).

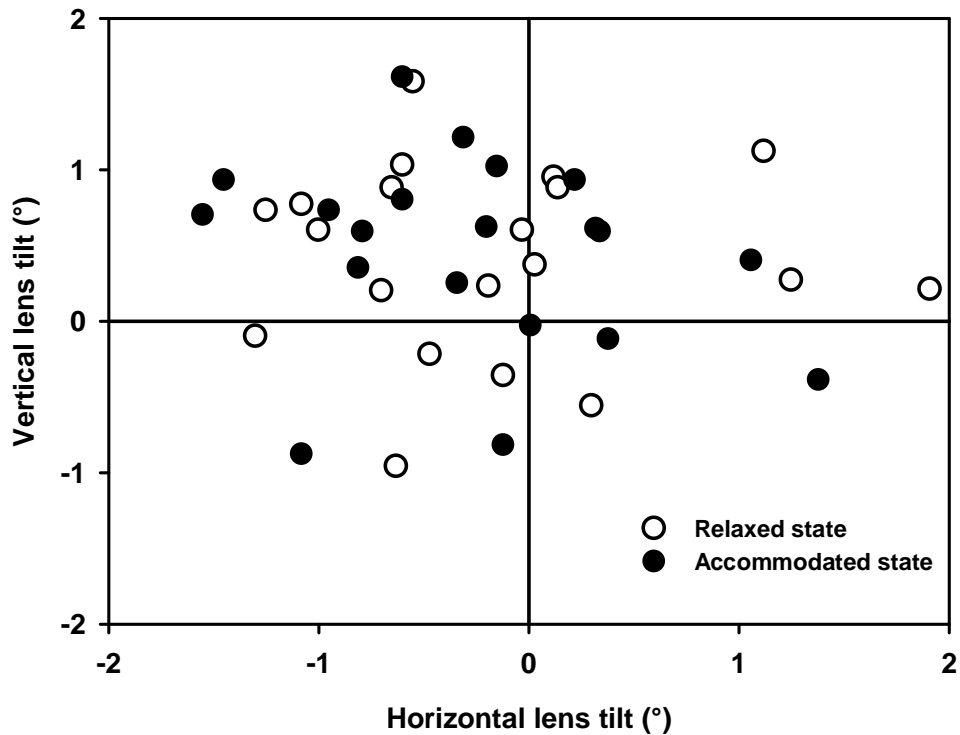


Figure 5.9. Lens tilt in the unaccommodated state, and in response to an 8.0 D stimulus. $n = 20$ young subjects. No significant accommodative difference was identified in either horizontal or vertical lens tilt.

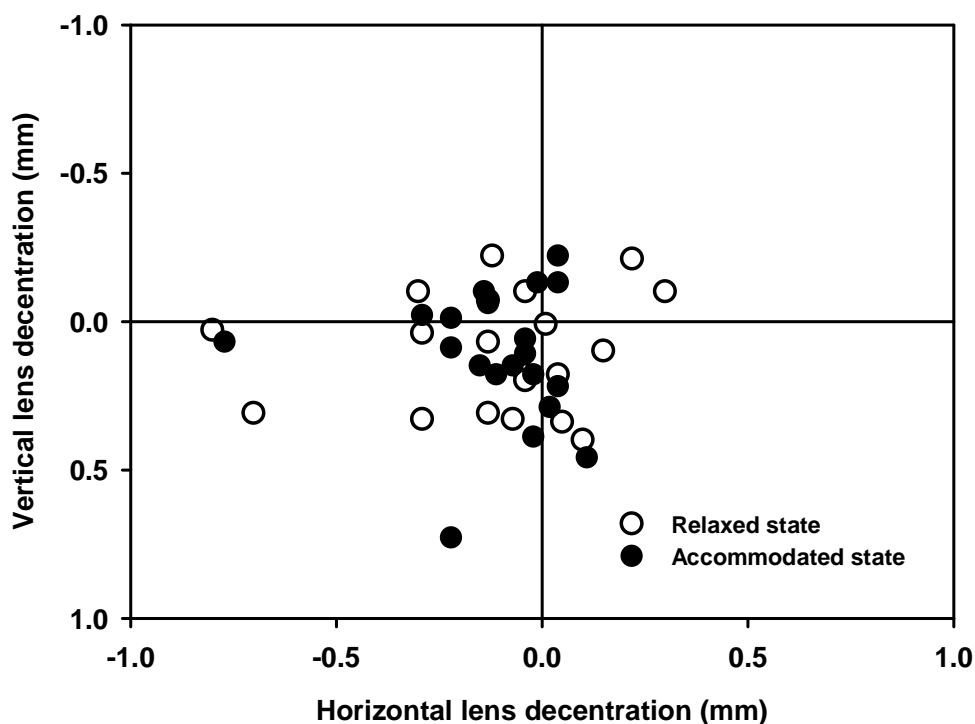


Figure 5.10. Lens decentration in the unaccommodated state, and in response to an 8.0 D stimulus. $n = 20$ young subjects. No significant difference was identified in either horizontal or vertical lens decentration relative to the cornea, with accommodation.

5.4. Discussion

There is a paucity of published data reporting the effects of accommodation on phakic lens tilt and alignment relative to the cornea. This study is the first to describe a method for analysis of lenticular tilt and decentration using AS-OCT. Whilst most previous investigations into human ocular surface alignment have required bespoke apparatus (e.g. Barry *et al.*, 2001; Kirschkamp *et al.*, 2004; Rosales and Marcos, 2006; He *et al.*, 2010), this study is based upon use of a non-modified commercially available instrument.

The data indicate relatively good alignment between the lens and cornea in the unaccommodated state, with mean tilt values of $0.185 \pm 0.845^\circ$ horizontally (i.e. nasal tilt) and $0.411 \pm 0.628^\circ$ vertically (i.e. superior edge of lens moved forwards). The lens was, on average, displaced inferio-nasally by 0.111 ± 0.271 mm (nasal displacement) and 0.102 ± 0.196 (inferior displacement), relative to the cornea. However, there was significant inter-individual variation in these parameters, as reflected by the standard deviations of the measures, and depicted in Figures 5.8 and 5.9. The mean values and standard deviations obtained in this study for lens tilt are similar to those obtained using phakometry by Kirschkamp *et al.* (2004), Dunne *et al.* (2005) and Rosales and Marcos (2006; Table 5.1),

although significantly smaller than the values reported by Chang *et al.* (2007) using MRI and Schaeffel (2008), utilising phakometry. Furthermore, the decentration values reported here compare well with the results of all of the investigations summarised in Table 5.1, although the standard deviations of decentration measures are generally higher in the present study. A variety of factors could contribute to these discrepancies: the definitions of tilt and decentration vary between studies, for example, Schaeffel (2008) describes tilt relative to the fixation axis, rather than the corneal axis, as applied in the present study. The measures of lens decentration reported by Rosales and Marcos (2006) and Schaeffel (2008) are relative to the pupil centre, whereas the current study describes decentration from the corneal axis. The findings of Chang *et al.* are obtained from a cohort of just 6 participants (possibly due to the expense and time-consuming nature of MRI), thus the results should be considered with caution. Higher standard deviations of lens decentration reported here, compared to earlier studies could be due to either genuine population differences or the combination of factors in the present study which could lead to variability in the data, including operator input in manual location of landmarks during image analysis and the potential for subject head movements between collection of the anterior and posterior images (although participants were instructed to keep their heads as still as possible during data acquisition, and scans were repeated if head motion was suspected).

Accommodation to an 8.0 D target was found to cause no significant difference in either lens tilt or decentration, relative to the cornea. These findings are in agreement with the phakometry-based study of Kirschkamp *et al.* (2004), which utilised a 4.0 D accommodative stimulus. According to the broadly-accepted Helmholtzian mechanism of accommodation, the reduction in zonular tension following ciliary muscle contraction would be expected to cause reduced lens stability and a change in lens tilt and decentration due to gravity. Previous investigations that have failed to identify a significant change in lens stability during accommodation (Sokolowska and Thorn, 2003; Kirschkamp *et al.*, 2004; Schachar *et al.*, 2007) have been cited as evidence in support of the mechanism of accommodation proposed by Schachar (Schachar, 2006; Schachar, 2007), which is based upon an increase in zonular tension with accommodation. Although the present study has not measured a significant accommodative difference in lens tilt and decentration, there are other plausible explanations for the findings: it is possible that any changes in lens tilt and decentration are too small to be detected using the methodology developed here, given the inherent variability of the technique resulting from the semi-automated image analysis techniques. Additionally, significant changes in lens stability may only occur when the zonules are maximally slackened, i.e. at the subjective amplitude of accommodation. The present investigation utilised a standard accommodative demand level of 8.0 D which is below the

subjective amplitude that would be expected for many of the participants (Duane, 1922; Turner, 1958). A further possibility is that the lens is offered some degree of support during accommodation by the vitreous, meaning that reduced zonular tension does not result in significant lenticular instability. Several previous authors have proposed that vitreous support may be a key element in the mechanism of accommodation and assist in bringing about lenticular shape changes (Coleman, 1970; Coleman, 1986; Ljubimova and Eriksson, 2005). The data obtained in the present study could provide support for such hypotheses.

In addition to the potential sources of error previously identified, namely, subject head movements between scans and subjective operator input during image analysis, there are several further limitations to be addressed. The analysis programme is based on the assumption that the corneal and lenticular surfaces are rotationally symmetric. Non-rotationally symmetric surfaces would affect the determination of the corneal and lenticular axes, and lead to error in the calculated values of tilt and decentration. The subjective identification of surface apices can be difficult, particularly for the anterior lens surface, which is relatively flat, meaning that precise location of the most anterior portion is less accurate, adding to the variability in results associated with user input. Furthermore, due to the process by which the anterior and posterior surfaces of the lens are located by the operator in order to identify the midpoint values for determination of the lens axis, an artefactual level of lens tilt would be calculated, in the presence of lenticular decentration alone. Therefore, eyes with zero lens tilt but significant decentration, relative to the cornea, would produce a measurement of lens tilt, using the protocol described. In order to investigate the maximum possible effect this factor could have on the data, a sample image based on an AS-OCT scan was constructed using *PowerPoint* presentation software and analysed with the bespoke programme. The lens in the sample image was assigned zero lens tilt, but was decentred by the equivalent of 0.3 mm to reflect the maximum mean lens decentration reported by previous investigators (Table 5.1). The decentration of 0.3 mm resulted in an artificial value of 0.36° of lens tilt, representing the greatest amount one could expect lenticular tilt values to vary due to decentration alone.

A number of assumptions and sources of error associated with the methodology have been identified and discussed, with an attempt to quantify the effect on the data wherever possible. Whilst the factors described could affect the absolute values of lens tilt and decentration obtained, the same confounding factors would apply in both the relaxed and accommodated states. Therefore, the ability of the technique to identify changes in lens tilt and decentration, which are relevant to the mechanism of accommodation, should not be impaired as a consequence.

5.5. Conclusion

Estimates of lens tilt and decentration relative to the cornea can be obtained from AS-OCT images and application of the image analysis software developed by the author. The lens appears generally well aligned with the cornea in both the relaxed and accommodated states. The data suggest that the lens does not demonstrate significant instability during accommodation, which could be interpreted as evidence favouring a model centred on increased zonular tension with ciliary muscle contraction, although there are a number of alternative explanations for the findings. Further work enabling visualisation of the lens equatorial region, using high-resolution three dimensional MRI techniques, could provide further clarification of the effect of ciliary muscle contraction on zonular tension, by examination of changes in lens diameter with accommodation.

CHAPTER 6

THREE-DIMENSIONAL MAGNETIC RESONANCE IMAGING OF THE PHAKIC CRYSTALLINE LENS DURING ACCOMMODATION

6.1. Introduction

For over a decade, high resolution magnetic resonance imaging (MRI) techniques have been available for *in vitro* and *in vivo* analysis of the accommodative structures. As issues such as inadequate resolution and signal to noise ratio (SNR) limitations have been overcome through use of higher field strengths and specialised radiofrequency (RF) coils, application of this technique in accommodation and presbyopia research has become relatively more common (Strenk *et al.*, 1999; Richdale *et al.*, 2009). MRI offers several notable advantages over conventional ocular imaging techniques such as Scheimpflug photography, ultrasound biomicroscopy (UBM) and anterior segment optical coherence tomography (AS-OCT) in that images free from optical distortion may be acquired non-invasively in any desired plane (Strenk *et al.*, 1999; Jones *et al.*, 2007). Furthermore, the entire crystalline lens and its relationship with neighbouring ocular structures can be visualised.

Hitherto, the majority of published MRI studies relating to phakic accommodation have utilised a two-dimensional (2-D) approach, imaging a single axial slice of finite thickness, through the eye. Particular attention has been paid to the crystalline lens and ciliary muscle, and the accommodative and age-dependent changes that occur in these structures. Table 6.1 summarises the results and implications of notable *in vivo* MRI accommodation studies. Strenk *et al.* (1999) provided firm evidence for the first time that the human ciliary muscle maintains its *in vivo* contractile ability well into old age. The diameter of the ciliary muscle ring was found to reduce in response to an 8.0 D accommodative stimulus, even in advanced presbyopes, and furthermore, a significant age-dependent reduction in this diameter was identified. A later study (Strenk *et al.*, 2006) with a larger cohort confirmed these findings and established that the accommodative and age-dependent reductions in ciliary muscle ring diameter were not affected by IOL implantation. Persistence of ciliary muscle contractile ability in the ageing eye supports the Hess-Gullstrand theory (Hess, 1896; von Gullstrand, 1924) of presbyopia development which states that lenticular changes underlie the loss of accommodation and that the ciliary muscle loses its ability to modify lens shape as a result of increased lenticular stiffness.

More recently, the antero-posterior position of the ciliary muscle apex during accommodation has been analysed using MRI. Strenk *et al.* (2010) observed no forward accommodative movement of the muscle apex in subjects aged 22-91 years, contravening the widely-accepted theory that the ciliary muscle moves anteriorly and inwards during accommodation to reduce tension on the zonules. However, AS-OCT findings reported in Chapter 3, using a stimulus of the same vergence (-8.0 D) as Strenk and colleagues, indicate that the ciliary muscle does move anteriorly with accommodation, by $110 \pm 86 \mu\text{m}$, and $223 \pm 108 \mu\text{m}$ on the nasal and temporal sides, respectively. Changes of this magnitude may be difficult to detect using MRI: Strenk *et al.* (2010) stated the absolute error of their technique to be $78 \mu\text{m}$.

In addition to ciliary muscle studies, MRI has provided a wealth of information on the optical and morphological changes in the crystalline lens with age and accommodation. Techniques to map the refractive index distribution throughout the lens have been developed (Moffat *et al.*, 2002a; Moffat *et al.*, 2002b; Jones and Pope, 2004) and applied to human eyes *in vitro* (Jones *et al.*, 2005) and *in vivo* (Jones *et al.*, 2007; Kasthurirangan *et al.*, 2008). A central plateau region of high refractive index, surrounded by a zone of sharp decline is present throughout life, although the peripheral reduction is steepest in older lenses (Jones *et al.*, 2005; Kasthurirangan *et al.*, 2008). The equatorial diameter of the central plateau zone increases with age, and decreases with accommodation (Kasthurirangan *et al.*, 2008).

Author & study title	Cohort characteristics	Demand levels	Results	Implications
Strenk et al. 1999 Age-related changes in human ciliary muscle and lens: a magnetic resonance imaging study.	n = 25 (range 22-83 years).	0.1 and 8.0 D	In unaccommodated state, ciliary muscle (CM) ring diameter decreases with age. CM retains contractile ability with age. Lens ability to change shape in response to CM contraction, reduces to zero with age.	Supports lenticular theory of presbyopia. CM remains active after loss of accommodation. Lenticular changes could be secondary to reduced tension resulting from decreased CM ring diameter with age.
Strenk et al. 2004 Magnetic resonance imaging study of the effects of age and accommodation on the human lens cross-sectional area.	n = 25 (range 22-50 years)	0.1 and 8.0 D	Total lens cross-sectional area (CSA) and CSA of anterior portion increase with age in both accommodative states. CSA of posterior portion not dependent on either age or accommodative state.	Lens growth during life appears confined to the anterior portion of the lens. Properties of the anterior capsule, the position of zonular attachments or the location of foetal nucleus may be responsible for lens CSA changes being confined to anterior portion.
Strenk et al. 2006 Magnetic resonance imaging of aging, accommodating, phakic, and pseudophakic ciliary muscle diameters.	n = 40 (range 22-91 years) 32 phakic, 8 pseudophakic	0.1 and 8.0 D	Change in CM diameter with accommodative effort not altered by age or intraocular lens implantation.	Strategies to restore accommodation may rely on a functioning ciliary muscle, but must also take into account the effect of decreased CM diameter on zonular tension.
Jones et al. 2007 Changes in lens dimensions and refractive index with age and accommodation	n = 44 (range 18-59 years)	0.17 and 6.67 D	Unaccommodated lens thickness (LT) increases with age. Lens diameter (LD) is independent of age. LT and LD change by $+0.050 \pm 0.024$ and -0.067 ± 0.030 mm/ D with accommodation.	Findings are consistent with the Helmholtzian mechanism of accommodation.
Kasthurirangan et al. 2008 <i>In vivo</i> study of changes in	n = 30, 15 young (19-29	0.16 D and maximum	A central region of high refractive index and sharp peripheral decline is present in all ages.	Lens central refractive index does not change with age or accommodation.

refractive index distribution in the human crystalline lens with age and accommodation.	years) and 15 older (60-70 years)	subjective amplitude	Peripheral decline in refractive index is steepest in older lenses. Equatorial diameter of central plateau increases with age, and decreases with accommodation	The central plateau region of high refractive index increases in size with age.
Hermans <i>et al.</i> 2009 Constant volume of human lens and decrease in surface area of capsular bag during accommodation: an MRI and Scheimpflug study.	n = 5 (range 18-35 years)	0.5 D and maximum subjective amplitude	Lens volume unchanged during accommodation, but lens surface area decreases by mean of 8.4 mm ² from 0.5 D to maximum stimulus level.	Lens material appears to be incompressible, and capsular bag undergoes elastic deformation during accommodation. Findings should be interpreted with caution as small cohort size and no repeatability data is provided for the 3-D MRI technique employed.
Strenk <i>et al.</i> 2010 Magnetic resonance imaging of the anteroposterior position and thickness of the aging, accommodating, phakic and pseudophakic ciliary muscle	n = 32 phakic, and 8 pseudophakic (range 22-91 years)	0.1 and 8.0 D	CM shifts anteriorly, towards cornea with age. No anterior movement of CM during accommodation observed at any age. CM is restored to its youthful position by cataract surgery with IOL implantation.	Contradicts classic theory that CM moves anteriorly and inwards during accommodation. Forces created as a result of continued lens growth are removed by cataract surgery, allowing choroidal elasticity to restore the CM to a more posterior position.

Table 6.1. Summary of notable *in vivo* MRI studies of human phakic accommodation.

The accommodative morphological changes of the crystalline lens observed from 2-D MRI studies to date have provided evidence to support von Helmholtz' (1855) theory of accommodation. Several authors have documented a significant increase in lens axial thickness, and reduction in equatorial diameter during accommodation (Strenk *et al.*, 1999; Jones *et al.*, 2007; Kasthurirangan *et al.*, 2008). Jones *et al.* (2007) reported mean changes in lens thickness and equatorial diameter of $+0.050 \pm 0.024$ mm/ D and -0.067 ± 0.030 mm/ D, respectively, although these values relate to stimulus demand level, rather than objective accommodation response. Analysis of lens cross-sectional area (CSA; Strenk *et al.*, 2004) shows an accommodative increase, with changes confined to the anterior portion of the lens. The increase in lens CSA with accommodation was hypothesised to be a result of lens compression in the unaccommodated state, and expansion when zonular tension reduces following ciliary muscle contraction. However, changes in CSA do not necessarily correspond to a change in lens volume (Judge and Burd, 2004; Hermans *et al.*, 2009).

Whilst the published MRI studies to date have undoubtedly furthered understanding of the action and ageing of accommodative structures, 2-D approaches have inherent limitations. Image acquisition planes could potentially vary between the relaxed and accommodated states, as a result of subject head movements, and the convergent and excyclotorsional eye movements that accompany accommodation. Schachar *et al.* (2008) analysed the MR images included in the publication of Jones *et al.* (2007) of an eye in the relaxed and accommodated states, finding that the globe diameter was smaller in the accommodating eye. As globe size does not decrease during accommodation (Drexler *et al.*, 1998; Ziebarth *et al.*, 2005; Mallen *et al.*, 2006), Schachar postulated that the accommodative reduction in lens diameter observed by Jones *et al.* (2007) was due to methodological error, which would have confounded the results of previous authors (e.g. Strenk *et al.*, 1999; Kasthurirangan *et al.*, 2008). It may be unlikely that image planes would vary significantly compared to overall slice thickness (usually 3 mm), but it is apparent that there is ongoing debate over the validity of 2-D methodologies to study lens equatorial diameter. Furthermore, 2-D data cannot provide direct information on lens volume. Several authors have utilised *in vitro* techniques to calculate lens volume, but *in vivo* measures are much more difficult to acquire. The lens is widely believed to be incompressible due to its high water content, thus its volume would not be expected to vary during accommodation. However, Gerometta *et al.* (2007) predicted a 2.6 % accommodative increase in human lens volume from a geometric model developed using published data on lenticular dimensions, and Strenk *et al.* (2004) suggested that reduced CSA in the unaccommodated state was due to lens compression. Furthermore, bovine

lenses have been shown *in vitro* to expand during simulated accommodation using a lenticular stretching device (Zamudio *et al.*, 2008). A completely 3-D high-resolution MRI methodology is required to provide clarification on *in vivo* changes in lens volume and equatorial diameter during human accommodation.

Singh *et al.* (2006) provided the first description of the shape of the whole eye in 3-D from MRI data. Previous authors had only assumed 3-D shape from a limited number of 2-D slices, but the acquisition of MRI data with high resolution in all three dimensions facilitated the generation of complete 3-D surface models, providing information on ocular volume, surface area, axial length and width. In addition to describing variations in human eye shape, the image analysis techniques described by Singh *et al.* (2006) have been applied to the developing chick eye, scanned with a 9.4 Tesla (T) small animal scanner (Goodall *et al.*, 2009). *In vivo* human eye studies have generally used lower field strengths (typically 1.5 or 3.0 T), although Richdale *et al.* (2009) have recently reported a protocol to generate optimised 3-D images of the human eye at 7.0 T. The very high resolution MR scans, with a voxel size of 0.1 x 0.1 x 0.5 mm allowed fine structures such as the ciliary body and iris to be clearly visualised. However, the protocol required subjects to have their eyelids taped closed to reduce motion artefacts due to blinking, thus the methodology described could not be used to examine accommodative changes in ocular structures in response to visual stimuli. Furthermore, Langner *et al.* (2010) have examined *in vivo* rabbit eyes and several species of *ex vivo* eyes (including a single human eye) in three dimensions at 7.1 T, providing volumetric and surface area data. The protocol utilised a small inner-tube diameter (200.5 mm) scanner, unsuitable for examination of human subjects *in vivo*.

To date, one published study has reported accommodated and unaccommodated lens dimensions, including volume, obtained using a 3-D MRI approach. Hermans *et al.* (2009) generated estimates of lens volume and surface area in 5 subjects using a 1.5 T scanner to acquire T₁-weighted 3-D MRI scans. Application of a Canny filter to the images to determine the lens interface in eight principle meridians, and calculation of volume and surface area of each of the eight segments allowed summation of these values to describe the parameters of the whole lens. No significant accommodative change in lens volume was observed (mean 160.1 ± 2.8 mm³ in the relaxed state), although surface area decreased with accommodation (mean 175.9 ± 2.5 mm² and 167.5 ± 2.9 mm² in the relaxed and fully accommodated states, respectively). The findings imply that the human crystalline lens mass is indeed incompressible, and the capsular bag undergoes elastic deformation during accommodation. However, the results should be considered with

caution due to the very small cohort size, and the lack of reported repeatability data relating to the 3-D imaging and analysis techniques.

MRI, therefore, represents a unique methodology permitting visualisation of the entire lens and surrounding structures in scans free from optical distortion. The majority of previously-published MRI studies on accommodation have utilised a 2-D approach, but collection of data with high resolution in all three dimensions is now possible. 3-D MRI techniques have been used to model *in vivo* the complete human eye (Singh *et al.*, 2006; Richdale *et al.* 2009), rabbit eye (Langner *et al.* 2010), and more recently, the human lens during accommodation (Hermans *et al.*, 2009). All previous accommodation studies based on MRI have analysed just two stimulus vergence levels (usually minimal, and near maximal subjective amplitude), providing no information on the rate of change of various lenticular parameters.

The aim of this study is to develop an MRI protocol enabling 3-D imaging of the complete crystalline lens during accommodation. The protocol will be applied to a larger cohort than the previously-published 3-D study of accommodation, and intermediate stimulus levels will be explored for the first time using MRI. Changes in lenticular dimensions will be considered in relation to objectively-measured accommodative response rather than stimulus demand, providing a more valid description of changes occurring in the human lens during accommodation. The study develops the author's previous work by utilising an additional advanced *in vivo* technique to analyse biometric changes during accommodation, and overcomes some of the limitations of AS-OCT, most significantly, the lack of ability to visualise the lens equator.

6.2. Methods

Prior to the main investigation, it was necessary to conduct developmental work to standardise a protocol for MR imaging of the lens at sufficiently high, isotropic resolution, to enable 3-D analysis and generation of complete lenticular surface models. The study was a collaboration between Aston University's Ophthalmic Research Group (ORG) and neuroimaging physicists from the School of Psychology at Cardiff University. Subject recruitment and preliminary data collection took place at Aston University, whilst all MRI work was conducted at the Cardiff University Brain Repair and Imaging Centre (CUBRIC). The ethics committees of both Aston University and Cardiff University approved the study, which was performed in accordance with the tenets of the Declaration of Helsinki. Written, informed consent was obtained from all participants following explanation of the nature and possible consequences of the study. Subjects consented to the initial stages of the

study at Aston University (see Appendix 2 for consent form), and completed MRI initial screening and consent forms (see Appendix 4) to ensure suitability for the subsequent stages of the investigation. A second screening form (see Appendix 4) was completed at CUBRIC, immediately before scanning.

6.2.1 MRI Protocol Development

Generation of complete ocular surface models from MRI data has been previously described by Singh *et al.* (2006). However, to apply similar analysis techniques for smaller, lenticular models, a novel scanning protocol was required, optimised for imaging the crystalline lens. Furthermore, it was necessary to develop a method of presenting accommodative stimuli within the confines of the scanner.

Rather than using the body coil integrated into the 3.0 T General Electric HDx system, a birdcage-design head coil was needed to improve the signal to noise ratio (SNR), which also acted as a mount for a mirror, positioned at an angle of 45°, to allow supine subjects to see out of the scanner (Figure 6.1). Cushioned pads were positioned between the head coil and the subject to minimise head movements. A static, high-contrast (85 %) Maltese cross target, visible through the mirror during scanning, was used for fixation, positioned on the window of the MRI control room, providing a stimulus vergence of -0.17 D for emmetropic subjects. Functional emmetropia was ensured for ametropic subjects by the wearing of disposable soft contact lenses (*Focus Dailies* or *Focus Dailies Toric*: nelfilcon A, 69 % water content; Ciba Vision, Duluth, Georgia, USA). A static cross target was used to avoid possible saccadic eye movements during scanning, which can cause motion artefacts. Accommodative stimulus levels of 4.0 and 8.0 D were selected to complement the author's previous work on ciliary muscle morphology (detailed in Chapters 3 and 4) which used the same vergence demands. To vary accommodative demand, subjects wore a non-metallic trial frame under the head coil, into which an occluder was placed in the left aperture, and a -4.00 or -8.00 DS trial lens in front of the right eye. The left eye was occluded to avoid convergent eye movements, and only the right eyes of all subjects were analysed. Figure 6.1 illustrates the subject set-up for MRI data collection.

Initial MRI work involved scanning sample subjects multiple times over several weeks to ascertain the ideal protocol that allowed images of sufficient resolution to be obtained, whilst keeping scan times down to a comfortable duration. MRI parameters including bandwidth, acquisition matrix, field-of-view, slice thickness, number of slices and number of signal averages were adjusted to optimise the protocol. Sagittal, axial and coronal localiser (scout) scans were performed initially on each subject to verify the location of the

crystalline lens and inform slice placement for the main scan. After the first and second major scans, subjects were moved out of the scanner to enable the trial lens to be altered to adjust stimulus vergence. A further localiser scan was therefore necessary before imaging the second and third accommodative states in case subject head movement had occurred whilst being moved out of, and back into, the scanner. T₂-weighted images, in which the fluid-filled regions of the eye appear hyperintense, were required for analysis purposes and were collected using the vendor's fast-spin echo (FSE) sequence, the most commonly used pulse sequence in current MRI protocols (Liney, 2005a).

The final protocol involved twenty-four oblique-axial slices of 0.8 mm thickness, with no inter-slice gaps, to visualise the crystalline lens fully in all three dimensions. FSE images were acquired with a bandwidth of ± 15.63 kHz, echo train length 24, sequence repetition time 8580 ms and echo time 500 ms. The acquisition matrix was square; 256 * 256, with a 205 mm field of view. Voxels within the images therefore had a 0.8 mm isotropic resolution. Three signal averages were performed, resulting in a total scan duration of 5 minutes 18 seconds. Although increasing the number of signal averages would provide improved SNR by reducing the effects of random artefacts, an unacceptable scan duration of 10 minutes per accommodative state would have resulted from 4 averages. Local shimming was performed prior to each scan to eliminate inhomogeneities in the magnetic field around the eyes, which cause geometric distortions (Liney, 2005b; Singh *et al.*, 2006). Total time spent in the scanner for each subject was approximately 45- 60 minutes, comprising of localiser scans, main scans, and repetition of longer scans, if necessary, due to blink/ motion artefacts.

The inherent motion sensitivity of the MRI protocol necessitated a means of eliminating blinking from the scans. A single blink during the main scan resulted in significant motion artefacts (due to the low number of signal averages) which would have rendered the images unsuitable for analysis. Initial experimental planning involved the use of topical corneal anaesthetic (e.g. benoxinate 0.4 %) to reduce the blink reflex. Although the blink reflex is suppressed by anaesthetics, it is not completely eliminated, as required for the scans. Furthermore, the Troxler effect, which causes a stimulus to disappear during prolonged viewing (Lou, 2008) and could result in unpredictable eye movements, would not have been solved by topical anaesthetic. A system was therefore developed to allow the scan to be paused as required for blinking and refixation. Subjects were provided with a button box (Fig. 6.1), connected to a PC in the MRI control room, that when pressed caused the monitor to change colour from grey to white, and back to grey when released.

Participants could therefore alert the MRI operator to pause the scan as frequently as required for blinking, and recommence once refixated on the stimulus.

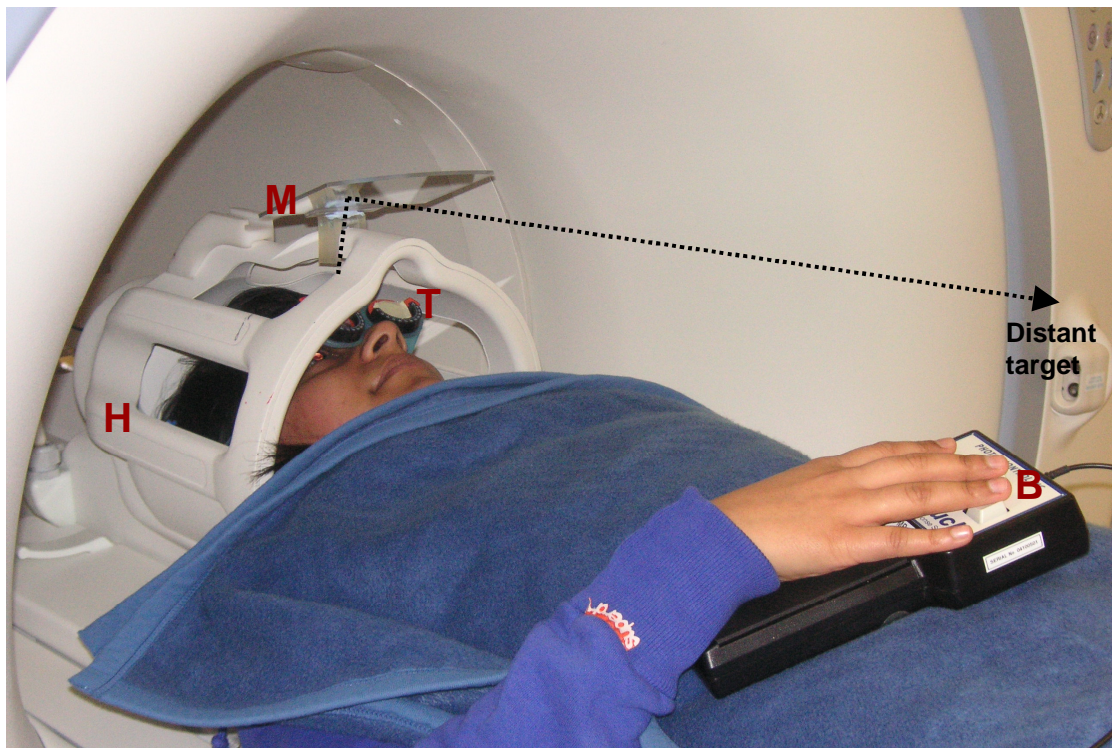


Figure 6.1. Subject set-up for MRI. Participants viewed a distant (-0.17 D) Maltese cross target, through a mirror (M), mounted at 45°, on the head coil (H). The left eye was occluded during scanning and -4.00 D and -8.00 DS trial lenses were inserted into the trial frame (T) to stimulate accommodation. Participants alerted the MRI operator when blink pauses were required by using a button box (B) connected to a PC in the control room.

6.2.2 Main protocol

Nineteen pre-presbyopic volunteers (7 male, 12 female), aged 19 to 30 years (mean age 25.8 ± 4.5 years) with no previous history of ocular abnormality or intraocular surgery were recruited using general email announcements at Aston University. Subjects with all types of refractive error were included, provided their prescription was amenable to correction with daily disposable soft contact lenses (*Focus Dailies* and *Focus Dailies Toric*). The parameter ranges for these contact lenses meant subjects with spherical refractive errors greater than -10.00 DS or +6.00 DS were excluded from the investigation, as were those with oblique cylinders > 0.50 DC, or orthogonal cylinders > 1.50 DC. Additionally, potential subjects were asked to complete an initial MRI screening form which excluded participants with implanted metallic devices (e.g. pacemakers, metal plates), those with possible metal fragments in the eyes or elsewhere in the body, migraine sufferers and females who may have been pregnant, for safety reasons.

All measurements were taken from the right eye only. Refractive error was determined from the mean of five open-view distance autorefractor readings obtained with the Grand Seiko Auto Ref/ Keratometer *WAM-5500* (Grand Seiko Co. Ltd., Hiroshima, Japan; Sheppard and Davies, 2010a). Subjects with spherical or astigmatic refractive error > 0.50 D were corrected with disposable soft contact lenses. Functional emmetropia was necessary to ensure near-identical accommodative demand for each subject.

Objective accommodative responses were determined using the *WAM-5500* autorefractor whilst subjects fixated Maltese cross targets in free space at -4 D and -8 D stimulus vergences, presented in random order. The targets subtended a constant angular subtense of 4.6° . Average target luminance and Michelson contrast values were 34.0 cd/m^2 and 82% , and 30.5 cd/m^2 and 80% , for the 4 D and 8 D stimuli, respectively. The left eye was occluded with a patch during measurement of the response and subjects were instructed to “carefully focus” (Stark and Atchison, 1994) on the centre of the Maltese cross to induce both voluntary and reflex accommodation (Radhakrishnan and Charman, 2007a). It was ensured at this stage that participants had sufficient subjective accommodative amplitude to maintain clarity of the 8 D stimulus, which would be required for subsequent MRI data collection. Five readings were obtained at each stimulus level, and the mean of these values was used in conjunction with the distance autorefractor results to determine the objective accommodative response. Axial lengths were obtained from the mean of five partial coherence laser interferometry (PCI) readings, using the *IOLMaster* (Carl Zeiss Meditec, Inc., Dublin, California, USA; Santodomingo-Rubido *et al.*, 2002). For those subjects corrected with soft contact lenses, axial length measurement was conducted at the end of initial data collection, following lens removal.

MRI data collection took place approximately 2 weeks later, depending on scanner availability, at CUBRIC. Participants completed a second MRI screening form to ensure none of the initial responses had changed, and a CUBRIC consent form. While undergoing scanning, ametropic subjects wore contact lenses of the specification determined in the earlier stage of the study. Scans were performed according to the protocol previously described, at randomly-ordered stimulus vergence levels of -0.17 , -4.0 and -8.0 D.

6.2.3 MRI data analysis

Image analysis was performed using a specially modified version of the freeware software package *mri3dX* (www.jiscmail.ac.uk/lists/mri3dX.html), described by Singh *et al.* (2006)

for semi-automated 3-D characterisation of complete eye shape. The T₂-weighted images, in which the fluid-filled regions of the eye appear hyperintense, are loaded into *mri3dX*, and the dark crystalline lens manually identified (Fig. 6.2a). A 3-D flood-filling algorithm is used to label the voxels comprising the lens and shade them yellow (Fig. 6.2b). Thresholds for voxel intensity were set at 0-73 for all crystalline lenses in the study following analysis of pilot MRI data from 3 subjects. This range was found to most accurately shade the lenticular region, although manual editing (to a precision of 0.1 mm) of the shaded area can be performed if necessary, in all three dimensions, to ensure complete characterisation of the lens. Manual editing of the shaded crystalline lens was only required for approximately 25 % of images. Subsequently, the operator manually identifies the crystalline lens anterior pole with the cursor, and a sphere consisting of 32, 768 triangular polygons is automatically generated to completely envelop the shaded lens voxels. An iterative shrink-wrap process is executed until the vertices of each polygon intersect a shaded voxel. The ensuing polygonal model appears ribbed, due to tight wrapping of the mesh to surface voxels, thus a rapid smoothing process is executed to average local vertex positions and generate a more regular 3-D representation of the lens. The number of smoothing iterations is user-defined, and was set at 200 throughout the investigation as pilot analysis found this level to produce the most realistic 3-D lens models; insufficient smoothing (0-100 iterations) caused a bumpy lens surface, whilst excessive smoothing (>300 iterations) resulted in a blocky lens model.

Three-dimensional lens representations are visualised using freeware *Geomview* software (www.geomview.org), allowing the model to be rotated and viewed at any orientation. The parameters of lens surface area; volume; anterior and posterior radii of curvature; axial thickness and equatorial diameter are displayed in the *Geomview* window, along with the lens model (Fig. 6.3). The radius of the area over which surface curvature is described is defined by the operator, and was set at 3.5 mm for all analysis to ensure that the whole region (of 7.0 mm in diameter) fitted onto the lens model surface.

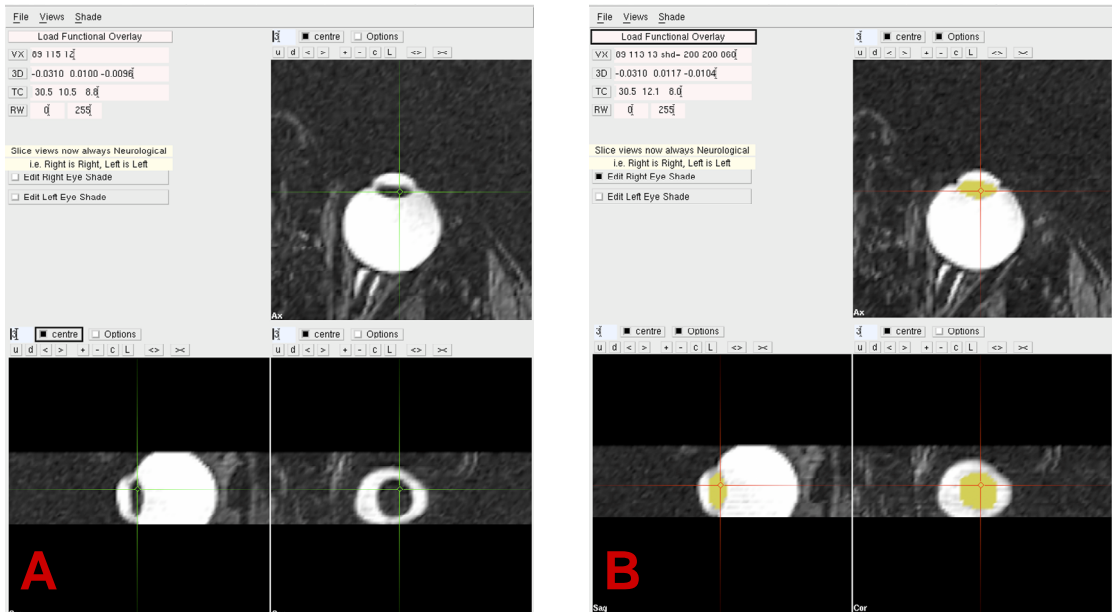


Figure 6.2. Image analysis using *mri3dX*. The lens is identified by the operator on the T_2 -weighted images (A), and a flood filling algorithm is employed to shade the crystalline lens voxels yellow (B).

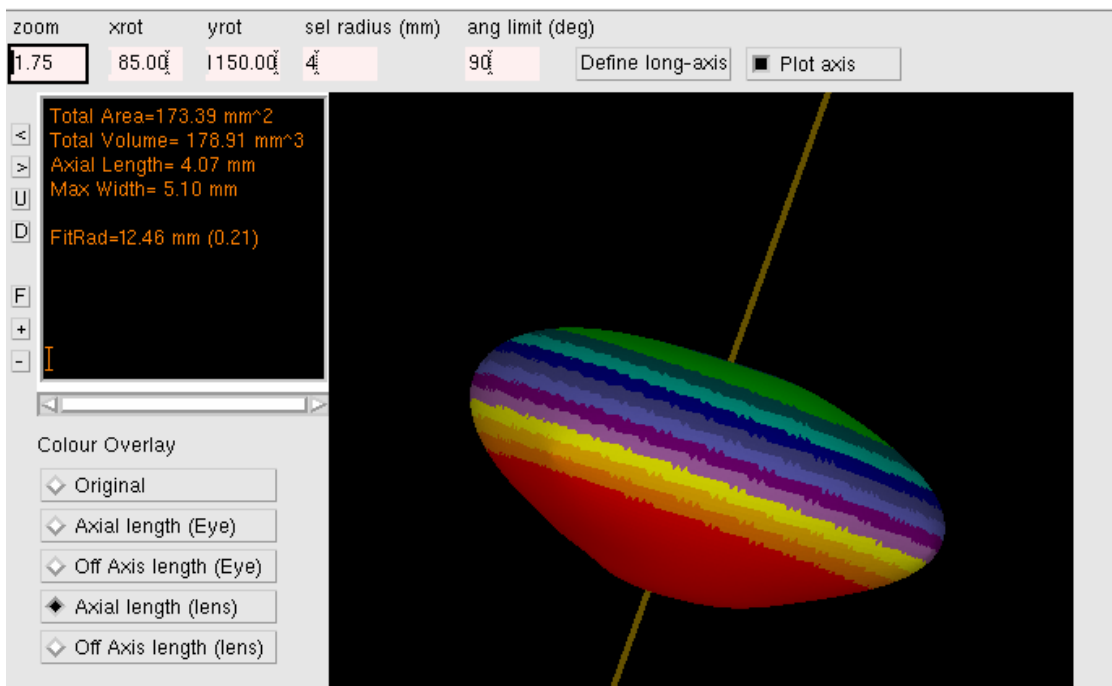


Figure 6.3. Visualisation of 3-D lens model using *Geomview* freeware software. The programme allows the lens be rotated and viewed from any orientation, in addition to providing the calculated values of area, volume, thickness, diameter and anterior and posterior radii of curvature.

6.2.4 Repeatability

The repeatability of both the image analysis methodology and the complete MRI experimental protocol were investigated as this study is the first to examine the crystalline lens in 3-D utilising the techniques described. Firstly, to determine the repeatability of semi-automated image analysis with *mri3dX*, the images of a single, randomly-selected

subject at the 0.17 D demand level, were analysed 10 times. The mean value of each of the 6 lens parameters was calculated, in addition to the standard deviation (SD) and standard error (SE) of the measures.

To assess intersession repeatability of the entire MRI protocol, a single subject was imaged five times at the 0.17 D and 4.0 D accommodative states. Multiple repetitions of the 8.0 D level were not feasible due to the problem of subject fatigue. Whilst assessing repeatability, the participant was removed from the scanner after the acquisition of each long scan. Images were analysed for the two accommodative states, and the mean, standard deviation and standard error of each parameter was calculated.

6.2.5 Statistical analysis

The relationships between axial length/ refractive error and the six lens parameters measured were explored using linear regression analysis, performed with *SigmaPlot* graphing and statistical software (Version 11, Systat Software Inc., Chicago, Illinois, USA). One-way repeated measures ANOVAs, using *SPSS* statistical software (Version 15, SPSS Inc., an IBM Company, Chicago, Illinois, USA) were executed to determine if accommodation caused significant changes in lens biometric characteristics. Demand, the within subjects factor, was assigned three levels, of 0.19, 4.0 and 8.0 D. A significance level of $\alpha = 0.05$ was used throughout analysis.

6.3. Results

6.3.1 Repeatability

The results obtained from analysing a single image set ten times are displayed in Table 6.2, whilst the intersession repeatability data of the complete MRI technique are shown in Table 6.3. Both the image analysis and complete MRI techniques appear robust, with intersession standard deviation (SD) and standard error (SE) values for lens thickness, diameter and anterior and posterior radii being within the voxel size of the original scans. Interestingly, the SDs and SEs of lens parameters are very similar at the 0 D and 4 D levels (Table 6.3), suggesting that subject fatigue in the accommodated state is not of significant detriment to the results. Use of the button box to pause scanning as necessary may reduce fatigue, providing more consistent data.

<i>Repeat</i>	<i>Surface area (mm²)</i>	<i>Volume (mm³)</i>	<i>Axial thickness (mm)</i>	<i>Equatorial diameter (mm)</i>	<i>Anterior radius of curvature (mm)</i>	<i>Posterior radius of curvature (mm)</i>
1	172.24	177.00	4.04	9.94	13.87	6.32
2	172.46	177.27	4.03	9.90	14.13	6.36
3	172.46	177.27	4.04	10.00	13.82	6.3
4	172.46	177.27	4.04	10.14	13.96	6.38
5	172.46	177.27	4.04	9.92	13.77	6.42
6	172.46	177.27	4.04	10.10	13.75	6.27
7	172.46	177.27	4.02	9.90	13.86	6.29
8	174.24	179.87	4.06	10.16	14.13	6.34
9	172.46	177.27	4.05	10.14	13.64	6.31
10	172.46	177.27	4.04	10.08	13.47	6.22
Mean	172.62	177.50	4.04	10.03	13.84	6.32
SD	0.58	0.84	0.01	0.11	0.20	0.06
SE	0.18	0.26	0.01	0.03	0.07	0.02

Table 6.2. Repeatability of *mri3dX* image analysis techniques. A single image set was analysed 10 times.

	<i>Surface area (mm²)</i>	<i>Volume (mm³)</i>	<i>Axial thickness (mm)</i>	<i>Equatorial diameter (mm)</i>	<i>Anterior radius of curvature (mm)</i>	<i>Posterior radius of curvature (mm)</i>
Mean: 0 D	172.45	177.45	3.95	9.78	11.18	6.42
SD	1.45	1.11	0.08	0.09	0.61	0.40
SE	0.73	0.56	0.04	0.04	0.31	0.20
Mean: 4 D	168.17	177.35	4.09	9.60	10.20	5.95
SD	2.11	1.45	0.09	0.12	0.58	0.32
SE	0.95	0.65	0.04	0.05	0.26	0.14

Table 6.3. Intersession repeatability of complete MRI technique. A single subject was scanned 5 times at the 0 D and 4 D stimulus levels, and images analysed with *mri3dX*.

6.3.2 Main investigation

Mean spherical equivalent (MSE) refractive error of the 19 participants ranged from -6.00 to +0.19 D (mean -2.38 ± 2.09 D). Mean objective accommodative responses to the 4.0 D and 8.0 D stimuli were 2.91 ± 0.66 D and 5.65 ± 1.12 D, respectively. Images of sufficient clarity for analysis purposes were obtained from all subjects at the 3 stimulus levels, although occasional motion artefacts required a proportion of scans (approximately 15 %) to be repeated, during the same session. Figure 6.4 is an example of the raw T₂-weighted axial images of a single subject at the -0.17 and -8.0 D vergence levels, and the resultant 3-D lens models generated by *mri3dX*. The accommodated lens is visibly thicker (4.24 *versus* 4.09 mm), with a smaller equatorial diameter (9.88 *versus* 9.50 mm).

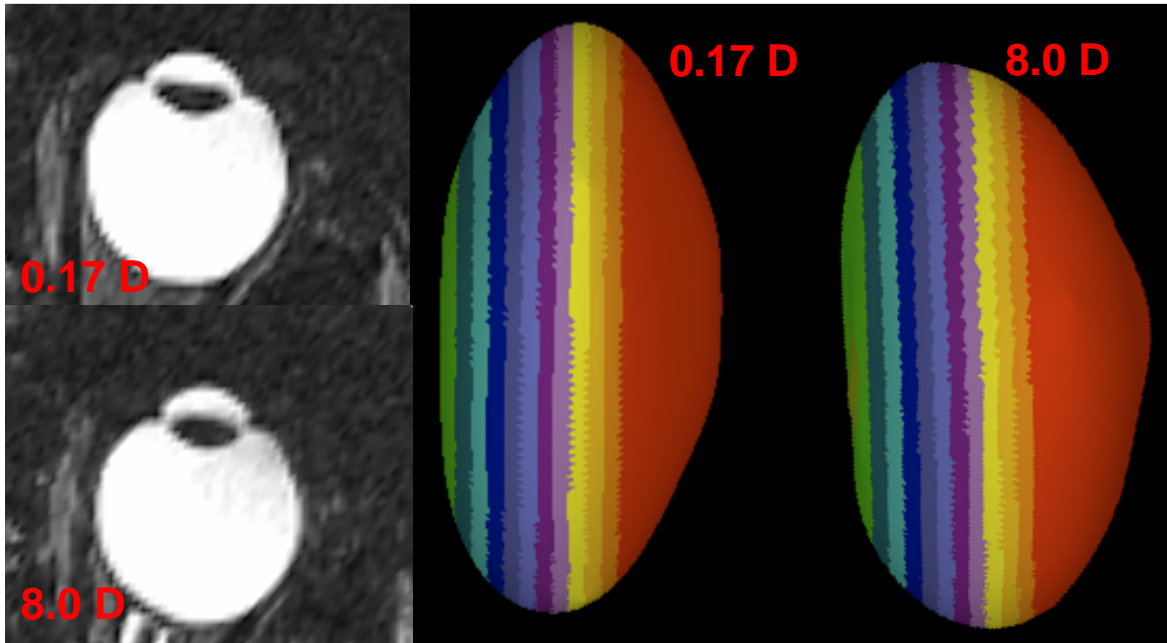


Figure 6.4. Raw T₂-weighted axial images (left) of a 20 year old subject scanned at the 0.17 and 8.0 D stimulus levels, and the corresponding 3-D lens models generated by *mri3dX* (right). The coloured bands on the 3-D models relate to axial distance from the anterior lens apex. Lens thickness measures in the relaxed and accommodated states were 4.09 mm and 4.24 mm, respectively, whilst lens equatorial diameters were 9.88 mm (0.17 D level) and 9.50 mm (8.0 D level).

Across the whole cohort, mean unaccommodated lens thickness was 3.75 ± 0.35 mm, which significantly increased with accommodation ($F = 33.39$, $P < 0.001$) at both of the accommodative vergence levels. From the 0.17 to 4.0 D level, mean change in lens thickness was $+0.06 \pm 0.08$ mm per dioptre of accommodative response (D_{Resp}), whilst between the 4.0 and 8.0 D levels, the increase was 0.09 ± 0.12 mm/ D_{Resp} . Figure 6.5 illustrates the change in lens thickness (and equatorial diameter) with accommodation. Mean lens equatorial diameter was 9.49 ± 0.45 mm in the relaxed state, with a significant accommodative reduction observed ($F = 24.00$, $P < 0.001$), which was greatest between the 0.17 and 4.0 D levels. Between the 0.17 and 4.0 D levels, mean change in lens equatorial diameter was -0.14 ± 0.17 mm/ D_{Resp} , but between the 4.0 and 8.0 D levels, the mean change was much smaller, at -0.01 ± 0.16 mm/ D_{Resp} . No significant correlation was identified between either unaccommodated lens thickness or equatorial diameter and axial length/ refractive error.

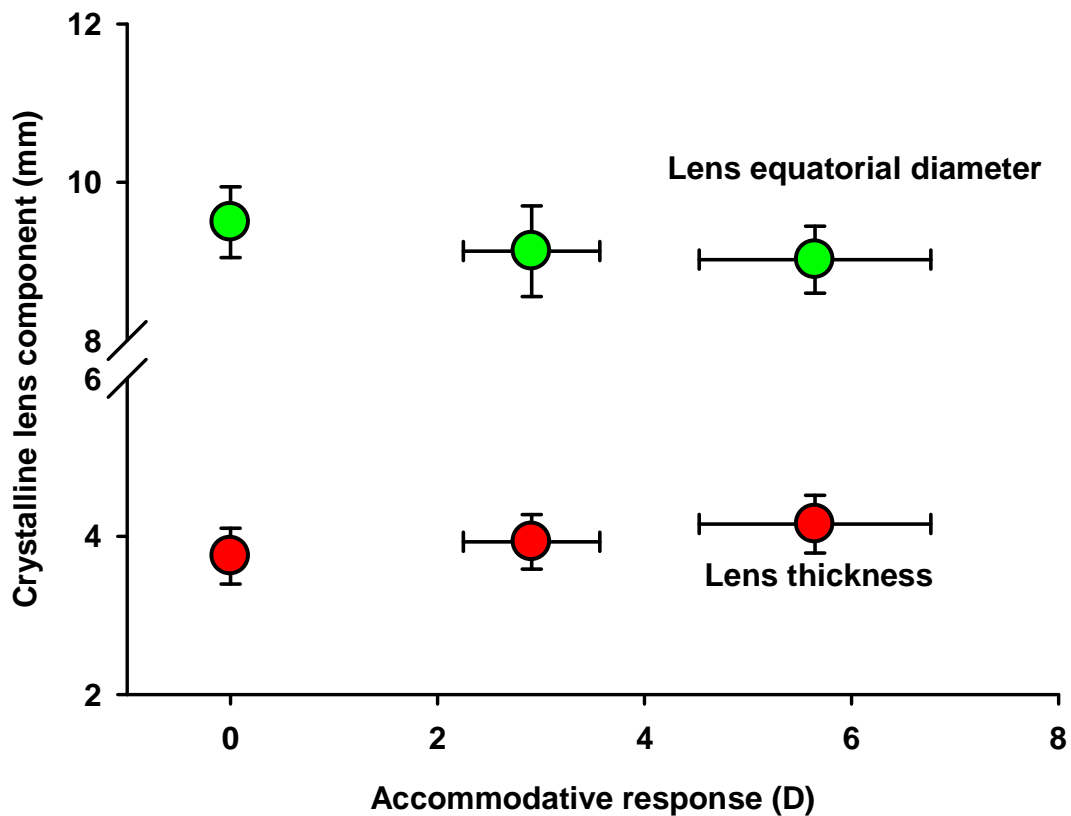


Figure 6.5. Change in lens equatorial diameter (green symbols) and lens thickness (red symbols) with accommodation. $n = 19$ young subjects. Error bars represent ± 1 standard deviation. A statistically significant reduction in lens equatorial diameter, and increase in lens thickness was observed with accommodation.

Regarding surface curvatures, the posterior lens surface was steeper at all three demand levels. In the relaxed state, mean anterior and posterior radii of curvature were 11.89 ± 2.75 mm and 6.12 ± 0.75 mm, respectively. Linear regression analysis identified a significant negative correlation between MSE refractive error and anterior lens radius of curvature ($R = 0.53$, $P = 0.02$), but no such relationship was present for the posterior lens radius ($R = 0.09$, $P = 0.71$). Furthermore, neither the anterior or posterior radius of curvature demonstrated a correlation with axial length ($r = 0.08$, $P = 0.75$; $r = 0.19$, $P = 0.44$, for the anterior and posterior surfaces, respectively). Both lens surfaces, but particularly the anterior surface, showed a significant reduction in radius with accommodation ($F = 21.78$, $P < 0.001$; $F = 13.81$, $P < 0.001$, for anterior and posterior surfaces, respectively). Mean reductions in anterior radius were 0.82 ± 1.04 mm/ D_{Resp} between the 0.17 and 4.0 D stimulus levels, and 0.63 ± 1.19 mm/ D_{Resp} between the 4.0 and 8.0 D levels. The posterior lens surface curvature steepened by 0.15 ± 0.23 mm/ D_{Resp} and 0.46 ± 1.45 mm/ D_{Resp} between the 0.17 to 4.0 D, and 4.0 to 8.0 D levels,

respectively. Figure 6.6 illustrates the change in anterior and posterior lens surface curvature with accommodation.

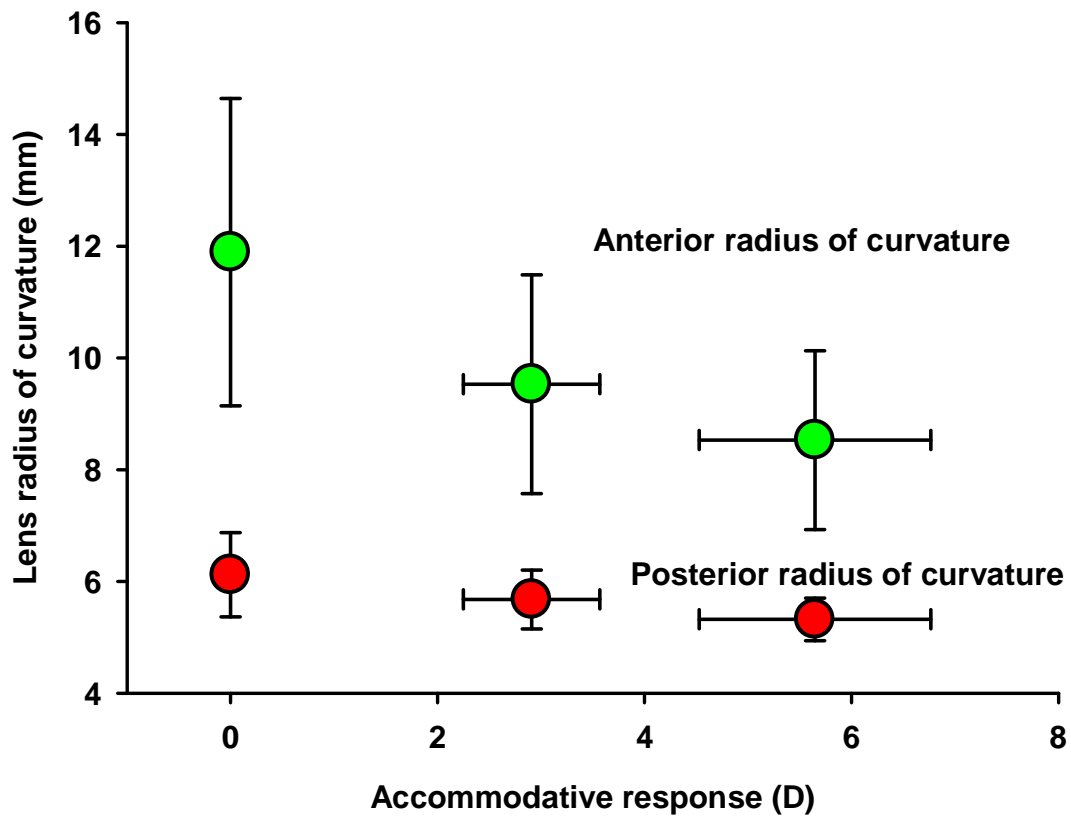


Figure 6.6. Change in anterior (green symbols) and posterior (red symbols) lens surface radii of curvature during accommodation. Error bars represent ± 1 standard deviation. A statistically significant reduction in both surface curvatures was identified during accommodation, although the anterior lens surface showed the greatest steepening.

Mean lens surface area in the relaxed state was $157.72 \pm 11.59 \text{ mm}^2$, which reduced significantly with accommodation ($F = 7.04$, $P = 0.003$). Between the 0.17 and 4.0 D levels, lens surface area reduced on average by 4.75 mm^2 , which represents a decrease of $1.73 \pm 2.01 \text{ mm}^2 / D_{\text{Resp}}$. Between 4.0 and 8.0 D, a small increase in lens surface area was measured, of $0.69 \pm 3.27 \text{ mm}^2$, although a paired t-test indicated that this change was not statistically significant ($t = -0.41$, $P = 0.68$). Figure 6.7 shows the change in lens surface area with accommodation.

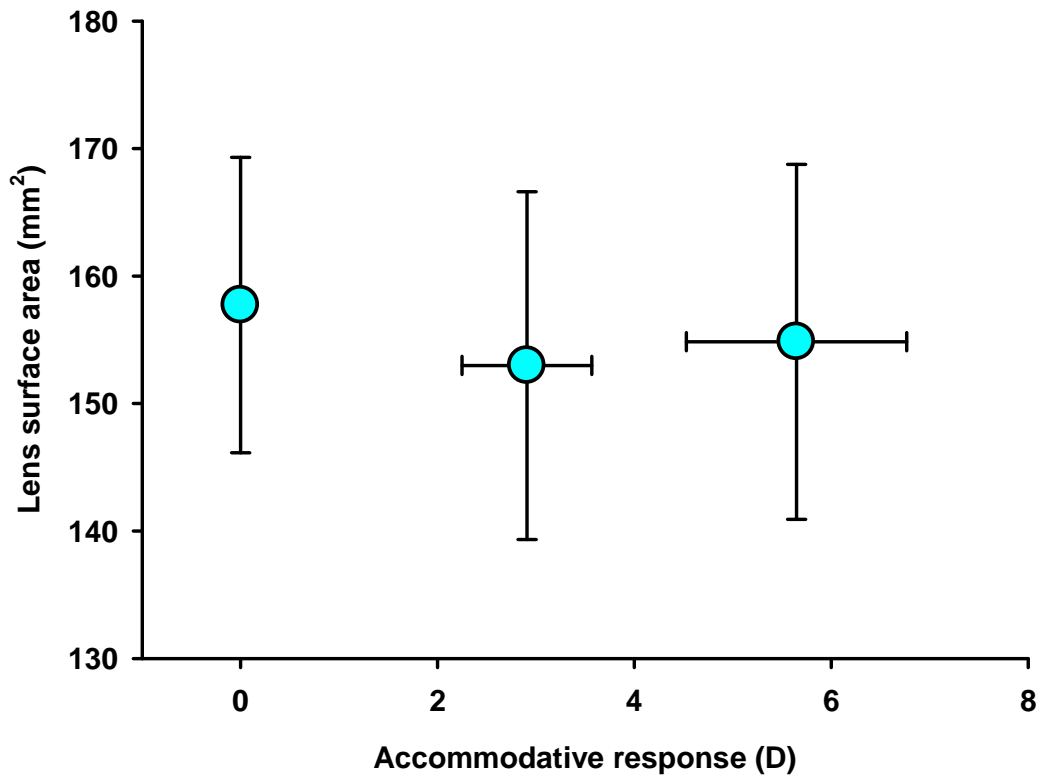


Figure 6.7. Change in lens surface area with accommodation. Error bars represent ± 1 standard deviation. Overall, a significant reduction in surface area was observed with accommodation, although the change consisted of a large, significant reduction between 0.17 and 4.0 D, accompanied by a small and insignificant increase between the 4.0 and 8.0 D levels.

Whilst lens surface area demonstrated an overall reduction with accommodation, mean lens volume increased significantly ($F = 6.06$, $P = 0.005$), from $154.52 \pm 19.00 \text{ mm}^3$ in the relaxed state to $158.08 \pm 22.89 \text{ mm}^3$ at 8.0 D stimulus vergence, a mean change of $+0.65 \pm 1.62 \text{ mm}^3 / D_{\text{Resp}}$. The overall mean increase in volume from the relaxed state to 8.0 D level was composed of a large increase between the 4.0 and 8.0 D stimulus levels, of $2.36 \pm 5.71 \text{ mm}^3 / D_{\text{Resp}}$, which was preceded by a non-significant ($t = 1.73$, $P = 0.11$) reduction in volume of $-1.24 \pm 3.13 \text{ mm}^3 / D_{\text{Resp}}$ from the relaxed state to the 4.0 D level. Figure 6.8 illustrates the change in lens volume measured during accommodation.

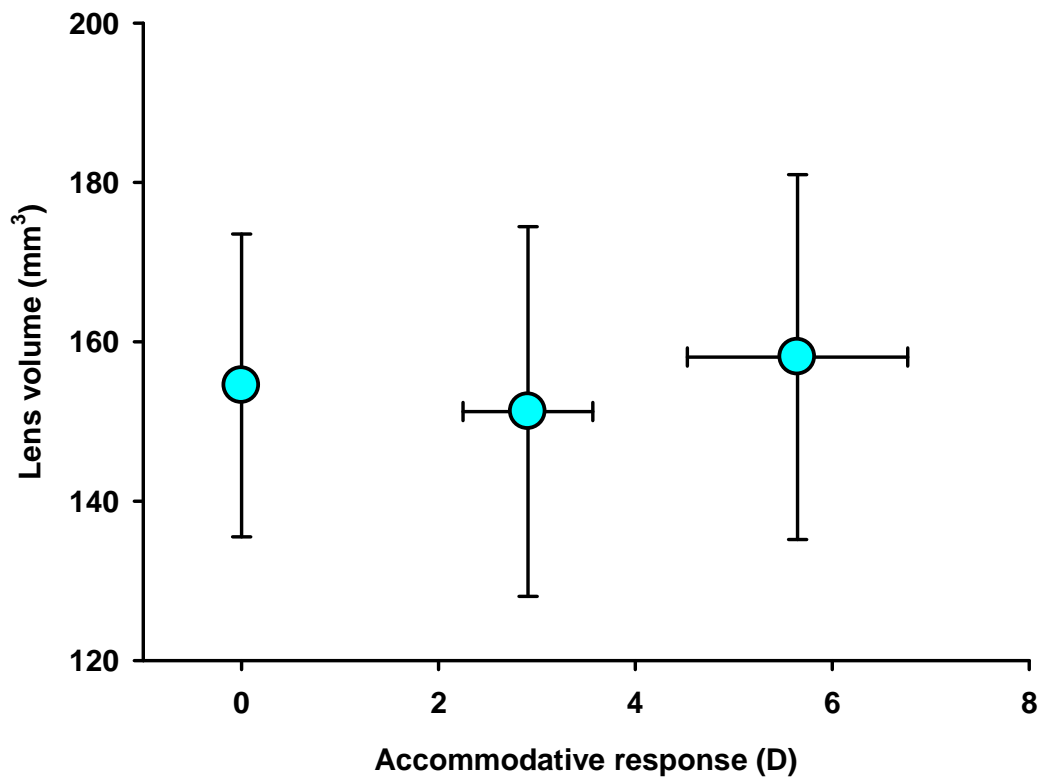


Figure 6.8. Change in lens volume with accommodation. Error bars represent ± 1 standard deviation. A significant increase in lens volume between the relaxed state and the 8.0 D demand level was identified.

Lens Parameter	Mean value at 0.17 D and accommodative change observed in present study	Mean value in relaxed state and accommodative change reported previously	
		Relaxed	Accommodative change and author/ study type
Axial thickness	3.75 ± 0.35 mm	3.66 ± 0.14 mm	+0.06 ± 0.03 mm/ D _{Resp} (3-D MRI; Hermans <i>et al.</i> 2009)
	+0.08 ± 0.05 mm/ D _{Resp}	3.78 ± 0.22 mm	+0.07 ± 0.04 mm/ D _{Resp} (2-D MRI; Kasthurirangan <i>et al.</i> 2008)
		4.05 ± 0.20 mm	+0.05 ± 0.02 mm/ D _{Resp} (AS-OCT; Richdale <i>et al.</i> 2008)
		3.73 mm*	+0.05 ± 0.02 mm/ D _{Stim} (2-D MRI; Jones <i>et al.</i> 2007)
		3.63 ± 0.07 mm	+0.04 ± 0.01 mm/ D _{Stim} (Scheimpflug; Dubbelman <i>et al.</i> 2005)
		3.70 ± 0.10 mm	+0.05 ± 0.03 mm/ D _{Stim} (A-scan ultrasound; Kirschkamp <i>et al.</i> 2004)
		3.63 ± 0.26 mm	+0.05 ± 0.04 mm/ D _{Stim} ** (2-D MRI; Strenk <i>et al.</i> 1999)
Equatorial diameter	9.49 ± 0.45 mm	9.58 ± 0.26 mm	-0.07 ± 0.01 mm/ D _{Resp} (3-D MRI; Hermans <i>et al.</i> 2009)
	-0.09 ± 0.065 mm/ D _{Resp}	9.12 ± 0.33 mm	-0.09 ± 0.08 mm/ D _{Resp} (2-D MRI; Kasthurirangan <i>et al.</i> 2008)
		9.33 ± 0.33 mm	-0.07 ± 0.03 mm/ D _{Stim} (2-D MRI; Jones <i>et al.</i> 2007)
		9.21 ± 0.29 mm	-0.08 ± 0.04 mm/ D _{Stim} ** (2-D MRI; Strenk <i>et al.</i> 1999)
Anterior radius of curvature	11.89 ± 2.75 mm	11.45 ± 1.7 mm	-0.51 ± 0.50 mm/ D _{Resp} (3-D MRI; Hermans <i>et al.</i> 2009)
	-0.63 ± 0.50 mm/ D _{Resp}	12.3 ± 0.8 mm	-0.93 ± 0.30 mm/ D _{Stim} (Phakometry; Kirschkamp <i>et al.</i> 2004)
		11.25 ± 0.4 mm	-0.61 ± 0.15 mm/ D _{Stim} (Scheimpflug; Dubbelman <i>et al.</i> 2001 & 2005)
Posterior radius of curvature	6.12 ± 0.75 mm	6.11 ± 1.4 mm	-0.14 ± 0.13 mm/ D _{Resp} (3-D MRI; Hermans <i>et al.</i> 2009)
	-0.15 ± 0.18 mm/ D _{Resp}	6.10 ± 0.2 mm	-0.20 ± 0.05 mm/ D _{Stim} (Phakometry; Kirschkamp <i>et al.</i> 2004)
Surface area	157.72 ± 11.59 mm ²	175.9 ± 2.8 mm ²	-1.4 ± 0.2 mm ² / D _{Resp} (3-D MRI; Hermans <i>et al.</i> 2009)
	-0.54 ± 1.08 mm ² / D _{Resp}		

Volume	154.52 ± 19.0 mm ³	160.1 ± 2.5 mm ³	No significant accommodative change (3-D MRI; Hermans <i>et al.</i> 2009)
	+0.65 ± 1.62 mm ³ / D _{Resp}		

Table 6.4. Mean values (± standard deviation) of the six lens parameters measured in the current investigation, and the change in these parameters with accommodation, (assuming a linear response profile from the 0.17 to 8.0 D levels). Previously published data are provided for comparison. D_{Resp} and D_{Stim} are dioptries of accommodative response, and dioptries of stimulus demand, respectively. * Based on linear regression results, for a 25- year old subject. ** Based on reported values for the ten youngest participants (aged 22- 31 years).

6.4. Discussion

Advances in MRI data collection and image analysis tools have recently facilitated complete 3-D modelling of the human crystalline lens *in vivo*. MRI overcomes several disadvantages associated with conventional ocular imaging techniques, and may now be utilised to measure lenticular changes with accommodation. To date, this study is the largest to provide data on crystalline lens biometric characteristics, in the relaxed and accommodated states, using an *in vivo* 3-D MRI methodology.

The crystalline lens accommodative changes observed are in accordance with the widely-accepted Helmholtzian theory. A statistically significant accommodative increase in lens thickness and reduction in equatorial diameter was accompanied by a steepening of surface curvatures. The increase in lens thickness with accommodation has been well documented previously, using *in vivo* imaging techniques including MRI (Strenk *et al.*, 1999; Jones *et al.*, 2007; Kasthurirangan *et al.*, 2008; Hermans *et al.*, 2009), Scheimpflug photography (Dubbleman *et al.*, 2005), AS-OCT (Richdale *et al.*, 2008) and ultrasonography (e.g. Kirschkamp *et al.*, 2004). However, the inability to view the equatorial region of the lens, due to the presence of the iris, has hindered *in vivo* determination of the effect of accommodation on human lens diameter. Previous 2-D MRI studies reporting a reduction in lens equatorial diameter during accommodation (Strenk *et al.*, 1999; Jones *et al.*, 2007) have received criticism for the possibility that the lenticular changes observed were due to differing acquisition planes, rather than accommodative state (Levy, 2000; Schachar *et al.*, 2008). According to the theory postulated by Schachar (1994; 2006), accommodation causes the lens equator to move outwards towards the sclera, secondary to increased equatorial zonular tension. However, the results of the present 3-D study, in which the errors associated with imaging just a single slice of finite thickness are removed, provide evidence in direct opposition to Schachar's non-conformist theory. Between the 0.17 and 8.0 D stimulus levels, the mean change in equatorial diameter with accommodation was -0.09 ± 0.07 mm/ D_{Resp} , representing an overall mean reduction of 4.95 %.

The protocol enabled anterior and posterior lens surface curvatures to be measured without the need to correct for optical distortion. A significant negative correlation ($r = 0.53$, $P = 0.02$) was identified between anterior lens radius of curvature and refractive error (i.e. higher myopes have flatter anterior lens surfaces). No such relationship was found regarding the posterior lens surface. Previous authors have identified no dependence of anterior lens radius on refractive error using phakometry (Goss *et al.*, 1997) and corrected Scheimpflug imaging (Dubbelman and Van der Heijde, 2001). However, the crystalline lens is known to become more steeply curved with age (Brown, 1974; Olbert, 1988; Dubbelman and Van der

Heijde, 2001), so it is possible that any relationship between anterior lens curvature and refractive error would be most apparent in young subjects, such as the participants in this study. Further investigation using alternative imaging methodology, to allow a greater volume of data to be collected, is required to confirm a link between anterior lens radius and refractive error, and explore the cause of any relationship, although such work is beyond the scope of the present investigation.

The observed decreases in lens radii of curvature with accommodation were most significant for the anterior lens surface, although the posterior surface remained steeper at all stimulus levels. Previous authors have described similar accommodative changes in lens surface curvatures, using Scheimpflug imaging (Koretz *et al.*, 2002; Dubbleman *et al.*, 2005) and phakometry (Garner and Yap, 1997; Kirschkamp *et al.*, 2004). The present study indicates that MRI represents a further methodology for analysis of changes in lens radii during accommodation. The measured curvature changes were non-linear in nature, particularly for the posterior lens surface. Between the 0.17 and 4.0 D levels, the anterior and posterior radii decreased by 0.82 ± 1.04 and 0.15 ± 0.23 mm/ D_{Resp} , respectively, whilst from the 4.0 to the 8.0 D levels, there was a small reduction in the anterior surface response, to -0.63 ± 1.19 mm/ D_{Resp} , but a three-fold increase in the posterior radius change, to -0.46 ± 1.45 mm/ D_{Resp} . Previous AS-OCT data regarding lenticular surface position during accommodation (Davies *et al.*, 2008) has suggested that significant accommodative changes in the posterior lens surface only occur above the 1.5 D response level; before this, lenticular changes are limited to the anterior portion of the lens. Further investigation is required to confirm the nature of the accommodative response of the posterior lens surface, through application of techniques such as AS-OCT, phakometry and Scheimpflug imaging to a substantial cohort of young subjects, with high amplitudes of accommodation, at a range of intermediate vergence levels.

The creation of fully 3-D lens models allowed determination of *in vivo* lens surface area and volume changes during accommodation, in the largest cohort described to date. A significant overall reduction in surface area ($P = 0.003$), and an increase in lens volume ($P = 0.005$) was observed. A mean 4.78 % accommodative decrease in lens surface area, but maintenance of constant lens volume was measured by Hermans *et al.* (2009), with MRI data from 5 subjects. The present study has identified a mean reduction in lens surface area of 1.82 % from the relaxed state to the 8.0 D stimulus, with an increase in volume of 2.30 %. The results suggest that the capsular bag undergoes elastic deformation during accommodation, causing reduced surface area, whilst the volumetric changes oppose the theory that the lens is incompressible due to its high water content. During distance viewing,

when the zonules are taut, the lens appears to be compressed, with expansion occurring when zonular tension reduces during accommodation. The data support the assertion that lens mechanics cannot be modelled as a simple incompressible fluid-filled sac (Weale, 1989). The observed 2.3 % increase in lens volume is in accordance with the theoretical +2.6 % accommodative change calculated by Gerometta *et al.* (2007), based on geometric modelling of the human lens. The dual occurrence of increased volume, and reduced surface area, has been predicted previously by Zamudio *et al.* (2008) by further mathematical modelling of mammalian and human lenses, based on their elliptical forms. The present study is the first to provide *in vivo* support of the theory developed by Gerometta *et al.* (2007) and modified by Zamudio *et al.* (2008).

For comparison purposes, the results of the present study are summarised in Table 6.4, along with recent *in vivo* studies that have applied MRI and alternative imaging techniques to measure changes in lens parameters with accommodation. It is apparent that the unaccommodated lens dimensions reported here compare well with previously published data, providing further evidence for the validity of the novel MRI acquisition and image analysis techniques described. Furthermore, the measured changes in lens thickness, equatorial diameter and radii of curvature are very similar to those documented by earlier studies that have reported differences based on accommodative response, rather than stimulus demand. Only one previous study has described *in vivo* lens surface area and volume characteristics. Hermans *et al.* (2009) reported larger values for both mean surface area ($175.9 \pm 2.8 \text{ mm}^2$ versus $157.7 \pm 11.6 \text{ mm}^2$) and lens volume ($160.1 \pm 2.5 \text{ mm}^3$ versus $154.5 \pm 19.0 \text{ mm}^3$) than the present investigation, with lower associated standard deviations, a possible consequence of the smaller sample size. No alternative technique to MRI, for validation of the measures, is currently available for measurement of lens volume and surface area *in vivo*.

Whilst evaluating the results and implications of the current study, it is also important to consider also the limitations of the protocol. The strong field strength used in MRI, preventing use of metallic machinery in the scanning room, and the physical limitations of the scanner borehole, prohibit measurement of accommodative response during image acquisition. Accommodative responses to the 4.0 and 8.0 D stimuli were therefore determined before the MRI session, with the subject sitting upright. The supine scanning position however, may reduce accommodative amplitude by over a dioptre (Fincham, 1937; Atchison *et al.*, 1994) due to backward movement of the accommodated lens under gravity. Whilst it may be technically difficult to objectively record the accommodative response of a

supine subject, future studies should ensure that participants have sufficient subjective amplitude to maintain clarity of the stimuli whilst lying down, with the head facing upwards.

Although the results compare favourably with previously-published data, the resolution of the technique is limited by the 0.8 mm isotropic voxel size. Image acquisition with 0.7 mm voxels reduced the SNR unacceptably for data analysis purposes. Image quality, and potentially variability of the results, could have been improved by increasing the number of signal averages to 4, but the required scan length of 10 minutes per accommodative state was too demanding for participants and resulted in greater variability. Thus, a compromise in image quality was needed to limit acquisition times. Richdale *et al.* (2009) have recently described 7.0 T 3-D imaging of the human eye *in vivo* with superior resolution and visualisation of the crystalline lens, although the scanning protocol requires subjects to have their eyelids taped closed to minimise motion artefacts, thus preventing the viewing of accommodative stimuli. However, pharmacological manipulation of accommodative state, with use of topical agents such as cyclopentolate and pilocarpine, to prevent and induce accommodation, respectively would permit imaging of the relaxed and maximally accommodated lens, using their 7.0 T protocol. Similar analysis techniques to the current investigation could be applied to describe more precisely the relaxed and fully accommodated lens in 3-D, using MRI.

6.5 Conclusion

3-D MRI techniques are now available for modelling the relaxed and accommodated crystalline lens *in vivo*. The accommodative changes observed support the classic Helmholtzian theory of accommodation and are in agreement with the findings of previous 2-D MRI investigations. An overall decrease in lens surface area, and increase in lens volume with accommodation has been observed for the first time *in vivo*. The findings suggest that the lens material is compressed in the unaccommodated state, and undergoes expansion when zonular tension reduces secondary to ciliary muscle contraction.

CHAPTER 7

IN VIVO ANALYSIS OF ACCOMMODATIVE MORPHOLOGICAL CHANGES IN THE POSTERIOR SEGMENT

7.1. Introduction

There is a clear association between refractive error and ocular conformation, with myopic eyes generally exhibiting longer axial lengths, as a result of enlargement of the vitreous chamber (Curtin, 1985; Wildsoet, 1998; Stone and Flitcroft, 2004). An axial bias to the expansion of the vitreous chamber during myopigenesis has been identified (Zhou *et al.*, 1996; Mutti *et al.*, 2000; Atchison *et al.*, 2004; Logan *et al.*, 2004), causing the myopic eye to exhibit a relatively prolate posterior profile. In contrast, hyperopic eyes tend to be more oblate, and emmetropic eyes either spherical or oblate (Mutti *et al.*, 2000; Seidemann *et al.*, 2002).

The mechanism responsible for the prolate distortion of myopic eyes is unclear, although previous investigators have suggested a number of possible explanations. It is feasible that anatomical factors could restrict ocular expansion in the equatorial, but not axial direction (Mutti *et al.*, 2000; Atchison *et al.*, 2004). The orbital walls are in closer proximity to the globe in the vertical, compared to the horizontal, direction (Atchison *et al.*, 2004), meaning that soft tissues surrounding the eye including the extraocular muscles, orbital fat and connective tissue, could limit ocular growth. Alternatively, restrictive forces exerted by the extraocular muscles and distributed unevenly over the globe could be important; surgical modification of the tone of the extraocular muscles in the rabbit eye causes variation in the degree of artificially induced myopia (Mohan *et al.*, 1977). A further potential explanation is that local retinal regions control ocular growth, such that the axial and transverse dimensions are regulated differently (Atchison *et al.*, 2004; Logan *et al.*, 2004). Evidence to support a model of regional control is provided by animal studies that have induced myopia in a particular sector of the field, dependent upon visual experience. Chicks raised in a low-ceiling environment demonstrate significantly more myopia in the upper field than control animals inhabiting a high-ceiling location (Miles and Wallman, 1990). Additionally, partial occlusion of the retina (with hemifield occluders) in the chick induces myopia only in the deprived region of the retina; the non-deprived portion remains virtually emmetropic (Wallman *et al.*, 1987). In nature, several species of bird, including the pigeon (Fitzke *et al.*, 1985), quail, chick and crane (Hodos and Erichsen, 1990) are known to exhibit lower field myopia, allowing the ground to be kept in focus during foraging, whilst simultaneously

monitoring distance locations for predators. It is plausible that this lower field myopia is the result of regional growth induced by hyperopic defocus in early life.

Although the chick has been extensively used in previous myopia research, and appears to demonstrate an axial bias to myopic expansion similar to humans (Rada *et al.*, 2002), the chick eye has an additional scleral cartilaginous layer. This layer is lacking from the fibrous human sclera, and may be important in myopigenesis in chicks (Kusakari *et al.*, 2001), thus chick models of myopia may not be directly applicable to humans. Mutti *et al.* (2000) proposed a further theory for prolate distortion of the myopic eye, based on data from 822 children, whereby the crystalline lens fails to thin during growth of the globe, creating tension within the lens, ciliary body and choroid. It is hypothesised that ocular growth in the equatorial plane is restricted by tension at the equator, whilst axial elongation is accelerated.

Hitherto, ocular shape has been most frequently inferred indirectly, from measures of peripheral refractive error, relative to the visual axis. More direct analysis of ocular conformation has been performed using techniques such as magnetic resonance imaging (MRI; Cheng *et al.*, 1992; Atchison *et al.*, 2004; Singh *et al.*, 2006), x-ray measurement (Deller *et al.*, 1947) and computed tomography (CT) scanning (Zhou *et al.*, 1996). Ferree *et al.* (1931) made the first measures of peripheral refractive error, and highlighted that the data could be used to describe the conformation of the retinal surface (Ferree and Rand, 1933). Myopic eyes generally demonstrate relative peripheral hyperopia, as a consequence of axial elongation, whereas hyperopic eyes are typically relatively myopic in the periphery (Rempt *et al.*, 1971; Millodot, 1981; Mutti *et al.*, 2000; Logan *et al.*, 2004; Stone and Flitcroft, 2004; Atchison *et al.*, 2005; Mutti *et al.*, 2007). Children (Mutti *et al.*, 2007) and young adults (Hoogerheide *et al.*, 1971) with relative peripheral hyperopia are at high risk of myopia development, and it is hypothesised that peripheral hyperopic defocus may activate compensatory ocular growth and axial myopia. In support of this model, infant rhesus monkeys with lens-induced relative peripheral hyperopia become myopic, even following laser ablation of the fovea (Smith *et al.*, 2009), highlighting the importance of peripheral refraction on development of central refractive errors. According to this theory, spectacle or contact lens correction of axial myopia would increase axial expansion and myopia, by restoration of relative peripheral hyperopia.

A range of methodologies have been applied to determine peripheral ocular refractive error, including subjective refraction (Ronchi, 1971; Thibos *et al.*, 1996; Lundstrom *et al.*, 2005), retinoscopy (Hoogerheide *et al.*, 1971; Rempt *et al.*, 1971; Lotmar and Lotmar, 1974), manual optometers (Ferree *et al.*, 1931; Millodot and Lamont, 1974; Dunne and Barnes,

1990), the double-pass technique (Jennings and Charman, 1978; Navarro *et al.*, 1993; Gustaffson *et al.*, 2001), photorefractometry (Seidemann *et al.*, 2002; Lundstrom *et al.*, 2005), autorefraction (Dunne *et al.*, 1993; Mutti *et al.*, 2000; Logan *et al.*, 2004; Calver *et al.*, 2007) and aberrometry (Navarro *et al.*, 1998; Atchison and Scott, 2002; Atchison, 2004). Of these techniques, autorefraction has been the most widely used, with commercially available binocular open-view instruments (e.g. Canon Autorefractometer R-1, Shin-Nippon SRW5000 and Shin Nippon NVision-K 5001) requiring no modification for determination of horizontal peripheral refraction, except for a method of presenting stimuli at a range of eccentricities. Although simple and rapid to perform, autorefraction determination of peripheral refractive error is limited to a maximum horizontal eccentricity of approximately 35- 40° (Wang *et al.*, 1996; Love *et al.*, 2000; Logan *et al.*, 2004) due to the design of the viewing window and surrounding casing (Sheppard and Davies, 2010a), which also hinders vertical assessment. In contrast, horizontal peripheral refraction measures at eccentricities of 60- 80° have been reported using retinoscopic techniques (Rempt *et al.*, 1971; Leibowitz *et al.*, 1972; Johnson and Leibowitz, 1974), and Tabernero and Schaeffel (2009) have recently reported measurements out to 90° with a fast scanning infrared photoretinoscope. Regardless of the technique used, peripheral refraction measures represent an indirect measurement of retinal contour. Published studies generally consider peripheral refraction in terms of the mean spherical equivalent (MSE; sphere + cylinder/ 2), and it is assumed that the image shell is spherical, which is probably an oversimplified approach (Dunne, 1995; Logan *et al.*, 1995; Stone and Flitcroft, 2004). Furthermore, levels of peripheral astigmatism are influenced by numerous variables including the gradient index of the crystalline lens, misalignment of the ocular components, and ocular surface asphericity.

Relatively few studies have made direct measurements of the conformation of the retinal surface across various refractive groups. An x-ray based investigation of 15 subjects (Deller *et al.*, 1947) indicated a prolate retinal contour in myopes, as axial length was found to be the longest ocular dimension. Emmetropes and hyperopes exhibited oblate, spherical or prolate ocular shapes. More recent studies utilising B-scan echography (Vohra and Good, 2000), CT scanning (Zhou *et al.*, 1996) and MRI (Atchison *et al.*, 2004) have typically supported these findings, although Cheng *et al.* (1992) concluded from the MRI data of 21 participants that myopic eyes expanded equally in all dimensions, and were not distorted into a prolate shape.

Recent advances in MR imaging, including scanning at higher field strengths and use of newer-design radiofrequency (RF) coils have facilitated the acquisition of ocular shape data with high resolution in all three dimensions (Singh *et al.*, 2006). Application of specialist

analysis techniques to ocular MRI data now permits construction of complete 3-D surface models of animal (Goodall *et al.*, 2009) and human eyes (Singh *et al.*, 2006; Gilmartin *et al.*, 2007; Nagra *et al.*, 2009), and acquisition of volumetric data. The first description of a methodology to completely characterise the conformation of the eye in 3-D, using MRI data, was provided by Singh *et al.* (2006). Previous studies that had inferred 3-D ocular shape (e.g. Cheng *et al.*, 1992; Atchison *et al.*, 2004; Atchison *et al.*, 2005) had done so from just a limited number of 2-D slices through the eye. The data of Singh *et al.* (2006) highlighted that the absolute size of eyes could vary significantly, even in subjects with similar refractive errors. Amongst the cohort of seven participants, no clear relationship was evident between axial length and refractive error, although nasal-temporal asymmetry in ocular shape, previously reported in the eyes of whites (Logan *et al.*, 2004), could be identified with the technique. Subsequent 3-D MR imaging has indicated ocular sphericity, regardless of refractive error, between 25 and 75 % of overall axial length, with just the conformation of the posterior quartile speculated to be affected by vision-dependent growth (Gilmartin *et al.*, 2007). Significant steepening or flattening was identified in the majority of subjects in the last quartile, the angular subtense of which is approximately equal to the region of overlap in visual field with the fellow eye. More recently, a tendency for a temporal bulge in the ocular shape of myopes, compared to emmetropes, has been identified (Nagra *et al.*, 2009).

Although high-resolution MRI techniques now facilitate the acquisition of 3-D data regarding ocular shape, the associated expense and relative inaccessibility are limitations to large-scale studies. Additionally, a proportion of potential subjects could be excluded from participation on safety grounds (e.g. implanted metal devices, previous penetrating metallic injuries, migraneurs). Mallen and Kashyap (2007) described an adaptation of the commercially available Zeiss *IOLMaster* (Carl Zeiss Ltd., Welwyn Garden City, Hertfordshire, UK) to allow direct measurement of the central 80° of retinal contour (40° superior, inferior, nasal and temporal to fixation). The *IOLMaster* is a non-contact device that employs partial coherence interferometry (PCI) to measure axial lengths, with a resolution of 0.01 mm and high repeatability (Santodomingo-Rubido *et al.*, 2002). Conventionally, axial length measures are acquired along the visual axis, whilst the subject fixates an internal light. An apparatus consisting of a 50 % transmission/ 50 % reflection beamsplitter; a Badal optometer providing correction of ametropia and enabling stimulation of accommodation; a high-contrast Maltese cross target, and a goniometer to allow the angle of measurement to be varied, may be mounted on the *IOLMaster* headrest to acquire peripheral measurements (Mallen and Kashyap, 2007). The arrangement of these components is shown in Figure 7.1. Pilot data provided by Mallen and Kashyap (2007) provided further evidence of nasal versus temporal asymmetry in ocular conformation amongst myopic subjects.

In addition to the variation in eye shape with refractive error, accommodation is now known to cause a temporary change in ocular conformation (Smith *et al.*, 1988; Drexler *et al.*, 1998; Walker and Mutti, 2002; Uozato *et al.*, 2003; Calver *et al.*, 2007; Davies and Mallen, 2009; Charman and Radhakrishnan, 2010). Direct and indirect measures have indicated that the eye elongates and becomes more prolate in shape during accommodation. It is hypothesised that these transient changes are due to the contracting ciliary muscle applying an inward pulling force to the neighbouring choroid and sclera (Drexler *et al.*, 1998). A backwards movement of the most posterior region of the globe is hypothesised to occur in order to maintain a constant ocular volume (Mallen *et al.*, 2006).

Several studies have identified a correlation between refractive error, and amount (Adams and McBrien, 1992; Parsinnen and Lyyra, 1993; Mutti *et al.*, 2002) or intensity (Ip *et al.*, 2008) of accommodation/ near work. Possible links between myopia, ocular conformation and near work/ accommodation represent a justification for the study of change in ocular shape with accommodation. Investigations based on peripheral refraction measures have shown that peripheral astigmatism increases (Smith *et al.*, 1988) and that relative peripheral refractive error (RPRE) becomes increasingly hyperopic with accommodation (Mutti *et al.*, 2002; Walker and Mutti, 2002), indicating a more prolate ocular conformation.

Regarding differences between refractive groups with accommodation, both Calver *et al.* (2007) and Davies and Mallen (2009) found no significant relationship between refractive error and changes in peripheral refraction induced by accommodation. However, direct measurement of the change in axial length with accommodation, using PCI, indicates possible differences in the response between emmetropes and myopes. Drexler *et al.* (1998) concluded that elongation of the globe during accommodation was more pronounced for emmetropes than myopes. The mean changes observed in axial length when viewing a target at the near point, compared to the far point, were 12.7 μm and 5.2 μm for the emmetropic and myopic groups, respectively. The results of Mallen *et al.* (2006) contradict this study, with axial elongation found to be significantly greater amongst the myopic cohort. Mean change in axial length in response to a 6 D stimulus was 37 μm in emmetropes, and 58 μm in myopes. A possible explanation for the discrepancy in results is that Drexler *et al.* (1998) used an accommodative stimulus at the subjective near point, whereas Mallen *et al.* (2006) used a fixed 6 D stimulus vergence. It is feasible that the near point was not accurately determined amongst the myopic subjects in the earlier study, due to the close proximity of this point to the eye in young myopes, thus the true accommodative demand was different between refractive groups.

Whilst it is well-known that accommodation induces changes in ocular conformation, whether these changes are dependent upon refractive error is less obvious. Indirect measures of retinal contour (peripheral refractions) indicate no notable differences between emmetropes and myopes, whilst direct measurements using PCI imply that considerable differences between refractive error groups may exist. To date, direct measurements of posterior ocular shape change with accommodation have been limited to on-axis determination of axial length using PCI. New high-resolution MRI techniques allow the acquisition of 3-D data to describe ocular shape, but these methods have been applied only to the unaccommodated eye.

The aim of this study, therefore, is to investigate the potential value of 3-D MRI techniques to analyse changes in ocular conformation with accommodation. MRI offers the key advantages of being free from optical distortion, and able to characterise the shape of the complete eye. The technique could therefore represent a novel and powerful method for analysis of accommodative changes in globe conformation. Youthful subjects, with high accommodative amplitudes will be investigated, as it is feasible that any changes will be more obvious when a high degree of accommodation is exerted.

7.2. Methods

Eight pre-presbyopic participants (aged 19.3- 31.5 years) with no history of ocular abnormality or intraocular surgery were recruited for the investigation using email announcements at Aston University. The cohort comprised 4 emmetropes and 4 axial myopes, with refractive errors amenable to correction with single use disposable soft contact lenses (*Focus Dailies* and *Focus Dailies Toric*: nelfilcon A, 69 % water content; Ciba Vision, Duluth, Georgia, USA). The parameter ranges for these contact lenses meant subjects with spherical myopic refractive errors greater than -10.00 DS were excluded from the investigation, as were those with oblique cylinders > 0.50 DC, or orthogonal cylinders > 1.50 DC.

The study was a collaboration between Aston University's Ophthalmic Research Group (ORG) and neuroimaging physicists from the School of Psychology at Cardiff University. Subject recruitment and preliminary data collection took place at Aston University, whilst all MRI work was conducted at the Cardiff University Brain Repair and Imaging Centre (CUBRIC). The ethics committees of both Aston University and Cardiff University approved the study, which was performed in accordance with the tenets of the Declaration of Helsinki. Written, informed consent was obtained from all participants following explanation of the

nature and possible consequences of the study. Subjects consented to the initial stages of the study at Aston University (see Appendix 2 for consent form), and completed an MRI initial screening form (Appendix 4) to ensure suitability for the subsequent stages of the investigation. Volunteers with implanted metallic devices (e.g. pacemakers, metal plates), those with possible metal fragments in the eyes or elsewhere in the body, migraine sufferers and females who may have been pregnant, were excluded from the investigation for safety reasons. A second screening form (Appendix 4) and MRI consent form (Appendix 4) was completed at CUBRIC, immediately before scanning.

The initial visit involved determination of objective refractive error and accommodative responses and direct analysis of retinal contour with accommodation, using the IOLMaster. All measurements were taken from the right eye only. Refractive error was determined from the mean of five open-view distance autorefractor readings obtained with the Grand Seiko Auto Ref/ Keratometer WAM-5500 (Grand Seiko Co. Ltd., Hiroshima, Japan; Sheppard and Davies, 2010). Subjects with spherical or astigmatic refractive error > 0.50 D were corrected with Focus Dailies or Focus Dailies Toric disposable soft contact lenses. Functional emmetropia was necessary to ensure near-identical accommodative demand for each subject.

Objective accommodative responses were measured using the WAM-5500 autorefractor whilst subjects fixated Maltese cross targets in free space at -4 D and -8 D stimulus vergences, presented in random order. The targets subtended a constant angular subtense of 4.6° . Average target luminance and Michelson contrast values were 34.0 cd/m^2 and 82% , and 30.5 cd/m^2 and 80% , for the 4 D and 8 D stimuli, respectively. The left eye was occluded with a patch during measurement of the response and subjects were instructed to “carefully focus” (Stark and Atchison, 1994) on the centre of the Maltese cross to induce both voluntary and reflex accommodation (Radhakrishnan and Charman, 2007). It was ensured at this stage that participants had sufficient subjective accommodative amplitude to maintain clarity of the 8 D stimulus, which would be required for subsequent IOLMaster and MRI data collection. Five readings were obtained at each stimulus level, and the mean of these values was used in conjunction with the distance autorefractor results to determine the objective accommodative response.

Direct determination of horizontal peripheral ocular dimensions in the relaxed and accommodated states was performed with the Zeiss *IOLMaster* and the adaptation described by Mallen and Kashyap (2007), shown in Figure 7.1. Myopic subjects removed their contact lenses prior to acquisition of these data. The Badal optometer features a lens of power 20.8 D, enabling correction of ametropia and stimulation of accommodation. Eye

length measures were recorded at nasal and temporal eccentricities of 0, 10, 20 and 30°, in the relaxed state, and at 4.0 and 8.0 D accommodative demand levels. Demand level and eccentricity were randomly ordered. For measurement of unaccommodated eye length, the illuminated Maltese cross was positioned in the Badal system at the most positive/ least negative point that allowed the subject to see the target clearly. Following determination of this position within the system, the Maltese cross could be adjusted to provide each subject with 4.0 and 8.0 D accommodative demand levels. Subjects were instructed to maintain clarity and “carefully focus” on the cross target during data acquisition. The mean of 5 measures (with a signal to noise ratio; SNR, of at least 2.0) at each eccentricity and demand level was used for analysis purposes.

Intersession repeatability of relaxed and accommodated peripheral retinal contour measures with the *IOLMaster* was explored as this is the first study to apply the technique to the accommodating eye. Temporal eye length measures in the unaccommodated state, and at 8.0 D stimulus vergence, were acquired at 0, 10, 20 and 30° eccentricities from 10 youthful volunteers. Participants returned for the second data collection session within a week of the initial measures. The bias for each eccentricity at both vergence levels, was calculated from the mean difference in measures between visits, and paired t-tests used to determine whether the levels of bias were significantly different to zero. The limits of agreement (LoA) were established using the standard deviation (SD) of differences with the following formula:

$$\text{LoA} = \text{bias} \pm (1.96 * \text{SD of differences})$$

Equation 3

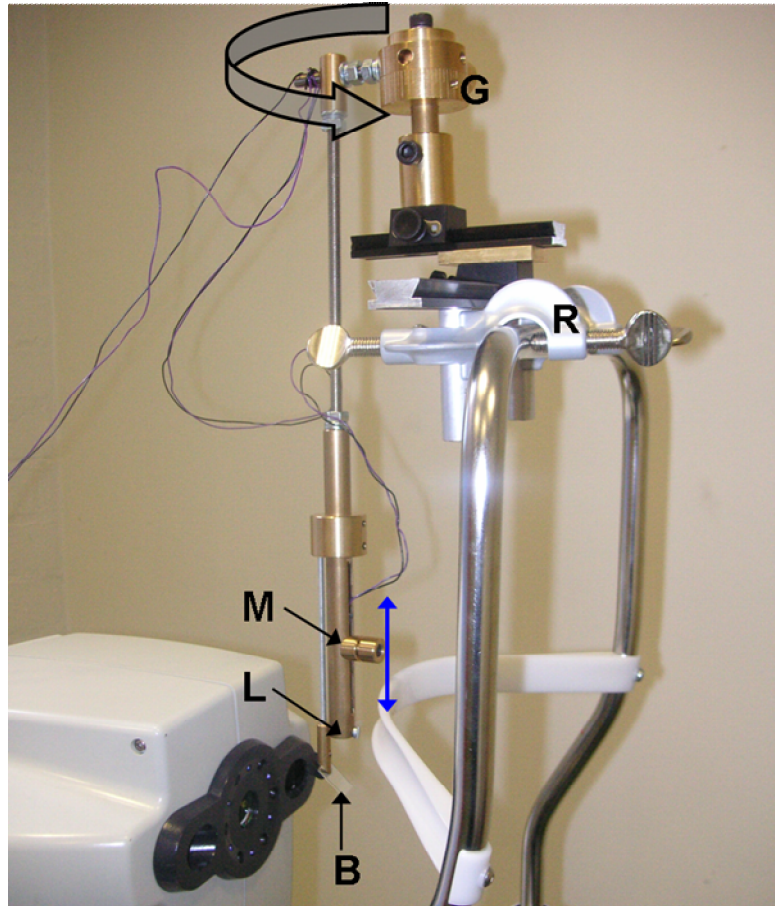


Figure 7.1. Adaptation of the Zeiss *IOLMaster* for determination of horizontal peripheral ocular dimensions. A movable internal Maltese cross target (M) is viewed via a beam splitter (B), through which the measurement beam of the *IOLMaster* also passes. A goniometer (G) attached to the instrument forehead rest using retort clamps (R) allows the illuminated Maltese cross, Badal lens (L) and beam splitter to be rotated around the vertical axis, so that the eye rotates relative to the *IOLMaster* measurement axis.

Three-dimensional MRI data collection took place approximately 2 weeks later, depending on scanner availability, at CUBRIC. Participants completed a second MRI screening form to ensure none of the initial responses had changed, and a CUBRIC consent form. Whilst undergoing scanning, ametropic subjects wore contact lenses of the specification determined in the earlier stage of the study. The subject set-up for MRI was as detailed in Chapter 6, and participants were scanned at 0.17, 4.0 and 8.0 D demand levels, using the blink-pause box. The scanning protocol was adjusted to enable acquisition of high resolution images featuring the entire eye in all three dimensions. The whole-eye protocol involved 54 oblique-axial slices of 0.7 mm thickness, with no inter-slice gaps, to visualise the complete eye in all three dimensions. FSE images were acquired with a bandwidth of ± 23.40 kHz, echo train length 24, sequence repetition time 25000 ms and echo time 300 ms. The acquisition matrix was square; $192 * 192$, with a 134 mm field of view. Voxels within the images therefore had a 0.7 mm isotropic resolution. One signal average was performed,

resulting in a total scan duration of 3 minutes 45 seconds. Overall time spent in the scanner for each subject was approximately 40- 60 minutes, comprising of localiser scans, main scans, and repetition of longer scans, if necessary, due to blink/ motion artefacts.

7.2.1. MRI data analysis

The initial stages of MRI data analysis were conducted using a similar methodology to that described in Chapter 6. T₂-weighted 3-D MR images were loaded into *mri3dX* (www.jjiscmail.ac.uk/lists/mri3dX.html), and the approximate centre of the globe manually identified. A 3-D flood filling algorithm was used to shade voxels of intensities between 55 and 128, corresponding to the fluid-filled regions of the eye. The shaded volume was manually edited to include the crystalline lens, and ensure complete characterisation of the eye. Following subsequent location of the anterior pole, a sphere consisting of 32,768 triangular polygons was automatically generated to completely envelop the shaded voxels. An iterative shrink-wrap process was executed until the vertices of each polygon intersected a shaded voxel, then a rapid smoothing process performed on the polygonal model to average local vertex positions and generate a more regular 3-D characterisation of the eye. The number of smoothing iterations was set at 200 throughout the investigation.

Three-dimensional ocular representations (Fig. 7.2) were visualised using *Geomview* software (www.geomview.org), allowing the model to be rotated and viewed at any orientation. Overall ocular volume at the 0.17 D demand level was obtained from the *Geomview* window, in addition to the surface curvature around the posterior pole of the eye at all vergence levels. The radius of the area over which surface curvature was described was set at 8.0 mm for all analyses to identify any change which would indicate local changes in posterior ocular conformation with accommodation.

Measures of vitreous volume and anterior eye volume were additionally acquired using *mri3dX*. To obtain vitreous volume at 0.17, 4.0 and 8.0 D stimulus levels, initial shading was performed as previously described, but the editing process was used to eliminate voxels shading the anterior region of the eye. The vitreous volume at 0.17 D, obtained from viewing the resultant 3-D model with *Geomview*, was subtracted from the overall ocular volume to determine anterior eye volume (corresponding to the lens and anterior chamber) in the relaxed state.

Further analysis of the MRI data was performed in order to explore accommodative changes in the conformation of the nasal and temporal quadrants (the superior and inferior quadrant data were not used for analysis purposes), and identify any regional asymmetry which could

be linked to the findings of Chapter 3 of a greater contractile response of the temporal, compared to nasal, ciliary muscle aspect. Following the iterative shrink-wrap and smoothing processes, *mri3dX* produces a text file of the *x* and *y* surface co-ordinates of the nasal, temporal, superior and inferior quadrants. Each quadrant is represented by over 8,000 sets of co-ordinates, thus the data were copied into an *Excel* spreadsheet (Microsoft, Richmond, Washington, USA) and a systematic sampling process employed to reduce the volume of data by a factor of 10. The *x* and *y* co-ordinates representing the region from 25- 75 % of overall axial length were then plotted using *SigmaPlot* (Version 11; Systat Software Inc., Chicago, Illinois, USA) graphing and statistical software and a second order polynomial (represented by the equation $y = ax^2 + bx + c$) fitted to the data. In order to determine the co-ordinates of the maximum point of the polynomial (and minimal point for the temporal polynomial), *x* was derived from the equation $x = -b/ 2a$, and subsequently used to calculate *y*, given that $y = ax^2 + bx + c$. The process was repeated for the nasal and temporal quadrants at each accommodative state to ascertain whether the locus of the vertex changed significantly with accommodation.

7.2.2. Statistical analysis

Regarding 3-D MRI data, the relationships between axial length and unaccommodated ocular volume parameters (complete eye volume, anterior volume and vitreous volume) were explored using linear regression analysis, performed with *SigmaPlot* graphing and statistical software (Version 11, Systat Software Inc., Chicago, Illinois, USA). One-way repeated measures analyses of variance (ANOVAs), using *SPSS* statistical software (Version 15, SPSS Inc., an IBM Company, Chicago, Illinois, USA) were conducted to determine if accommodation caused any significant change in vitreous volume, curvature of the posterior region of the eye, or the *x* and *y* co-ordinates of the vertex of the second order polynomial fitted to the MRI data representing 25- 75 % of overall axial length on the nasal and temporal sides. Demand, the within subjects factor, was assigned three levels, of 0.19, 4.0 and 8.0 D for ANOVA purposes. A significance level of $\alpha = 0.05$ was used throughout analysis.

7.3 Results

Mean spherical equivalent (MSE) refractive error of the 8 participants ranged from -6.00 to +0.19 D (mean -2.07 ± 2.19 D). Mean objective accommodative responses to the 4.0 D and

8.0 D stimuli were 2.64 ± 0.37 D and 5.69 ± 0.99 D, respectively. MRI data indicated that complete eye volume varied widely amongst the cohort, from 5288 to 6898 mm³ in the unaccommodated state. Ocular volume was significantly and positively correlated with axial length ($r = 0.85$, $P = 0.007$), as was vitreous volume ($r = 0.86$, $P = 0.006$). Mean complete eye volume was 5999 ± 515 and 6444 ± 328 mm³ in the emmetropic and myopic groups, respectively, whilst mean vitreous volume in the same refractive groups was 5611 ± 474 and 6027 ± 261 mm³. Anterior ocular volume was not dependent on axial length ($r = 0.343$, $P = 0.406$), with a mean of 388 ± 105 mm³ across the whole cohort. During accommodation, vitreous volume was statistically unchanged ($F = 0.608$, $P = 0.558$). Figure 7.2 illustrates sample vitreous and whole eye models for a single subject, at the 0.17 D demand level.

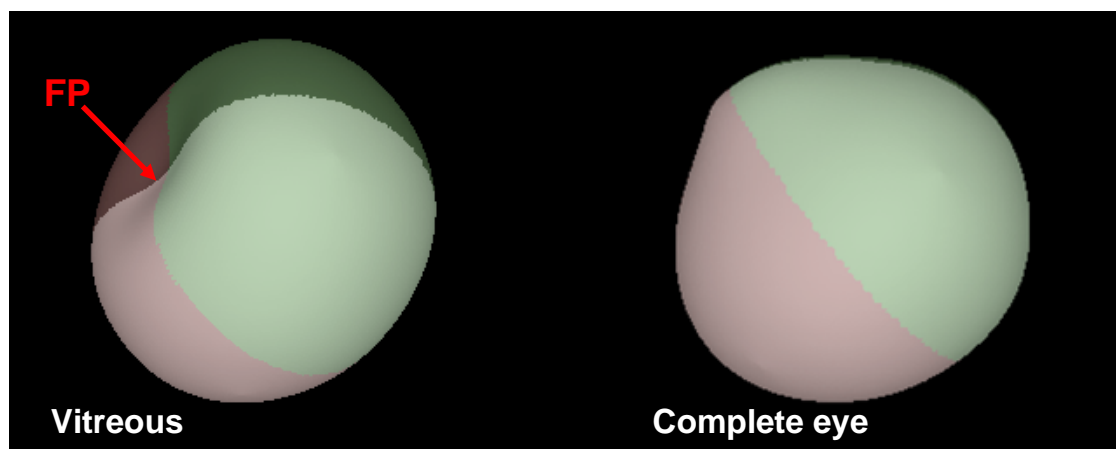


Figure 7.2. Sample 3-D models of the vitreous body (left) and complete eye (right) of a 20 year old emmetrope, viewed using *Geomview* software. The *fossa patellaris* (FP) is clearly visible on the vitreous model.

7.3.1. IOLMaster derived retinal contour

Table 7.1 details the intersession repeatability of temporal retinal contour measures in the relaxed and accommodated states. None of the amounts of bias reported are statistically significantly different from zero, at either the minimal or maximal accommodative stimulus level.

Eccentricity (°)	0 D stimulus level			8 D stimulus level		
	Bias (mm)	SD of differences	95 % LoA	Bias (mm)	SD of differences	95 % LoA
0	0.00	0.04	-0.078, 0.078	-0.02	0.04	-0.098, 0.058
10	-0.02	0.03	-0.079, 0.039	0.00	0.03	-0.059, 0.059
20	0.01	0.05	-0.088, 0.108	-0.01	0.03	-0.088, 0.108
30	-0.01	0.03	-0.068, 0.049	-0.01	0.05	-0.108, 0.088

Table 7.1. Intersession repeatability of temporal retinal contour measures with the *IOLMaster*, in the relaxed and accommodated states. Ten participants attended two data acquisition sessions, separated by no longer than a week.

Amongst the main cohort, there was a significant difference in axial length measures between the refractive groups, with myopes exhibiting the longest eyes (mean axial lengths were 23.67 ± 0.64 and 25.08 ± 0.81 mm for the emmetropic and myopic groups, respectively; $P = 0.013$). Figure 7.3 illustrates graphically the relationship between field angle and mean eye length in the relaxed and accommodated states, for both refractive groups. Temporal retinal contour in the relaxed state is visibly steeper in the myopic eyes (Fig. 7.3b) than the emmetropes (Fig. 7.3a; $P = 0.045$), with no significant difference between refractive groups on the nasal side ($P = 0.96$).

Across the whole cohort, accommodation was associated with a statistically significant increase in eye length measures at all eccentricities except at 10° and 20° nasally. Table 7.2 details mean eye lengths and the mean changes in eye length in response to 4.0 and 8.0 D stimuli for each eccentricity measured.

Eccentricity (°)	Mean eye length at 0.0 D (mm)	Mean change from 0.0 to 4.0 D (μm)	Mean change from 0.0 to 8.0 D (μm)	F	P
-30	24.02	+ 7.5 \pm 13	+ 26 \pm 23	5.989	0.013*
-20	24.18	+ 15 \pm 17	+ 50 \pm 30	13.012	0.001*
-10	24.25	+ 28 \pm 24	+ 48 \pm 36	8.273	0.004*

0	24.37	+ 15 ± 12	+ 55 ± 52	7.223	0.007*
10	24.21	+ 48 ± 58	+ 46 ± 26	3.353	0.065
20	23.95	+ 21 ± 21	+ 48 ± 18	21.078	<0.001*
30	23.66	+ 38 ± 65	+ 54 ± 75	2.070	0.169

Table 7.2. Mean eye length measures, and change with accommodation measured with the *IOLMaster*. Negative eccentricities correspond to temporal measures of eye length. * indicates a statistically significant change with accommodation, as determined by repeated measures ANOVA.

7.3.2 MRI derived ocular conformation

Figure 7.4 illustrates the nasal and temporal quadrant shapes from 25- 75% of overall axial length of a single participant at the three demand levels. The polynomials appear very similar for all accommodative levels, a finding which was consistent amongst the 8 participants. One-way repeated measures ANOVA testing found no significant change with accommodation in the location of either the x or y co-ordinates of the maxima or minima of the polynomials representing the nasal ($F = 0.828$, $P = 0.457$, and $F = 2.006$, $P = 0.200$, for x and y, respectively) and temporal ($F = 0.907$, $P = 0.908$, and $F = 0.553$, $P = 0.587$, for x and y, respectively) quadrants.

Regarding the surface curvature of the circular area with an 8.0 mm radius, centred on the most posterior region of the eye, the curvature in the relaxed state was found to be significantly and positively linked refractive error ($r = 0.715$, $P = 0.046$), with myopic eyes demonstrating steeper posterior ocular contours. Posterior curvature ranged from 10.23 to 12.87 mm at the 0.17 D demand level, and did not change significantly with accommodation ($F = 0.569$, $P = 0.579$).

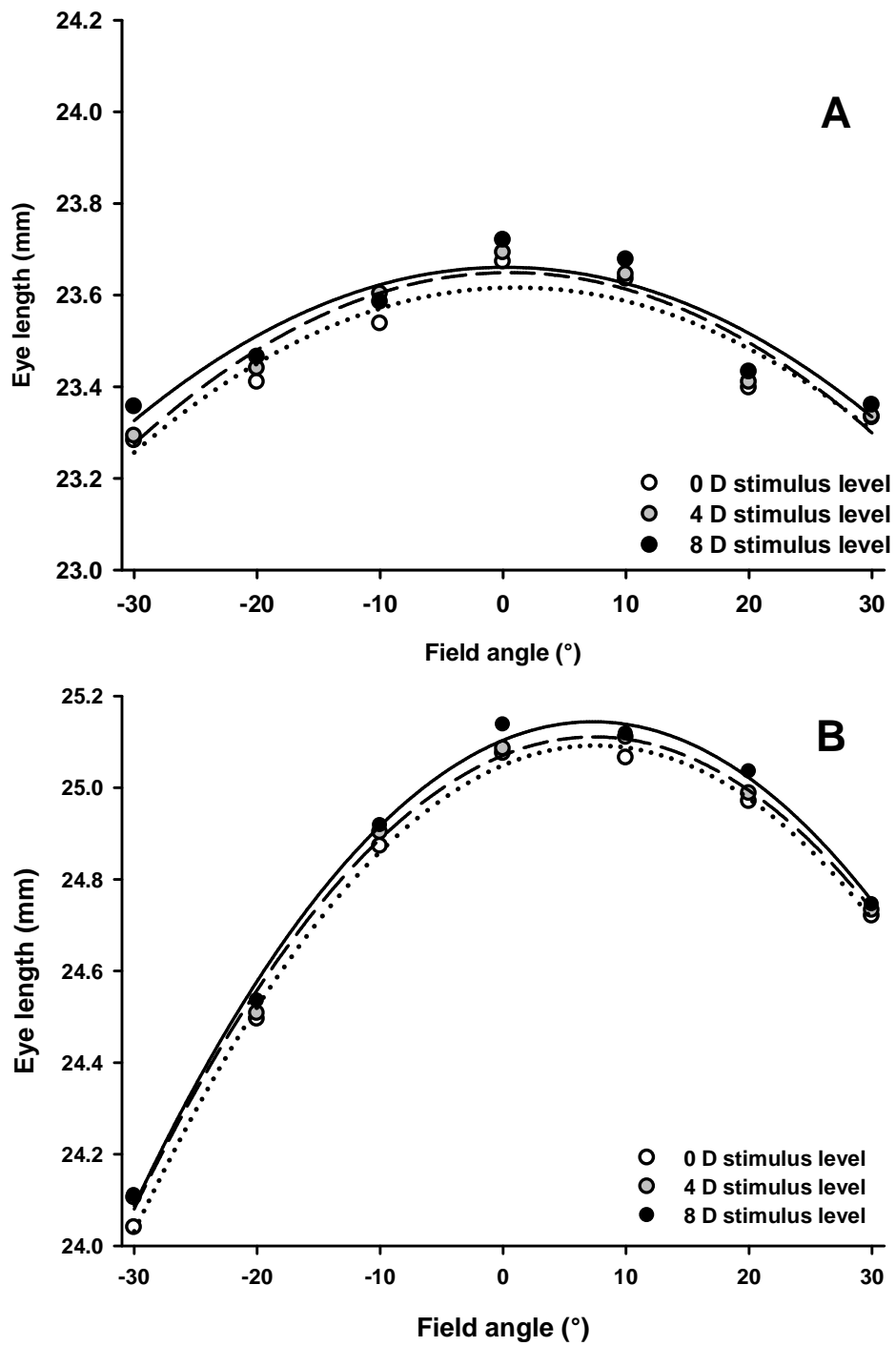


Figure 7.3. Mean eye length (obtained from the *IOLMaster*) as a function of field angle for emmetropic (A; upper plot) and myopic (B; lower plot) subjects at 0, 4 and 8 D stimulus vergences. Negative field angles correspond to the temporal side, and positive angles, the nasal aspect.

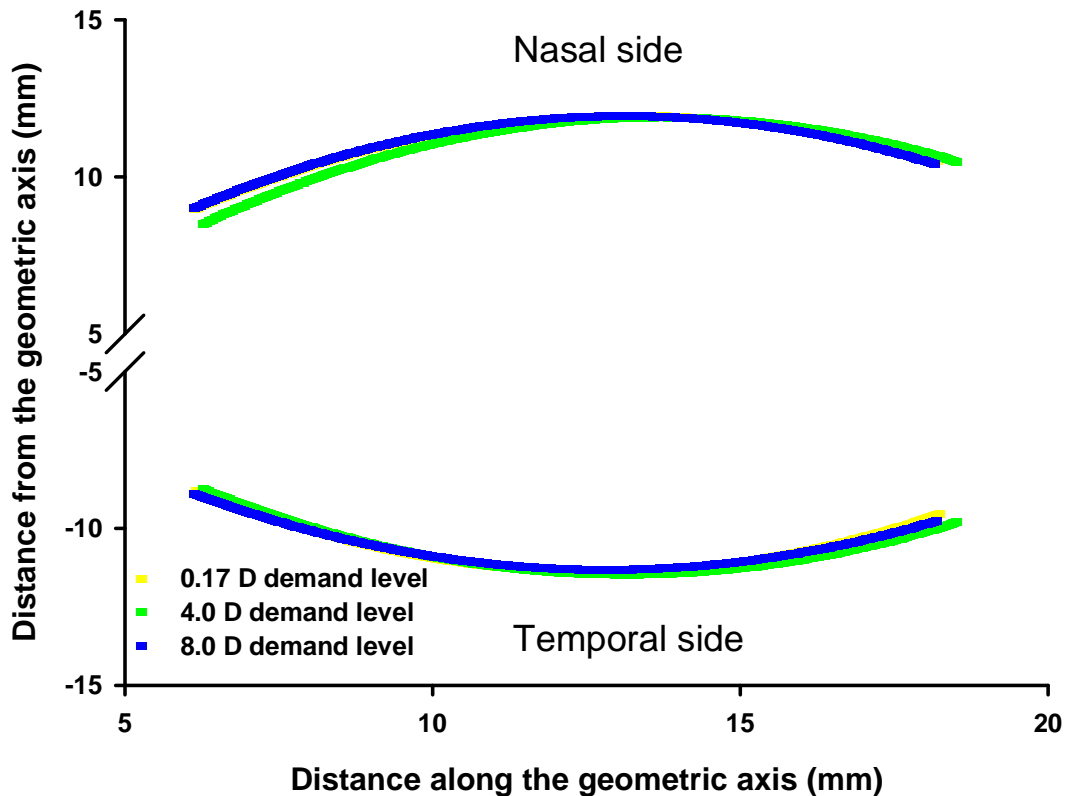


Figure 7.4. Polynomial plots of nasal and temporal ocular contours from 25-75 % of axial length at 0.17 (yellow line), 4.0 (green line) and 8.0 D (blue line) stimulus levels. Myopic subject (MSE -2.50 D), aged 19 years. Note the plot for the 0.17 D demand level is mostly obscured by that for the 4.0 D level.

7.4. Discussion

Advances in MRI have allowed several previous authors to investigate the relationship between ocular shape and refractive error. However, this is the first study to apply 3-D MRI techniques to explore accommodative changes in ocular conformation. Furthermore, reports of axial length changes with accommodation, measured using PCI, have been limited hitherto to on-axis measurements. The present study provides data on retinal contour to an eccentricity of 30° in the nasal and temporal directions, using the adaptation to the IOLMaster described by Mallen and Kashyap (2007).

The 3-D MRI data highlights a significant dependence of both vitreous volume and complete ocular volume, on axial length in the unaccommodated state. However, no relationship between anterior volume and axial length was identified. This finding is in agreement with

the recently published data of Read *et al.* (2010), based on optical low coherence reflectometry measures of ocular biometric characteristics in emmetropes and myopes. No significant relationship was identified between anterior axial distances (central corneal thickness, anterior chamber depth, lens thickness and anterior segment length) and refractive error group, but both vitreous chamber depth and axial length were significantly greater in the myopic participants.

IOLMaster eye length data were obtained from all participants at eccentricities up to 30° nasally and temporally in the present study. Pupil size limitations prevented acquisition of eye length data at greater eccentricities, particularly for the accommodated states. A significant increase in eye length with accommodation was determined at all eccentricities, except for 10° and 30° nasally, which may be a consequence of the relatively small cohort size. Whilst no previous study has measured directly the changes in peripheral eye length values with accommodation, the values for on-axis elongation (0° eccentricity) are generally comparable with previously published data. The present study observed mean increases in axial length across the whole cohort of $15 \pm 12 \mu\text{m}$ and $55 \mu\text{m} \pm 52 \mu\text{m}$ for the 4.0 and 8.0 D stimulus levels, respectively. Drexler *et al.* (1998) detected mean axial elongations of 12.7 μm in emmetropes and 5.2 μm in myopes, in response to a target at the near point. Conversely, Mallen *et al.* (2006) observed the greatest axial length changes in myopic subjects, with a mean increase of 58 μm , compared to 37 μm in emmetropes, when viewing a 6 D stimulus. Most recently, Read *et al.* (2010) documented a mean axial length increase of $24.1 \pm 22.7 \mu\text{m}$ in response to a 6.0 D stimulus, with no significant difference in response between emmetropes and myopes. The accommodative axial elongation observed in previously published studies has been suggested as a mechanism allowing the maintenance of a constant ocular volume whilst contraction of ciliary smooth muscle pulls the choroid and sclera adjacent to the ciliary body inwards (Drexler *et al.*, 1998; Mallen *et al.*, 2006). Three-dimensional MRI data from the present investigation provides the first *in vivo* evidence to support the assertion that vitreous chamber volume remains unchanged during accommodation.

Nasal and temporal quadrant MRI data indicated no significant change with accommodation in either the x or y co-ordinates of the maximum or minimum points of the polynomials fitted to the data points. The maintenance of a constant ocular profile during accommodation on both the nasal and temporal sides of the globe implies that changes in ocular conformation with accommodation may be limited to the posterior region of the eye (as axial length is known to increase with accommodation). In this case, it would be expected that the surface curvature of the posterior region of the eye would increase during accommodation.

However, the 3-D MRI data indicated no significant accommodative change in curvature of the posterior portion of the eye.

It is feasible that the changes occurring in the posterior segment of the eye during accommodation are very slight, and are likely overestimated by the raw *IOLMaster* data. The *IOLMaster* uses an average refractive index within the eye, which would vary with accommodation, due to the axial thickening of the crystalline lens and reduction in anterior chamber depth. Atchison and Smith (2004) proposed a formula to reduce the error associated with determining accommodative axial length changes, which requires input of lens thickness and the change in lens thickness with accommodation. However, precise values for these parameters were not available in the present investigation as the *IOLMaster* does not provide lens thickness measurements and the only internal measurement provided by the device from PCI is axial length. Read *et al.* (2010) have recently reported corrected values of axial length changes during accommodation, obtained using the commercially available *LenStar LS900* (Haag-Streit Koeniz, Switzerland; Buckhurst *et al.*, 2009). This instrument employs optical low coherence reflectometry (OLCR) to acquire anterior chamber depth, lens thickness and axial length measures, thus the data obtained can more readily adjusted to account for variations in ocular refractive index during accommodation. The corrected data of Read *et al.* (2010) identified a mean increase in axial length of $7.4 \pm 18.9 \mu\text{m}$ to a 6 D stimulus, compared to the mean of uncorrected values of $24.1 \pm 22.7 \mu\text{m}$. This $7.4 \mu\text{m}$ mean corrected increase in axial length is approximately 8 times smaller than the elongation reported in the present investigation (to an 8.0 D stimulus) and in myopic subjects (to a 6.0 D stimulus) by Mallen *et al.* (2006), from raw *IOLMaster* data. The *LenStar* could be modified, therefore, with a similar adaptation to that used with the *IOLMaster* in the present investigation to provide more realistic corrected values of eye length changes during accommodation.

The current investigation employed 3.0 T MRI scanning, although Richdale *et al.* (2009) have described 3-D MRI of the human eye *in vivo* at 7.0 T. The improved image quality from scans acquired at 7.0 T may provide more accurate data regarding ocular conformation in the relaxed state. However, such high-field techniques are not currently applicable to the study of natural accommodative changes in ocular conformation due to the requirement of the lids to be taped closed during scanning to minimise motion artefacts, thus preventing the viewing of visual stimuli. Pharmacological stimulation of accommodation could be employed, although pilocarpine is a known superstimulus to accommodation, and does not reflect the normal physiological response (Kriechbaum *et al.*, 2005).

7.5. Conclusion

The present study sought to explore the worth of 3-D MRI techniques in the analysis of posterior ocular changes during accommodation. The volume of the vitreous appears to remain constant with accommodation, as has been predicted by previous authors, but not supported hitherto with empirical data. Changes in ocular conformation during accommodation were not detected using the 3-D MRI techniques employed, although PCI data indicated a small accommodative elongation of the eye, in alignment with previously published studies. Methodologies based upon OLCR or PCI may be more appropriate than current MRI techniques for the study of accommodative changes in ocular conformation. However, optical data regarding the effect of accommodation on eye length require *post hoc* correction to avoid significantly overestimating the magnitude of the changes induced.

CHAPTER 8

CONCLUSIONS AND PLANS FOR FUTURE WORK

8.1. General conclusions

The central experimental theme of the thesis has been *in vivo* analysis of ocular morphological changes during human accommodation, with particular attention paid to the ciliary muscle and crystalline lens. The *in vivo* investigations have avoided the use of pharmacological agents in order to examine the natural, physiologic accommodative system. Application of newly developed techniques, such as three dimensional magnetic resonance imaging (MRI) and anterior segment optical coherence tomography (AS-OCT), have provided an improved insight into human phakic accommodation.

AS-OCT has been employed for the first time to examine the morphology of human ciliary muscle during accommodation, and to assess the refractive and age-dependent characteristics of this structure (Chapters 3 and 4). The ciliary muscle was found to be longer, both in terms of overall length, and anterior length, in eyes with axial myopia, implying that the muscle grows in the antero-posterior direction as the globe elongates, with the scleral spur as the fixed anchor point. The muscle does not, however, appear to be simply stretched during axial elongation, as suggested by the *in vitro* globe expansion work conducted by van Alphen (1986), as the myopic ciliary muscle was not found to be thinner than in emmetropic subjects, indeed no relationship between muscle thickness and refractive error was identified. With accommodative effort, the ciliary muscle demonstrates a contractile shortening, and thickening of the anterior region, even in eyes with established presbyopia, supporting a lenscentric model of presbyopia development. Nasal *versus* temporal asymmetries in ciliary muscle characteristics have been documented for the first time *in vivo*, notably thickening of the muscle, and greater contractile response, on the temporal side.

The observed regional differences in ciliary muscle characteristics could potentially impact on lens stability during accommodation, thus a bespoke methodology allowing quantification of lens tilt and decentration, relative to the cornea, using AS-OCT data was developed and is described in Chapter 5. Although AS-OCT has been suggested as a useful tool for analysis of IOL position (Montes-Mico *et al.*, 2009), there are no previous accounts in the literature of this technique being employed in the determination of phakic lens tilt and centration. Application of the novel technique in a cohort of young subjects indicated that the lens is generally well aligned with the cornea, in both the relaxed and accommodated states.

The implied stability of the lens during accommodation may be as a consequence of vitreous support, rather than indicative of increased equatorial zonular tension following ciliary muscle contraction, as predicted by Schachar (1994; 2006).

Support for the Helmholtzian mechanism of accommodation is provided from 3-D MRI of the phakic crystalline lens (Chapter 6). In addition to axial thickening and steepening of surface curvatures, the equatorial diameter of the lens was observed to decrease significantly during accommodation. The 3-D techniques used negated the potential problem of varying acquisition planes between the relaxed and accommodated states, and the findings are in direct opposition to Schachar's theory of accommodation, which is based upon increased equatorial zonular tension during accommodation, causing a movement of the lens edges outwards towards the sclera, increasing lenticular diameter (Schachar, 1994; Schachar, 2006).

The creation of fully 3-D lens models enabled *in vivo* determination of lens surface area and volume changes during accommodation, in the largest cohort described to date. The volumetric data suggest that the crystalline lens is compressed in its unaccommodated state, and undergoes expansion during accommodation, challenging the assumption that this structure is incompressible due to its high water content. The capsular bag appears to undergo elastic deformation, causing its surface area to reduce with accommodation. The dual occurrence of reduced lenticular surface area and increased volume has been predicted from mathematical modelling of primate lenses (Gerometta, 2007; Zamudio, 2008), but the data presented in Chapter 6 is the first *in vivo* support of this theory.

Whilst 3-D MRI techniques are clearly of great value in the study of lenticular changes with accommodation (Chapter 6) and analysis of complete eye shape (Singh *et al.* 2006; Gilmartin *et al.* 2007; Nagra *et al.* 2009), their current worth in the investigation of changes in ocular conformation with accommodation appears limited. The MRI data presented in Chapter 7 showed no significant change in nasal and temporal ocular conformation in the region from 25- 75 % of total axial length, or surface curvature of the area centred on the posterior pole. Amongst the same cohort, *IOLMaster* results demonstrated significant axial elongation at the majority of eccentricities measured, although these data are likely to overestimate true axial length changes due to the accommodative thickening of the crystalline lens and the impact this has on the mean refractive index of the ocular media. Investigation of changes in ocular shape with accommodation is unfortunately still restricted to indirect measures (peripheral refraction) and devices such as the *IOLMaster* and *Lenstar* which require adaptation to acquire off-axis data.

8.2. Evaluation of experimental work: suggestions for improvement and plans for future research

Ciliary muscle biometry was investigated using the *Visante* AS-OCT, for which a software update (Version 2.0) became available during the data acquisition phase of the thesis. The new software update provides a novel enhanced high resolution imaging mode which generates images of improved quality by automatically averaging the data from several scans. Future ciliary muscle imaging with the *Visante* will be conducted in this mode, rather than the standard high-resolution setting to reduce the variability of measurements. Furthermore, the development of bespoke image analysis software employing edge detection algorithms to enable automated determination of ciliary muscle boundaries is planned by the author, thus improving on the current subjective technique.

The investigation of ageing ciliary muscle detailed in Chapter 4 was limited to phakic volunteers, yet the impact of cataract extraction and intraocular lens (IOL) implantation on ciliary muscle morphology and contractility is very relevant to research directed at restoration of accommodation to presbyopic eyes. All techniques currently available to provide accommodation to the ageing eye rely on continued function of the ciliary muscle throughout life. Previous studies of the effect of cataract surgery on ciliary muscle action have provided some contradictory results, for example, Park *et al.* (2008) identified a significant increase in ciliary muscle centripetal movement in response to pilocarpine post-operatively, whereas the MRI data of Strenk *et al.* (2010) identified no thickening of the ciliary muscle in pseudophakic eyes with accommodative effort. Phakic volunteers aged up to 91 years however, showed an accommodative thickening, suggesting that cataract surgery causes at least a partial reduction in ciliary muscle response. Comparison of age-matched phakic and pseudophakic volunteers, or cataract patients pre- and post-operatively, utilising the methodology detailed in Chapters 3 and 4 could provide clarification of the effects of cataract surgery and IOL implantation on the contractile response of human ciliary muscle.

The 3-D MRI and analysis methodology detailed in Chapter 6 allowed the *in vivo* determination of lens equatorial diameter with a good level of intersession repeatability. The data confirmed an accommodative reduction in lens diameter, consistent with the Helmholtzian theory of accommodation. However, due to time and cost constraints, the study was limited to youthful subjects. Further research could apply the techniques described to a larger cohort, with a wider age range, to ascertain the effect of age on lens equatorial diameter. These data would be valuable in the understanding of the mechanism responsible for presbyopia development, particularly because the scientific basis of scleral

expansion surgery (Schachar, 2000) which aims to reverse the reduction in zonular tension that occurs secondary to an age-related increase in lens diameter, remains unproven.

MRI data presented in Chapters 6 and 7 is based upon the assumption that subjects exert the same degree of accommodation whilst sitting upright at an autorefractor, and supine during MRI scanning. It is possible that the supine position necessary for MRI data acquisition may reduce accommodative amplitude due to posterior movement of the accommodated lens under the influence of gravity, whilst zonular tension is relaxed. No previously published studies have quantified the degree of posterior displacement of the accommodating human crystalline lens. The recently developed *LenStar LS900* (Haag-Streit Koeniz, Switzerland; Buckhurst *et al.*, 2009) ocular biometry device utilises optical low coherence reflectometry to measure axial distances including corneal thickness, anterior chamber depth, crystalline lens thickness and axial length, and could be adapted to allow assessment of supine subjects. Mallen and Kashyap (2009) described modification of the *IOLMaster* by replacement of the chinrest with a headrest to support the subject's head horizontally and incorporation of a mirror to direct the measurement beam into the eye to facilitate ocular biometric measurement of a subject in a supine position. A similar adaptation could be utilised with the *LenStar* to compare anterior chamber depth of accommodating subjects in both the upright and supine positions to clarify whether backwards movement of the accommodated lens could influence MRI data analysis.

The data acquisition phase for Chapter 7 suggested a qualitative link between axial length changes with accommodation as determined with the *IOLMaster*, and subject age. Amongst the relatively small cohort of 8 subjects (aged 19- 31 years), accommodative elongation appeared more pronounced in the younger participants. The study of a range of subjects, from youths to incipient presbyopes could provide information relevant to the understanding of presbyopia. Loss of choroidal compliance has been suggested as a key factor in presbyopia development (Bito and Miranda, 1989) and data relating to any change in accommodative axial elongation (hypothesised to result from the contracting ciliary muscle applying an inward pulling force to the neighbouring choroid and sclera) with age, would provide an insight into the validity of this theory. Furthermore, Mallen *et al.* (2006) suggested that investigation was required to determine the axial expandability of the eyes of children, which could be relevant to the development of myopia. There is clear scope, therefore, for further research into the change in accommodative ocular elongation with age.

8.3. Concluding statement

The investigations detailed in the thesis have explored some of the aspects of human ocular accommodation which remain poorly understood, despite vast literary coverage of the subject. The findings provide further support for both the Helmholtzian mechanism of accommodation, and lenscentric models of presbyopia development. New information regarding the relationship between ciliary muscle morphology and refractive error could also be relevant to the understanding of myopigenesis.

The MRI and AS-OCT based methodologies described represent non-invasive techniques which can be employed to examine the accommodative structures *in vivo*, removing issues such as *post mortem* tissue changes and disruption of the complete system, which are associated with *ex vivo* studies. High resolution 3-D MRI allows the crystalline lens to be modelled and provides important information on lenticular volume and diameter, whilst AS-OCT is a commercially available and more accessible tool that can be applied for the investigation of ciliary muscle morphology. In addition to providing greater insight into several aspects of human accommodation which are not fully understood, the findings detailed form a platform for numerous future investigations in an exciting and expansive field of research, the ultimate goal of which is the restoration of accommodative ability to the presbyopic eye.

REFERENCES

- Abad, J. C., Rubinfeld, R. S., Del Valle, M., Belin, M. W., Kurstin, J. M. and Vertical, D. (2007). A novel topographic pattern in some keratoconus suspects. *Ophthalmology*. **114**, 1020-1026.
- Adams, D. W. and McBrien, N. A. (1992). Prevalence of myopia and myopic progression in a population of clinical microscopists. *Optometry and Vision Science*. **69**, 467-473.
- Aiello, A. L., Tran, V. T. and Rao, N. A. (1992). Postnatal development of the ciliary body and pars plana. *Archives of Ophthalmology*. **110**, 802-805.
- Altman, D. G. and Bland, J. M. (1983). Measurement in medicine: The analysis of method comparison studies. *The Statistician*. **32**, 307.
- Anderson, R. S. and Thibos, L. N. (1999). Relationship between acuity for gratings and for tumbling-E letters in peripheral vision. *Journal of the Optical Society of America A- Optics and Image Science*. **16**, 2321-2333.
- Ardiemand, N., Hau, S., McAlister, J. C., Bunce, C., Galaretta, D. and Tuft, S. J. (2007). Quality of vision and graft thickness in deep anterior lamellar and penetrating corneal allografts. *American Journal of Ophthalmology*. **143**, 228-235.
- Arnulf, A. and Dupuy, O. (1960). Contribution à l'étude des microfluctuations d'accommodation de l'oeil [French]. *Revue d'Optique, Paris*. **39**, 195-208.
- Atchison, D. A. (1991). Design of aspheric intraocular lenses. *Ophthalmic and Physiological Optics*. **11**, 137-146.
- Atchison, D. A. (1995). Accommodation and presbyopia. *Ophthalmic and Physiological Optics*. **15**, 255-272.
- Atchison, D. A. (2004). Anterior corneal and internal contributions to peripheral aberrations of human eyes. *Journal of the Optical Society of America A- Optics and Image Science*. **21**, 355-359.

- Atchison, D. A., Capper, E. J. and McCabe, K. L. (1994). Critical subjective measurement of amplitude of accommodation. *Optometry and Vision Science*. **71**, 699-706.
- Atchison, D. A., Jones, C. E., Schmid, K. L., Pritchard, N., Pope, J. M., Strugnell, W. E. and Riley, R. A. (2004). Eye shape in emmetropia and myopia. *Investigative Ophthalmology and Visual Science*. **45**, 3380-3386.
- Atchison, D. A., Markwell, E. L., Kasthurirangan, S., Pope, J. M., Smith, G. and Swann, P. G. (2008). Age- related changes in optical and biometric characteristics of emmetropic eyes. *Journal of Vision*. **8**, 1-20.
- Atchison, D. A., Pritchard, N. and Schmid, K. L. (2006). Peripheral refraction along the horizontal and vertical visual fields in myopia. *Vision Research*. **46**, 1450-1458.
- Atchison, D. A., Pritchard, N., Schmid, K. L., Scott, D. H., Jones, C. E. and Pope, J. M. (2005). Shape of the retinal surface in emmetropia and myopia. *Investigative Ophthalmology and Visual Science*. **46**, 2698-2707.
- Atchison, D. A. and Scott, D. H. (2002). Monochromatic aberrations of human eyes in the horizontal visual field. *Journal of the Optical Society of America A- Optics and Image Science*. **19**, 2180-2184.
- Atchison, D. A. and Smith, G. (2004). Possible errors in determining axial length changes during accommodation with the IOLMaster. *Optometry and Vision Science*. **81**, 282-285.
- Augusteyn, R. C. (2010). On the growth and internal structure of the human lens. *Experimental Eye Research*. **90**, 643-654.
- Ayrshire Study Circle (1964). An investigation into accommodation. *British Journal of Physiological Optics*. **21**, 31-35.
- Baïkoff, G. (2006). Anterior segment OCT and phakic intraocular lenses: a perspective. *Journal of Cataract and Refractive Surgery*. **32**, 1827-1835.
- Baïkoff, G., Lutun, E., Ferraz, C. and Wei, J. (2004a). Static and dynamic analysis of the anterior segment with optical coherence tomography. *Journal of Cataract and Refractive Surgery*. **30**, 1843-1850.

- Baïkoff, G., Lutun, E., Wei, J. and Ferraz, C. (2004b). Anterior chamber optical coherence tomography study of human natural accommodation in a 19-year-old albino. *Journal of Cataract and Refractive Surgery*. **30**, 696-701.
- Baïkoff, G., Lutun, E., Ferraz, C. and Wei, J. (2005). Analysis of the eye's anterior segment with optical coherence tomography: static and dynamic study [French]. *Journal Francais d'Ophthalmologie*. **28**, 343-352.
- Bailey, M. D., Sinnott, L. T. and Mutti, D. O. (2008). Ciliary body thickness and refractive error in children. *Investigative Ophthalmology and Visual Science*. **49**, 4353-4360.
- Bakri, S. J., Sears, J. E. and Lewis, H. (2007). Management of macular hole and submacular hemorrhage in the same eye. *Graefes Archives of Clinical and Experimental Ophthalmology*. **245**, 609-611.
- Banks, M. S. (1980). Infant refraction and accommodation. *International Ophthalmology Clinics*. **20**, 205-232.
- Barry, J.-C., Dunne, M. C. M. and Kirschkamp, T. (2001). Phakometric measurement of ocular surface radius of curvature and alignment: evaluation of method with physical model eyes. *Ophthalmic and Physiological Optics*. **21**, 450-460.
- Ben Simon, G. J., Annunziata, C. C., Fink, J., Villablanca, P., McCann, J. D. and Goldberg, R. A. (2005). Establishing guidelines for interpreting orbital imaging studies and evaluating their predictive value in patients with orbital tumors. *Ophthalmology*. **112**, 2196-2207.
- Benjamin, W. J. (2006) Borish's Clinical Refraction, St. Louis, Butterworth Heinemann Elsevier pp 99-105.
- Beers, A. P. A. and Van der Heijde, G. L. (1994). *In vivo* determination of the biomechanical properties of the component elements of the accommodation mechanism. *Vision Research*. **34**, 2897-2905.
- Bito, L. Z., DeRousseau, C. J., Kaufman, P. L. and Bitto, J. W. (1982). Age-dependent loss of accommodative amplitude in rhesus monkeys: an animal model for presbyopia. *Investigative Ophthalmology and Visual Science*. **23**, 23-31.

- Bito, L. Z. and Miranda, O. C. (1989). Accommodation and presbyopia. *In : Ophthalmology Annual 1989*. (R. D. Reinecke, Ed) Raven Press, New York, USA. pp. 103-128.
- Bland, J. M. and Altman, D. G. (1986). Statistical methods for assessing agreement between two methods of clinical measurement. *The Lancet*. **1**, 307-310.
- Borish, I. M. (1975) *Clinical Refraction*, 3rd Edition. Professional Press Inc. New York, USA.
- Bours, J. and Fodisch, H. J. (1986). Human fetal lens: wet and dry weight with increasing gestational age. *Ophthalmic Research*. **18**, 363-368.
- Brookman, K. E. (1983). Ocular accommodation in human infants. *American Journal of Optometry and Physiological Optics*. **60**, 91-99.
- Brown, N. (1972). An advanced slit-image camera. *British Journal of Ophthalmology*. **56**, 624-631.
- Brown, N. P. (1973a). The change in shape and internal form of the lens of the eye on accommodation. *Experimental Eye Research*. **15**, 441-459.
- Brown, N. (1974a). The change in lens curvature with age. *Experimental Eye Research*. **19**, 175-183.
- Brown, N. P. (1973b) Lens change with age and cataract; slit image photography. *In: The Human Lens in Relation to Cataract*, CIBA Symposium Foundation, Elsevier, Amsterdam, The Netherlands, pp 65-78.
- Buckhurst, P. J., Wolffsohn, J. S., Shah, S., Naroo, S. A., Davies, L. N. and Berrow, E. J. (2009). A new optical low coherence reflectometry device for ocular biometry in cataract patients. *British Journal of Ophthalmology*. **93**, 949-953.
- Buehl, W., Stojanac, D., Sacu, S., Drexler, W. and Findl, O. (2006). Comparison of three methods of measuring corneal thickness and anterior chamber depth. *American Journal of Ophthalmology*. **141**, 7-12.
- Buehren, T., Collins, M. J., Loughridge, J., Carney, L. G. and Iskander, D. R. (2003). Corneal topography and accommodation. *Cornea*. **22**, 311-316.

Bullimore, M. A., Adams, C. W., Fusaro, R. E., Bauman, M., Cottler, R. M., Sarver, J. N., Twelker, D. and Graham, A. D. (1996). Patient acceptance of autorefractor prescriptions: a randomised clinical trial. *In: Vision Science and its Applications*. Technical Digest Series, Vol. 1. Optical Society of America, Washington D. C., USA. pp 194-197.

Bullimore, M. A., Fusaro, R. E. and Adams, C. W. (1998). The repeatability of automated and clinician refraction. *Optometry and Vision Science*. **75**, 617-622.

Calver, R., Radhakrishnan, H., Osuobeni, E. and O'Leary, D. (2007). Peripheral refraction for distance and near in emmetropes and myopes. *Ophthalmic and Physiological Optics*. **27**, 584-593.

Campbell, F. W. (1954). The minimum quantity of light required to elicit the accommodation reflex in man. *Journal of Physiology*. **123**, 357-366.

Campbell, F. W. and Westheimer, G. (1960). Dynamics of accommodation responses of the human eye. *Journal of Physiology (London)*. **151**, 285-295.

Chang, Y., Wu, H.-M. and Lin, Y.-F. (2007). The axial misalignment between ocular lens and cornea observed by MRI (I)- At fixed accommodative state. *Vision Research*. **47**, 71-84.

Charman, W. N. (2008). The eye in focus: accommodation and presbyopia. *Clinical and Experimental Optometry*. **91**, 207-225.

Charman, W. N. and Heron, G. (1988). Fluctuations in accommodation: a review. *Ophthalmic and Physiological Optics*. **8**, 153-164.

Charman, W. N. and Radhakrishnan, H. (2010). Peripheral refraction and the development of refractive error: a review. *Ophthalmic and Physiological Optics*. **30**, 321-338.

Chau, C., Fung, K., Pak, K. and Yap, M. (2004). Is eye size related to orbit size in human subjects? *Ophthalmic and Physiological Optics*. **24**, 35-40.

Chaudhry, I. A., Shamsi, F. A., Elzaridi, E., Arat, Y. O. and Riley, F. C. (2007). Congenital cystic eye with intracranial anomalies: a clinicopathologic study. *International Ophthalmology Clinics*. **27**, 223-233.

Cheng, H., Barnett, J. K., Vilipuru, A. S., Marsack, J. D., Kasthurirangan, S., Applegate, R. A. and Roorda, A. (2004). A population study on changes in wave aberrations with accommodation. *Journal of Vision*. **4**, 272-280.

Cheng, H.-M., Singh, O. S., Kwong, K., Xiong, J., Woods, B. T. and Brady, T. J. (1992). Shape of the myopic eye as seen with high-resolution magnetic resonance imaging. *Optometry and Vision Science*. **69**, 698-701

Chien, C.-H. M., Huang, T. and Schachar, R. A. (2006). Analysis of human crystalline lens accommodation. *Journal of Biomechanics*. **39**, 672-680.

Cleary, G., Spalton, D. J., Patel, P. M., Lin, P.-F. and Marshall, J. (2009). Diagnostic accuracy and variability of autorefractometry by the Tracey Visual Function Analyzer and the Shin-Nippon NVision-K 5001 in relation to subjective refraction. *Ophthalmic and Physiological Optics*. **29**, 173-181.

Cogan, D. G. (1937). Accommodation and the autonomic nervous system. *Archives of Ophthalmology*. **18**, 739-766.

Coleman, D. J. (1970). Unified model for accommodative mechanism. *American Journal of Ophthalmology*. **69**, 1063-1079.

Coleman, D. J. (1986). On the hydraulic suspension theory of accommodation. *Transcripts of the American Ophthalmology Society*. **84**, 846-868.

Collins, M., Davis, B. and Wood, J. (1995). Microfluctuations of steady-state accommodation and the cardiopulmonary system. *Vision Research*. **35**, 2491-2502.

Crawford, K. S., Kaufman, P. L. and Bito, L. Z. (1990). The role of the iris in accommodation of rhesus monkeys. *Investigative Ophthalmology and Visual Science*. **31**, 2185-2190.

Crawford, K., Terasawa, E. and Kaufman, P. L. (1989). Reproducible stimulation of ciliary muscle contraction in the cynomolgus monkey via a permanent indwelling midbrain electrode. *Brain Research*. **503**, 265-272.

Croft, M. A., Glasser, A., Heatley, G., McDonald, J., Ebbert, T., Dahl, D. B., Nadkarni, N. V. and Kaufman, P. L. (2006a). Accommodative ciliary body and lens function in rhesus

monkeys I: normal lens, zonule and ciliary process configuration in the iridectomized eye. *Investigative Ophthalmology and Visual Science*. **47**, 1076-1086.

Croft, M. A., Glasser, A., Heatley, G., McDonald, J., Ebbert, T., Nadkarni, N. V. and Kaufman, P. L. (2006b). The zonula, lens, and circumlental space in the normal iridectomized rhesus monkey eye. *Investigative Ophthalmology and Visual Science*. **47**, 1087-1095.

Croft, M. A., Glasser, A. and Kaufman, P. L. (2001). Accommodation and presbyopia. *International Ophthalmology Clinics*. **41**, 33-46.

Croft, M. A., McDonald, J. P., James, R. J., Heatley, G. A., Lin, T. L., Lütjen-Drecoll, E. and Kaufman, P. L. (2008). Surgical intervention and accommodative responses I: centripetal ciliary body, capsule and lens movements in rhesus monkeys of various ages. *Investigative Ophthalmology and Visual Science*. **49**, 5484-5494.

Croft, M. A., McDonald, J. P., Nadkarni, N. V., Lin, T. L. and Kaufman, P. L. (2009). Age-related changes in centripetal ciliary body movement relative to centripetal lens movement in monkeys. *Experimental Eye Research*. **89**, 824-832.

Curtin, B. J. (1985). The components of refraction and their correlation. In: *The Myopias: Basic Science and Clinical Management*. Harper and Row, Philadelphia, USA.

Davies, L. N., Dunne, M. C. M., Gibson, G. A. and Wolffsohn, J. S. (2010) Vergence analysis reveals the influence of axial distances on accommodation with age and axial ametropia. *Ophthalmic and Physiological Optics*. **30**, 371-378.

Davies, L. N., Gibson, G. A., Sheppard, A. L. and Wolffsohn, J. S. (2008). *In vivo* biometric evaluation of phakic and pseudophakic eyes during accommodation with optical coherence tomography. *Investigative Ophthalmology and Visual Science*. **49**, E-Abstract 3777.

Davies, L. N. and Mallen, E. A. (2009). Influence of accommodation and refractive status on the peripheral refractive profile. *British Journal of Ophthalmology*. **93**, 1186-1190.

Davies, L. N., Mallen, E. A., Wolffsohn, J. S. and Gilmartin, B. (2003). Clinical evaluation of the Shin-Nippon NVision-K 5001/ Grand Seiko WR-5100 K autorefractor. *Optometry and Vision Science*. **80**, 320-324.

- Davson, H. (1990) *Physiology of the Eye*, 5th Edition. Macmillan, London, UK. pp 767-782.
- Daxecker, F. (1992). Christopher Scheiner's eye studies. *Documenta Ophthalmologica*. **81**, 27-35.
- Day, M., Strang, N. C., Seidel, D., Gray, L. S. and Mallen, E. A. H. (2006). Refractive group differences in accommodation microfluctuations with changing accommodation stimulus. *Ophthalmic and Physiological Optics*. **26**, 88-96.
- de Castro, A., Rosales, P. and Marcos, S. (2007). Tilt and decentration of intraocular lenses in vivo from Purkinje and Scheimpflug imaging. *Journal of Cataract and Refractive Surgery*. **33**, 418-429.
- Deller, J. F. P., O'Connor, A. D. and Sosby, A. (1947). X-ray measurement of the diameters of the living eye. *Proceedings of the Royal Society of London B: Biological Sciences*. **134**, 456-467.
- Demer, J. L., Kono, R. and Wright, W. (2003). Magnetic resonance imaging of human extraocular muscles in convergence. *Journal of Neurophysiology*. **89**, 2072-2085.
- Denieul, P. (1982). Effects of stimulus vergence on mean accommodation response, microfluctuations of accommodation and optical quality of the human eye. *Vision Research*. **22**, 561-569.
- Deubel, H. and Bridgeman, B. (1995). Fourth Purkinje image signals reveal eye-lens deviations and retinal image distortions during saccades. *Vision Research*. **35**, 529-538.
- Dick, H. B. (2005). Accommodative intraocular lenses: current status. *Current Opinion in Ophthalmology*. **16**, 8-26.
- Dirckx, J. J., Kuypers, L. C. and Decraemer, W. F. (2005). Refractive index of tissue measured with confocal microscopy. *Journal of Biomedical Optics*. **10**, 044014 doi:10.1117/1.1993487
- Drexler, W. (2007). Latest technological developments in ophthalmic optical coherence tomography [German]. *Spektrum der Augenheilkunde*. **21**, 3-12.

- Drexler, W., Baumgartner, A., Findl, O., Hitzemberger, C. K. and Fercher, A. F. (1997). Biometric investigation of changes in the anterior eye segment during accommodation. *Vision Research*. **37**, 2789-2800.
- Drexler, W., Findl, O., Schmetterer, L., Hitzemberger, C. K. and Fercher, A. F. (1998). Eye elongation during accommodation in humans: differences between emmetropes and myopes. *Investigative Ophthalmology and Vision Science*. **39**, 2140-2147.
- Drexler, W. and Fujimoto, J. G. (2007). Optical coherence tomography in ophthalmology. *Journal of Biomedical Optics*. **12**, (4) 041201.
- Duane, A. (1922). Studies in monocular and binocular accommodation with their clinical applications. *American Journal of Ophthalmology*. **5**, 865-877.
- Duane, A. (1925). Are the current theories of accommodation correct? *American Journal of Ophthalmology*. **8**, 196-202.
- Dubbelman, M. and Van der Heijde, G. L. (2001). The shape of the aging human lens: curvature, equivalent refractive index and the lens paradox *Vision Research*. **41**, 1867-1877.
- Dubbleman, M., Van der Heijde, G. L., Weeber, H. A. and Vrensen, G. F. J. M. (2003). Changes in the internal structure of the human crystalline lens with age and accommodation. *Vision Research*. **43**, 2363-2375.
- Dubbleman, M., Van der Heijde, G. L. and Weeber, H. A. (2005). Change in shape of the aging human crystalline lens with accommodation. *Vision Research*. **45**, 117-132.
- Duke-Elder, S. (1961) The anatomy of the visual system. *In: System of Ophthalmology, Vol. 2 The Anatomy of the Visual System*. London, Henry Kimpton. pp 146-167.
- Duke-Elder, S. (1970) *System of Ophthalmology*, St. Louis, Missouri, C.V.Mosby Company pp 220-265.
- Dunne, M. C. M. (1995). A computing scheme for determination of retinal contour from peripheral refraction, keratometry and A-scan ultrasonography. *Ophthalmic and Physiological Optics*. **15**, 133-143.

- Dunne, M. C. M. and Barnes, D. A. (1990). Modelling oblique astigmatism in eyes with known peripheral refraction and optical dimensions. *Ophthalmic and Physiological Optics*. **10**, 46-48.
- Dunne, M. C. M., Davies, L. N., Mallen, E. A. H., Kirschkamp, T. and Barry, J. (2005). Non-invasive phakometric measurement of corneal and crystalline lens alignment in human eyes. *Ophthalmic and Physiological Optics*. **25**, 143-152.
- Dunne, M. C. M., Davies, L. N. and Wolffsohn, J. S. (2007). Accuracy of cornea and lens biometry using anterior segment optical coherence tomography. *Journal of Biomedical Optics*. **12**, 064023:1-5.
- Dunne, M. C. M., Mission, G. P., White, E. K. and Barnes, D. A. (1993). Peripheral astigmatic asymmetry and angle alpha. *Ophthalmic and Physiological Optics*. **13**, 303-305.
- Edwards, K. and Llewellyn, R. (1988) *Optometry*. Butterworths, London.
- Ehrmann, K., Ho, A. and Parel, J.-M. (2008). Biomechanical analysis of the accommodative apparatus in primates. *Clinical and Experimental Optometry*. **91**, 302-312.
- Elder, M. J., Murphy, C. and Sanderson, G. F. (1996). Apparent accommodation and depth of field in pseudophakia. *Journal of Cataract and Refractive Surgery*. **22**, 615-619.
- Elliott, M., Simpson, T., Richter, D. and Fonn, D. (1997). Repeatability and accuracy of automated refraction: a comparison of the Nikon NRK-8000, the Nidek AR-1000, and subjective refraction. *Optometry and Vision Science*. **74**, 434-438.
- Eng, J. (2003). Sample size estimation: how many individuals should be studied? *Radiology*. **227**, 309-313.
- Farnsworth, P. N. and Burke, P. (1977). Three-dimensional architecture of the suspensory apparatus of the lens of the rhesus monkey. *Experimental Eye Research*. **25**, 563-577.
- Farnsworth, P. N. and Shyne, S. E. (1979). Anterior zonular shifts with age. *Experimental Eye Research*. **28**, 291-297.
- Fedtke, C., Ehrmann, K. and Holden, B. A. (2009). A review of peripheral refraction techniques. *Optometry and Vision Science*. **86**, 429-446.

- Ferree, C. E. and Rand, G. (1933). Interpretations of refractive conditions in the peripheral field of vision. *Archives of Ophthalmology*. **9**, 925-938.
- Ferree, C. E., Rand, G. and Hardy, C. (1931). Refraction for the peripheral field of vision. *Archives of Ophthalmology*. **5**, 717-731.
- Fincham, E. F. (1937). The mechanism of accommodation. *British Journal of Ophthalmology Supplement*. **8**, 5-80.
- Fisher, R. F. (1969). Elastic constants of the human lens capsule. *Journal of Physiology*. **201**, 1-19.
- Fisher, R. F. (1977). The force of contraction of the human ciliary muscle during accommodation. *Journal of Physiology (London)*. **270**, 51-74.
- Fisher, R. F. (1982). The vitreous and lens in accommodation. *Transcripts of the Ophthalmology Society of the United Kingdom*. **102**, 318-322.
- Fisher, R. F. (1983). Is the vitreous necessary for accommodation in man? *British Journal of Ophthalmology*. **67**, 206.
- Fisher, R. F. (1986). The ciliary body in accommodation. *Transcripts of the Ophthalmology Society of the United Kingdom*. **105**, 208-219.
- Fisher, R. F. and Pettet, B. E. (1973). Presbyopia and the water content of the human crystalline lens. *Journal of Physiology (London)*. **234**, 443-447.
- Fitzke, F. W., Hayes, B. P., Hodos, W., Holden, A. L. and Low, J. C. (1985). Refractive sectors in the visual field of the pigeon eye. *Journal of Physiology*. **369**, 33-44.
- Fledelius, H. C. (1997). Ultrasound in ophthalmology. *Ultrasound in Medicine and Biology*. **23**, 365-375.
- Fletcher, R. J. (1951). Astigmatic accommodation: Parts I- III. *British Journal of Physiological Optics*. **8**, 73-94.

Garner, L. F. and Yap, M. K. (1997). Changes in ocular dimensions and refraction with accommodation. *Ophthalmic and Physiological Optics*. **17**, 12-17.

Gerometta, R., Zamudio, A. C., Escobar, D. P. and Candia, O. A. (2007). Volume change of the ocular lens during accommodation. *American Journal of Physiology- Cell Physiology*. **293**, C797-C804.

Gilmartin, B. (1986). A review of the role of sympathetic innervation of the ciliary muscle in ocular accommodation. *Ophthalmic and Physiological Optics*. **6**, 23-37.

Gilmartin, B. (1995). The aetiology of presbyopia: a summary of the role of lenticular and extralenticular structures. *Ophthalmic and Physiological Optics*. **15**, 431-437.

Gilmartin, B. (1998) Autonomic correlates of near-vision in emmetropia and myopia. *In :Myopia and Near Work*. Oxford, Butterworth Heinemann.

Gilmartin, B. (2004). Myopia: precedents for research in the twenty-first century. *Clinical and Experimental Ophthalmology*. **32**, 305-324.

Gilmartin, B., Hogan, R. E. and Thompson, S. M. (1984). The effect of timolol maleate on tonic accommodation, tonic vergence, and pupil diameter. *Investigative Ophthalmology and Visual Science*. **25**, 763-770.

Gilmartin, B., Logan, N. S. and Singh, K. (2007). Determining regional variations in globe conformation using 3-D ocular MRI. *Investigative Ophthalmology and Vision Science*. **48**, E-abstract 1215.

Gilmartin, B., Mallen, E. A. and Wolffsohn, J. S. (2002). Sympathetic control of accommodation: evidence for inter-subject variation. *Ophthalmic and Physiological Optics*. **22**, 366-371.

Glasser, A. (2008). Restoration of accommodation: surgical options for correction of presbyopia. *Clinical and Experimental Optometry*. **91**, 279-295.

Glasser, A. and Campbell, M. C. W. (1998). Presbyopia and the optical changes in the human crystalline lens with age. *Vision Research*. **38**, 209-229.

Glasser, A. and Campbell, M. C. W. (1999). Biometric, optical and physical changes in the isolated human crystalline lens in relation to presbyopia. *Vision Research*. **39**, 1991-2015.

Glasser, A., Croft, M. A., Brumback, L. and Kaufman, P. L. (2001). Ultrasound biomicroscopy of the aging rhesus monkey ciliary region. *Optometry and Vision Science*. **78**, 417-424.

Glasser, A. and Kaufman, P. L. (1999). The mechanism of accommodation in primates. *Ophthalmology*. **106**, 863-872.

Glasser, A., Wendt, M. and Ostrin, L. (2006). Accommodative changes in lens diameter in rhesus monkeys. *Investigative Ophthalmology and Visual Science*. **47**, 278-286.

Goldsmith, J. A., Li, Y., Chalita, M. R., Westphal, V., Patil, C., Rollins, A., Izatt, J. and Huang, D. (2005). Anterior chamber width measurement by high speed optical coherence tomography. *Ophthalmology*. **113**, 238-244.

Goss, D. A., van Veen, H. G., Rainey, B. B. and Feng, B. (1997). Ocular components measured by keratometry, phakometry and ultrasonography in emmetropic and myopic optometry students. *Optometry and Vision Science*. **74**, 489-495.

Gray, L. S., Gilmartin, B. and Winn, B. (2000). Accommodation microfluctuations and pupil size during sustained viewing of visual display terminals. *Ophthalmic and Physiological Optics*. **20**, 5-10.

Gray, L. S., Winn, B. and Gilmartin, B. (1993a). Accommodative microfluctuations and pupil diameter. *Vision Research*. **33**, 2083-2090.

Gray, L. S., Winn, B. and Gilmartin, B. (1993b). Effect of target luminance on microfluctuations of accommodation. *Ophthalmic and Physiological Optics*. **13**, 258-265.

Gustaffson, J., Terenius, E., Buchheister, J. and Unsbo, P. (2001). Peripheral astigmatism in emmetropic eyes. *Ophthalmic and Physiological Optics*. **21**, 393-400.

Guyton, D. L., Uozato, H. and Wisnicki, H. J. (1990). Rapid determination of intraocular lens tilt and decentration through the undilated pupil. *Ophthalmology*. **97**, 1259-1264.

Gwiazda, J., Thorn, F., Bauer, J. and Held, R. (1993). Myopic children show insufficient accommodative response to blur. *Investigative Ophthalmology and Visual Science*. **34**, 690-694.

Gwiazda, J., Thorn, F. and Held, R. (2005). Accommodation, accommodative convergence, and response AC/A ratios before and at the onset of myopia in children. *Optometry and Vision Science*. **82**, 273-278.

Han, W., Kwan, W., Wang, J., Yip, S. P. and Yap, M. (2007). Influence of eyelid position on wavefront aberrations. *Ophthalmic and Physiological Optics*. **27**, 66-75.

Harocopos, G. J., Shui, Y. B., McKinnon, M., Holekamp, N. M., Gordon, M. O. and Beebe, D. C. (2004). Importance of vitreous liquefaction in age-related cataract. *Investigative Ophthalmology and Visual Science*. **45**, 77-85.

Hayashi, K., Harada, M., Hayashi, H., Nakao, F. and Hayashi, F. (1997). Decentration and tilt of polymethyl methacrylate, silicone and acrylic soft intraocular lenses. *Ophthalmology*. **104**, 793-798.

He, J. C., Burns, S. A. and Marcos, S. (2000). Monochromatic aberrations in the accommodated human eye. *Vision Research*. **40**, 41-48.

He, L., Donnelly III, W. J., Stevenson, S. B. and Glasser, A. (2010). Saccadic lens instability increases with accommodative stimulus in presbyopes. *Journal of Vision*. **10**, 1-16.

Heath, G. G. (1956). Components of accommodation. *American Journal of Optometry and Archives of American Academy of Optometry*. **33**, 569-579.

Hemenger, R. P., Garner, L. F. and Ooi, C. S. (1995). Change with age of the refractive index gradient of the human ocular lens. *Investigative Ophthalmology and Visual Science*. **36**, 703-707.

Hermans, E. A., Dubbelman, M., van der Heijde, R. and Heethar, R. (2007). The shape of the human lens nucleus with accommodation. *Journal of Vision*. **7**, 1- 10.

Hermans, E. A., Pouwels, P. J. W., Dubbelman, M., Kuijer, J. P. A., van der Heijde, R. G. L. and Heethar, R. M. (2009). Constant volume of the human lens and decrease in surface

area of the capsular bag during accommodation: an MRI and Scheimpflug study. *Investigative Ophthalmology and Visual Science*. **50**, 281-289.

Heron, G. and Schor, C. M. (1995). The fluctuations of accommodation and ageing. *Ophthalmic and Physiological Optics*. **15**, 445-449.

Hess, C. (1896). Arbeiten aus Gebiete der Akkommodationsiehr [German]. *Graefes Archiv für klinische und experimentelle Ophthalmologie*. **42**.

Heys, K. R., Cram, S. L. and Truscott, R. J. (2005). Massive increase in the stiffness of the lens nucleus with age: the basis for presbyopia? *Molecular Vision*. **10**, 256-263.

Hodos, W. and Erichsen, J. T. (1990). Lower-field myopia in birds: An adaptation that keeps the ground in focus. *Vision Research*. **30**, 653-657.

Hoogerheide, J., Rempt, F. and Hoogenboom, W. P. (1971). Acquired myopia in young pilots. *Ophthalmologica*. **163**, 209-215.

Hopkins, G. and Pearson, R. (2007) *Ophthalmic Drugs. Diagnostic and Therapeutic Uses*. Edinburgh, Butterworth Heinemann Elsevier. pp 85-106.

Hornak, J. P. (2008). The Basics of MRI: an Online Book on magnetic resonance imaging., Rochester Institute of Technology, Rochester, NY. Available online at <http://www.cis.rit.edu/htbooks/mri>. Accessed August 10th 2010.

Huber, C. (1981). Myopic astigmatism as a substitute for accommodation in pseudophakia. *Developments in Ophthalmology*. **5**, 17-26.

Hung, G. K. and Ciuffreda, K. J. (2000). A unifying theory of refractive error development. *Bulletin of Mathematical Biology*. **62**, 1087-1108.

Hurwitz, B. S., Davidowitz, J., Chin, N. B. and Breinin, G. B. (1972). The effects of the sympathetic nervous system on accommodation: 1. Beta sympathetic nervous system. *Archives of Ophthalmology*. **87**, 668-674.

- Ip, J. M., Saw, S. M., Rose, K. A., Morgan, I. G., Kifley, A., Wang, J. J. and Mitchell, P. (2008). Role of Near Work in Myopia: Findings in a Sample of Australian School Children. *Investigative Ophthalmology and Vision Science*. **48**, 2903-2910.
- Izatt, J. A., Hee, M. R., Schuman, J. S. and Fujimoto, J. G. (1994). Micrometer-scale resolution imaging of the anterior eye in vivo with optical coherence tomography. *Archives of Ophthalmology*. **112**, 1584-1589.
- Jackman, W. T. and Webster, J. D. (1886). On photographing the retina of the living human eye. *Philadelphia Photographer*. **23**, 275.
- Jennings, J. A. and Charman, W. N. (1978). Optical image quality in the peripheral retina. *American Journal of Optometry and Physiological Optics*. **55**, 582-590.
- Johnson, C. (1976). Effects of luminance and stimulus distance on accommodation and visual resolution. *Journal of the Optical Society of America*. **66**, 138-142.
- Johnson, C. A. and Leibowitz, H. W. (1974). Practice, refractive error, and feedback as factors influencing peripheral motion thresholds. *Perception and Psychophysics*. **15**, 276-280.
- Jones, C. E., Atchison, D. A., Meder, R. and Pope, J. M. (2005). Refractive index distribution and optical properties of the isolated human lens measured using magnetic resonance imaging. *Vision Research*. **45**, 2352-2366.
- Jones, C. E., Atchison, D. A. and Pope, J. M. (2007). Changes in lens dimensions and refractive index with age and accommodation. *Optometry and Vision Science*. **84**, 990-995.
- Jones, C. E. and Pope, J. M. (2004). Measuring optical properties of an eye lens using magnetic resonance imaging. *Magnetic Resonance Imaging*. **22**, 211-220.
- Judge, S. J. and Burd, H. J. (2004). The MRI data of Strenk *et al.* do not suggest lens compression in the unaccommodated state (E-letter). *Investigative Ophthalmology and Vision Science*. **45**, 539.

Jumblatt, J. E. (1999) Innervation and pharmacology of the iris and ciliary body., *In: Nervous Control of the Eye* (G. Burnstock and A. M. Sillito Eds), Amsterdam, Harwood Academic. pp.1- 40.

Kasthurirangan, S. and Glasser, A. (2006). Age-related changes in accommodative dynamics in humans. *Vision Research*. **46**, 1507-1519.

Kasthurirangan, S., Markwell, E. L., Atchison, D. A. and Pope, J. M. (2008). *In vivo* study of changes in refractive index distribution in the human crystalline lens with age and accommodation. *Investigative Ophthalmology and Visual Science*. **49**, 2531-2540.

Kaufman, P. L. (1992) Accommodation and presbyopia: neuromuscular and biophysical aspects, *In: Adler's Physiology of the Eye, Clinical Application. 9th Edition* (ed. W. M. Hart, Jr.) C. V. Mosby, St Louis, Missouri, USA. pp. 391-411.

Kaufman, P. L. and Alm, A. (2003). Accommodation and presbyopia. *In: Adler's Physiology of the Eye, Clinical Application. 10th Edition*. Mosby Year Book Inc. St. Louis, Missouri, USA. pp. 195-233.

Kaufman, P. L., Bito, L. Z. and DeRousseau, C. J. (1982). The development of presbyopia in primates. *Transcripts of the Ophthalmology Society of the United Kingdom*. **102**, 323-326.

Kinge, B., Milelfart, A. and Jacobsen, G. (1996). Clinical evaluation of the Allergan Humphrey 500 autorefractor and the Nidek AR-1000 autorefractor. *British Journal of Ophthalmology*. **80**, 35-39.

Kirschkamp, T., Dunne, M. C. M. and Barry, J-C. (2004). Phakometric measurement of ocular surface radii of curvature, axial separations and alignment in relaxed and accommodated human eyes. *Ophthalmic and Physiological Optics*. **24**, 65-73.

Koeppl, C., Findl, O., Kriechbaum, K. and Drexler, W. (2005). Comparison of pilocarpine-induced and stimulus-driven accommodation in phakic eyes. *Experimental Eye Research*. **80**, 795-800.

Kolk, A., Pantke, C., Wiener, E., Plodor, O. and Neff, A. (2005). A novel high-resolution magnetic resonance imaging microscopy coil as an alternative to multislice computed tomography in postoperative imaging of orbital fractures and computer-based volume measurement. *Journal of Oral and Maxillofacial Surgery*. **63**, 492-498.

- Konstantopoulos, A., Hossain, P. and Anderson, D. F. (2007). Recent advances in ophthalmic anterior segment imaging: a new era for ophthalmic diagnosis? *British Journal of Ophthalmology*. **91**, 551-557.
- Koopmans, S. A., Terwee, T. T., Barkhof, J., Haitjema, H. J. and Kooijman, A. C. (2003). Polymer refilling of presbyopic human lenses in vitro restores the ability to undergo accommodative changes. *Investigative Ophthalmology and Visual Science*. **44**, 250-257.
- Koretz, J. F., Bertasso, A. M., Neider, M. W., True-Gabelt, B. A. and Kaufman, P. L. (1987a). Slit-lamp studies of the rhesus monkey eye: II. Changes in crystalline lens shape, thickness and position during accommodation and aging. *Experimental Eye Research*. **45**, 317-326.
- Koretz, J. F., Cook, C. A. and Kaufman, P. L. (2001). Aging of the human lens: changes in lens shape at zero-diopter accommodation. *Journal of the Optical Society of America*. **18**, 265-272.
- Koretz, J. F., Cook, C. A. and Kaufman, P. L. (2002). Aging of the human lens: changes in lens shape upon accommodation and with accommodative loss. *Journal of the Optical Society of America A-Optics and Image Science*. **19**, 144-151.
- Koretz, J. F. and Handelman, G. H. (1986). Modeling age-related loss in the human eye. *Mathematical Modelling*. **7**, 1003-1014.
- Koretz, J. F. and Handelman, G. H. (1988). How the human eye focuses. *Scientific American*. **259**, 64-71.
- Koretz, J. F. and Handelman, G. H. (1982). Model of the accommodative mechanism in the human eye. *Vision Research*. **22**, 917-927.
- Koretz, J. F., Kaufman, P. L., Neider, M. W. and Goeckner, P. A. (1989). Accommodation and presbyopia in the human eye- aging of the anterior segment. *Vision Research*. **29**, 1685-1692.

Koretz, J. F., Neider, M. W., Kaufman, P. L., Bertasso, A. M., DeRousseau, C. J. and Bitó, L. Z. (1987b). Slitlamp studies of the rhesus monkey eye I: survey of the anterior segment. *Experimental Eye Research*. **44**, 307-318.

Koretz, J. F., Strenk, S. A., Strenk, L. M. and Semmlow, J. L. (2004). Scheimpflug and high-resolution magnetic resonance imaging of the anterior segment: a comparative study. *Journal of the Optical Society of America*. **21**, 346-354.

Kotulak, J. C. and Schor, C. M. (1986). Temporal variations in accommodation during steady state conditions. *Journal of the Optical Society of America*. **3**, 223-227.

Kotulak, J. C. and Schor, C. M. (1987). The effects of optical vergence, contrast, and luminance on the accommodative response to spatially bandpass filtered targets. *Vision Research*. **27**, 1797-1806.

Krag, S. and Andreassen, T. T. (2003). Mechanical properties of the human posterior lens capsule. *Investigative Ophthalmology and Visual Science*. **44**, 691-696.

Krag, S., Olsen, T. and Andreassen, T. T. (1997). Biomechanical characteristics of the human anterior lens capsule in relation to age. *Investigative Ophthalmology and Visual Science*. **38**, 357-363.

Kriechbaum, K., Findl, O., Koepl, C., Menapace, R. and Drexler, W. (2005). Stimulus-driven versus pilocarpine-induced biometric changes in pseudophakic eyes. *Ophthalmology*. **112**, 453-459.

Kusakari, T., Sato, T. and Tokoro, T. (2001). Visual deprivation stimulates the exchange of the fibrous sclera into the cartilaginous sclera in chicks. *Experimental Eye Research*. **73**, 533-546.

Kuszak, J. R. (1995). Development of sutures in the lens. *Progress in Retinal and Eye Research*. **14**, 567-591.

Lackner, B., Schmidinger, G., Pieh, S., Funovics, M. A. and Skorpik, C. (2005). Repeatability and reproducibility of central corneal thickness measurement with Pentacam, Orbscan and ultrasound. *Optometry and Vision Science*. **82**, 892-899.

- Langaas, T., Riddell, P. M., Ystenaes, A. E., Langeeggen, I. and Bruenech, J. R. (2008). Variability of the accommodation response in early onset myopia. *Optometry and Vision Science*. **85**, 37-48.
- Langner, S., Martin, H., Terwee, T., Koopmans, S. A., Krüger, P. C., Hosten, N., Schmitz, K. P., Guthoff, R. F. and Stachs, O. (2010). 7.1T MRI to Assess the Anterior Segment of the Eye. *Investigative Ophthalmology and Visual Science*. In press doi:10.1167/iovs.09-4865.
- Leibowitz, H. W., Johnson, C. A. and Isabelle, E. (1972). Peripheral motion detection and refractive error. *Science*. **177**, 1207-1208.
- Levy, N. S. (2000). Comparing MRIs with movement artifact (E-letter). *Investigative Ophthalmology and Vision Science*. Available at: <http://www.iovs.org/cgi/eletters/40/6/1162>. Accessed 16th August 2010.
- Li, Y., Shekhar, R. and Huang, D. (2006). Corneal pachymetry mapping with high-speed optical coherence tomography. *Ophthalmology*. **113**, 792-799.
- Lim, J. C., Walker, K. L., Sherwin, T., Schey, K. L. and Donaldson, P. J. (2009). Confocal microscopy reveals zones of membrane remodelling in the outer cortex of the human lens. *Investigative Ophthalmology and Visual Science*. **50**, 4304-4310.
- Liney, G. P. (2005a) Magnetic Resonance Imaging Physics Lectures. Available online at http://www.hull.ac.uk/mri/lectures/gpl_page.html Accessed August 10th 2010.
- Liney, G. P. (2005b) MRI from A to Z: a definitive guide for medical professionals, Cambridge University Press, Cambridge. pp 3- 247.
- Ljubimova, D. and Eriksson, A. (2005). Numerical study of the effect of vitreous support on eye accommodation. *Acta of Bioengineering and Biomechanics*. **7**, 3-16.
- Logan, N. S., Gilmartin, B. and Dunne, M. C. M. (1995). *Computation of retinal contour in anisomyopia*. *Ophthalmic and Physiological Optics*. **15**, 363-366.
- Logan, N. S., Gilmartin, B., Wildsoet, C. F. and Dunne, M. C. M. (2004). Posterior retinal contour in adult human anisomyopia. *Investigative Ophthalmology and Visual Science*. **45**, 2152-2162.

- Lotmar, W. and Lotmar, T. (1974). Peripheral astigmatism in the human eye: experimental data and theoretical model predictions. *Journal of the Optical Society of America*. **64**, 510-513.
- Lou, L. (2008). Troxler effect with dichoptic stimulus presentations: Evidence for binocular inhibitory summation and interocular suppression. *Vision Research*. **48**, 1514-1521.
- Love, J., Gilmartin, B. and Dunne, M. C. M. (2000). Relative peripheral refractive error in adult myopia and emmetropia. *Investigative Ophthalmology and Vision Science*. **41**, S302.
- Lundstrom, L., Gustaffson, J., Svenson, I. and Unsbo, P. (2005). Assessment of objective and subjective eccentric refraction. *Optometry and Vision Science*. **82**, 298-306.
- Lutjen-Drecoll, E., Kaufman, P. L., Wasilewski, R., Ting-Li, L. and Croft, M. A. (2010). Morphology and accommodative function of the vitreous zonule in human and monkey eyes. *Investigative Ophthalmology and Visual Science*. **51**, 1554-1564.
- Lutjen, E. (1966). Histometric studies on the ciliary muscle in primates [German]. *Graefes Archiv für klinische und experimentelle Ophthalmologie*. **171**, 121-133.
- Ma, J. and Chen, X. (2004). Dynamic changes of configuration and position of human ciliary body during accommodation [Chinese]. *Zhonghua Yan Ke Za Zhi*. **40**, 590-596.
- Mafee, M. F., Valvassori, G. E. and Becker, M. (2005) *Valvassori's Imaging of the Head and Neck. Second edition*. Thieme, New York. pp. 140-143.
- Mallen, E. A. and Kashyap, P. (2007). Technical note: Measurement of retinal contour and supine axial length using the Zeiss IOLMaster. *Ophthalmic and Physiological Optics*. **27**, 404-411.
- Mallen, E. A. H., Kashyap, P. and Hampson, K. M. (2006). Transient axial length change during the accommodation response in young adults. *Investigative Ophthalmology and Visual Science*. **47**, 1251-1254.

- Mallen, E. A. H., Wolffsohn, J. S. W., Gilmartin, B. and Tsujimura, S. (2001). Clinical evaluation of the Shin-Nippon SRW-5000 autorefractor in adults. *Ophthalmic and Physiological Optics*. **21**, 101-107.
- Manny, R. E., Fern, K. D., Zervas, H. J., Cline, G. E., Scott, S. K., White, J. M. and Pass, A. F. (1993). 1 % cyclopentolate hydrochloride: another look at the time course of the cycloplegia using an objective measure of the accommodative response. *Optometry and Vision Science*. **70**, 651-665.
- Marchini, G., Ghilotti, G., Bonadimani, M. and Babighian, S. (2003). Effects of 0.005 % Latanoprost on ocular anterior structures and ciliary body thickness. *Journal of Glaucoma*. **12**, 295-300.
- Mathews, S. (1999). Scleral expansion surgery does not restore accommodation in human presbyopia. *Ophthalmology*. **106**, 873-877.
- Mays, L. E. and Gamlin, P. D. R. (1995). Neuronal circuitry controlling the near response. *Current Opinion in Neurobiology*. **5**, 763-768.
- McBrien, N. and Millodot, M. (1985). Clinical Evaluation of the Canon Autorefr R-1. *American Journal of Optometry and Physiological Optics*. **62**, 786-792.
- Mester, U., Sauer, T. and Kaymak, H. (2009). Decentration and tilt of a single-piece aspheric intraocular lens compared with the lens position in young phakic eyes. *Journal of Cataract and Refractive Surgery*. **35**, 485-490.
- Miege, C. and Denieul, P. (1988). Mean response and oscillations of accommodation for various stimulus vergences in relation to accommodation feedback control. *Ophthalmic and Physiological Optics*. **8**, 165-171.
- Miles, F. A. and Wallman, J. (1990). Local ocular compensation for imposed local refractive error. *Vision Research*. **30**, 339-349.
- Millodot, M. (1981). Effect of ametropia on peripheral refraction. *American Journal of Optometry and Physiological Optics*. **58**, 691-695.
- Millodot, M. (2008) Dictionary of Optometry and Visual Science, Oxford, Butterworth Heinemann.

Millodot, M. and Lamont, A. (1974). Letter: Refraction of the periphery of the eye. *Journal of the Optical Society of America*. **64**, 110-111.

Moffat, B. A., Atchison, D. A. and Pope, J. M. (2002). Age-related changes in refractive index distribution and power of the human lens as measured by magnetic resonance micro imaging in vitro. *Vision Research*. **42**, 1683-1693.

Mohan, M., Rao, V. A. and Dada, V. K. (1977). Experimental myopia in the rabbit *Experimental Eye Research*. **25**, 33-38.

Montes-Mico, R., Cervino, A. and Ferrer-Blasco, T. (2009). Intraocular lens centration and stability: efficacy of current technique and technology. *Current Opinion in Ophthalmology*. **20**, 33-36.

Morgan, A. J., Harper, J., Hosking, S. L. and Gilmartin, B. (2002). The effect of corneal thickness and corneal curvature on pneumatonometer measurements. *Current Eye Research*. **25**, 107-112.

Muftuoglu, O., Flosal, B. M., Karel, F. and Zilefioglu, G. (2005). Drug-induced intraocular lens movement and near visual acuity after AcrySof intraocular lens implantation. *Journal of Cataract and Refractive Surgery*. **31**, 1298-1305.

Muftuoglu, O., Hosal, B. M. and Zilelioglu, G. (2009). Ciliary body thickness in unilateral high axial myopia. *Eye (London)*. **23**, 1176-1181.

Mutlu, F. M., Bayer, A., Erduman, C. and Bayraktar, M. Z. (2005). Comparison of tilt and decentration between phacoemulsification and phacotrabeculectomy. *Ophthalmologica*. **219**, 26-29.

Mutti, D. O. (2010). Hereditary and environmental contributions to emmetropization and myopia. *Optometry and Vision Science*. **87**, 255-259.

Mutti, D. O., Enlow, N. L. and Mitchell, G. L. (2001). Accommodation and induced with-the-rule astigmatism in emmetropes. *Optometry and Vision Science*. **78**, 6-7.

Mutti, D. O., Hayes, J. R., Mitchell, G. L., Jones, L. A., Moeschberger, M. L., Cotter, S. A., Kleinstejn, R. N., Manny, R. E., Twelker, J. D. and Zadnik, K. (2007). Refractive error, axial

length, and relative peripheral refractive error before and after the onset of myopia. *Investigative Ophthalmology and Vision Science*. **48**, 2510-2519.

Mutti, D. O., Mitchell, G. L., Hayes, J. R., Jones, L. A., Moeschberger, M. L., Cotter, S. A., Kleinstein, R. N., Manny, R. E., Twelker, D. and Zadnik, K. (2006). Accommodative lag before and after the onset of myopia. *Investigative Ophthalmology and Visual Science*. **47**, 837-846.

Mutti, D. O., Mitchell, G. L., Moeschberger, M. L., Jones, L. A. and Zadnik, K. (2002). Parental myopia, near work, school achievement, and children's refractive error. *Investigative Ophthalmology and Visual Science*. **43**, 3633-3640.

Mutti, D. O., Sholtz, R. I., Friedman, N. E. and Zadnik, K. (2000). Peripheral refraction and ocular shape in children. *Investigative Ophthalmology and Visual Science*. **41**, 1022-1030.

Nagra, M., Gilmartin, B., Logan, N. S., Furlong, P., Wilkinson, E. and Singh, K. (2009). Conformation of sagittal and axial meridians in human myopia. *Investigative Ophthalmology and Vision Science*. **50**, E-abstract 3941.

Nakazawa, M. and Ohtsuki, K. (1983). Apparent accommodation in pseudophakic eyes after implantation of posterior chamber intraocular lenses. *American Journal of Ophthalmology*. **96**, 435-438.

Navarro, R., Artal, P. and Williams, D. R. (1993). Modulation transfer of the human eye as a function of retinal eccentricity. *Journal of the Optical Society of America A- Optics and Image Science*. **10**, 201-212.

Navarro, R., Moreno, E. and Dorronsoro, C. (1998). Monochromatic aberrations and point-spread functions of the human eye across the visual field. *Journal of the Optical Society of America A- Optics and Image Science*. **15**, 2522-2529.

Neider, M. W., Crawford, K., Kaufman, P. L. and Bito, L. Z. (1990). *In vivo* videography of the rhesus monkey accommodative apparatus. *Archives of Ophthalmology*. **108**, 69-74.

Nickla, D. and Wallman, J. (2010). The multifunctional choroid. *Progress in Retinal and Eye Research*. **29**, 144-168.

- Nishida, S. and Mizutani, S. (1992). Quantitative and morphometric studies of age-related changes in human ciliary muscle. *Japanese Journal of Ophthalmology*. **36**, 380-387.
- Nolan, W. P. (2008). Anterior segment imaging: ultrasound biomicroscopy and anterior segment optical coherence tomography. *Current Opinion in Ophthalmology*. **19**, 115-121.
- Nolan, W. P., See, J. L., Chew, P. T. K., Friedman, D. S., Smith, S. D. and Radhakrishnan, S. (2007). Detection of primary angle closure glaucoma using anterior segment optical coherence tomography in Asian eyes. *Ophthalmology*. **114**, 33-39.
- Nordmann, J., Fink, H. and Hockwin, O. (1974). Die wachstumskurve der menschlichen linsen. *Graefes Archiv für klinische und experimentelle Ophthalmologie*. **191**, 165-175.
- Nubile, M., Calienno, R., Lanzini, M. and Mastropasqua, L. (2008). Applications for Visante OCT. *Cataract and Refractive Surgery Today Europe*. Available online at <http://www.crstodayeurope.com/Pages/whichArticle.php?id=323>. Accessed August 10th 2010.
- Obata, T., Uemura, K., Nonaka, H., Tamura, M., Tanada, S. and Ikehira, H. (2006). Optimizing T2-weighted magnetic resonance sequences for surface coil microimaging of the eye with regard to lid, eyeball and head moving artifacts. *Magnetic Resonance Imaging*. **24**, 97-101.
- Olbert, D. (1988). Problems of lens biometry by Scheimpflug photos. *Lens Research*. **5**, 73-81.
- Oliveira, C., Tello, C., Liebmann, J. M. and Ritch, R. (2005). Ciliary body thickness increases with increasing axial myopia. *American Journal of Ophthalmology*. **140**, 324-325.
- Ostrin, L. A. and Glasser, A. (2004). Accommodation measurements in a prepresbyopic and presbyopic population. *Journal of Cataract and Refractive Surgery*. **30**, 1435-1444.
- Ostrin, L. A. and Glasser, A. (2007a). Edinger-Westphal and pharmacologically stimulated accommodative refractive changes and lens and ciliary process movements in rhesus monkeys. *Experimental Eye Research*. **84**, 302-313.

Ostrin, L. A. and Glasser, A. (2007b). Effects of pharmacologically manipulated amplitude and starting point on Edinger-Westphal-stimulated accommodative dynamics in rhesus monkeys. *Investigative Ophthalmology and Visual Science*. **48**, 313-320.

Ostrin, L. A., Kasthurirangan, S. and Glasser, A. (2004). Evaluation of a satisfied scleral expansion band patient. *Journal of Cataract and Refractive Surgery*. **30**, 1445-1453.

Owens, H. (1991). The effect of beta-adrenergic receptor agonists on the temporal accommodation response. PhD thesis, Aston University, Birmingham, UK, Ch. 5, pp. 90-101.

Owens, H., Bhat, K. and Jacobs, R. J. (1994). Maxwellian and real pupils: effects on accommodative microfluctuations. *Investigative Ophthalmology and Visual Science*. **35**, S1280.

Pardue, M. T. and Sivak, J. G. (2000). Age-related changes in human ciliary muscle. *Optometry and Vision Science*. **77**, 204-210.

Park, K.-H., Yun, J.-H. and Kee, C. (2008). The effect of cataract extraction on the contractility of ciliary muscle. *American Journal of Ophthalmology*. **146**, 8-14.

Parsinnen, O. and Lyyra, A. L. (1993). Myopia and myopic progression among schoolchildren: a three-year follow-up study. *Investigative Ophthalmology and Vision Science*. **34**, 2794-2802.

Patel, C. K. and Bron, A. J. (2002) The Ageing Lens. *In: Cataract Referral and Management*. Association of Optometrists, London. pp. 24-30.

Patnaik, B. (1967). A photographic study of accommodative mechanisms: changes in lens nucleus during accommodation. *Investigative Ophthalmology*. **6**, 601-611.

Pau, H. and Kranz, J. (1991). The increasing sclerosis of the human lens with age and its relevance to accommodation and presbyopia. *Graefe's Archives of Clinical and Experimental Ophthalmology*. **229**, 294-296.

- Pavlin, C. J., Harasiewicz, K. and Foster, F. S. (1992). Ultrasound biomicroscopy of anterior segment structures in normal and glaucomatous eyes. *American Journal of Ophthalmology*. **113**, 381-389.
- Pepose, J. S. (2008). Maximising satisfaction with presbyopia-correcting intraocular lenses: the missing links. *American Journal of Ophthalmology*. **146**, 641-648.
- Phillips, P., Perez-Emmanuelli, J., Rosskothan, H. D. and Koester, C. J. (1988). Measurement of intraocular lens decentration and tilt *in vivo*. *Journal of Cataract and Refractive Surgery*. **14**, 129-135.
- Pieroni, C. G., Witkin, A. J. and Ko, T. H. (2006). Ultrahigh resolution optical coherence tomography in non-exudative age related macular degeneration. *British Journal of Ophthalmology*. **26**, 14-20.
- Pierscionek, B. K. and Weale, R. A. (1995). Presbyopia- a maverick of human aging. *Archives of Gerontology and Geriatrics*. **20**, 229-240.
- Polito, A., Del Borello, M., Polini, G., Furlan, F., Isola, M. and Bandello, F. (2006). Diurnal variation in clinically significant diabetic macular edema measured by the stratus OCT. *Retina*. **26**, 14-20.
- Pope, J. M., Atchison, D. A. and Jones, C. E. (2008). Authors' reply: changes in lens dimensions and refractive index with age and accommodation. *Optometry and Vision Science*. **85**, 282-283.
- Poyer, J. F., Kaufman, P. L. and Flügel, C. (1993). Age does not affect contractile responses of the isolated rhesus monkey ciliary muscle to muscarinic agonists. *Current Eye Research*. **12**, 413-422.
- Provine, R. R. and Enoch, J. M. (1975). On voluntary ocular accommodation. *Perception and Psychophysics*. **17**, 209-212.
- Pugh, J. R., Eadie, A. S., Winn, B. and Heron, G. (1987). Power spectrum analysis in the study of ocular mechanisms. *Ophthalmic and Physiological Optics*. **7**, 321-324.

- Pugh, J. R. and Winn, B. (1988). Modification of the Canon Autorefractometer R1 for use as a continuously recording infra-red optometer. *Ophthalmic and Physiological Optics*. **8**, 460-464.
- Rabbetts, R. B. (1998). Bennett and Rabbetts' Clinical Visual Optics. Third Edition. Butterworth-Heinemann. Edinburgh, U. K. pp 290-292.
- Rabsilber, T. M., Khoramnia, R. and Auffarth, G. U. (2006). Anterior chamber measurements using Pentacam rotating Scheimpflug camera. *Journal of Cataract and Refractive Surgery*. **32**, 456-459.
- Rada, J. A., Johnson, J. M., Achen, V. R. and Rada, K. G. (2002). Inhibition of scleral proteoglycan synthesis blocks deprivation-induced axial elongation in chicks. *Experimental Eye Research*. **74**, 205-215.
- Radhakrishnan, H. and Charman, W. N. (2007a). Age-related changes in static accommodation and accommodative miosis. *Ophthalmic and Physiological Optics*. **27**, 342-352.
- Radhakrishnan, H. and Charman, W. N. (2007b). Changes in astigmatism with accommodation. *Ophthalmic and Physiological Optics*. **27**, 275-280.
- Radhakrishnan, H. and Charman, W. N. (2008). Peripheral refraction measurement: does it matter if one turns the eye or the head? *Ophthalmic and Physiological Optics*. **28**, 73-82.
- Radhakrishnan, H., Goldsmith, J. and Westphal, V. (2005). Comparison of optical coherence tomography and ultrasound biomicroscopy for detection of narrow anterior chamber angles. *Archives of Ophthalmology*. **123**, 1053-1059.
- Ramrattan, R. S., van der Schaft, T. L., Mooy, C. M., de Bruijn, W. C., Mulder, P. G. H. and de Jong, P. (1994). Morphometric analysis of Bruch's membrane, the choriocapillaris and the choroid in aging. *Investigative Ophthalmology and Visual Science*. **35**, 2857-2864.
- Read, S. A., Collins, M. J., Woodman, E. C. and Cheong, S. H. (2010). Axial length changes during accommodation in myopes and emmetropes. *Optometry and Vision Science*. **87**, DOI: 1040-5488/10/8709-0001/0.

- Remington, L. A. (2005) *Clinical Anatomy of the Visual System*, St. Louis, Missouri, Elsevier Butterworth Heinemann. pp 87-101.
- Rempt, F., Hoogerheide, J. and Hoogenboom, W. P. (1971). Peripheral retinocopy and the skiagram. *Ophthalmologica*. **162**, 1-10.
- Richdale, K., Bullimore, M. A., and Zadnik, K. (2008). Lens thickness with age and accommodation by optical coherence tomography. *Ophthalmic and Physiological Optics*. **28**, 441-447.
- Richdale, K., Wassenaar, P., Bluestein, K. T., A., A., Christoforidis, J. A., Lanz, T., Knopp, M. V. and Schmalbrock, P. (2009). 7 Tesla MR imaging of the human eye *in vivo*. *Journal of Magnetic Resonance Imaging*. **30**, 924-932.
- Rohen, J. W. (1979). Scanning electron microscopic studies of the zonular apparatus in human and monkey eyes. *Investigative Ophthalmology and Visual Science*. **18**, 133-144.
- Roman, F. (1995). The discovery of accommodation. *British Journal of Ophthalmology*. **79**, 375.
- Ronchi, L. (1971). Absolute threshold before and after correction of oblique-ray astigmatism. *Journal of the Optical Society of America*. **61**, 1705-1709.
- Roorda, A. and Glasser, A. (2004). Wave aberrations of the isolated crystalline lens. *Journal of Vision*. **4**, 250-261.
- Rosales, P. and Marcos, S. (2006). Phakometry and lens tilt and decentration using a custom-developed Purkinje imaging apparatus: validation and measurements. *Journal of the Optical Society of America*. **23**, 509-520.
- Rosales, P., Wendt, M., Marcos, S. and Glasser, A. (2008). Changes in crystalline lens radii of curvature and lens tilt and decentration during dynamic accommodation in rhesus monkeys. *Journal of Vision*. **8**, 1-12.
- Rosen, A. M., Denham, D. B., Fernandez, V., Borja, D., Ho, A., Manns, F., Parel, J.-M. and Augusteyn, R. C. (2006). *In vitro* dimensions and curvatures of human lenses. *Vision Research*. **46**, 1002-1009.

- Rosenfield, M. and Ciuffreda, K. J. (1991). Effect of surround propinquity on the open-loop accommodative response. *Investigative Ophthalmology and Visual Science*. **32**, 142-147.
- Rosenfield, M., Ciuffreda, K. J. and Hung, G. K. (1991). The linearity of proximally induced accommodation and vergence. *Investigative Ophthalmology and Visual Science*. **32**, 2985-2991.
- Rosenfield, M., Ciuffreda, K. J., Hung, G. K. and Gilmartin, B. (1993). Tonic accommodation: a review I. Basic aspects. *Ophthalmic and Physiological Optics*. **13**, 266-284.
- Rosenfield, M. and Cohen, A. S. (1996). Repeatability of clinical measurements of the amplitude of accommodation. *Ophthalmic and Physiological Optics*. **16**, 247-249.
- Sa, H. S., Kyung, S. E. and Ob, S. Y. (2005). Extraocular muscle imaging in complex strabismus. *Ophthalmic Surgery, Lasers and Imaging*. **36**, 487-493
- Sakabe, I., Oshika, T., Lim, S. J. and Apple, D. J. (1998). Anterior shift of zonular insertion into the anterior surface of human crystalline lens with age. *Ophthalmology*. **105**, 295-299.
- Sakata, L. M., Lavanya, R., Friedman, D. S., Aung, H. T., Seah, S. K., Foster, P. J. and Aung, T. (2008). Assessment of the scleral spur in anterior segment optical coherence tomography images. *Archives of Ophthalmology*. **126**, 181-185.
- Saladin, J. J. and Stark, L. (1975). Presbyopia: new evidence from impedance cyclography supporting the Hess-Gullstrand theory. *Vision Research*. **15**, 537-541.
- Santodomingo-Rubido, J., Mallen, E. A. H., Gilmartin, B. and Wolffsohn, J. S. (2002). A new non-contact device for ocular biometry. *British Journal of Ophthalmology*. **86**, 458-462.
- Schachar, R. A. (1992). Cause and treatment of presbyopia with a method for increasing the amplitude of accommodation. *Annals of Ophthalmology*. **24**, 445-452.
- Schachar, R. A. (1994). Pathophysiology of accommodation and presbyopia: understanding the clinical implications. *Journal of the Florida Medical Association*. **81**, 268-271.
- Schachar, R. A. (2000). Theoretical basis for the scleral expansion band procedure for surgical reversal of presbyopia. *Annals of Ophthalmology*. **32**, 271-278.

Schachar, R. A. (2005). Growth patterns of fresh human crystalline lenses measured by in vitro photographic biometry. *Journal of Anatomy*. **206**, 575-580.

Schachar, R. A. (2006). The mechanism of accommodation and presbyopia. *International Ophthalmology Clinics*. **46**, 39-61.

Schachar, R. A. (2007). Letter to the Editor: the lens is stable during accommodation. *Ophthalmic and Physiological Optics*. **27**, 520-521.

Schachar, R. A. and Cudmore, D. P. (1994). The effect of gravity on the amplitude of accommodation. *Annals of Ophthalmology*. **26**, 65-70.

Schachar, R. A., Cudmore, D. P. and Black, T. D. (1993a). Experimental support for Schachar's hypothesis of accommodation. *Annals of Ophthalmology*. **25**, 404-409.

Schachar, R. A., Davila, C., Pierscionek, B. K., Chen, W. and Ward, W. W. (2007). The effect of human *In vivo* accommodation on crystalline lens stability. *British Journal of Ophthalmology*. **91**, 790-793.

Schachar, R. A., Huang, T. and Huang, X. (1993b). Mathematical proof of Schachar's hypothesis of accommodation. *Annals of Ophthalmology*. **25**, 5-9.

Schachar, R. A., Kamangar, F. and Pierscionek, B. K. (2008). To the editor: changes in lens dimensions and refractive index with age and accommodation. *Optometry and Vision Science*. **85**, 281-282.

Schachar, R. A. and Koivula, A. (2008). The stress on the anterior lens surface during human *In vivo* accommodation. *British Journal of Ophthalmology*. **92**, 348-350.

Schachar, R. A., Tello, C., Cudmore, D. P., Liebmann, J. M., Black, T. D. and Ritch, R. (1996). *In vivo* increase of the human lens equatorial diameter during accommodation. *American Journal of Physiology- Regulatory, Integrative and Comparative Physiology*. **271**, 670-676.

Schaeffel, F. (2008). Binocular lens tilt and decentration measurements in healthy subjects with phakic eyes. *Investigative Ophthalmology and Visual Science*. **49**, 2216-2222.

- Schor, C. M., Kotulak, J. C. and Tsuetaki, T. (1986). Adaptation of tonic accommodation reduces accommodative lag and is masked in darkness. *Investigative Ophthalmology and Visual Science*. **27**, 820-827.
- Schultz, K. E., Sinnott, L. T., Mutti, D. O. and Bailey, M. D. (2009). Accommodative fluctuations, lens tension and ciliary body thickness in children. *Optometry and Vision Science*. **86**, 677-684.
- Seidemann, A., Schaeffel, F., Guirao, A., Lopez-Gil, N. and Artal, P. (2002). Peripheral refractive errors in myopic, emmetropic, and hyperopic young subjects. *Journal of the Optical Society of America A- Optics and Image Science*. **19**, 2363-2373.
- Siebinga, I., Vrensen, G. F. J. M., De Mu, F. F. and Greve, J. (1991). Age-related changes in local water and protein content of human eye lenses measured by Raman Spectroscopy. *Experimental Eye Research*. **153**, 233-239.
- Sheppard A.L. and Davies L. N. (2009a). Changes in human ciliary muscle biometry with accommodation: an anterior segment optical coherence tomography study. *Ophthalmic and Physiological Optics*. **29**, 668 (Abstract).
- Sheppard, A. L. and Davies, L. N. (2009b). *In vivo* changes in human ciliary muscle biometry with accommodation. *Investigative Ophthalmology and Visual Science*. **50**, E-Abstract 2796.
- Sheppard, A. L. and Davies, L. N. (2010a). Clinical evaluation of the Grand Seiko Auto Ref/Keratometer WAM-5500. *Ophthalmic and Physiological Optics*. **30**, 143-151.
- Sheppard A.L. and Davies L. N. (2010b). *In vivo* analysis of ciliary muscle morphological changes with accommodation and axial ametropia. *Investigative Ophthalmology and Visual Science*. In press. doi: 10.1167/iovs.10-5787
- Sheppard, A. L., Bashir, A., Wolffsohn, J. S. and Davies, L. N. (2010). Accommodating Intraocular Lenses: a review of design concepts, usage and assessment methods. *Clinical and Experimental Optometry*. In press.

- Singh, M., Chew, P. T. K. and Friedman, D. S. (2007). Imaging of trabeculectomy blebs using anterior segment optical coherence tomography. *Ophthalmology*. **114**, 47-53.
- Singh, K. D., Logan, N. S. and Gilmartin, B. (2006). Three-dimensional modeling of the human eye based on magnetic resonance imaging. *Investigative Ophthalmology and Visual Science*. **47**, 2272-2279.
- Smith, E. L. R., Hung, L. F. and Huang, J. (2009). Relative peripheral hyperopic defocus alters central refractive development in infant monkeys. *Vision Research*. **49**, 2386-2392.
- Smith, G. (1983). The accommodative resting states, instrument accommodation and their measurement. *Journal of Modern Optics*. **30**, 347-359.
- Smith, G., Millodot, M. and McBrien, N. (1988). The effect of accommodation on oblique astigmatism and field curvature of the human eye. *Clinical and Experimental Optometry*. **71**, 119-125.
- Snell, R. S. and Lemp, M. A. (1998) *Clinical Anatomy of the Eye*. Second edition. (Malden, M. A., Ed.) Blackwell Science pp3-15 and 197-205.
- Sokolowska, A. and Thorn, F. (2003). Accommodation induced changes in crystalline lens position. *Investigative Ophthalmology and Visual Science*. **44**, E-Abstract 4072.
- Stachs, O., Martin, H., Kirchhoff, A., Stave, J., Terwee, T. and Guthoff, R. (2002). Monitoring accommodative ciliary muscle function using three-dimensional ultrasound. *Graefe's Archives of Clinical and Experimental Ophthalmology*. **240**, 906-912.
- Stachs, O., Schneider, H., Beck, R. and Guthoff, R. (2006). Pharmacological-induced haptic changes and the accommodative performance in patients with the AT-45 accommodative IOL. *Journal of Refractive Surgery*. **22**, 145-150.
- Stafford, M. J. (2001). The histology and biology of the lens. *Optometry Today*. **41** (1), 23-30.
- Stark, L. R. and Atchison, D. A. (1994). Subject instructions and methods of target presentation in accommodation research. *Investigative Ophthalmology and Visual Science*. **35**, 528-537.

- Stark, L. R. and Atchison, D. A. (1997). Pupil size, mean accommodation response and the fluctuations of accommodation. *Ophthalmic and Physiological Optics*. **17**, 316-323.
- Strang, N. C., Gray, L. S., Winn, B. and Pugh, J. R. (1998). Clinical evaluation of patient tolerance to autorefractor prescriptions. *Clinical and Experimental Optometry*. **81**, 112-118.
- Streeten, B. W. (1985) Ciliary body. *In: Biomedical Foundations of Ophthalmology* (Duane T. D. and Jaeger, E. A., Eds) Harper and Row, Philadelphia, USA. Chapter 13, pp 1-28.
- Steffen, H., Walker, M. F. and Zee, D. S. (2000). Rotation of Listing's plane with convergence: independence from eye position. *Investigative Ophthalmology and Visual Science*. **41**, 715-721.
- Stone, R. A. and Flitcroft, D. I. (2004). Ocular shape and myopia. *Annals, Academy of Medicine, Singapore*. **33**, 7-15.
- Strenk, S. A., Semmlow, J. L., Strenk, L. M., Munoz, P., Gronlund-Jacob, J. and De Marco, J. K. (1999). Age-related changes in human ciliary muscle and lens: a magnetic resonance imaging study. *Investigative Ophthalmology and Visual Science*. **40**, 1162-1169.
- Strenk, S. A., Strenk, L. M. and Guo, S. (2006). Magnetic resonance imaging of aging, accommodating, phakic, and pseudophakic ciliary muscle diameters. *Journal of Cataract and Refractive Surgery*. **32**, 1792-1798.
- Strenk, S. A., Strenk, L. M. and Guo, S. (2010). Magnetic resonance imaging of the anteroposterior position and thickness of the aging, accommodating, phakic and pseudophakic ciliary muscle. *Journal of Cataract and Refractive Surgery*. **36**, 235-241.
- Strenk, S. A., Strenk, L. M. and Koretz, J. F. (2005). The mechanism of presbyopia. *Progress in Retinal and Eye Research*. **24**, 379-393.
- Strenk, S. A., Strenk, L. M., Semmlow, J. L. and De Marco, J. K. (2004). Magnetic resonance imaging study of the effects of age and accommodation on the human lens cross-sectional area. *Investigative Ophthalmology and Visual Science*. **45**, 539-545.
- Swegmark, G. (1969). Studies with impedance cyclophography on human accommodation at different ages. *Acta Ophthalmologica*. **47**, 1186-1206.

- Tabernerero, J. and Schaeffel, F. (2009). Fast scanning photoretinoscope for measuring peripheral refraction as a function of accommodation. *Journal of the Optical Society of America A- Optics and Image Science*. **26**, 2206-2210.
- Tamm, E. R. and Lütjen-Drecoll, E. (1996). Ciliary body. *Microscopy Research and Technique*. **33**, 390-439.
- Tamm, E. R., Lütjen-Drecoll, E., Jungkunz, W. and Rohen, J. W. (1991). Posterior attachment of ciliary muscle in young, accommodating old, presbyopic monkeys. *Investigative Ophthalmology and Visual Science*. **32**, 1678-1692.
- Tamm, S., Tamm, E. R. and Rohen, J. W. (1992a). Age-related changes of the human ciliary muscle: a quantitative morphometric study. *Mechanisms of Ageing and Development*. **62**, 209-221.
- Tamm, E., Croft, M. A., Jungkunz, W., Lütjen-Drecoll, E. and Kaufman, P. L. (1992b). Age-related loss of ciliary muscle mobility in the rhesus monkey: role of the choroid. *Archives of Ophthalmology*. **110**, 871-876.
- Tearney, G. J., Brezinski, M. E., Southern, J. F., Bouma, B. E., Hee, M. R. and Fujimoto, J. G. (1995). Determination of the refractive index of highly scattering human tissue by optical coherence tomography. *Optics Letters*. **20**, 2258-2261.
- Thibos, L. N., Still, D. L. and Bradley, A. (1996). Characterization of spatial aliasing and contrast sensitivity in peripheral vision. *Vision Research*. **36**, 249-258.
- Thibos, L. N., Wheeler, W. and Horner, D. (1997). Power vectors: an application of Fourier analysis to the description and statistical analysis of refractive error. *Optometry and Vision Science*. **74**, 367-375.
- Toates, F. M. (1972). Accommodation function of the human eye. *Physiology Reviews*. **52**, 828-863.
- Törnqvist, G. (1966). Effect of cervical sympathetic stimulation on accommodation in monkeys. *Acta Physiologica Scandinavica*. **67**, 363-372.

- Törnqvist, G. (1967). The relative importance of the parasympathetic and sympathetic nervous systems for accommodation in monkeys. *Investigative Ophthalmology and Visual Science*. **6**, 612-617.
- Truscott, R. J. (2009). Presbyopia. Emerging from a blur towards and understanding of the molecular basis for this most common eye condition. *Experimental Eye Research*. **88**, 241-247.
- Tscherning, M. (1909) H. v. Helmholtz et la theorie de l'accommodation, Octave Doin, Paris.
- Tsukamoto, M., Nakajima, T., Nishino, J., Hara, Y., Uozato, H. and Saishin, M. (2000). Accommodation causes with-the-rule astigmatism in emmetropes. *Optometry and Vision Science*. **77**, 150-155.
- Turner, M. J. (1958). Observations on the normal subjective amplitude of accommodation. *British Journal of Physiological Optics*. **15**, 70-100.
- Uozato, H., Shimizu, K., Minei, R. and Suzuki, H. (2003). Effect of accommodation on axial length measurement in optical coherence biometry. *Investigative Ophthalmology and Vision Science*. **44**, E-Abstract 4080.
- Uthoff, D., Holland, D., Hepper, D., Gulati, A., Koch, L. and Haigis, W. (2009). Laserinterferometric measurements of accommodative changes in the position of an optic-shift intraocular lens. *Journal of Refractive Surgery*. **25**, 416-420.
- van Alphen, G. W. (1986). Choroidal stretch and emmetropization. *Vision Research*. **26**, 723-734.
- Van der Heijde, G. L., Beers, A. P. A. and Dubbelman, M. (1996). Microfluctuations of steady-state accommodation measured with ultrasonography. *Ophthalmic and Physiological Optics*. **16**, 216-221.
- Van Heyningen, R. (1972). The human lens 3. Some observations on the post-mortem lens. *Experimental Eye Research*. **13**, 155-160.

- Verbruggen, K. H., Rozema, J. J. and Gobin, L. (2007). Intraocular lens centration and visual outcomes after bag-in-the-lens implantation. *Journal of Cataract and Refractive Surgery*. **33**, 1267-1272.
- Vezella, F. and Calossi, A. (1993). Multifocal effect of against-the-rule myopic astigmatism in pseudophakic eyes. *Refractive and Corneal Surgery*. **9**, 58-61.
- Vilipuru, A. S. and Glasser, A. (2005). The relationship between refractive and biometric changes during Edinger-Westphal stimulated accommodation in rhesus monkeys. *Experimental Eye Research*. **80**, 349-360.
- Vohra, S. B. and Good, P. A. (2000). Altered globe dimensions of axial myopia as risk factors for penetrating ocular injury during peribulbar anaesthesia. *British Journal of Anaesthesiology*. **85**, 242-245.
- von Gullstrand, A. (1924) Mechanism of accommodation, in *Handbuch der Physiologischen Optik*, Vol. 1. Optical Society of America. pp. 382-415.
- von Helmholtz, H. (1855). Über die akkommodation des auges. *Archives of Ophthalmology*. **1**, 1-74.
- Walker, T. W. and Mutti, D. O. (2002). The effect of accommodation on ocular shape. *Optometry and Vision Science*. **79**, 424-430.
- Wallman, J., Gottlieb, M. D., Rajaram, V. and Fugate-Wentzek, L. A. (1987). Local retinal regions control local growth and myopia. *Science*. **237**, 73-77.
- Wang, Y. Z., Thibos, L. N., Lopez, N., Salmon, T. and Bradley, A. (1996). Subjective refraction of the visual field using contrast detection acuity. *Journal of the American Optometry Association*. **67**, 584-589.
- Wasilewski, R., McDonald, J. P., Heatley, G., Lütjen-Drecoll, E., Kaufman, P. L. and Croft, M. A. (2008). Surgical intervention and accommodative responses II: forward ciliary body accommodative movement is facilitated by zonular attachments to the lens capsule. *Investigative Ophthalmology and Visual Science*. **49**, 5495-5502.

- Weale, R. A. (1989). Presbyopia towards the end of the 20th century. *Surveys in Ophthalmology*. **34**, 15-30.
- Weale, R. A. (1992). *The Senescence of Human Vision*, Oxford University Press, Oxford, UK.
- Weale, R. A. (1999). On potential causes of presbyopia. *Vision Research*. **39**, 1263-1272.
- Weale, R. A. (2000). Why we need glasses before a zimmer-frame. *Vision Research*. **40**, 2233-2240.
- Weeber, H. A., Eckert, G., Pechhold, W. and Van der Heijde, R. G. L. (2007). Stiffness gradient in the crystalline lens. *Graefes Archives of Clinical and Experimental Ophthalmology*. **245**, 1357-1366.
- Werner, L., Lovisolo, C., Chew, J., Tetz, M. and Müller, M. (2008). Meridional differences in internal dimensions of the anterior segment in human eyes evaluated with 2 imaging systems. *Journal of Cataract and Refractive Surgery*. **34**, 1125-1132.
- Wildsoet, C. F. (1998). Structural correlates of myopia. In: *Myopia and Nearwork*. Rosenfield M and Gilmartin B Eds. Oxford, UK. Butterworth-Heinemann. pp 31-56.
- Wilson, R. S. (1997). Does the lens diameter increase or decrease during accommodation? Human accommodation studies: a new technique using infra-red retro-illumination video photography and pixel analysis. *Transcripts of the American Optical Society*. **95**, 261-267.
- Winn, B. and Gilmartin, B. (1992). Current perspective on microfluctuations of accommodation. *Ophthalmic and Physiological Optics*. **12**, 252-256.
- Winn, B., Pugh, J. R., Gilmartin, B. and Owens, H. (1990). Arterial pulse modulates steady-state ocular accommodation. *Current Eye Research*. **9**, 971-975.
- Win-Hall, D. M., Ostrin, L. A., Kasthurirangan, S. and Glasser, A. (2007). Objective accommodation measurement with the Grand Seiko and Hartinger coincidence refractometer. *Optometry and Vision Science*. **84**, 879-887.

- Wirbelauer, C., Gochmann, R. and Pham, D. T. (2005). Imaging of the anterior eye chamber with optical coherence tomography [German]. *Klinische Monatsblätter für Augenheilkunde*. **222**, 856-862.
- Wold, H. E., Hu, A., Chen, S. and Glasser, A. (2003). Subjective and objective measurement of human accommodative amplitude. *Journal of Cataract and Refractive Surgery*. **29**, 1878-1888.
- Wolffsohn, J. S. (2008) Ophthalmic imaging. *In: Eye Essentials* (Doshi, S. and Harvey, W., Eds). Butterworth Heinemann Elsevier, Edinburgh.
- Wolffsohn, J. S. and Davies, L. N. (2007a). Advances in anterior segment imaging. *Current Opinion in Ophthalmology*. **18**, 32-38.
- Wolffsohn, J. S. and Davies, L. N. (2007b). Advances in ocular imaging. *Expert Reviews in Ophthalmology*. **2**, 755-767.
- Wolffsohn, J. S., Gilmartin, B., Mallen, E. A. H. and Tsujimura, S. (2001). Continuous recording of accommodation and pupil size using the Shin-Nippon SRW-5000 autorefractor. *Ophthalmic and Physiological Optics*. **21**, 108-113.
- Wolffsohn, J. S., O'Donnell, C. O., Charman, W. N. and Gilmartin, B. (2004). Simultaneous continuous recording of accommodation and pupil size using the modified Shin-Nippon SRW-5000 autorefractor. *Ophthalmic and Physiological Optics*. **24**, 142-147.
- Wolffsohn, J. S. and Peterson, R. C. (2006). Anterior ophthalmic imaging. *Clinical and Experimental Optometry*. **89**, 205-214.
- Young, T. (1801). The Bakerian Lecture. On the mechanism of the eye. *Philosophical Transactions of the Royal Society of London*. 23-88.
- Zamudio, A. C., Candia, O. A., Kong, C. W., Wu, B. and Gerometta, R. (2008). Surface change of the mammalian lens during accommodation. *American Journal of Physiology-Cell Physiology*. **294**, C1430–C1435.
- Zeiss (2006). Visante OCT Model 1000 User Manual.

Zhou, X. D., Wang, F. R., Zhou, S. Z. and Shi, J. S. (1996). A computed tomographic study of the relation between ocular axial biometry and refraction. In: *Myopia Updates: Proceedings of the 6th International Conference on Myopia; September 24-26th, Hakone, Japan*. Tokoro, T., Ed. Springer, Tokyo, 1997. pp 112-116.

Ziebarth, N. M., Borja, D., Arrieta, E., Aly, M., Manns, F., Dortonne, I., Nankivil, D., Jain, R. and Parel, J.-M. (2008). Role of the lens capsule on the mechanical accommodative response in a lens stretcher. *Investigative Ophthalmology and Visual Science*. **49**, 4490-4496.

Ziebarth, N. M., Manns, F., Uhlhorn, S., Venkatraman, A. S. and Parel, J.-M. (2005). Non-contact optical measurement of lens capsule thickness in human, monkey and rabbit post-mortem eyes. *Investigative Ophthalmology and Visual Science*. **46**, 1690-1697.